Determining the origin of localised subsidence features in the Kawerau Geothermal Field, Bay of Plenty, New Zealand

---

A thesis submitted in partial fulfilment of the requirements for the degree

of

Masters of Science in Engineering Geology

at the

University of Canterbury

by

Hayden Thomas Mackenzie

Department of Geological Sciences,

University of Canterbury,

Christchurch, New Zealand

2012

Acknowledgements

This report takes the form of a thesis, which was supported by grants from Mighty River Power and The Australasian Institute of Mining and Metallurgy, for which I am thankful.

I wish to sincerely thank my thesis supervisors Dr Darren Gravely and Dr David Nobes for their guidance, assistance in the collection and processing of data and their reviews of this manuscript.

Mighty River Power staff, in particular Ben Pezaro who pulled everything together in the North Island, organising site access, background history, access to data and constant help and communication. Thanks so much Ben. Also from Mighty River Power, thanks to Joe Gamman and Tom Powell for all your help.

I thank the Department of Geological Sciences at Canterbury University and the input of various staff members, particularly Jim Cole for motivating me in the very beginning and setting up the original discussions with Mighty River Power. Thank you John Southward for all your assistance with the computers, I wouldn't have got very far without your help. Thanks to David Bell for your input and discussion on investigation techniques and the engineering geological model as well as all your help with part one of Masters; your input, especially towards the end of my thesis has been invaluable. Thanks to the technical staff for providing all the field gear I needed and assistance with lab work, particularly Cathy, Vanessa, Chris and Sacha.

Thanks to all the students who have helped out, particularly Georgina Richards for all your help with the geophysics field work, I truly appreciate your help and the swims, barbecues and bottles of wine at the end of each day. Thanks to Andrew Klahn for your help with the soil augering, your help on this is greatly appreciated. Thanks to Brendan Duffy for help with LiDAR and GPS data and GIS. Your ideas, advice and help is greatly appreciated.

A great deal of thanks is due to the landowners whose land I worked on, without access we wouldn't have had much data to work with.

Thanks to staff at Environment Bay of Plenty for providing valuable data, aerial photographs, LiDAR data and records.

Thanks to Leapfrog staff for free software and tutorials, trouble shooting, pre-releases of software and modifications to the software as required.

Thanks to Anthony Olsen for your local knowledge and the cultural background you provided as well as your opinions and maps.

Thanks to Whakatane Historical Society, particularly secretary Meri Low for scanning records and sending me information on the Rangitaiki Plains.

Thanks also to all my flatmates over the years, you have been my family in Christchurch and all of you have been amazing to live with.

I owe a great deal of thanks to Andrew Klahn for your motivation, support, frequent discussions and opinions, trips away to get work done, study sessions and social organisation over the last 7 years, uni really wouldn't have been the same without you and your help.

Thanks to everyone at CRL Energy, most of you have contributed with discussions at some point and were very flexible and accommodating to me while I was studying. The experiences and contacts I made through CRL have been invaluable and I thoroughly enjoyed my time working with you all.

Above all, thanks are due to my Family. My parents spent my childhood taking us all tramping, pointing out geological features and getting us in to the outdoors. They gave me the education and support I needed to start it all and they have supported me being at University, even though it turned out to be a lot longer than planned. Thanks to Andrew and Kate for being great siblings, thanks for the comments on my thesis Kate. Perhaps the greatest thanks is due to Dr Paul Fitzgerald, a very good family friend who is a geologist who has spent his career researching in amazing locations such as Antarctica and Papua New Guinea. It is due to his glamorisation of the geology industry that got me so excited about the field from such an early age.

Thank you to all others who helped me in this project in some way.

Abstract

Kawerau is located in the Bay of Plenty on the north-east coast of the North Island, New Zealand. Kawerau is an active geothermal field where fluids have been extracted for energy use since the 1950's when a pulp and paper mill was constructed due to the close proximity to forestry areas and the geothermal energy source. Kawerau has seen significant development in the last 10 years with the commissioning of a 100 MW geothermal power station by Mighty River Power in 2005. Kawerau is located on the south-western edge of the Rangitaiki Plains; these plains have been modified considerably over the last 125 years since the 1886 Tarawera eruption by both natural and anthropogenic mechanisms. Processes at work in the Kawerau area include active volcanism, rifting, fluvial processes, shallow and deep water extraction, anthropogenic river modification and diversion, and construction of buildings and factories.

Subsidence is an issue in geothermal and oil fields worldwide and Kawerau is no different. This research aims to determine the origin of localised subsidence features identified by levelling surveys within the Kawerau Geothermal Field. Ground subsidence surrounding the pulp and paper mill, geothermal power station and residential properties in Kawerau has been monitored with levelling surveys since the 1970's. The potential effects of continued subsidence and tilt within this area could negatively affect the operation of the industry in the area, particularly the pulp and paper mill due to the sensitivity of the paper rollers to tilt. Subsidence in Kawerau occurs on two scales: the first is a large, field-wide subsidence feature, the second is a series of smaller, localised subsidence features which this thesis focuses on.

First, identifying the location and characterising the properties of historic river channels, as well as their response to human demand, such as land and water use has been the primary approach in determining the origin of subsidence features. This helped build a picture of how the area appeared 125 years ago and add to our understanding of the history and landscape of the Rangitaiki Plains.

Second, to determine the cause(s) and mechanism(s) of the subsidence in Kawerau, field and laboratory investigations were undertaken. Site investigations included geomorphological mapping, ground penetrating radar (GPR), electrical imaging, hand augering and face logging. Laboratory investigations included permeability testing, determination of Atterberg Limits, dispersion testing, grain size distributions, microscopy and allophane detection testing.

Aerial photograph and LiDAR interpretation as well as a literature review has shown the approximate location of where the Tarawera River used to flow before it was diverted to aid in the draining of the Rangitaiki Plains. In the approximate location of the old Tarawera River, the geophysical survey identified an extension of the Onepu fault. This fault may have influenced the original location of the Tarawera River by creating low points in the topography as the result of seismic events. The Tarawera River path was diverted to its current path in the early 1900s following the large outbreak flood from Lake Tarawera.

Basin wide subsidence at Kawerau has been attributed to geothermal fluid extraction and the resulting contraction and/or cooling of the reservoir. This has caused low rates of subsidence across the whole field. This subsidence is unlikely to cause any damage to surface features due to its low rate and low angles of tilt. Basin wide subsidence is not the focus of this thesis so is not covered in detail.

This thesis focuses on two main sites of subsidence. Site 1 lies between the mill site and the Mighty River Power geothermal power station. Site 2 lies in farm land to the north of the mill and the old air strip. The mechanisms controlling subsidence at these sites is believed to be acting independently of each other. Primary mechanisms of subsidence at Site 1 include indirect seismic activity, direct disturbance by construction, vibration, apparent subsidence, the influence of drainage through the site, and wetting and drying sequences associated with rainfall and the soak ponds immediately adjacent to Site 1. Subsidence at Site 2 is likely to be caused by direct seismic activity, indirect seismic activity, consolidation of sediment due to changes in the groundwater table, and the influence of perched water tables.

Table of Contents

Acknowledgements 1
Abstract 3
Table of Contents 5
List of Figures 7
List of Tables 10
List of Equations 10
Chapter 1: Introduction 11
1.1 Subsidence 11
1.2 Subsidence in geothermal and oil field settings 12
1.3 Subsidence in drained areas 16
1.4 Thesis objectives 18
1.5 Structure 18
Chapter 2: Background geologic and geomorphic setting for Kawerau 19
2.1 Site location 19
2.2 Regional setting 22
2.3 Local setting 41
Chapter 3: Previous subsidence studies at Kawerau 49
3.1 Introduction 49
3.2 Levelling surveys 49
3.3 Geotechnical drill holes 60
3.4 Cone penetrometer tests 61
3.5 Aerial photograph interpretation 63
3.6 Computer modelling 64
3.7 Laboratory testing of materials 65
3.8 Geological and Nuclear Science reports 67
Chapter 4: Preliminary site investigation 69
4.1 Site investigation approach and objectives 69
4.2 Aerial photograph interpretation 69
4.3 Initial site visit 75
4.4 Engineering geological mapping 78
4.5 Site hydrogeology 81
Chapter 5: Shallow subsurface investigations 83
5.1 Introduction 83

5.2 Geophysical investigation 83
5.3 Leapfrog model and LiDAR 101
5.4 Invasive investigation 107
5.5 Laboratory investigation objectives and approach 118
5.5.1 Sample history 118
5.5.2 Water content 118
5.5.3 Atterberg limits 120
5.5.4 Emerson Aggregate Test 125
5.5.5 Grain size distribution 128
5.5.6 Microscopy 132
5.5.7 Detection of allophane in soils 134
5.5.8 Falling head permeability test 136
5.5.9 Constant head permeability test 139
5.5.10 Permeability summary 142
5.5.11 Implications of laboratory investigations to subsurface model 143
Chapter 6: Subsidence model 145
6.1 Evaluation of current theories on subsidence mechanisms 145
6.2 Key results 152
6.3 Preferred subsidence model 153
6.4 Explanation of patterns identified in levelling surveys 157
6.5 Predictions for future evolution of subsidence and assumptions 158
6.6 Kawerau in relation to other settings 158
Chapter 7: Conclusions and Recommendations 161
7.1 Project methods 161
7.2 Summary of results 161
7.3 Further Work 164
7.4 Implications for Future Development and Land Use in the Kawerau Area 165
References 166
Appendices 173
Appendix A: Results from compressibility and thermal expansion tests 174
Appendix B: Aerial photographs 178
Appendix C: Mill construction photographs 198
Appendix D: Geophysical principles 206
Appendix E: Ground penetrating radar profiles 210

Appendix F: Electrical imaging profiles 224
Appendix G: Auger logs 233
Appendix H: Rolled thread results 237
Appendix I: Cone penetration results 239
Appendix J: Emerson Aggregate Test methods 246
Appendix K: Emerson Aggregate Test results and photographs 251
Appendix L: Laser sizer results 267

List of Figures

Figure 1: Location of geothermal fields in the Taupo Volcanic Zone (TVZ) (Powell, 2011) 12
Figure 2: Location of Kawerau, Bay of Plenty, New Zealand 19
Figure 3: Locality map showing Kawerau and the specific field area 20
Figure 4: Location of the main subsidence bowls in Kawerau. Contours are 20 mm/year intervals for total cumulative subsidence from 2006 to 2010. 22
Figure 5: Location of the Kawerau geothermal field (red circle) within the TVZ and Whakatane Graben (Nairn & Beanland, 1989). Filled squares mark andesite/dacite and are volcanoes; outcropping greywacke is dot stippled. Star marks location of the 1987 March Edgecumbe earthquake main shock. 24
Figure 6: High resolution LiDAR-derived digital elevation model showing active fault traces across the Rangitaiki Plains (Begg & Mouslopoulou, 2010). The field area is located within the red square to the bottom left of the figure. 25
Figure 7: Fault zones in the Kawerau geothermal field adapted from Beanland at al. (1989), and Nairn and Beanland (1989). Purple lines show inferred buried fault displacements within the geothermal field, from Nairn and Beanland (1989). 26
Figure 8: Location of geotechnical drill holes G1 (yellow dot), G2 (red dot), G3 (blue dot), and KA41 (green dot) (SKM, 2005). 27
Figure 9: Simplified NW – SE cross section of the Kawerau Geothermal Field, based on well logging (Milicich, et al., 2011) 32
Figure 10: Sketch of stratigraphy and structures inferred in the eastern Kawerau Geothermal Field (Nairn & Beanland, 1989) 33
Figure 11: Regional geology of the Rangitaiki Plains and Kawerau area (Gordon, 2002) 35
Figure 12: Quaternary geology of the Rangitaiki Plains. (Begg & Mouslopoulou, 2010) 36
Figure 13: Map showing location of Tarawera River descriptions 39
Figure 14: Photograph showing typical banks of the Tarawera River 40
Figure 15: Photograph of the Tarawera River showing typical shape, width and flow 40
Figure 16: Map post-1913 showing original and current location of the Tarawera River 43
Figure 17: Location of major geothermal energy producers in the Kawerau area (Spinks, et al., 2007) 46
Figure 18: Benchmark number K0669 on the concrete base of a pipe support 50
Figure 19: Photograph showing typical location of benchmarks (Brock, 2006) 50
Figure 20: Photograph of typical conditions in site 1 and the location of a benchmark 51
Figure 21: Benchmark along the side of Onepu Springs Road within a concrete box with a steel lid 51
Figure 22: Benchmark locations at the mill site, and sites 1 and 2 54
Figure 23: Location of main subsidence bowls in Kawerau area. Contours are 20 mm/year intervals 55

FIGURE 24: IMAGES SHOWING PROGRESSION OF SUBSIDENCE BOWLS IN KAWERAU SINCE 2000, RATES ARE IN MM/YEAR. 56
FIGURE 25: PHOTOGRAPH OF SITE 1 IN HEAVY RAINFALL (BROCK, 2006) 60
FIGURE 26: ELECTRICAL FRICTION CONE WITH CUT-AWAY FRICTION SLEEVE (BROUWER, 2007) 62
FIGURE 27: 1945 AERIAL PHOTOGRAPH OF MILL SITE. RED CIRCLE SHOWING THE APPROXIMATE LOCATION OF SITE 1. VICINITY OF CLOSED DEPRESSION COMMENT IS IN THE SOUTHERN PART OF SITE 2. COMMENTS BY BROCK (2006). 71
FIGURE 28: 1966 AERIAL PHOTOGRAPHS SHOWING MILL DEVELOPMENTS AND SITES 1 (BLUE CIRCLE) AND 2 (RED OVAL) 72
FIGURE 29: 1987 AIR PHOTO OF THE FIELD AREA, SAME ANNOTATION AS ABOVE. COMMENTS BY BROCK (2006). 72
FIGURE 30: 2000 AERIAL PHOTO OF THE FIELD AREA – SITE 2 INDICATED BY RED CIRCLE. GREEN CIRCLES INDICATE INCREASES IN VEGETATION. ALSO OBVIOUS IN THE MAP ARE HISTORIC BRAIDED STREAM CHANNELS TO THE NORTH AND NORTH EAST OF SITE 2. 73
FIGURE 31: AERIAL PHOTOGRAPH OF THE PROPOSED MILL SITE (PHOTO DATED 1951) 74
FIGURE 32: AERIAL PHOTOGRAPH OF THE MILL SITE DURING CONSTRUCTION (CIRCA 1955). SITE 1 APPROXIMATELY SHOWN BY BLUE CIRCLE. 74
FIGURE 33: PHOTOGRAPH OF MILL UNDER CONSTRUCTION, THIS PHOTOGRAPH SHOWS CONSIDERABLE GROUND DISTURBANCE AND FOUNDATION PREPARATION (9 NOVEMBER 1955) 75
FIGURE 34: STEAM PIPELINE AT SITE 1 IN DRAINAGE CHANNEL 76
FIGURE 35: HISTORIC RAILWAY TRACKS - CREATE NOISE ON GPR PROFILES 77
FIGURE 36: STEAM PIPELINES, FENCES AND POWER LINES AT SITE 1. PIPELINE FOUNDATIONS IN SOFT, SATURATED GROUND. 77
FIGURE 37: HISTORIC RIVER CHANNEL AT SITE 2 78
FIGURE 38: ENGINEERING GEOLOGICAL MAP OF THE FIELD AREA INCLUDING LAND USE AND INVESTIGATION LOCATIONS 79
FIGURE 39: MAP OF FIELD AREA SHOWING WATER TABLE DEPTHS CALCULATED BY SPLINE INTERPOLATION OF DEPTHS TO WATER TABLE IN VARIOUS GROUNDWATER MONITORING WELLS. 82
FIGURE 40: IMAGE SHOWING THE LOCATION OF GPR LINES IN TWO MAIN LOCATIONS – SITE 1 TO THE SOUTH AND SITE 2 TO THE NORTH 84
FIGURE 41: PHOTOGRAPH SHOWING GPR COMPONENTS AND SET UP 85
FIGURE 42: USING GPR IN THE FIELD 86
FIGURE 43: CMP SURVEY IN PROGRESS 86
FIGURE 44: CMP ANALYSIS RESULTS SHOWING A PLOT OF VELOCITY MEASUREMENTS FROM WITHIN THE SUBSURFACE OF EPAD 3 .. 87
FIGURE 45: GPR LINE NML2 BETWEEN AND UNDER STEAM PIPELINES DELIVERED NOISY PROFILES 89
FIGURE 46: BASIC PROCESSING OF NML2 SHOW HIGH LEVELS OF NOISE AND NO REAL STRUCTURE FOR INTERPRETATION 90
FIGURE 47: PROCESSED (A.) AND INTERPRETED (B.) GPR PROFILES FOR EPAD1 91
FIGURE 48: PROCESSED (A.) AND INTERPRETED (B.) GPR PROFILES FOR WPAD1 92
FIGURE 49: PROCESSED (A.) AND INTERPRETED (B.) GPR PROFILES FOR MILL2 93
FIGURE 50: EXAMPLE OF FAULT IDENTIFICATION FROM YETTON AND NOBES (1998) 95
FIGURE 51: FIGURE SHOWING ACTIVE FAULTS IN THE KAWERAU AREA - ONEPU FAULT IN CENTRE, SITE 2 WITHIN RED CIRCLE (GNS, 2011) 96
FIGURE 52: IMAGE SHOWING NEW MAPPED LOCATION OF THE ONEPU FAULT 97
FIGURE 53: CAMPUS TIGRE RESISTIVITY UNIT AND LAPTOP PROTECTED WITHIN BLUE BOX 99
FIGURE 54: PHOTOGRAPH OF ELECTRODE LAYOUT AND ELECTRODE CABLE 99
FIGURE 55: TYPICAL RESISTIVITY PROFILE SHOWING VARIOUS PROCESSING FORMS FOR RESISTIVITY LINE KAWRES1 100
FIGURE 56: LIDAR IMAGE PROJECTED IN LEAPFROG 3D 102
FIGURE 57: 3D IMAGE OF LIDAR AND GPR PROFILES, THIS ALLOWS CLEAR VISUALISATION OF SUB-SURFACE PROFILES. GPR PROFILES ARE APPENDED (APPENDIX E) 103
FIGURE 58: PROJECTION OF FAULTS TO THE SURFACE AS EXTRAPOLATED FROM GPR PROFILES. THE IRREGULAR SHAPE AND STEPOVERS SUGGEST EN ECHELON OR OVERLAPPING FAULTS. GPR PROFILES ARE APPENDED (APPENDIX E). THIS FIGURE DOES NOT SHOW PREDICTED FAULT LOCATION, BUT WAS USED AS A TOOL TO IDENTIFY FAULT MORPHOLOGY. WITH FURTHER PROCESSING OF DATA, THIS COULD SHOW MORE ACCURATE FAULT LOCATIONS 103
FIGURE 59: ADDING AERIAL PHOTOGRAPHS TO LIDAR AND GPR PROFILES ALLOW THE VIEWER TO SEE LOW POINTS IN THE LANDSCAPE AND WHERE THE POTENTIAL FAULTS MEET THE SURFACE 104

Figure 60: Full view of LiDAR data set and GPR profiles. Leapfrog 3D also allows you to import GIS files such as the ones here which show the pathways of old rivers (Tarawera River is the blue line) 104
Figure 61: Leapfrog images of A: Aerial photograph of suspected river channels (centre of image) and, B: LiDAR image which shows there is a change in elevation around the location of possible river channels 105
Figure 62: Drill hole data can be imported in to Leapfrog 3D 105
Figure 63: Drill hole data can be interpreted to model features and lithology. This figure shows an unmodified or processed model made purely from drill hole data with no faults added. The figure has close resemblance to the most up to date geological model of the area. 106
Figure 64: The most recent geological model of the Kawerau Geothermal Field (Milicich, et al., 2011) shows close resemblance to the unprocessed Leapfrog model (Figure 63). 106
Figure 65: Location of hand auger holes and face logs 108
Figure 66: Location of hand auger holes and face logs at Site 1 109
Figure 67: Location of hand auger holes and face logs at Site 2 110
Figure 68: Photograph of hand auger in operation 111
Figure 69: Image of a soil auger head similar to what was used in Kawerau (AMS, 2011) 111
Figure 70: Face log 1 112
Figure 71: Hand auger log for Hole 3 113
Figure 72: Hand auger log for Hole 8 114
Figure 73: Hand auger log for Hole 10 114
Figure 74: Tributary to the Tarawera River - the incised channels show the ready erodability of the material around Kawerau 116
Figure 75: Photograph of the banks of the Tarawera River showing very loose sand eroding easily into the river 117
Figure 76: Rolled thread breaking apart 121
Figure 77: Soil sample is mixed thoroughly 123
Figure 78: Sample is placed into cone penetration cup 123
Figure 79: Cup is placed under cone, button on grey box to the right is pressed and cone pushes into sample 123
Figure 80: Penetration distance is measured 124
Figure 81: Soil sample cubes in distilled water 126
Figure 82: Slaked soil sample 127
Figure 83: Dispersed soil sample 127
Figure 84: Sieve shaker 129
Figure 85: Sample after being in the sieve shaker - grains are sorted in to sieves depending on size 129
Figure 86: Each grain size is weighed to 0.01 of a gram 129
Figure 87: A sample of grains <1 mm is processed in the laser sizer 130
Figure 88: Microscope photo 10 times magnification Sample 1 132
Figure 89: Microscope photograph 40 times magnification Sample 1 133
Figure 90: Microscope photograph 40 times magnification Sample 1 showing fibrous pumice shard 133
Figure 91: Microscope photograph 10 times magnification Sample 2 133
Figure 92: Microscope photograph 40 times magnification Sample 2 134
Figure 93: Photograph of samples on indicator paper after adding sodium fluoride 135
Figure 94: Falling head permeameter 137
Figure 95: Photograph of falling head permeameter set up 138
Figure 96: Typical intrinsic and hydraulic conductivity values for a variety of rocks (grey bars) and sediments (blue bars) (Hornberger, et al., 1998). 139
Figure 97: Photographs of constant head set up (left) and constant head permeameter unit (right) 141
Figure 98: Schematic drawing of infiltration at Kawerau with perched water table 142
Figure 99: Discharge point on steam pipeline at Site 1 144
Figure 100: Location of faults as interpreted from GPR and literature review and their spatial relationship with subsidence bowls and river channels 148

Figure 101: Buried waste material found at Site 1 153
Figure 102: Progression of conditions at Site 2. A: Fault rupture causes low point in topography, B: River forms in low point in topography, C: Tarawera River is diverted and original river channel dries up, D: Rangitaiki Plains are drained, water table drops and sediment compacts. 155
Figure 103: Waikamihi Stream on Rangitaiki Plains following a flood (February 2011) 156
Figure 104: Flood deposits on the banks of Waikamihi Stream on the Rangitaiki Plains (February 2011) 156
Figure 105: Graph of rainfall vs. subsidence rates at Kawerau. 1987 earthquake data removed 157
Figure 106: Cumulative subsidence, Kawerau vs. Wairakei (Spinks, et al., 2007). Blue and black lines refer to Kawerau, future scenario is predicted basin-wide subsidence as calculated by computer modelling, and actual subsidence is measured by levelling surveys. Purple dashed line refers to Wairakei. 159
Figure 107: Signal paths between a transmitter and a receiver on the surface. A is the direct airwave, G is the direct ground wave, R is the reflected wave, and C is the critically refracted wave. From Jol, (2009). 207
Figure 108: Simple reflection at a geological boundary showing incident wave raypath (black line), reflected wave (blue line) and, refracted wave (red line). Layer 1 velocity (v1) < Layer 2 velocity (v2) 208
Figure 109: GPR noise sources. From Jol, (2009). 208

List of Tables

Table 1: Descriptions of Tarawera River at various locations 38
Table 2: Summary of subsidence rates from 2004 to 2010 (Energy Surveys, 2010) 47
Table 3: Levelling survey sizes and subsidence results 1970 – 2011 53
Table 4: Average compaction and thermal expansion coefficients measured on Kawerau samples (Terralog Technologies, 2006) 66
Table 5: Comparison of pressure and temperature related compaction in Huka Falls Formation and greywacke (Terralog Technologies, 2006) 66
Table 6: Groundwater depths in monitored wells – Data valid until 22 April 2010 81
Table 7: Water content for various samples 119
Table 8: Plasticity index for samples tested for Atterberg limits 125
Table 9: Emerson Aggregate Test results summary 126
Table 10: Grain size distribution of samples from hand auger holes by sieving method 130
Table 11: Grain size distribution of samples from hand auger holes by laser sizer analysis of samples <1mm diameter 130
Table 12: Allophane detection test results 135
Table 13: Falling head permeability results 138
Table 14: Constant head permeability results 141

List of Equations

Equation 1: Water content 119
Equation 2: Plasticity index 120
Equation 3: Falling head permeability 137
Equation 4: Constant head permeability 140
Equation 5: Snell's law 207

Chapter 1: Introduction

Subsidence often occurs in geothermal fields as well as oil and gas fields around the world. The Kawerau Geothermal Field is no exception and has been regularly monitored for subsidence using levelling surveys since the 1970's. Until now not much work has been done on determining the origin and cause of the subsidence at Kawerau.

1.1 Subsidence

Subsidence is the sinking or settling of a section of the Earth's surface and can be the result of consolidation of material due to an increase in effective stress caused by water extraction; mineral changes; the collapse of underground cavities caused by erosion from water; or by anthropogenic processes such as mining. Subsidence is described as the vertical displacement of the ground surface.

In a stable, non-subsiding system, the weight of sediments is supported by both the rock matrix and pore fluid pressure. When fluid is removed, the pore pressure drops and more weight is transferred to the rock matrix, resulting in formation compaction (Terralog Technologies, 2006). Subsidence is common in geothermal fields due to the extraction of water at depth, and the gradual settling and consolidation of material above where the water has been extracted. This can be reduced by re-injecting the used water back into the system so that only a small percentage of water is lost from the total system. Subsidence in geothermal fields can also be due to thermal cooling and contraction of rocks.

Differential subsidence or tilt over short distances can lead to reduced support beneath structures. This can result in irreversible damage due to discontinuous foundation support. If subsidence occurs over large areas and differential subsidence over large distances is low, the effect on buildings may only be slight, or may not affect the structure at all.

1.2 Subsidence in geothermal and oil field settings

Introduction

The following section provides case studies and describes subsidence in geothermal fields, and touches on subsidence within oil fields. The following case studies provide good comparisons to Kawerau and provide context for geothermal field development.

1.2.1 New Zealand geothermal fields

Most of the geothermal fields and commercial geothermal power generation plants in New Zealand are located within the Taupo Volcanic Zone (TVZ) (Figure 1).

Ohaaki and Wairakei were chosen as case studies here as there have been many studies done to identify the mechanisms of subsidence in these areas. Wairakei has the highest amount of subsidence in New Zealand. Extraction of geothermal fluids at Wairakei began at around the same time as extraction in Kawerau. (Allis, 1982)

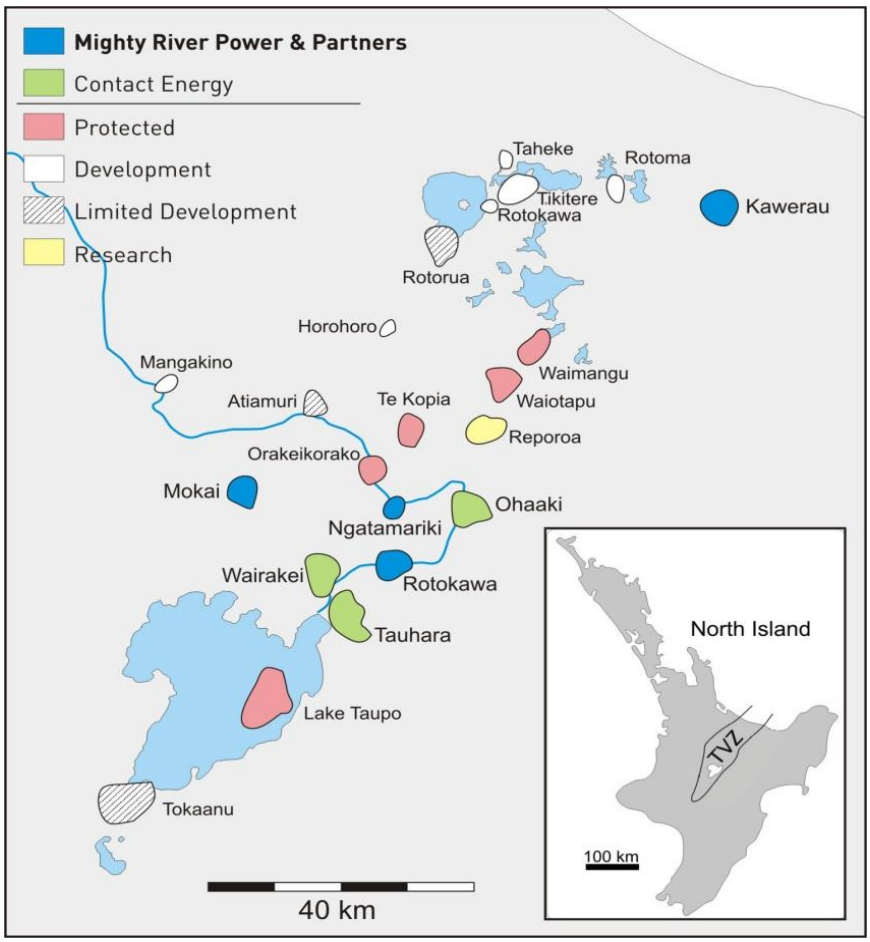

Figure 1: Location of geothermal fields in the Taupo Volcanic Zone (TVZ) (Powell, 2011)

Ohaaki Geothermal Field

Ohaaki geothermal field is located in the centre of the TVZ geothermal power generation area as seen in Figure 1.

In 2010 there were 23 production wells which extracted around 1,500 tonnes per hour (tph) of fluid in total, and six reinjection wells. The Ohaaki field generates approximately 47 MW of electricity (NZGA, 2011).

Subsidence bowls in Ohaaki are approximately 1 – 2 km across. Subsidence in Ohaaki occurs in response to host rock consolidation due to the propagation of deep pressure decline into the shallow, poorly permeable (0.05 – 0.3 mD) and highly compressible (10 – 30 $kbar^{-1}$) mudstones of the Huka Falls Formation (Rissman, et al., 2010).

When Ohaaki was first developed there was a test period where on average 25,000 tonnes of water per day (tpd) was extracted without reinjection. This resulted in a deep pressure decline of 1.5 MPa within 4 years (Rissman, et al., 2010). During this period, subsidence rates of up to 150 mm/year were determined from repeat levelling surveys. Following commissioning of the field in 1988, withdrawal increased to 45,000 tpd with approximately 28,000 tpd re-injected at the margins of the field (Rissman, et al., 2010). Subsidence rates increased to 500 mm/year and by the late 1990's a distinctive crescent shaped subsidence bowl formed over an area of approximately 1.5 km^2. The subsidence bowl was approximately 3 metres deep and had a subsidence rate of 100 mm/year (Rissman, et al., 2010). By 2000 subsidence rates were approximately 200 – 300 mm/year (Allis & Zhan, 2000). Current subsidence in the main Ohaaki subsidence bowl is comprised of four major subsidence features which form a crescent shaped feature. Subsidence rates are now around 60 mm/year (Samsonov & Tiampo, 2010). Subsidence rates at Ohaaki have slowed due to stabilisation of pressure at production depth (Allis & Zhan, 2000).

Wairakei Geothermal Field

Wairakei Geothermal Field is one of the oldest producing geothermal fields in the TVZ with development beginning in the 1950's. Wairakei is located to the north-east of Lake Taupo (Figure 1).

In 2010 there were 53 production wells which extracted around 5,300 tonnes per hour (tph) of fluid (1,500 tph steam plus 3,800 tph water), and six reinjection wells (NZGA, 2011). Well depths ranged between 0.3 and 2.4 km. Power generation from the Wairakei field is at approximately 220 MW.

Wairakei has two levels of subsidence, there are small subsidence bowls approximately 1-2 km across and there is a basin wide bowl which is more than 20 km^2 in area (O'Sullivan, et al., 2010). Total subsidence at Wairakei over the last 50 years is 15 ± 0.5 m. This is greater than at any other geothermal field in the world (Allis, et al., 2009);(Lawless, et al., 2003). Subsidence rates in the centre of the subsidence bowl have decreased from over 450 mm/year during the 1970's to 80 – 90 mm/year during 2000 – 2007 (Allis, et al., 2009). Subsidence is currently at a rate of approximately 58 mm/year (O'Sullivan, et al., 2010). Subsidence at Wairakei has decreased due to re-injection of geothermal fluids back in to the system, and the stabilisation of reservoir pressures (Allis & Zhan, 2000).

Subsidence at Wairakei is attributed to a pressure decline in relatively non-compacted, compressible sediments due to the extraction of geothermal water (Allis, et al., 2009). The greatest compaction in Wairakei is at 150 – 200 m depth. The cause of increased compressibility in this area is inferred to be higher clay content in the Huka Falls Formation due to intense hydrothermal alteration close to the natural fluid discharge areas (Allis, et al., 2009) and compression of hydrothermal eruption breccia between 35 m and 200 m deep (Bromley, et al., 2010). The 150 – 200 m depth of compaction at Wairakei has been identified by deformation of casing in wells at these depths (Bromley, et al., 2010).

It is important to note that the Huka Falls Formation is a general name for all lacustrine sediments within the TVZ. The formation at Ohaaki and Wairakei is a different unit from Kawerau and is more susceptible to compaction than the Huka Falls Formation at Kawerau (Milicich, et al., 2010).

1.2.2 International geothermal fields

The Geysers Geothermal Field, Mayacamas Mountains, California, USA

The Geysers Geothermal Field is a complex of 22 geothermal power plants located in the Mayacamas Mountains, 116 km north of San Francisco, California (DiPippo, 2008).

The Geysers has more than 460 extraction wells and 75 reinjection wells (Kahn, 2007) which have a production capacity of around 1,500 MW (Lund, et al., 2005). The Geysers is a dry steam field and peaked at 112 billion kilograms of steam production in 1987.

Subsidence rates at The Geysers between 1973 and 1977 peaked at 48 mm/year and 47 mm/year between 1977 and 1996 (Mossop & Segall, 1997). Subsidence rates are now approximately 10 to 30

mm/year (Floys, et al., 2010) and form bowls that are generally larger than 5 km across (Mossop & Segall, 1997). Subsidence at The Geysers has been attributed to the extraction of large amounts of water and has responded well to reinjection. Subsidence rates decreased once reinjection increased in 2003 (Kahn, 2007).

The geology of the geothermal energy producing area of The Geysers is a series of rhyolite domes, cones and flows overlain by Quaternary alluvium (Bacon, et al., 1974). The geothermal field is bounded by a fault system (Lowenstern & Janik, 2002).

Cerro Prieto Geothermal Field, Baja California, Mexico

Cerro Prieto Geothermal Field (CPGF) is located in South Mexicali, Baja California, Mexico. It is home to the world's largest geothermal power station with a generating capacity of 720 MW. CPGF has been generating geothermal electricity since 1973 (Gkowacka, et al., 2000). In 2002, CPGF had 138 production wells extracting on average 5,430 tph of steam, and had 13 reinjection wells in operation (Quijano-Leon & Gutierrez-Negrin, 2003). Between 1977 and 1987 the subsidence rate at the centre of the CPGF increased after every large, sustained production increase. Maps of subsidence rate for 1994-1997 show that the area with a subsidence rate ≥ 80 mm/year has an elliptical shape. There are localised areas with higher subsidence rates of around 120 mm/year. These areas coincide with the area of extracting wells (Gkowacka, et al., 2000). As of 2000, subsidence at CPGF had been attributed to geothermal fluid extraction. There was also no clear evidence that fluid reinjection decreased subsidence rates (Gkowacka, et al., 2000).

The CPGF consists of Upper Cretaceous granite which has intruded and metamorphosed Cretaceous and/or Palaeozoic deltaic sediments. Deltaic sediments have been divided in to two stratigraphic units:

A. unconsolidated Quaternary deltaic sediments composed of clays, sand and gravels; and
B. consolidated Tertiary deltaic sediments composed of siltstone, shales and sandstones.

Fault systems in the CPGF have created a step-faulted horst and graben structure striking NW – SE.

1.2.3 Oil fields

Wilmington Oil Field, Long Beach, California, USA

The Wilmington Oil Field is the third largest oil field in the United States and is located near Long Beach, California. The Wilmington Oil Field currently has over 1,550 active wells which extract a total average of 6,500 m^3 of oil per day (City of Long Beach, 2011). The Wilmington Field has been operating since 1932 (Otott & Clarke, 2007).

Subsidence in the Wilmington Field is in localised areas and has surface deformation rates in the order of 25 mm/year (Terralog Technologies, 2006). At its maximum, the Wilmington Field experienced approximately 9 m of subsidence at the surface (Otott & Clarke, 2007) and rates up to 750 mm/year (Fielding, et al., 1998). Sea water was pumped down old wells in 1953 to counteract subsidence. This water injection slowed subsidence and increased oil output (Otott & Clarke, 2007).

Although subsidence rates in the Wilmington field were initially high and there was considerable subsidence related damage to structures, pumping of sea water into the field has stabilised the ground and there has been no subsidence related impact on buildings and infrastructure in the last ten years (Terralog Technologies, 2006). This shows that subsidence can occur in sensitive environments with minimal damage so long as the rate remains low, and differential subsidence over short distances is small. Subsidence patterns in the Wilmington Oil Field are roughly elliptical in shape (Kosloff, et al., 1980).

1.3 Subsidence in drained areas

Subsidence is not always caused by extracting fluids from depth; it can also occur in areas where the land surface has been drained.

Many areas have been drained to increase useable land for various reasons including:

- farming on the Rangitaiki Plains,
- farming in the Netherlands, and
- expansion of cities such as Christchurch, New Orleans and Bangkok.

All of the locations mentioned above have been drained to improve the quality of the land for human use and all have had subsidence as a result. The very fact that the areas need draining

indicates that the local geology is generally saturated, comprised of some sort of mudstones or organic material (such as peat), has an abundant water supply, and/or floods frequently or is close to or below mean sea level.

The Netherlands is a well-known example of land reclamation. Around 20 percent of the country is situated below mean sea level and nearly 38 percent lies below high water level (Rietveld, 1983). Windmills were originally constructed in the Netherlands to pump water from farm land, but now more modern techniques are used. Approximately half of the surface of the Netherlands is covered by Holocene sediments of clay, sand and peat which attain thicknesses up to 20 m (Rietveld, 1983).

Subsidence rates across the Netherlands are approximately 10 – 20 mm/year (Andriesse, 1988). The shape of subsidence features in the Netherlands is determined by the shape of historic peat swamps and areas of the swamps that have been drained. Oxidation of peat occurs when the water table is drawn down and causes the peat to decrease in volume, creating subsidence (Cuenca, et al., 2007).

The Moanatuatua swamp on the Hauraki Plains, New Zealand was historically a peat swamp and has shown local subsidence rates of approximately 34 mm/year since 1925. This area had been drained to increase useable agricultural land (McKenzie & McLeod, 2004).

1.4 Thesis objectives

This study was initiated as a result of recommendations made by Mighty River Power (MRP). Many reports have attempted to describe subsidence in the Kawerau area (Allis, et al., 1993); (Bignall & Harvey, 2005); (Bloomer, 2005); (Brock, 2006); (Curie, 2011a); (Curie, 2011b) (Energy Surveys, 2009); (Energy Surveys, 2010); (Grindley, 1986); (Hole, et al., 2007); (Mighty River Power, 2005); (Milicich, et al., 2010); (Seiga, et al., 2011); (SKM, 2005); (Spinks, et al., 2007); (Terralog Technologies, 2006); (URS, 2005). Some of these studies have suggested causes of subsidence, but none have been proven.

The thesis objectives are:

1. To provide a geomorphological map of the field area with geomorphic site history reconstruction and its relevance to subsidence in the Kawerau Geothermal Field.
2. To identify the composition and character of the ground within the subsidence features.
3. To determine the cause(s) and mechanism(s) of the small, localised, linear and bowl shaped subsidence features within the Kawerau Geothermal Field.

This thesis does not aim to determine the origin of the larger, field wide subsidence feature.

1.5 Structure

This thesis is broken in to seven chapters consisting of an introduction to subsidence and subsidence in various settings. Chapter Two provides a background of the geological and geomorphological setting of the Kawerau area, including the regional setting and major geological units. Chapter Three reviews previous reports including levelling, engineering geological and scientific reports.

Chapter Four introduces the first phase of investigation including aerial photograph interpretation, initial site visit, mapping, and an investigation into local hydrogeology. Chapter Five discusses shallow surface investigations including a geophysical investigation, 3D modelling, hand augering, face logging, and laboratory work. Chapter Six brings the investigations together and presents a model of the subsidence in Kawerau. Chapter Seven provides conclusions on the investigation.

Chapter 2: Background geologic and geomorphic setting for Kawerau

2.1 Site location

Kawerau is located in the Bay of Plenty on the north east coast of the North Island, New Zealand (Figure 2).

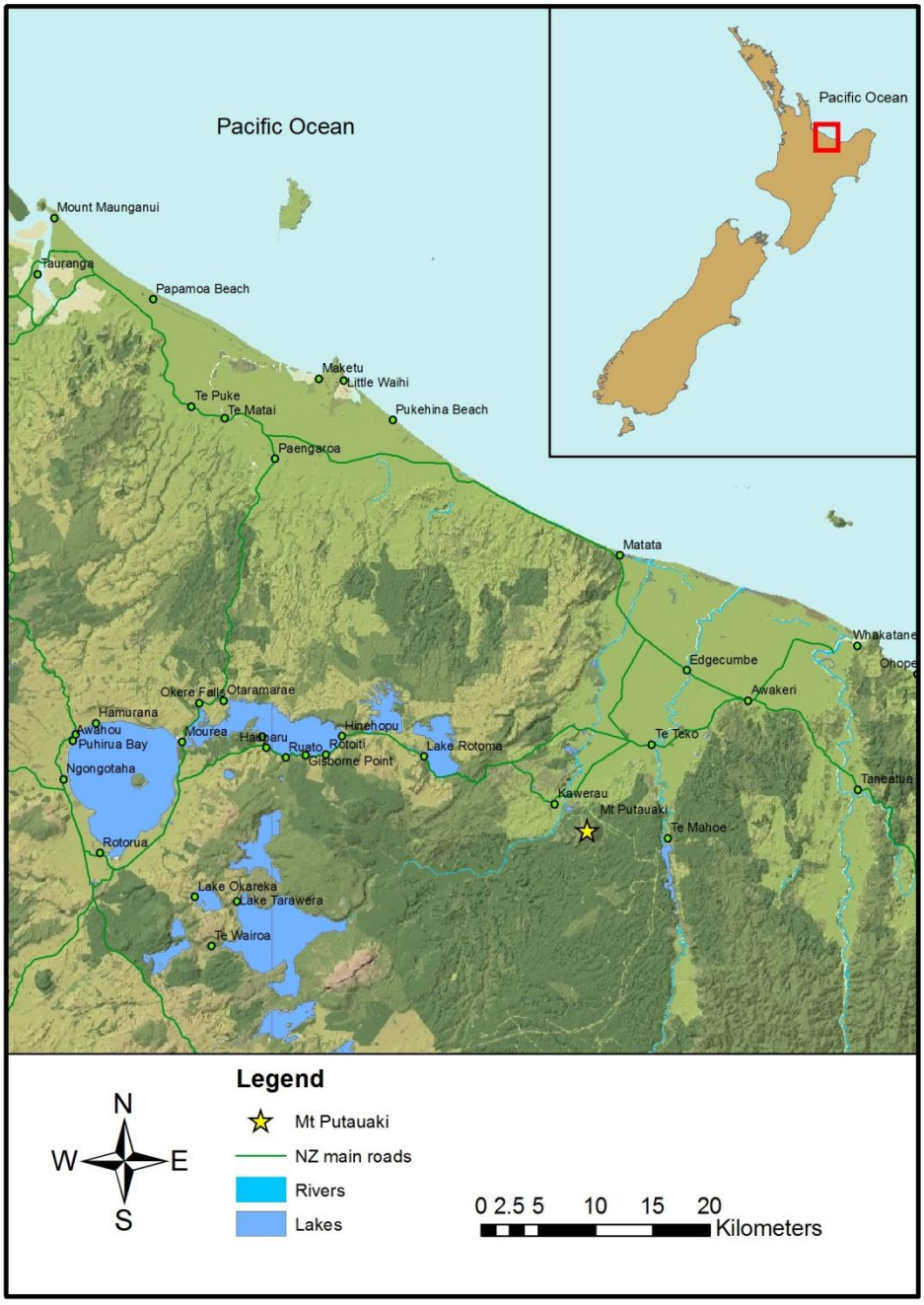

Figure 2: Location of Kawerau, Bay of Plenty, New Zealand

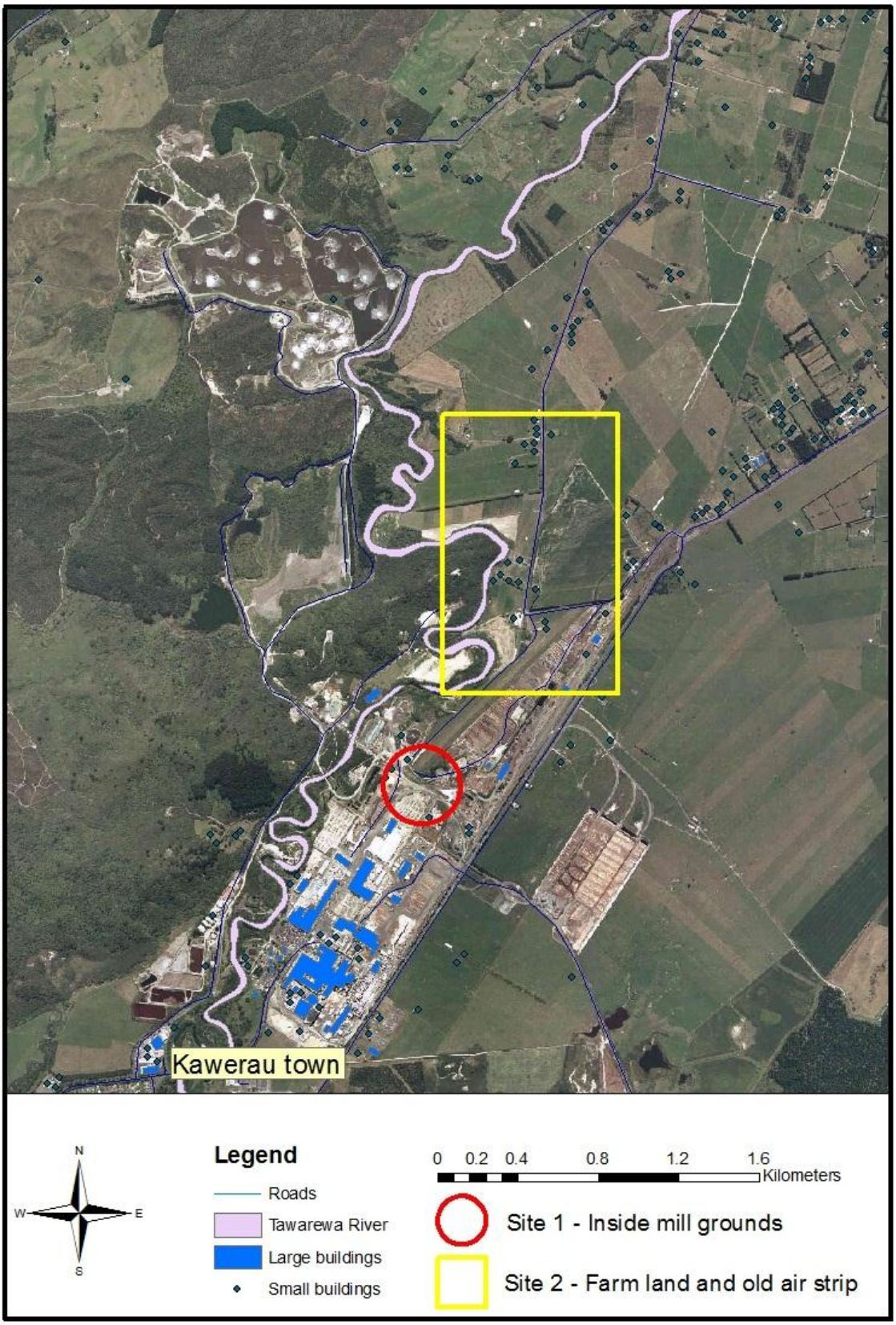

Figure 3: Locality map showing Kawerau and the specific field area

Subsidence in Kawerau has been monitored periodically since the 1970's due to its potential effect on buildings and infrastructure, in particular the pulp and paper mill which was constructed in the 1950's. The historical subsidence at Kawerau is relatively small compared to subsidence above other geothermal, oil and gas fields (Terralog Technologies, 2006). The total maximum subsidence measured at Kawerau from 1970 to 2004 was in the order of about 630 mm or about 19 mm/year. These data exclude the one-time jump induced by the 1987 Edgecumbe earthquake (Terralog Technologies, 2006). Due to the sensitivity of the pulp and paper mill to differential subsidence it is an issue which requires regular monitoring. Thorough research is important to prevent or at least understand subsidence at Kawerau as much as possible.

Kawerau currently has 13 production wells which extract up to 4,161 tph of geothermal water from between 950 m and 2100 m. There are also 11 injection wells which inject used fluid to depths between 300 m and 3000 m. There are 24 other monitoring wells throughout the Kawerau Geothermal Field, most of which are old production wells.

There are two levels of subsidence at Kawerau. The first is large, basin wide subsidence which is trending to the north to north-west of the mill site. The second level of subsidence comprises a number of localised, linear and round features within the large basin wide feature (Figure 4). This thesis focuses on two of the localised features as they have been exhibiting the maximum subsidence rates within the Kawerau Geothermal Field. The two sites are:

- Site 1: Lies within the mill grounds at Kawerau which is occupied by Mighty River Power, Carter Holt Harvey, Norske Skog Tasman, SCA Hygiene Australasia Ltd and Bay of Plenty Electricity.
- Site 2: Is in farm land used for grazing to the north of the mill and the old air strip.

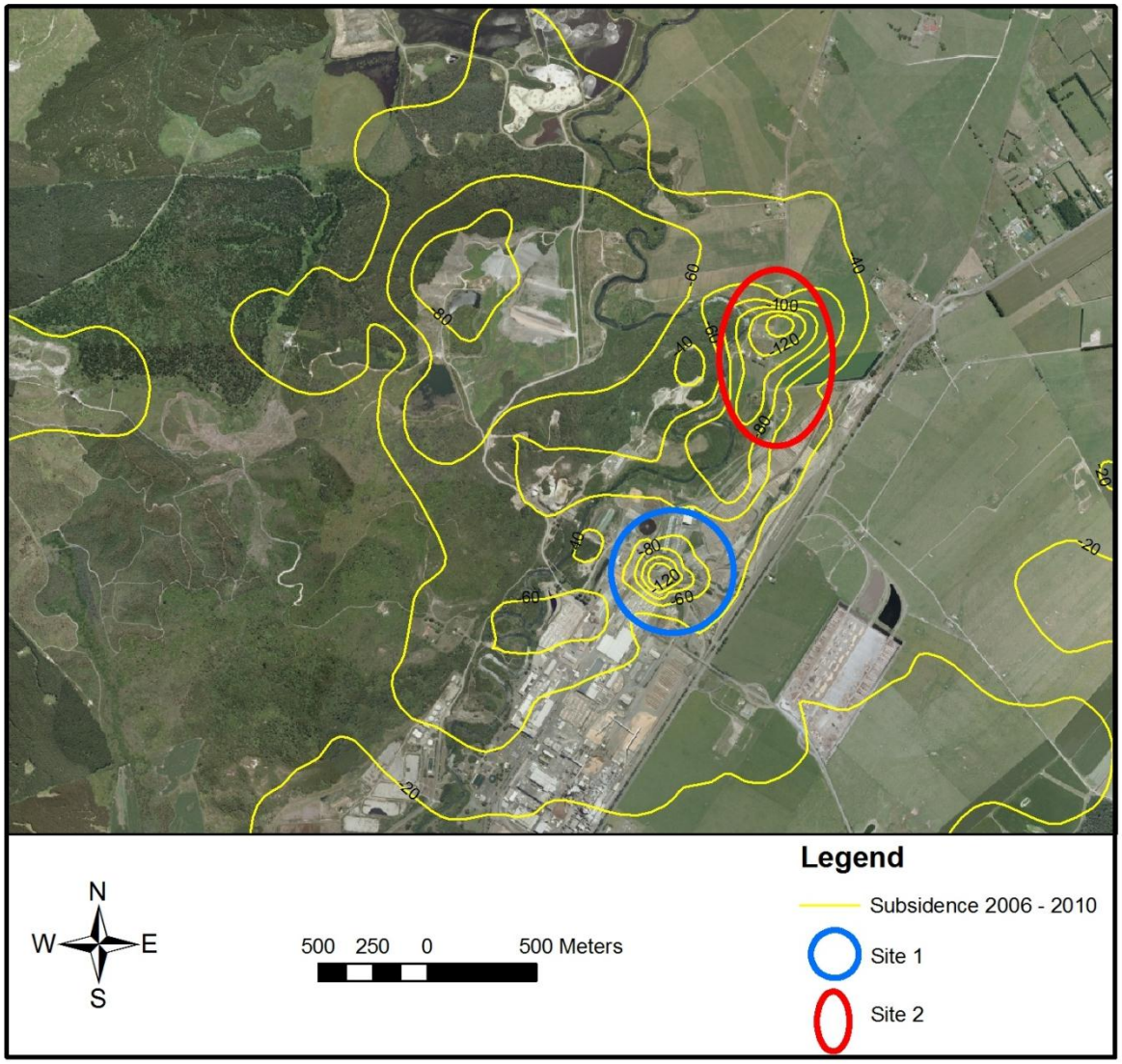

Figure 4: Location of the main subsidence bowls in Kawerau. Contours are 20 mm/year intervals for total cumulative subsidence from 2006 to 2010.

2.2 Regional setting

The objective of this section is to define aspects of regional geology that are relevant to subsidence in the Kawerau area. It will help build an understanding of the regional geology and how this may affect subsidence in Kawerau.

2.2.1 Regional geology

The Kawerau geothermal field lies within the Whakatane Graben on the north-eastern boundary of the Taupo Volcanic Zone (TVZ) and covers an area of 19 to 35km^2 with fluid temperatures exceeding 310°C (Bloomer, 1998). There are numerous faults throughout the region which generally strike

northeast with cross-faults also present (SKM, 2005); (Wood, et al., 2001) as shown on figures 5, 6 and 7. The TVZ is an area of active rifting and subsidence results from the oblique subduction of the Pacific plate (Wood, et al., 2001).

Unlike many of the geothermal fields within the central part of the TVZ, the Kawerau field is not located within, or on the faulted margins of a large rhyolite caldera. It is however only 10 km northeast of the very active Haroharo Caldera in the Okataina Volcanic Centre. Down hole temperatures indicate that mass flow of hot fluids at depth occurs in the southeast where the basement is at its highest elevation, field pressures are highest and there is evidence of a shallow magmatic heat source (Wood, et al., 2001). The geothermal heat source of the Kawerau Geothermal Field is likely to be provided by Mt Putauaki (Figure 2).

The greywacke basement rocks at Kawerau are generally considered to be largely impermeable, with hot water flowing up through a large micro-fracture network which can be associated with active and non-active faults (Pezaro, pers.comm., 2011). The basement in the vicinity of wells KA21 and KA36 contains very permeable fractures, and both of these wells have been good steam-producers (Wood, et al., 2001). Within the last million years, greywacke has been down faulted to 1 – 2 km below sea level. The resulting basin has been in-filled by Quaternary volcanic rocks and sediments. Much of the faulting occurred before the deposition of the overlying volcanic units, as the displacements decrease upward along the fault planes (Bignall & Harvey, 2005). The Okataina Volcanic Centre has been the main source of volcanic activity affecting the Kawerau area (Bignall & Harvey, 2005).

The geology of the site is complex with a number of rhyolite domes from a single source below the mill site. There are ignimbrite and tephra deposits which have wrapped around the rhyolite domes. There are also other considerable volcanic deposits such as the Kawerau Andesite, Caxton Rhyolite and the Onepu Rhyolite which is believed to be very extensive across the central portion of the field. Volcanic deposits are punctuated with marine transgressions and fluvial sediments.

The mill and geothermal power plant are located on alluvial sediments which are comprised of greywacke gravels, volcanic material, marine sediments, dune sands, swamp beds and sedimentary deposits (SKM, 2005). Alluvial sediments are up to 80 m thick and overlie the Matahina Ignimbrite and the Onepu Rhyolite. These are underlain by the Huka Falls Formation and other volcanic deposits with a greywacke basement (SKM, 2005).

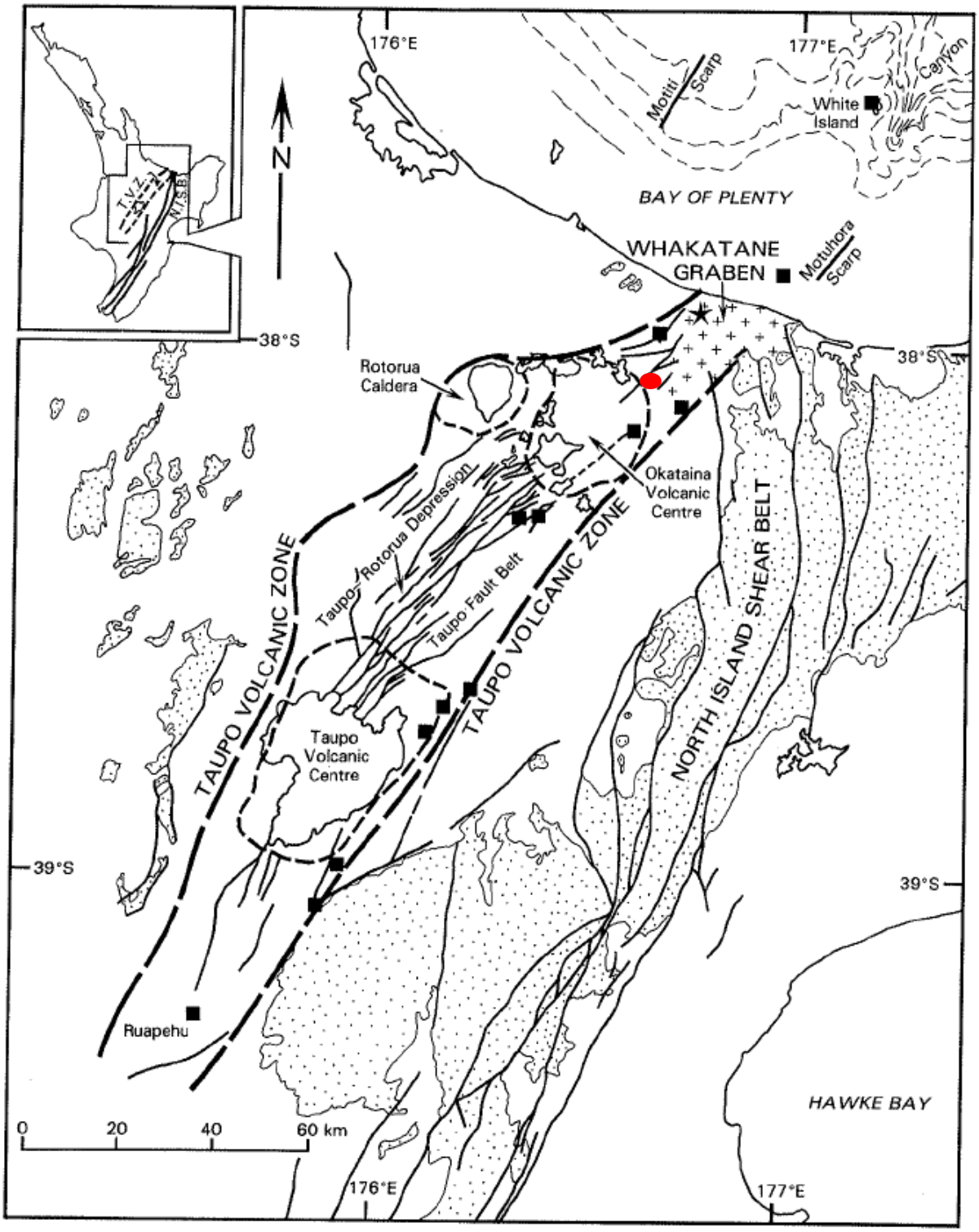

Figure 5: Location of the Kawerau geothermal field (red circle) within the TVZ and Whakatane Graben (Nairn & Beanland, 1989). Filled squares mark andesite/dacite and are volcanoes; outcropping greywacke is dot stippled. Star marks location of the 1987 March Edgecumbe earthquake main shock.

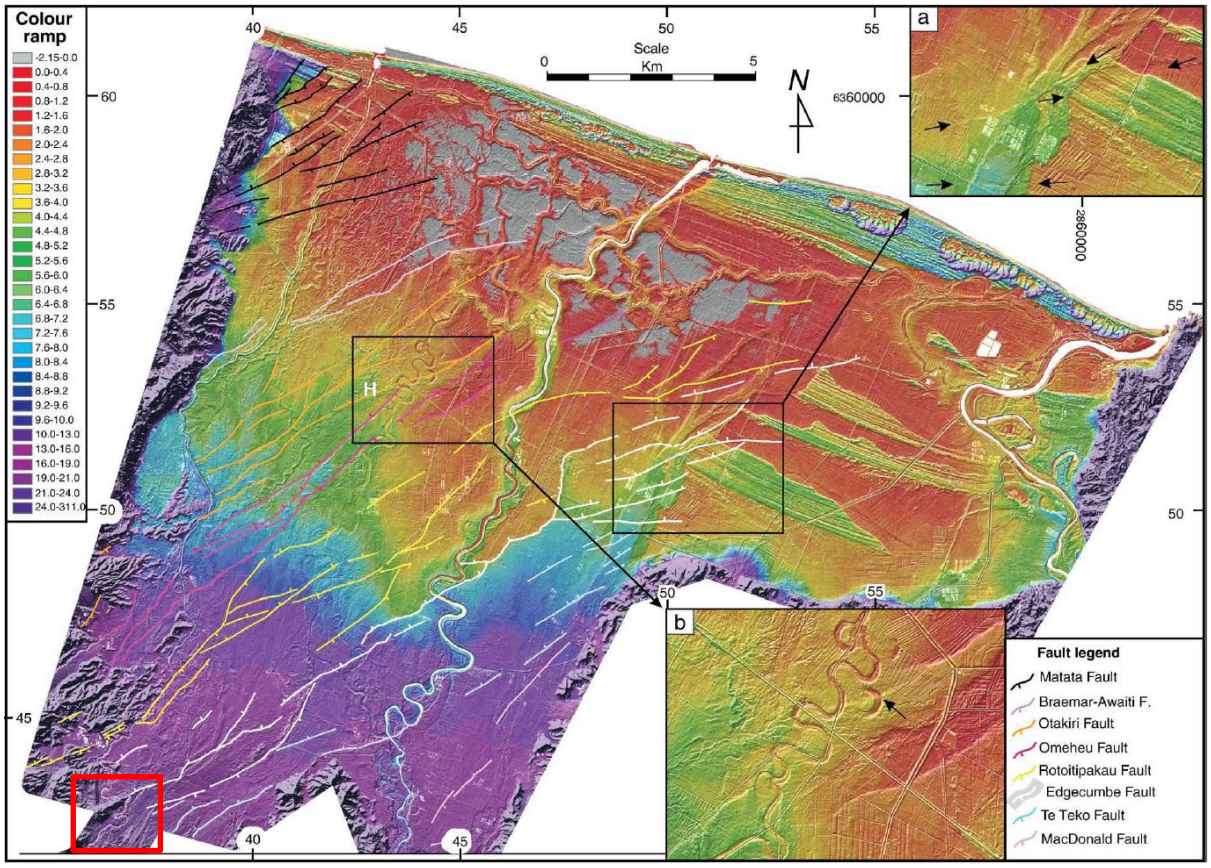

Figure 6: High resolution LiDAR-derived digital elevation model showing active fault traces across the Rangitaiki Plains (Begg & Mouslopoulou, 2010). The field area is located within the red square to the bottom left of the figure.

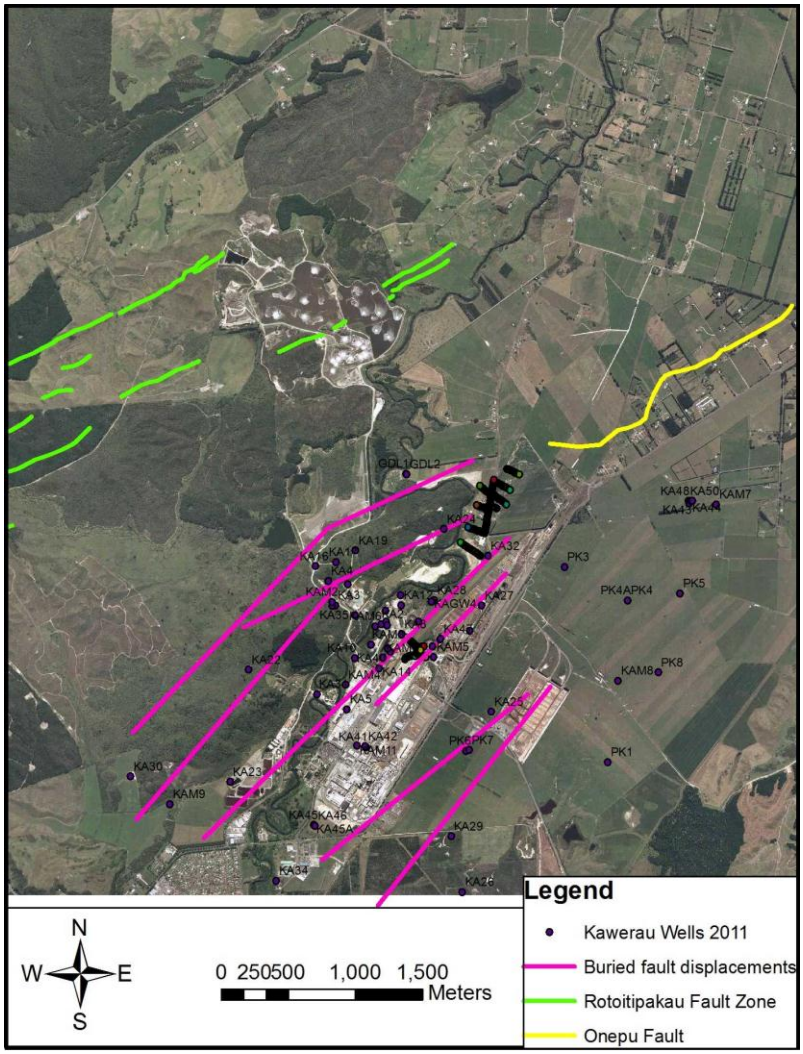

Figure 7: Fault zones in the Kawerau geothermal field adapted from Beanland at al. (1989), and Nairn and Beanland (1989). Purple lines show inferred buried fault displacements within the geothermal field, from Nairn and Beanland (1989).

2.2.2 Stratigraphy

The stratigraphy of the Kawerau area consists of Quaternary volcanics and alluvial deposits overlying Greywacke basement (Figure 9). Typical lithologies are rhyolite domes and ignimbrites from both proximal and distal vents.

Depths of lithologic units have been taken from geotechnical drill hole G2 (Figure 8) and description of units is primarily from SKM (2005) with any extra information as referenced. Drilling information was not available for all units.

Figure 8: Location of geotechnical drill holes G1 (yellow dot), G2 (red dot), G3 (blue dot), and KA41 (green dot) (SKM, 2005).

2.2.2.1 Volcanic alluvium and alluvial sediments

Depth

0 to 70 m

Description

Alluvial sediments are Holocene in age and consist of incompetent volcanic silty sands and gravels with occasional cobbles and boulders comprised of weathered pumice, ignimbrite, rhyolite and obsidian. Sand and gravels vary in grain size and grading, they are generally loose to medium density, grey, and wet below approximately 12 m. There are some thin clay and silt layers within the unit which vary in plasticity and dilatancy. Minor organic content occurs throughout the alluvium at varying depths (SKM, 2005).

There are boulders, gravels, and sand associated with the 1350 A.D. collapse of a natural dam at the eastern end of Lake Tarawera and some material is from the 700 B.P. Kaharoa eruption. Kaharoa pumice alluvium forms the present terrace surface that obscures structural features over much of the Kawerau Geothermal Field (Bignall & Harvey, 2005); (Grindley, 1986).

Drilling issues

Drilling through alluvial sediments is often challenging and recovery can be very limited. Drilling can be difficult in alluvial sediments as they are usually loose and unconsolidated. This means the water or mud pumped down the hole during drilling may be lost into the formation without maintaining pressure in the hole and keeping hole walls stable. Due to low pressure during drilling, the walls of the hole may collapse in, trapping the drill bit or rods.

Recovery is often poor as drilling washes away some or all of the sample and the core catcher cannot always pick up loose or unconsolidated sediments (SKM, 2005).

2.2.2.2 Matahina Ignimbrite

Depth

70 to 115 m

Description

The Matahina Ignimbrite formed from large (approximately 150 km^3) eruptions around 280 ka (Hodgson & Nairn, 2003).

The upper layers of the Matahina Ignimbrite are occasionally welded, fresh, moderately strong to very strong, and grey. Below 87 m the ignimbrite becomes less hydrothermally altered and less welded (although in some parts of the field welding increases), moderately weak to weak, and light grey. Some lithics and pumice are present although weaker pumice clasts appear to have been washed out by drilling giving the outside of the core a vesicular appearance. The general texture of the Matahina Ignimbrite is eutaxitic which is a result of flattened pumice and lithics (SKM, 2005). In G2 there were some weak tephra layers encountered below 106 m.

The Matahina Ignimbrite is a major regional unit covering approximately 2,000 km^2 across the northern TVZ (Milicich, et al., 2010), and is thought to pinch out towards the north, wedging out

against the rhyolite dome (SKM, 2005). The Matahina Ignimbrite has a central welded columnar unit which is an aquifer that is often targeted by irrigation bores (Mighty River Power, 2005).

Drilling issues

Drilling in the Matahina Ignimbrite is generally straightforward with excellent recovery (SKM, 2005).

2.2.2.3 Onepu Rhyolite

Depth

The Onepu Rhyolite was not intercepted in drill hole G2. In drill hole G3 (Figure 8) this unit was present between 81 m and the end of hole at 120 m and in drill hole KA41 from 70 m to the end of hole at 420 m (SKM, 2005).

Description

The only samples returned while drilling this unit were silt to fine sand-sized particles. Samples show the rhyolite to be a finely crystalline, strong to extremely strong, grey rock with only occasional hydrothermal alteration. There is an indication that the upper surface of the rhyolite may be somewhat brecciated (SKM, 2005). The Onepu Rhyolite is brecciated to massive, spherulitic and flow banded (Bignall & Harvey, 2005). The Onepu Rhyolite contains ash layers within the brecciated tops of lava flows (Pezaro, pers.comm., 2011).

The Onepu Rhyolite appears to be shallowest and thickest in the north west corner of the site and deepens to the south and therefore probably occurs at a greater depth than drilled in G1 and G2 (SKM, 2005).

Drilling issues

Drilling in rhyolite can often be difficult if the rhyolite is brecciated as the core often fractures and is pushed in front of the bit, rather than being collected in the core catcher. There was also a loss of circulation of drilling fluids in the upper 20 m of this unit whilst drilling KA41 (SKM, 2005).

2.2.2.4 Huka Falls Formation

Depth

Various thicknesses at depths between 250 m and 1,000 m (Milicich, et al., 2010)

Description

The sediments of the Huka Falls Formation are highly variable in thickness and range from 10 to 280 m thick (Milicich, et al., 2010). They are described as lacustrine, tuffaceous sandstone and siltstone. The Huka Falls Formation is a general name for all lacustrine sediments within the TVZ. At Kawerau, carbonaceous siltstones and sandstones, with variable proportions of pyroclastic and diatomaceous sediments are interbedded with welded pyroclastic flows of the underlying Kidnappers Ignimbrite and lower Onepu Rhyolite. Geophysical investigations indicate that the Huka Falls Formation may be thickest in eastern parts of the Kawerau geothermal field (Bignall & Harvey, 2005). The Huka Falls Formation at Kawerau may be partly of marine origin, and not entirely lacustrine (Mighty River Power, 2005).

This heterogeneous unit has low overall permeability and is not targeted or used for extraction of geothermal water (Pezaro, pers.comm., 2011).

2.2.2.5 Caxton Rhyolite

Depth

The Caxton Rhyolite occurs as concordant flows and/or sills separating the deeper ignimbrites and andesite between 500 and 1,000 m deep.

Description

Caxton Rhyolite is the name given to a series of rhyolite lavas that are older than the 1Ma Kidnappers Ignimbrite and Awakeri Formation encountered in Kawerau drillholes (Milicich, et al., 2010). The Caxton Rhyolite is a crystal-rich rhyolite lava containing diagnostic coarse, embayed quartz and plagioclase phenocrysts, altered amphibole and other mafic minerals. The Caxton rhyolite is chemically distinct from the Onepu rhyolites (Bignall & Harvey, 2005).

The Caxton Rhyolite is one of the units that geothermal fluid has been extracted from for geothermal energy generation (Pezaro, pers.comm., 2011).

2.2.2.6 Kawerau Andesite

Depth

Due to faulting, the Kawerau Andesite can be found between 550-1,350 m.

Description

The Kawerau Andesite is an important production aquifer in the western part of the Kawerau Geothermal Field with dense, grey-green andesitic lavas and breccias forming part of the buried truncated volcano near the north-western part of the field. The andesite consists of an upper (thinner) and lower (multiple-flow) member, and associated andesitic tuff that thicken towards an inferred vent-zone in the northwest part of the field (Bignall & Harvey, 2005).

The Kawerau Andesite is one of the units that geothermal fluid has been extracted from for geothermal energy generation (Pezaro, pers.comm., 2011).

2.2.2.7 Greywacke

Depth

800-1000 + (Mighty River Power, 2005).

Description

Greywacke is the basement unit in this area and is part of the Torlesse Terrane. It is exposed at the ground surface at Otamarakau to the west of Kawerau, in the Raungaehe Range. This low dipping basement rock may be attributed to northwest tilting, or progressive down-faulting.

The greywacke comprises medium-grained, volcanic litharenite (mainly andesite lavas with rare rhyolite lava and ignimbrite), with lenses of carbonaceous argillite that has been regionally metamorphosed to a prehnite-pumpellyite metamorphic assemblage/facies. Rare bedding dips steeply and variably. Wairakite-prehnite and quartz-calcite veining is widespread (Bignall & Harvey, 2005). Greywacke at Kawerau is hydrothermally altered, mostly moderately, but some intensely (Wood, et al., 2001). Fluid flow through the greywacke is dominantly along fractures (Mighty River Power, 2005). Greywacke is the primary unit geothermal fluid is now extracted from (Pezaro, pers.comm., 2011).

2.2.3 Cross section

The following schematic (Figure 9) shows the current understanding of the geology of the Kawerau geothermal field. Work is constantly being carried out on the local and regional structure of the Kawerau area, so this schematic may not be completely up to date. Sarah Milicich is currently working on a PhD titled 'Geological History and Structural Development of the Kawerau Geothermal Field' through Victoria University of Wellington which is considerably adding to the knowledge and model of the field.

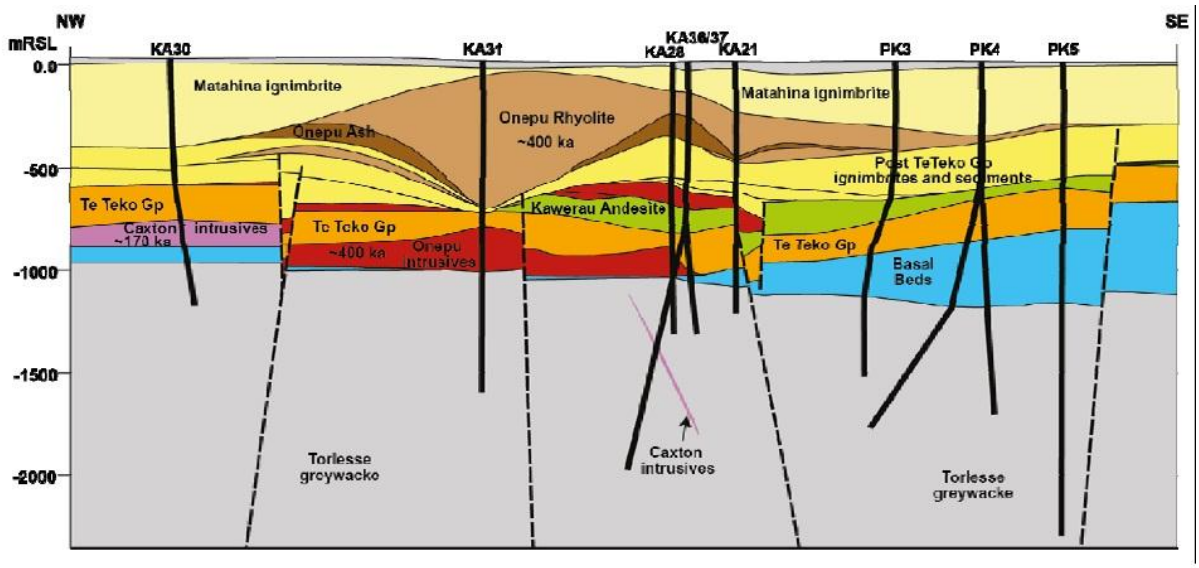

Figure 9: Simplified NW – SE cross section of the Kawerau Geothermal Field, based on well logging (Milicich, et al., 2011)

2.2.4 Structure

The Kawerau Geothermal Field is situated at the southern end of the northeast-trending Whakatane Graben in a zone where the northeast-striking active rift of the TVZ intersects the north-trending strike slip faults of the North Island Shear Belt (Milicich, et al., 2011). Basement at Kawerau is Mesozoic sandstone (greywacke) and argillite of the Torlesse terrane. This has been down faulted due to the active rifting and subsidence, resulting from the oblique subduction of the Pacific Plate beneath the North Island (Wood, et al., 2001). Basement at Kawerau is intersected at less than 1 km depth, which is considerably shallower than other fields in the TVZ. Pre-Quaternary formations have not been drilled in any other TVZ geothermal field (Wood, et al., 2001).

Drill hole stratigraphy has indicated that the basement greywacke is step-faulted down to the northwest on northeast-trending faults, to form a series of tilted fault blocks with northwest-

trending cross-faults, and a plunge to the northeast (Nairn & Beanland, 1989); (Wood, et al., 2001). These faults are believed to extend to above the Matahina Ignimbrite as this unit has been displaced 70 – 100 m by the same faults which have offset greywacke. However, the faults have displaced the greywacke by 430 m suggesting subsidence of the Whakatane Graben had started long before the 0.29 Ma Matahina eruptions (Nairn & Beanland, 1989).Basement faults at Kawerau are widely spaced, active, facilitate fluid flow and contain very permeable fractures (Wood, et al., 2001).

The Edgecumbe Fault in the top 2 km of the Rangitaiki Planes has been interpreted to have a fault plane dip in basement at approximately 55 degrees, or shallower and curves to near vertical in the top 100 m (Wood, et al., 2001).

Surface expression of faults on the Rangitaiki Plains is not common due to the burial of fault traces by young (< 800 years before present) fluvial deposits (Nairn & Beanland, 1989); (Wood, et al., 2001). Some fault ruptures were however traced following the 1987 Edgecumbe Earthquake.

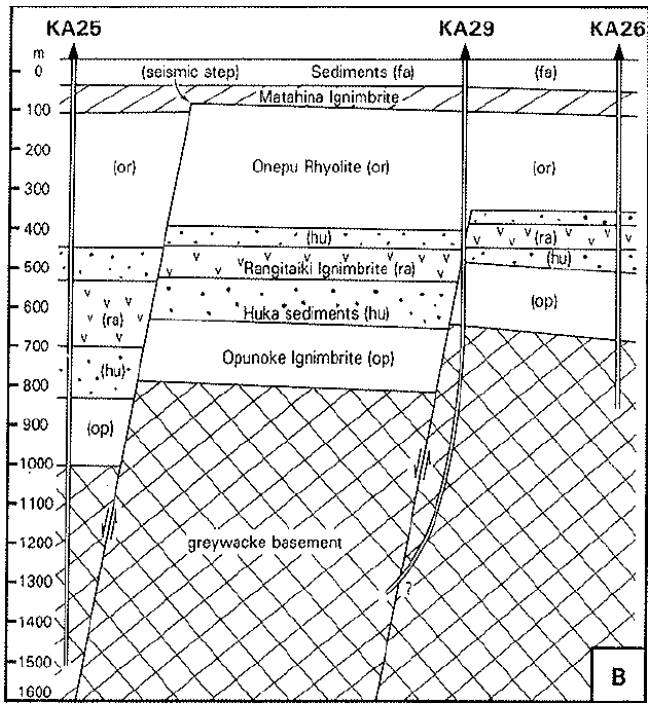

Figure 10: Sketch of stratigraphy and structures inferred in the eastern Kawerau Geothermal Field (Nairn & Beanland, 1989).

The Onepu Fault has a fault trace which is identifiable in aerial photographs and displaced the post 1850 and post 800 years before present sedimentary surfaces. Recent tectonic activity on the Rangitaiki Plains has been dominated by TVZ rifting (Nairn & Beanland, 1989).

2.2.5 Regional geomorphology

This section provides a summary of the current geomorphology of the Rangitaiki Plains. How these features have developed and changed in the last 150 years is discussed in Section 2.3.1.

The Rangitaiki Plains are a part of the Taupo Volcanic Zone (TVZ) and lie across the Whakatane Graben. Extension on the Rangitaiki Plains is approximately 15 – 20 mm/year (Begg & Mouslopoulou, 2010). To the east, west and southeast, the Rangitaiki Plains are bounded by early Holocene sea cliffs cut into materials ranging from Jurassic greywacke to Quaternary volcanic rocks and volcanogenic deposits when sea level stabilised around 6.5 kyr ago (Begg & Mouslopoulou, 2010). The volcanic Kaharoa plateau lies to the west and greywacke rocks form the Raungaehe Ranges to the east of the plains (Figure 11).

The most prominent feature in the regional landscape is Mt Putauaki, a dacite volcanic cone which rises to 820 m above sea level. The present large landscape features are controlled by extensional seismic activity in the Whakatane Graben; and volcanism, followed by partial burial by Quaternary marine and non-marine strata (Begg & Mouslopoulou, 2010).

The Rangitaiki Plains are primarily agricultural land with some industry including the pulp and paper mill at Kawerau, a Fonterra dairy factory at Edgecumbe and various power stations.

The Rangitaiki Plains were originally a swampy area (see 2.3.1). Due to significant human modification of drainage channels on the plains to make the land useable, the water table has dropped, drying out historic river channels, leaving many old river channel features across the plains including around Kawerau.

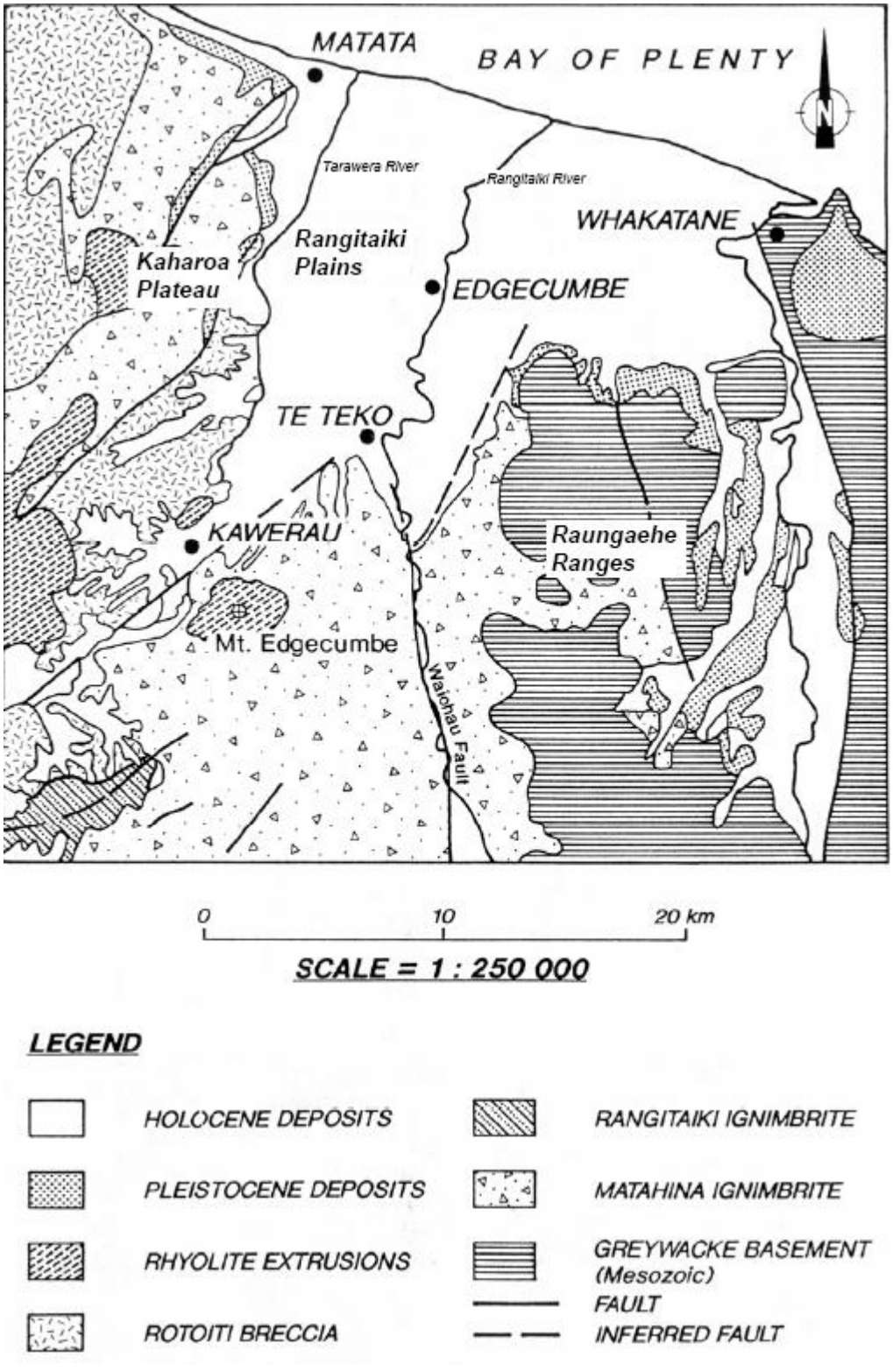

Figure 11: Regional geology of the Rangitaiki Plains and Kawerau area (Gordon, 2002)

Deposition on the plains has been dominated by tephra remobilisation following large rhyolitic volcanic eruptions from the TVZ. These eruptions swamped the upper catchments of the Whakatane, Rangitaiki and Tarawera rivers with pumice, which was later re-deposited during high

intensity rainfall (Begg & Mouslopoulou, 2010). The plains have prograded at least 10 km in the last 6500 years due to volcanoclastic sediment provided by the Whakatane, Rangitaiki and Tarawera rivers (Beanland & Berryman, 1992). Near the coast, a series of dune and beach ridges, peat swamps, back-beach lowlands, natural levee systems and active and ancient floodplains are obvious. These features are shown in Figure 12.

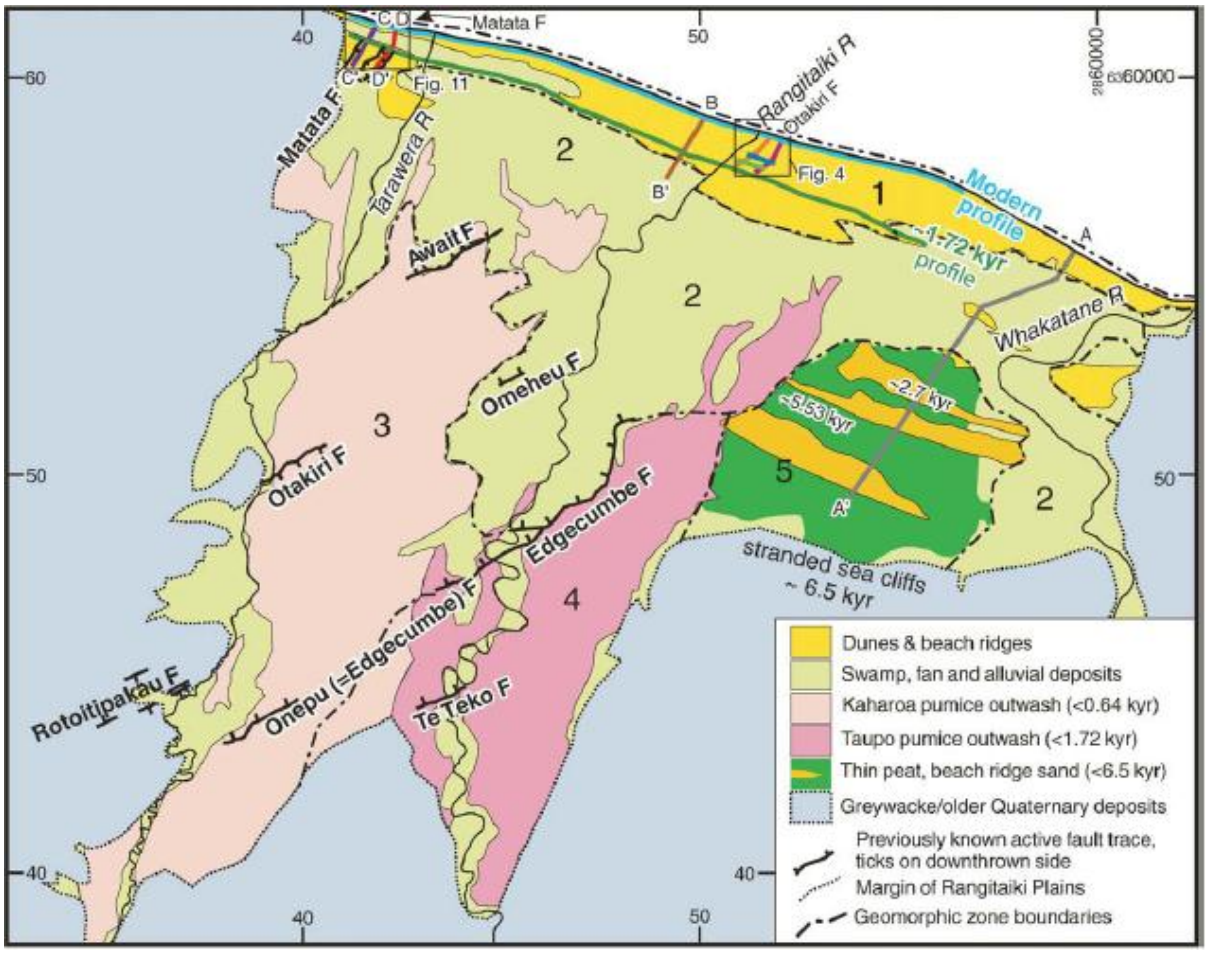

Figure 12: Quaternary geology of the Rangitaiki Plains. (Begg & Mouslopoulou, 2010)

2.2.6 Regional hydrogeology

This section is largely a review of Dougall Gordon's report to Environment Bay of Plenty in 2002 (Gordon, 2002).

Rainfall on the Rangitaiki Plains ranges between approximately 1000 and 2000 mm/year.
The regional hydrogeology of the Kawerau area and the Rangitaiki Plains consists of a system of unconfined aquifers to approximately 70 m and a series of confined aquifers to 400 m.
The Tarawera, Rangitaiki and Whakatane rivers flow north over the plains. The elevation of the plains ranges from 30 m above mean sea level in the south, to below sea level in the north (Gordon, 2002). Large areas of the northern plain are at, or slightly below sea level and require substantial artificial drainage (Gordon, 2002).
Shallow aquifers are found across most of the plains and the system is mostly found in alluvial material. The shallow aquifers are generally unconfined or semi-confined by layers of peat, clay and silt. Transmissivity values between 200 and 500 m^2/day are considered to be representative of the shallow aquifer system (Gordon, 2002).
Recharge to the shallow aquifer system is from two main sources: rainfall seepage from areas above the plains, and vertical leakage from deeper aquifer systems. Recharge from rivers and surface drainage are not considered significant recharge sources. Water level monitoring has indicated that the shallow aquifer system responds to rainfall events.
Shallow groundwater levels generally follow the topographic contours; however, groundwater levels on large areas of the plains are artificially controlled by drainage systems, pumping stations, flood gates and stop banks. Water levels in the shallow aquifers range from below mean sea level near the coast to between 11 and 13 m below ground surface at the head of the Tarawera and Rangitaiki River valleys, with annual changes typically ranging from 0.5 to 1.5 m (Gordon, 2002).

There are a number of significant springs on the plains with discharges ranging between 44 and 260 L/second. The deep aquifer system of the Rangitaiki Plains runs to a depth of 400 m and is comprised of unconsolidated alluvium including; gravel, sand, pumice, ash/silt/peat horizons and hard rock volcanic ignimbrites. Transmissivity across the plains varies considerably due to local geology changes from welded ignimbrites to pumiceous and greywacke gravels and sands. Transmissivity values of the deep aquifer system range between 18 and 6000 m^2/day. Most deep bores show no seasonal fluctuation in water level and generally have increasing head with depth suggesting a recharge source from beyond the plains (Gordon, 2002).

2.2.6.1 Tarawera River

The Tarawera River is one of three significant rivers on the Rangitaiki Plains and runs through the town of Kawerau and borders the field area.

Observations of the Tarawera River at a number of locations are described in Table 1. For locations of sites see Figure 13.

Table 1: Descriptions of Tarawera River at various locations

Site	River width (m)	River depth (m)	Description
1	15-20	Up to 1.5	Swift and clean, low sediment load, bottom covered in pumice and rocks up to 200 mm diameter. Banks medium sand to pebble sized grains. Stream entering river at this site looks very scoured out, very loose, friable banks.
2	20	1.5-2.0	Swift and clean, low sediment load. Silt to pebble base with some rocks up to 200 mm diameter. Outcrop on opposite side of river ~6 m high – grey, looks fine grained and similar grain size throughout.
3	15-20	Up to 2.0	Other side of river meander from Site 2. Swift, clear, very silty bottom. Soft, friable banks.
4	15-20	unknown	Swift moving, silty bottom, some stones up to 40 mm diameter. Bank on opposite side ~4 m high, easily eroded and very friable, looks like ash and lapilli layers, actively collapsing in to the river.
5	~10	unknown	River meandering, slower moving than earlier sites, water is black and dirty. River banks ~4 m high, reddish colour with angular rocks up to 100 mm diameter, moderately friable. Some armour stone around 100 m downstream suggesting site is easily erodible. Site is a washout, this shows ground is loose and easily erodible in flooding events.
6	~20	1-1.50	Swift moving, relatively clear water. Bottom very silty and has the appearance of ash with rocks up to 100 mm. River banks soft, friable light grey ash, some reddish horizons and weathering at top. On west side of river bank approximately 1.5-2 m high, bank on east side approximately 6m high.

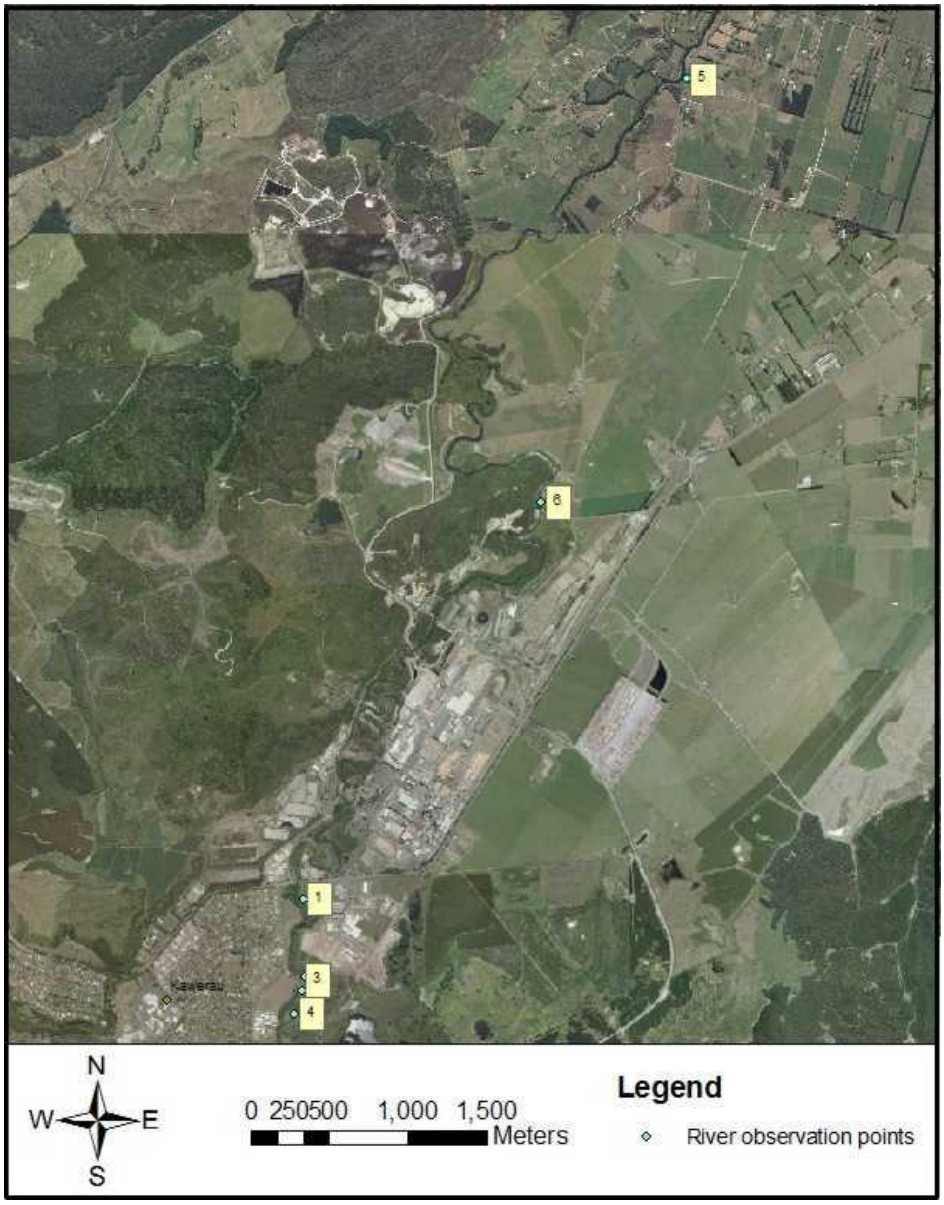

Figure 13: Map showing location of Tarawera River descriptions

Literature has shown that the Tarawera River has had its course changed by human modification in the early 1900's (Gibbons, 1990). One concern about how long the Tarawera River has been in its current location is that it appears to be a mature river with banks up to 10 m high. After examining the material in the river banks and observing the river on a calm day (Figures 14 and 15) it is clear that the loose, friable nature of the banks could easily be eroded into the river morphology we see today. This is supported by an observation in the book 'The Rangitaiki' by Walter Gibbons, commenting on a new drain, less than five years old. "In 1909 the Catchwater Drain was 35 ft wide instead of the 10 ft originally cut and in consequence a great deal of sand had been washed down

and deposited despite the absence of rain." This shows that the Tarawera River could easily appear to be a mature river after only 100 years following its current course.

This is further supported by descriptions of the river as reported in the Geoscientific Review of the Kawerau Geothermal Field (Bignall & Harvey, 2005), which quotes that the Tarawera River down cut 3 m between 1920 and 1950 in response to a lowered groundwater table.

Figure 14: Photograph showing typical banks of the Tarawera River

Figure 15: Photograph of the Tarawera River showing typical shape, width and flow

2.2.7 Implications of regional factors to field area

The Whakatane Graben is an extensional basin which has resulted in a number of fault lines. Begg and Mouslopoulou (2010) have identified that due to seismic activity across the Whakatane Graben, the Rangitaiki Plains have had a subsidence rate of approximately 3 mm/yr over the last 2,000 years between the Edgecumbe and Matata Faults. Indications that groundwater levels are generally high, follow the topography and respond to rainfall events show that wetting and drying sequences are likely to be common on the Rangitaiki Plains, especially in areas such as Site 1 where soak ponds are located immediately adjacent. With dewatering of sediments, it is likely that subsidence will occur to some degree in any situation. Deep aquifer systems seem to have little to no effect on the field area. Perhaps the most significant implication is that due to high water tables and frequent inundation of the plains, people have modified the drainage of the plains. This has lowered the water table in some areas and is causing consolidation within the field area.

2.3 Local setting

2.3.1 Kawerau in recorded history

The Rangitaiki Plains have been modified considerably over the last 125 years since the Tarawera eruption, by both natural and anthropogenic mechanisms.

Kawerau and the Rangitaiki Plains were originally covered in swamps and swamp vegetation such as flax, raupo and manuka. The area flooded often and roads were difficult to construct and maintain (Gibbons, 1990). The Rangitaiki had common peat swamps and much of the plains were often inundated due to flooding of the Rangitaiki. It wasn't until a series of drainage programs constructed drains and channels, diverted streams and rivers, and dredged existing waterways that the Rangitaiki Plains became a useable area. The following section describes the progression of the Kawerau area from wild swamp to how we see it today.

1868: Flood on the Rangitaiki Plains, details vague and implications uncertain (Gibbons, 1990)

June 10 1886: Mt Tarawera erupted covering more than 200 km^2 in $\geq$50 cm of basaltic scoria and ash (White, et al., 1997). It was also reported that 50 to 150 mm of ash fell between Te Teko and the Orini River (Gibbons, 1990). The eruption formed a natural dam at the outlet of Lake Tarawera, which resulted in the water level of the lake rising by approximately 12 m above its previous level (White, et al., 1997).

1890-1891: The Rangitaiki Plains were surveyed in to 500 acre sections with the hope that large sections would attract settlers with high private capital who could afford to drain the plains and create a large, fertile grain growing area (Gibbons, 1990). As a condition of land lease in the area, leaseholders had to provide 'substantial improvements (including reclamation from swamps) to the permanent character of the land' within 6 years of receiving the lease (Gibbons, 1990). This meant leaseholders had to drain the swamp land and make it suitable for agricultural use.

July 1892: A large flood filled the swampy Rangitaiki Plains and for several years gave the appearance of an inland lake behind the coastal sand hills (Gibbons, 1990). This indicates that until at least the end of the 19th Century, the Rangitaiki Plains were a very swampy and waterlogged area which flooded easily and often.

1893-1896: The first drainage board established by leaseholders made a strong effort to drain the Rangitaiki Plains. This was privately funded. With the plains so flooded it was impossible for leaseholders to generate income and many had to leave as they could not afford rent for their land. With leaseholders leaving, the first drainage board disbanded and sections were re-advertised (Gibbons, 1990).

August 1 1901: The second drainage board was established. This drainage board with the help of a recently created local council managed to dam and re-direct a number of streams and rivers on the plains and began the first drainage program. Drainage however had varied rates of success due to the fact that as water was drained from the land, the waterlogged ground and peat swamps began to subside and the water level effectively remained high (Gibbons, 1990).

November 8 1904: 18 years after the Tarawera eruption the natural dam at the outlet of Lake Tarawera failed and released water at a rate of up to 700 m^3/second into the Tarawera River causing an area of 150 km^2 to flood. In some areas the flood waters were so deep they rose above the windowsills of houses. The river continued to deposit sediment for years to come and by 1906 the riverbed had risen so much that the river began to overflow through the sand hills above Kawerau. The 1904 flooding of the Tarawera River is the first recorded flood event from this river. Before this the river level didn't fluctuate very much compared to the Rangitaiki as the Tarawera has a very limited catchment and is lake fed (Gibbons, 1990).

Unknown date between 1904 and 1918: As a response to the floods and filling of river channels, local settlers Thomas Seccombe and the Grieve brothers constructed stop banks near Kawerau to protect their properties and to divert the Tarawera River towards Lakes Rotoitipaku and Rotoroa,

and the Otarakuti Stream. The current location of the Tarawera River is the result of the stop banks and re-direction of the river.

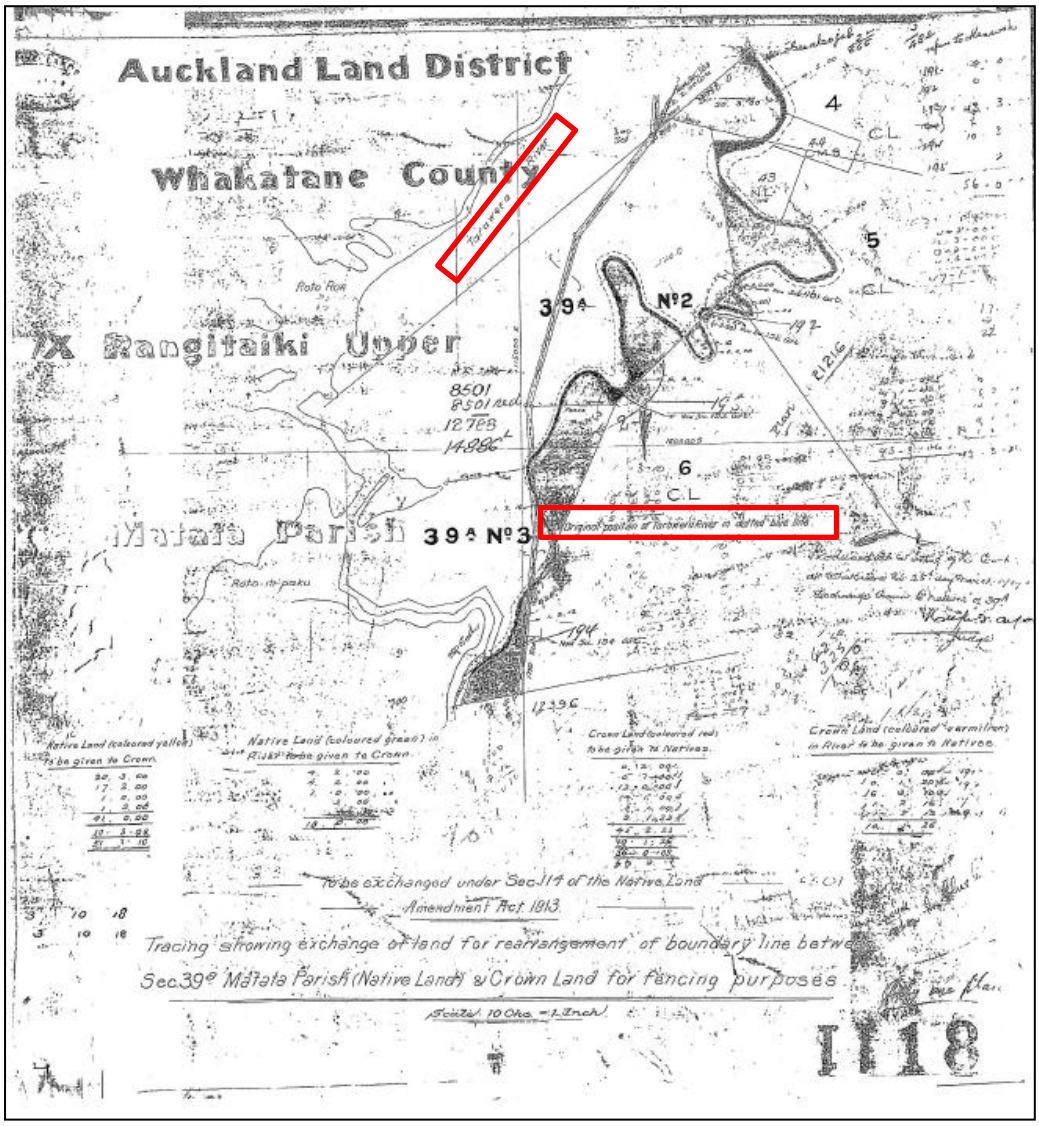

Figure 16: Map post-1913 showing original and current location of the Tarawera River

August 1st 1910: The second drainage board was abolished.

1918: By 1918 the Tarawera River no longer flowed along its original path, but along a new one where we see it today (Figure 16).

1911–1925: Canals on the Rangitaiki Plains were dredged and the Rangitaiki River was diverted to flow straight out to sea near Thornton where it reaches the sea now, rather than flowing north to Matata. The Tarawera River was also dredged to straighten and widen the river. This work was all carried out by the Lands Department.

1920's-1940's: Flooding commonly occurred on the Rangitaiki Plains. Swampy areas, in particular areas of deep peat continued to subside, some areas considerably, and gravity drainage was gradually lost (Gibbons, 1990).

1948: Control of drainage on the plains was handed over to the Works Department from the Lands Department.

1950's: Kawerau was chosen as a site for the Tasman Pulp and Paper Mill due to the geothermal energy resource.

1957: The first well came on to production for the mill making Kawerau the first producing geothermal field in New Zealand (NZGA, 2011). The original wells (KA1 to KA37) were drilled by Fletcher Challenge to supply steam to the mill.

1957: The third Drainage Board was established.

1957 – 1989: The third drainage board continued to drain the Rangitaiki Plains and maintain existing channels as well as install new pumps, stop banks and flood gates.

1979 – Fletcher Challenge sold its geothermal wells to the New Zealand Government as they were proving to be sub-economic (Carter & Hotson, 1992). The wells were then run by MB Century who continued to supply steam to the mill.

March 2 1987: The Edgecumbe Earthquake hit the Bay of Plenty with a magnitude of 6.3 on the Richter scale. Subsidence resulting from the earthquake ranged from millimetres to over two metres (Gibbons, 1990).

1993: By 1993 18 wells were cased to 300 m for production (Wigley, 1993). All of these wells terminated in volcanic deposits. Steam from these wells was provided to the Tasman Pulp and Paper Mill for industrial purposes.

2003: Mighty River Power began exploration for geothermal resources (Spinks, et al., 2007).

2005: The Crown transferred wells, steam field equipment, steam supply contracts and rights and obligations via Mighty River Power to Ngati Tuwharetoa Geothermal Assets (NTGA) for ownership (NZGA, 2011); (Spinks, et al., 2007); (Pezaro, pers.comm., 2011).

2011: Mighty River Power is currently consented to extract 55,000 tonnes of geothermal water per day to generate up to 104 MW of electricity in their geothermal power plant. All of Mighty River Power's wells take geothermal water from greywacke basement and are cased into the greywacke (Pezaro, pers.comm., 2011).

NTGA who is currently consented to extract 34,400 tonnes of geothermal water per day is a service provider. NTGA processes steam which is then sent to the mill for process heat, electricity generation and timber drying. This steam supply currently equates to half the world's total steam supply for industrial applications (NZGA, 2011). The brine from NTGA is then provided to Bay of Plenty Electricity who generates approximately 6 MW of electricity with geothermal power generators for domestic use. NTGA wells are cased to depths between 450 m and 1250 m, so some of these are in the volcanic and sedimentary units.

The Kawerau geothermal field is believed to be able to sustain further development for power generation. Although any further geothermal development in the area would require further monitoring and analysis to be confident that the extraction of geothermal water does not contribute towards subsidence or would not contribute towards an increase in subsidence rates.

2.3.2 Geothermal energy applications

Current geothermal operations in Kawerau

There are currently six companies commercially generating electricity from geothermal resources in New Zealand. The main producer in the Kawerau field is Mighty River Power who generates approximately 104 MW from 55,000 tonnes of geothermal water per day. Other producers in the Kawerau field include NTGA who utilise geothermal energy for industrial purposes and power generation extracting 34,400 tonnes per day and Bay of Plenty Electricity who produce 6 MW of electricity. There is a small operator in the area called Geothermal Development Limited (GDL) who is consented to extract 5,280 tonnes per day. The operations are all located within close proximity to each other (Figure 17). Bay of Plenty Electricity is located within the same area along the Tarawera River.

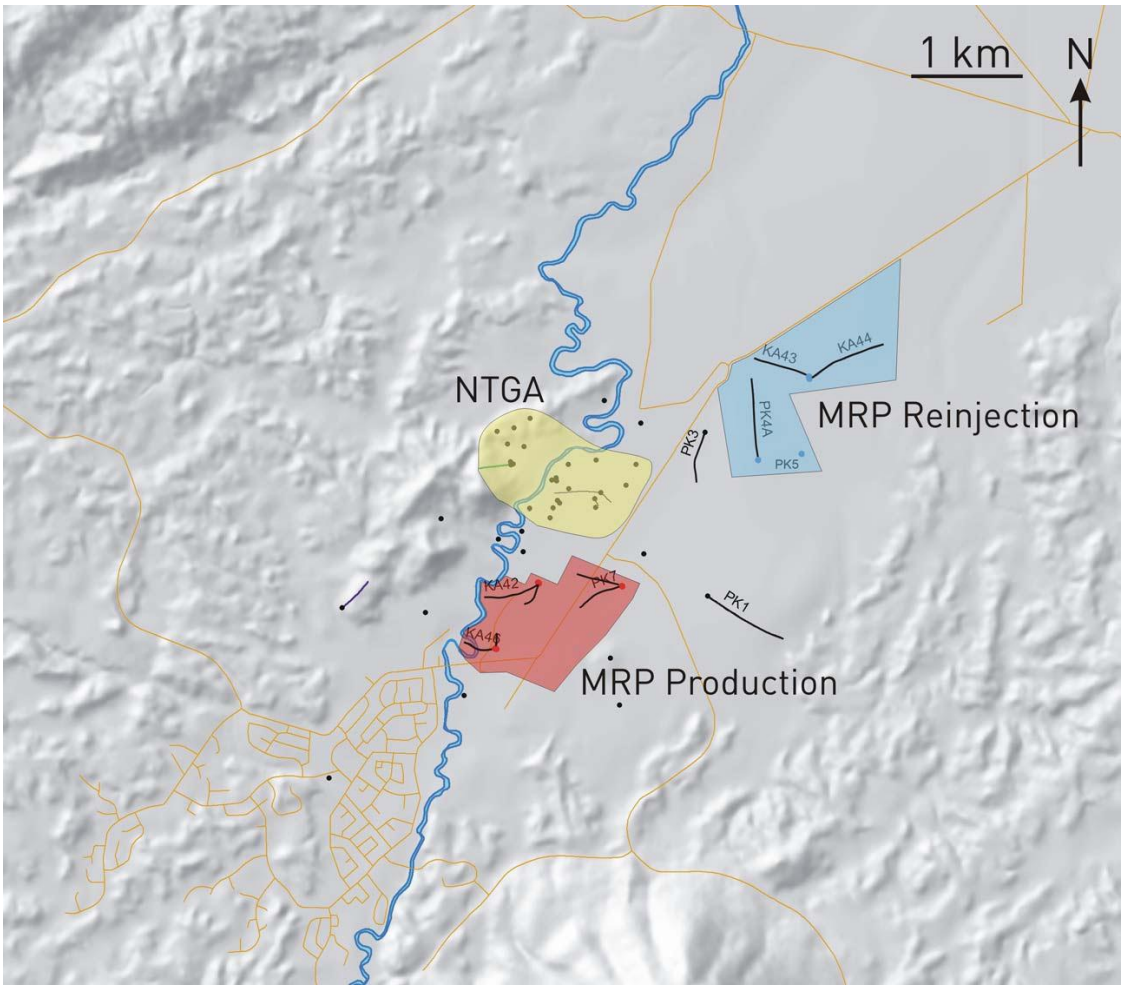

Figure 17: Location of major geothermal energy producers in the Kawerau area (Spinks, et al., 2007)

NTGA draws water from 850 to 1200 m in volcanic deposits, including the Caxton Rhyolite, Kawerau Andesite, Te Teko Ignimbrite and Basal Beds. NTGA then injects the water back in to the formation between 140 and 350m.

GDL produces geothermal water from the volcanic sediments and permeable zones around 500 and 1000 m and re-injects water at 190-240 m.

Mighty River Power currently draws 270°C to 300°C water from 6 production wells at 1,900 to 2,100 metres and re-injects the water through 4 injection wells at 1,900 to 3,000 metres, 2 kilometres north of the power station.

Until 2007 when the Mighty River Power geothermal power plant came on line, all geothermal water was extracted from rocks of volcanic origin such as the Kawerau Andesite, Caxton Rhyolite and

various ignimbrites (Figure 9). Extraction wells for the new power plant were drilled deeper than previous holes to give access to higher temperature rock and mitigate subsidence by extracting water from the much less compressible greywacke. Compression tests showed compression in the Huka Falls Formation is an order of magnitude more compressible than the greywacke (Terralog Technologies, 2006). See 3.7 for more details on compression tests.

Since increasing the depth of extraction wells, subsidence rates have not changed considerably even though production has increased (Spinks, et al., 2007). However, subsidence has been greater than that predicted in the 2005 assessment of environmental effects (Mighty River Power, 2005), which forecast a maximum subsidence rate of 8.5 mm/year between 2005 and 2050. This total rate may still be accurate if subsidence slows and/or stops in the future.

Table 2: Summary of subsidence rates from 2004 to 2010 (Energy Surveys, 2010)

Time period	Mean subsidence rate (mm)
2004 – 2006	-6.0
2006 – 2007	-9.5
2007 – 2008	-6.2
2008 – 2009	-9.7
2009 – 2010	-9.9

Geothermal water was not re-injected in the Kawerau Geothermal Field until 1991 (Bignall & Harvey, 2005).

A resource of approximately 350 MW has been estimated for the Kawerau field (NZGA, 2011).

2.3.3 Site geology

The geology of the area is fairly well understood, although more is being discovered regularly and the model of the sub-surface geology in the Kawerau area continues to change.

Local shallow sediments include recent alluvium, comprising peats, sands, gravels and unconsolidated or re-worked pyroclastics forming a layer of 10 to 50 m thickness. This overlies undifferentiated pyroclastics or Matahina Ignimbrites (Mighty River Power, 2005). The sediment

which forms the main surficial units at Kawerau are formed from the Whakatane (5.5 ka), Taupo (1.8 ka), Kaharoa (0.7 ka) and AD1886 eruption episodes (Hodgson & Nairn, 2003).
The site also has silt deposits related to the 1904 outbreak flood as mentioned in 2.3.1.

Literature review has shown that faults are mapped near the field area with the Onepu Fault almost reaching the western side of Site 2 (Beanland, et al., 1989); (Nairn & Beanland, 1989).

The sub-surface is described further in Chapter 5 – Shallow subsurface investigations.

Chapter 3: Previous subsidence studies at Kawerau

3.1 Introduction

This chapter reviews previous investigations associated with subsidence in Kawerau. The chapter is based on industry reports, survey monitoring data and personal observations from experts.

In 2006 Mighty River Power assumed responsibility for ensuring levelling surveys were carried out, as well as further investigation into potential subsidence in the Kawerau area. As part of Mighty River Power's resource consent to construct a geothermal power station, a thorough investigation on the likelihood of subsidence, and the potential impact of any subsidence was carried out between 2005 and 2006.

A number of investigations have been carried out on subsidence in the Kawerau geothermal field (Allis, et al., 1993); (Bignall & Harvey, 2005); (Bloomer, 2005); (Brock, 2006); (Curie, 2011a); (Curie, 2011b); (Energy Surveys, 2009); (Energy Surveys, 2010); (Grindley, 1986); (Hole, et al., 2007); (Mighty River Power, 2005); (Milicich, et al., 2010); (SKM, 2005); (Seiga, et al., 2011); (Spinks, et al., 2007); (Terralog Technologies, 2006); (URS, 2005). These studies usually coincide with development within the field due to requirements for resource consents.
Investigations have identified two levels of subsidence in Kawerau; the first is a large, field wide subsidence bowl which is likely to be controlled by subsidence at depth. The second is a series of linear and small, localised bowl shaped features which likely have near surface processes controlling subsidence (Figure 4).

3.2 Levelling surveys

The majority of subsidence monitoring that has been undertaken in Kawerau to date has been benchmark surveying. This is the process of surveying points around the mill site and surrounding areas relative to a fixed reference point which is not supposed to move at all, then repeating level surveys annually to identify any movement relative to the reference point.

Levelling surveys are a standard subsidence monitoring technique which is used in most geothermal fields around the world (Gkowacka, et al., 2000).

Benchmarks installed are 40 mm × M10 stainless domed top coach bolts drilled and glued with Hilti Hit glue (Figure 18). The studs were inserted through a 50×50×3 mm stainless washer with the benchmark name stamped on with red paint around the mark (Energy Surveys, 2009). Figures 19 and 20 show the typical location of benchmarks on structures, Figure 21 shows a benchmark within a concrete box with a steel lid along the side of Onepu Springs Road.

Figure 18: Benchmark number K0669 on the concrete base of a pipe support

Figure 19: Photograph showing typical location of benchmarks (Brock, 2006)

Figure 20: Photograph of typical conditions in site 1 and the location of a benchmark

Figure 21: Benchmark along the side of Onepu Springs Road within a concrete box with a steel lid

A total of 505 benchmarks were surveyed in the 2011 survey, this thesis does not present results for the 2011 survey as they were not yet available at the time of submission. Full surveys after the 1987 Edgecumbe earthquake were in 1988, 1994, 2000, 2006 and 2010. Two yearly or partial surveys were undertaken in the intervening years up to 2006, with more extensive annual partial surveys in 2007, 2008 and 2009 (Energy Surveys, 2009).

In 2011 more regular surveys were undertaken at Site 1 to identify any seasonal effects or discharge pond activity influences on the area. Extra surveys were undertaken as Site 1 shows the maximum subsidence rates in the field (Curie, 2011a). These surveys were carried out for the periods:

- June 2010 to March 2011,
- March 2011 to May 2011,
- May 2011 to July 2011 and,
- July 2011 to October 1011

Monitoring surveys in Kawerau started in 1970 (Energy Surveys, 2009) when a network of benchmarks were established to monitor ground movement. The size of the levelling surveys has increased considerably since its inception. The levelling survey to date is summarised in Table 3.

Table 3: Levelling survey sizes and subsidence results 1970 – 2011

Year	Benchmarks	Mean subsidence	Max subsidence	Min subsidence
1970	81			
1972	58	-1.4	-23	11
1976	99	-11.6	-34.6	1.6
1977	25	-1.4	-1.4	-1.4
1978	88	-1.1	-1.1	-1.1
1979	29	-0.2	-0.4	0
1981	25	-7.4	-13.5	-2.0
1982	182	-2.7	-9.9	0.5
1983	97	-4.0	-15.5	0
1984	117	-2.6	-11.4	2.0
1985	117	-6.1	-18.6	-1.1
1986	199	-3.4	-11.2	5.8
1987 (January)	122	-3.7	-21.3	0.3
1987 (April)	168	-113.4	-156.6	-65.5
1988	210	-5.8	-17.4	9.8
1990	342	-7.4	-25.9	6.4
1992	342	-9.1	-27.0	-2.4
1994	216	-12.5	-81.8	-2.4
1996	151	-11.3	-55.4	-3.3
1998	151	-12.7	-32.4	-3.4
2000	228	-9.9	-30.4	-2.3
2002	150	-9.4	-34.9	-1.0
2004	146	-11.5	-38.4	-1.8
2006	319	-6.0	-17.9	0.9
2007	341	-8.9	-36.5	2.5
2008	404	-5.7	-33.4	2.0
2009	431	-9.1	-47.5	26.2
2010 (June)	480	-9.9	-63.1	3.6
6/2010 – 7/2011	505			
6/2010 – 3/2011	49	-31.6	-53.5	-16.8
3/2011 – 5/2011	49	-31.3	-65.6	-10.1
5/2011 – 7/2011	49	-25.7	-43.5	-10.4
7/2011 – 10/2011	49	-30.5	-58.4	-6.3

Since 2006 surveys have been undertaken annually with more frequent surveys in areas of interest. The number of benchmarks has increased with each survey with significantly more benchmarks added in 2006, 2008 and 2010. Figure 22 shows the current distribution of levelling survey benchmarks around the field area.

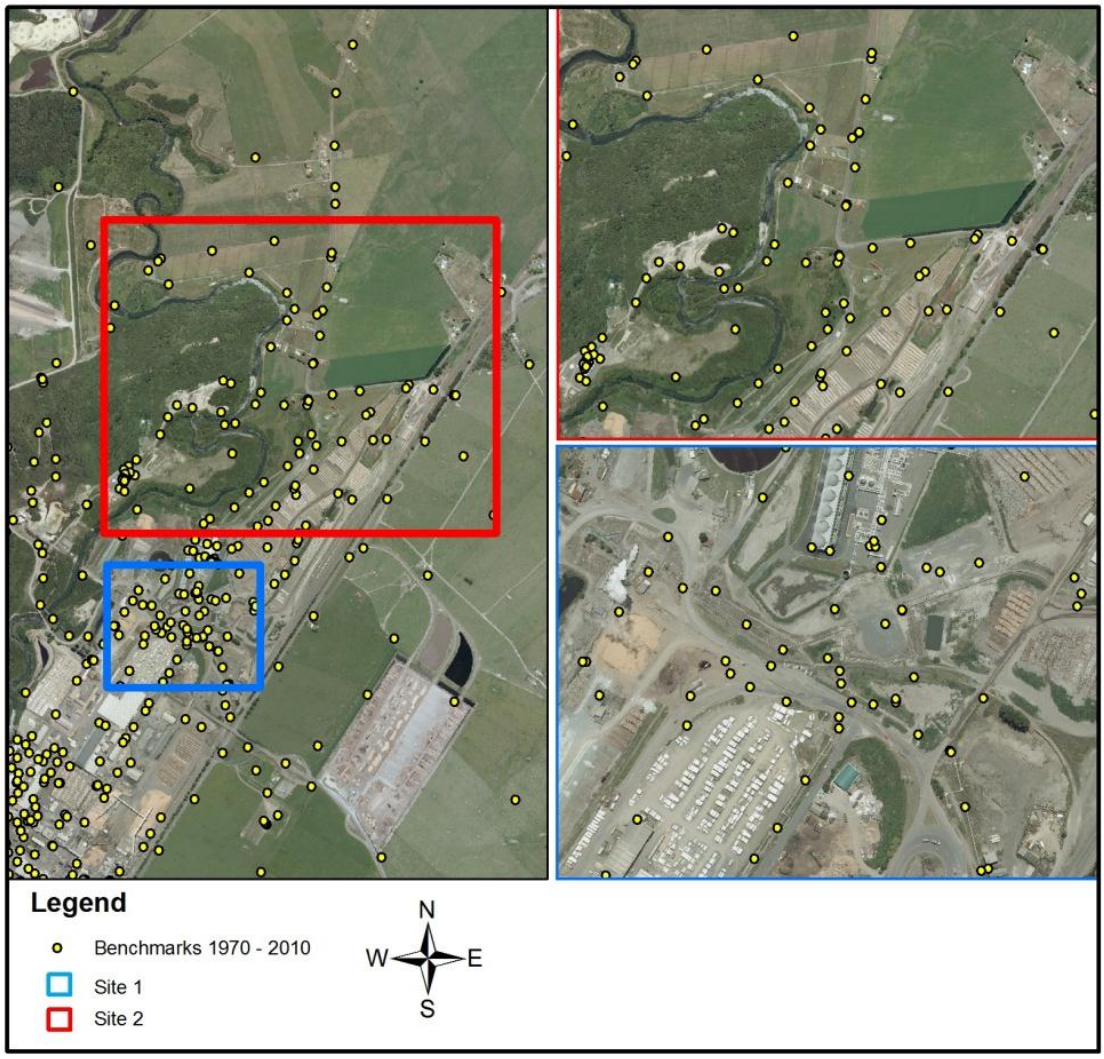

Figure 22: Benchmark locations at the mill site, and sites 1 and 2

There is currently one reference benchmark in the vicinity of the field against which all the partial (yearly) surveys are based. This benchmark links to the national benchmark system and is surveyed in the full (5-6 yearly) survey, results between the last full survey and the latest full survey will calibrate results from the intervening partial surveys (Energy Surveys, 2009).

Levelling surveys have identified three main subsidence bowls, two of which fall within the field area. The two bowls within the field area are shown in Figure 23. Site 1 has recently had more

benchmarks added and is being surveyed on a two monthly basis and has a current maximum rate of subsidence of approximately 63 mm/year, an increase from 48 mm/year for the period 2008-2009 and an increase from 18 mm/year from 2007-2008. This is the maximum subsidence rate recorded at Kawerau. Site 2 has a current maximum subsidence rate of 52 mm/year, an increase of 104 % from 25 mm/year for the previous period of 2008-2009.

The third subsidence bowl is much larger than the localised, linear subsidence features found at Sites 1 and 2 and is centred on Lake Rotoitipaku.

Site 1 is the most important feature to understand as it is closest to the mill and has the most potential to cause damage to buildings and infrastructure. Due to access to Site 1 and the infrastructure running through the area it is very difficult to conduct thorough surveys here. Site 2 however is generally in open agricultural land and was originally considered as a useful analogy to predict what is occurring in Site 1 without the interference of infrastructure.

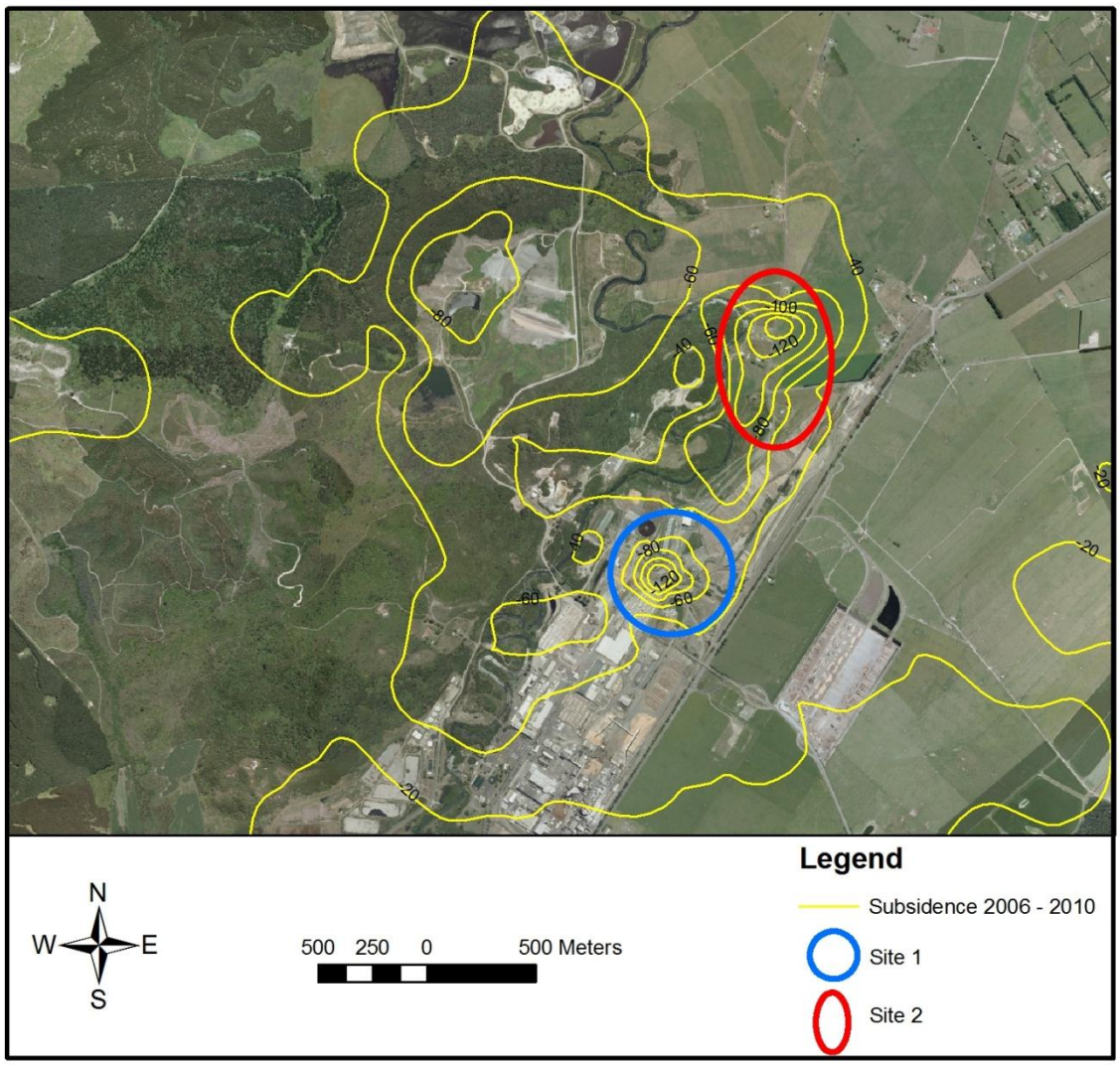

Figure 23: Location of main subsidence bowls in Kawerau area. Contours are 20 mm/year intervals

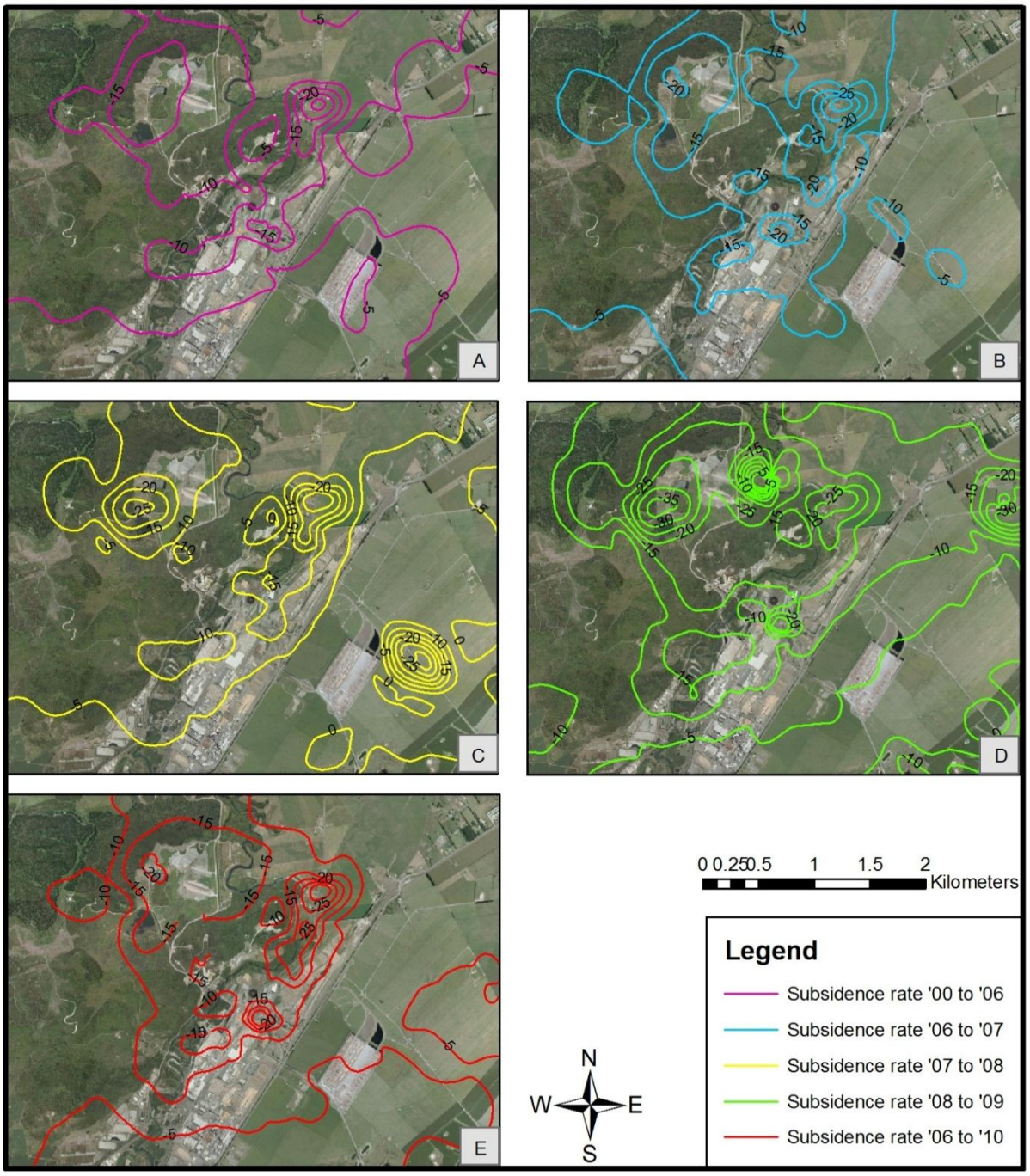

Figure 24: Images showing progression of subsidence bowls in Kawerau since 2000, rates are in mm/year.

Figure 24 shows the movement of subsidence bowls in the Kawerau area between 2000 and 2010. The shapes of bowls have not moved considerably, but have been refined due to the installation of more benchmarks around areas of interest. Interestingly features such as those in the south east corner of image C show a sizeable subsidence bowl, but no bowl in the same location in image D. This is also apparent in the top centre and upper right of image D. These anomalies may be explained by situations such as damage to the benchmark (such as someone driving over the benchmark) or nearby excavations reducing stability of the ground and allowing lateral spread,

measurement error or changes in the survey layout. Sites 1 and 2 however have remained present in all surveys since 2000, so are unlikely to simply be temporary anomalies such as the other features mentioned above.

Figures 24A and 24E are from full surveys, the 10 mm/year contour has significantly increased in size between figure 24A and 24E, this is likely to be a result of continued extraction of fluid at depth, but does not affect the localised features this thesis is focusing on. The area covered by the 10 mm/year contour for the 2010 survey was approximately 5 km^2, compared to 6 km^2 for the period 2008-2009, 2 km^2 for the period 2007-2008, 5 km^2 for the period 2006-2007 and 1 km^2 for the period 2004-2006 (Energy Surveys, 2010).

3.2.1 Results from benchmark surveys

Results from the latest survey (June 2009 to June 2010) have shown a mean subsidence rate for the field of 9.9 mm/year which is only a slight increase from 9.1 mm/year from the previous period of 2008-2009 (Energy Surveys, 2010). See Table 3 for full results.

Results from the 2010 levelling survey show that the area with current maximum subsidence is at Site 1 at the southern end of the airfield, or northern end of the mill site with benchmark K0669 subsiding at a rate of 63 mm/year. This is an increase from 48 mm/year for the 2008-2009 period and is an overall historic maximum rate recorded for the Kawerau field. Rates were 18 mm/year for 2007-2008 and 30 mm/year for 2006-2007. The benchmark K0669 was installed in 2006, so no data is available before this date. The maximum tilt in this area is 50 mm/100m/year for the June 2009 – June 2010 period. This is more than double the tilt rate at the previous survey where tilt was measured to be 24 mm/100m/year for the 2008-2009. Tilt is computed from the subsidence contour model, rather than being measured directly (Energy Surveys, 2010).

The area with the second highest level of subsidence was to the north-west of the airfield centred on benchmark H674 in Site 2 with a subsidence rate of 52 mm/year. This benchmark is located between the southwest corner of Onepu Springs Road and the Tarawera River. This subsidence rate is an increase of approximately 104 % from 25 mm/year for the previous period of 2008-2009. Subsidence in this area has shifted from benchmark HG8/1 between the 2009 and 2010 surveys. HG8/1 has a current maximum subsidence rate of 49 mm/year for the June 2009 to June 2010 period, an increase of around 48 % from 33 mm/year for the 2008-2009 period (Energy Surveys, 2010). HG8/1 had the highest subsidence rate for 2008-2009 with a rate of 33mm/year, for 2007-2008 at 33 mm/year, for

2006-2007 at 36 mm/year, 18 mm/year for 2004-2006 and, 38 mm/year for 2002-2004. This area has had the highest recorded subsidence since the post-Edgecumbe earthquake survey in 1988 at 639 mm (mean of 28 mm/year). Tilt in this area is around 66 mm/100m/year for the June 2009 to June 2010 survey, an increase of 50 % from 44 mm/100m/year for the 2008-2009 period. This area of subsidence includes the line of the old Tarawera River course (Energy Surveys, 2010).

Continued addition of more benchmarks has meant it has been possible to locate localised areas of subsidence and narrow this down to specific points.

Tilt over the mill area has been identified to be about 1.1 mm/100 m/year towards the west, with subsidence rates up to 2-5 mm/year around the NST mill paper machines (Energy Surveys, 2010).

3.2.2 Accuracy of levelling surveys

Strengths

- Benchmarks are relatively low cost and easy to install and survey which makes adding new benchmarks very easy. This helps narrow down areas of high subsidence as these areas can contain many benchmarks. This has been done in Kawerau with the addition of new points with nearly every survey, 25 new benchmarks were added in March 2011, mainly to further constrain subsidence rates at Site 1 (Curie, 2011a).
- Levelling surveys can be corrected very easily for errors to increase accuracy of measurements. Energy Surveys (2009) state that "All levelling observations were corrected for any instrumentation collimation error determined each day. The levelling was adjusted for misclosure by the snap least squares adjustment program. The small adjustment residuals and circuit closes confirm the high integrity of the observation data."

Limitations

- Errors of 4.9 mm/year were computed for the 2009-2010 subsidence rate (Energy Surveys, 2010).
- Surveys have traditionally been annual which doesn't show much in the way of seasonal variation of subsidence, however, this is required to get precise readings of such small

movements. With the new surveys being bi-monthly, the error has increased to 14 mm/year due to extrapolation of data (Curie, 2011b).

- Benchmarks are not always obvious and may be lost or destroyed accidently by other contractors who do not realise their importance.
- Benchmarks may be missed occasionally due to land access issues.
- The whole survey is based on one reference benchmark, if this benchmark moves or is damaged the system may be surveyed inaccurately and won't give an accurate indication of changes from the previous survey. The use of one secure reference point is the greatest weakness of this monitoring technique. If the reference benchmark has moved, this will make the whole survey pointless.
- Precision of surveys is based on the formula $\pm 5\sqrt{n}$ where n is the number of set ups during the run. For example, if there are 9 setups of equipment, you will allow for a 15 mm misclose, so the larger the area being surveyed, the more inaccurate you would expect results to be.
- Benchmarks don't provide horizontal displacement data.
- Surveys only provide a good indication of the change in elevation between surveys so long as the pattern of subsidence does not significantly shift (Energy Surveys, 2009).
- The location of benchmarks is critical when measuring subsidence. You need to be certain that the structures the benchmarks are on are not simply sinking in to soft sediment, and that what it is being measured is truly subsidence.
- The location of benchmarks may influence the shape of subsidence features by being spaced in a linear or biased direction. For example, the benchmarks around Site 2 are primarily located along the length of Onepu Springs Road; the resulting subsidence pattern is roughly parallel to Onepu Springs Road (Figure 22).

Figure 25: Photograph of Site 1 in heavy rainfall (Brock, 2006)

Figure 25 shows Site 1 in heavy rainfall conditions – this site is often inundated by water to some degree. Benchmarks are placed on heavy concrete footings which support the steam pipeline foundations. There is a chance that these heavy footings are sinking into the soft sediment on which they are resting, giving the appearance of subsidence rather than true subsidence actually occurring.

3.3 Geotechnical drill holes

Sinclair Knight Merz (SKM) carried out a geotechnical investigation in 2005. Three geotechnical drill holes were drilled to a maximum depth of 120m to investigate the geotechnical properties of shallow deposits across the mill grounds before the construction of the geothermal power station in 2007.

Geotechnical holes were drilled to increase knowledge of the local geological structure as well as to obtain samples for laboratory testing to determine compressibility, and thermal expansion and contraction properties to predict changes in the rock as pressure and temperature conditions change within the field due to water extraction.

Drilling was to be carried out until either 20 m of rhyolite was drilled, a depth of 120 m was reached or hole conditions lead to abandonment. Core was collected, logged and sampled.

Geotechnical boreholes identified that around the mill site there is pumice alluvium from surface to 65 to 80 m depth. Pumice alluvium is underlain by the Matahina Ignimbrite to a depth of up to 115.5 m except for hole G3 (Figure 8) where the Matahina Ignimbrite was not encountered. Instead the usually underlying unit, the Onepu Rhyolite, was found between 81 and 120 m.

The pumice alluvium seen in the drill holes has been described as silty sands and gravels, comprised from weathered pumice, ignimbrite, rhyolite and obsidian.

The geotechnical report as a result of the geotechnical borehole investigation highlights that significant differential subsidence from compaction in the alluvium is considered unlikely under the mill.

3.4 Cone penetrometer tests

Cone Penetrometer Test (CPT) investigations were carried out by URS in 2005 on behalf of Mighty River Power Ltd. CPT's were carried out in 24 locations along the air strip and at 31 locations around the mill complex. The purpose of the tests was to identify soil and groundwater conditions from ground surface to approximately 20 m depth. This was carried out to evaluate the potential for subsidence, compaction and consolidation beneath existing foundations (Brock, 2006).
The CPT is performed using a cylindrical penetrometer with a conical tip (cone) as shown in Figure 26. The penetrometer penetrates the ground at a constant rate of approximately 20 mm per second (Lankelma, 2010). During the penetration, the forces on the cone and the friction sleeve are measured. The measurements are carried out using electronic transfer and data logging, with a measurement frequency that can secure detailed information about the soil conditions (Brouwer, 2007).

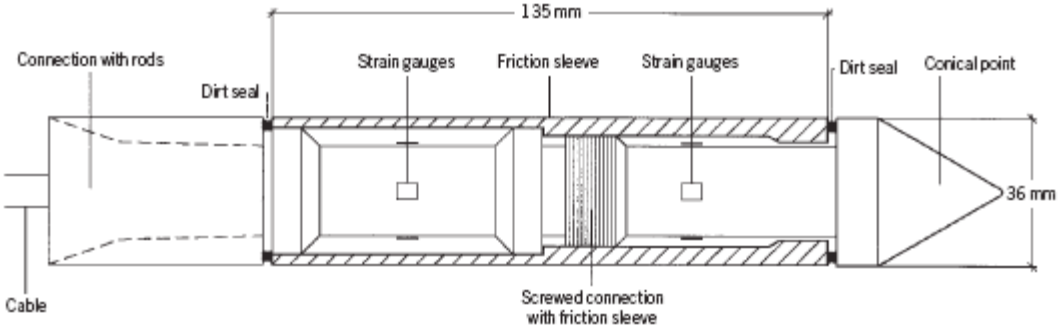

Figure 26: Electrical friction cone with cut-away friction sleeve (Brouwer, 2007)

CPT results are based on a ratio of tip and sleeve resistance, i.e. tip resistance is high in sands and low in clays, sleeve resistance is low in sands and high in clays (NEES, n.d.). CPT provides a soil profile, estimation of geotechnical parameters and an evaluation of groundwater conditions (NEES, n.d.).

A review of the URS CPT investigation was carried out by Dana Brock as part of expert evidence in response to Mighty River Powers application for resource consent for their geothermal power station in Kawerau. Brock found that the field area is blanketed with unconsolidated volcanic alluvium and that most of these deposits extend below the water table (2-12 m). Brock identified liquefiable areas which will be susceptible to settlement and collapse during seismic events and that there are also alluvial clays and silt which would be susceptible to consolidation, particularly if dewatered. Brock states that these conditions pre-existed the mill installations and are not related to geothermal reservoir processes (Brock, 2006).

Near Site 1 of the field area, Brock has interpreted CPT results to identify a blanket of very loose fill between 2 and 3 m below ground surface. The loose fill layer is underlain by medium dense alluvium, apart from when it is underlain by an alluvial clayey silt layer.

Near Site 2 of the field area, Brock interpreted CPT results to identify very loose pumiceous and quartzite alluvium to 3 m below ground surface underlain by alternating medium dense and dense alluvium to 13.5 m then ignimbrite of increasing density to a final depth of 19.5 m. Brock also identified fill to 1 m overlying 0.5 m of loose alluvium nearby. Groundwater in this area is shallow and reaches 2 – 2.5 m below ground surface (Brock, 2006).

Brock concludes that CPT results indicate that shallow soil and groundwater conditions in the field area could give rise to localised subsidence, lateral spreading and compaction (and where clays are present, consolidation) particularly when exposed to nearby loading, vibration, groundwater fluctuations, or loss of support due to nearby excavation.

CPT results identified the presence of tomos or piping in some of the boreholes. These would likely have formed naturally due to lateral drainage above a lower permeability layer (URS, 2005). During SPT testing in borehole BH5, at 13.8 m the sampling spoon dropped rapidly to 14.1 m suggesting a 300 mm thick cavity or a zone of very soft or very loose material (URS, 2005). As a response to this, dispersion and permeability tests were carried out on sands and very soft layers to test for susceptibility to erosion and permeability. This is discussed in section 5.5.

CPT results identified that groundwater in the area was consistently between 4.5 and 6.3 m below ground level. This was often difficult to measure due to soil collapse in the holes (URS, 2005).

3.5 Aerial photograph interpretation

Aerial photograph interpretation (API) was carried out by Dana Brock in 2006 (Brock, 2006). Advice was given on geologic hazards, specifically subsidence and liquefaction that might affect existing and proposed structures in response to Mighty River Powers application for resource consent for their geothermal power station in Kawerau.

Through API, Brock identified a number of features which may contribute to subsidence.

Three key features are:

- A depression within Site 2 appears to be an oxbow lake (1970) which has subsequently been filled by unknown means with unknown material (1973).
- A buried pipeline is located along the current alignment of the levelling survey marks on Onepu Springs Road. Depth and backfill characteristics are not indicated. Brock further states that most fill using site materials would tend to settle in comparison to surrounding in-place materials, creating a localised differential subsidence.
- Construction and operations disturbance in the vicinity of Site 1.

3.6 Computer modelling

Computer modelling of subsidence in Kawerau was carried out by Terralog Technologies USA, Inc. in 2006 (Terralog Technologies, 2006) and Industrial Research Ltd, Lower Hutt in 2005 (Young & White, 2005). Computer modelling is used to predict future subsidence rates and is generally only applicable to basin wide subsidence as it models reservoir behaviour at depth. It is therefore not suitable for modelling the localised, near surface features which this thesis is investigating, this section is however included as it provides context to the greater subsidence of the Kawerau field.

There are often many assumptions when predicting future reservoir behaviour through computer modelling including:

- The rate of water extraction will remain constant, or increase at pre-determined rates.
- Materials are going to continue to behave the way they have in the past.
- Lithologies that are prone to compaction, consolidation, thermal expansion or contraction are generally linear and will be well represented by samples (if any are collected) that have been tested in the laboratory for the conditions presented above.

Terralog Technologies has stated that surface subsidence is proportional to the magnitude of the pressure and temperature change of the reservoir and has calculated that Kawerau has an estimated formation thickness change of ~0.1% in response to pressure and temperature changes. The report further states that subsidence is proportional to the thickness of the compactable formation (In this case it is assumed to the Huka Falls Formation – see 2.2.2.4), the depth of burial, and the lateral extent of the subsurface compaction zone. This has allowed them to identify that subsidence may be mitigated by:

1. Reducing the magnitude of pressure or temperature change.
2. Increasing the depth at which pressure or temperature changes.
3. Reducing the lateral extent over which temperature and pressure changes, assuming the lateral extent is not large relative to the depth of burial.

Terralog Technologies expected subsidence rates to drop following the installation of Mighty River Power's power station due to the increase in depth of production wells and increase in injection rates.

Industrial Research Ltd (IRL) believe that the Kawerau field has a wide subsidence bowl attributed to pressure drawdown or thermal contraction due to geothermal fluid extraction. This is likely to be correct for the field-wide subsidence bowl, but the localised features at Sites 1 and 2 indicate a near-surface mechanism. They state that it is unlikely that the localised, near-surface subsidence features at Sites 1 and 2 could be related to pressure drawdown in the deeper reservoir (Young & White, 2005). The report on the Kawerau Geothermal Field by IRL focuses on the large scale subsidence features (see 2.1) and their future behaviour. IRL have calculated through modelling that the Kawerau Geothermal Field is likely to subside up to 500 mm over the period 2005 – 2050, or an annual rate of 11.11 mm/year with a temperature drop in the reservoir of 5° - 10°C depending on the well. This is considerably less than historic amounts where there has been 408 mm of subsidence between 1988 and 2004. This brings the average yearly subsidence rate down to ~11 mm/yr from ~25 mm/yr.

Both models from Terralog Technologies and IRL agree that subsidence rates are likely to decline. Both reports attribute this to increases in depth of production wells and increases in reinjection to maintain reservoir pressure. Computer modelling does have assumptions, but these are usually outweighed as they are usually modelled on worst case scenarios.

3.7 Laboratory testing of materials

Terralog Technologies oversaw mechanical property testing on core samples from the Kawerau field in 2006 to assess the compressibility and thermal expansion properties of the main lithologies found in the Kawerau Geothermal Field. Testing included 6 samples from Onepu Ash, 8 from Kidnappers Ignimbrite, 10 from Onepu Rhyolite, 8 from Huka Falls Formation and 10 from greywacke. Testing was also carried out to help strengthen computer modelling data (Terralog Technologies, 2006) which is described in 3.6.

Results from this report primarily focus on comparisons between the Huka Falls Formation and greywacke, however most fluid extraction has historically been from between these two units in permeable volcanic units. The main units water has historically been extracted from are the Kawerau Andesite, Caxton Rhyolite and various ignimbrites (Pezaro, pers.comm., 2011).

Laboratory testing found these key results:

- The Huka Falls Formation is about an order of magnitude more compressible than the greywacke where fluid extraction has recently shifted. Moving extraction to the greywacke will result in less pressure related compaction than historically occurred.
- Greywacke is slightly more responsive to temperature changes than the Huka Falls Formation, so similar or slightly more thermal related compaction is to be expected.
- Because greywacke is deeper, it means less surface subsidence will occur because subsidence transferred to the surface decreases with increasing depth of the compaction source.
- Temperature effects on subsidence in the Kawerau geothermal field are at least as large as the pressure effects. It is predicted that more than 90 % of the future compaction within the greywacke will be temperature related, rather than pressure related.

Table 4: Average compaction and thermal expansion coefficients measured on Kawerau samples (Terralog Technologies, 2006)

	Uniaxial compression coefficient		Thermal expansion coefficient ($\times10^{-6}$/°C)
	($\times10^{-6}$/psi)	($\times10^{-3}$/MPa)	
Huka Falls Formation	2.046	0.297	8.32
Greywacke	0.298	0.043	10.28

Table 5: Comparison of pressure and temperature related compaction in Huka Falls Formation and greywacke (Terralog Technologies, 2006)

	ΔP	ΔT	Thk	C_m	α	Pressure related compaction	Temperature related compaction	Total compaction
	MPa	°C	m	1/MPa	1/°C	m	m	m
Historical (Huka)	0.5	50	500	2.97E-06	8.32E-02	7.43E-02	2.08E-01	2.82E-01
Future (Greywacke)	0.5	50	500	4.30E-05	1.03E-02	1.08E-02	2.57E-01	2.68E-01

A summary of all compressibility and thermal expansion results are appended (Appendix A).

3.8 Geological and Nuclear Science reports

The Institute of Geological and Nuclear Sciences (GNS) has carried out a number of investigations into subsidence in Kawerau and surrounding areas. These reports provide geological information on the field area including recent and very thorough descriptions on the distribution, behaviour and local variations of geological units.

The Stratigraphic Correlation Study of the Kawerau Geothermal Field in 2010 (Milicich, et al., 2010) provided valuable information on the Matahina Ignimbrite, Huka Falls Formation, Kidnappers Ignimbrite (previously Rangitaiki Ignimbrite) and the deeper formations below the Kidnappers Ignimbrite.

The Geoscientific Review of the Kawerau Geothermal Field (Bignall & Harvey, 2005) is a thorough review of the Kawerau field and discusses the character, geology, chemical structure, geophysical structure, historical estimates of resource capacity and past effects of resource utilisation. This report also has a small section on subsidence in Kawerau. It highlights that although large scale cooling and contraction of a production zone can cause subsidence, it is unlikely to exceed 10 mm/year for present extraction rates. Whilst contraction may contribute to subsidence at Kawerau, it was unlikely to be the main cause of any geothermally induced subsidence.
This report raised some key ideas which include:

- The Edgecumbe earthquake of 1987 caused considerable subsidence in Kawerau (200 – 270 mm). Most of the subsidence happened during the earthquake, but as much as 30% occurred over the following 6 months.
- The identified NE-trending subsidence anomaly is likely to delineate a fault zone which moved during the 1987 earthquake.
- Despite the fields production rate increasing by close to 50% since 1979, there has been no systematic pattern of changing subsidence rate with time since the beginning of levelling surveys in 1970.
- The main cause of apparent variations in subsidence patterns are attributed to the distribution of benchmarks and the addition of new benchmarks.
- Bignall and Harvey have highlighted that in the vicinity of Site 2, before the Edgecumbe earthquake, subsidence rates were <5 mm/yr, but post-seismic subsidence was in the order of 5-9 mm/yr suggesting that seismic activity and relaxing of faults may be contributing to subsidence.

- Subsidence monitoring wells were installed at Site 1 to deduce the depth to the compacting layer in the area. Detailed measurements indicated ~0.5 mm/year of differential movement at the base of the well, compared to a subsidence rate of 13 mm/year at the surface. Measurements also indicated that variations in rock formation across the subsidence anomaly pointed to compaction being the primary cause of subsidence.

Chapter 4: Preliminary site investigation

This chapter explains the initial investigation that identified subsidence features and methods for further investigation which are discussed in Chapter 5.

4.1 Site investigation approach and objectives

The objective for the initial site investigation was to become more familiar with the field area at Kawerau, this involved:

1. Aerial photograph interpretation,
2. A site visit which involved:
    a. site familiarisation,
    b. identification of key features and areas
    c. identification of appropriate geophysical techniques, and
    d. planning geophysical investigation locations
3. Taking photographs of features at Kawerau

4.2 Aerial photograph interpretation

Aerial photograph interpretation (API) was carried out on photos obtained from Environment Bay of Plenty (Whakatane) records and scanned at high resolution. Photos were dated 1944, 1965, 1966, 1992, 1993, 1995, 1997, 2000 and 2001. Aerial photographs from Land Information New Zealand (LINZ) were examined from 2001. Aerial photographs from Google Earth were dated 2002 and 2004 and were examined. High resolution aerial photographs were obtained from Mighty River Power; these were taken in 2009 and are the most recent aerial photographs of the field area. Aerial photographs from Brock (2006) were also examined, and included aerial photos from 1945, 1987, 1995 and one undated oblique aerial photograph which was taken during mill construction (likely to be 1950's).

Photographs of the mill before and during construction were also found and examined, these were all provided by the Fletcher Trust Archives (Fletcher Trust Archive, 2011).

API helped identify the following key features:

1. river channels to the north east of the mill area,
2. historic river meanders, and
3. low points in the landscape

API helped identify these key changes through time:

1. 1944 and 1945 aerial photos show that the Tarawera River north of the field area looks relatively new with low amounts of vegetation on its banks and the absence of any buildings or construction. There are no depressions or channels near Site 1 visible in the 1945 photo (Figure 27).
2. An historic oblique aerial photograph (estimated to be 1950s) shows significant ground modification during the construction of the pulp and paper mill.
3. A 1965 aerial photo shows the installation of a train track to the mill, a lake to the north of the field area and a significant increase in water depth in the Tarawera River.
4. 1966 aerial photos show the installation of a geothermal pipeline across the Tarawera River, indicating an increase in development in the area, the construction of new houses and, increased development at the mill site. A photo of the mill area shows a train track and geothermal pipes running through Site 1, no development to the north of Site 1 and a clear drainage channel through the area (Figure 28).
5. A 1987 aerial photo shows a considerable drop in the water level of the Tarawera River compared to 1966, and also the disappearance of the lake to the north of the field area. An increase in vegetation in the field area and along the banks of the Tarawera River is also apparent (Figure 29)
6. A 1992 aerial photo does not show the mill area, is the first colour aerial photograph and doesn't show considerable change from 1987.
7. A 1993 aerial photograph is the first colour aerial photograph that shows the mill area and shows considerable ground modification. It does not however show considerable change since 1992 in the surrounding area.
8. 1995, 1997 and 2000 aerial photos show no notable changes since 1993 (Figure 30).
9. 2001 aerial photos show a decrease in vegetation at Site 2 and clearing of ground/ploughing of farmland to the south-west of the sharp bend in Onepu Springs Road
10. 2002 and 2004 aerial photos show no notable changes.
11. 2009 aerial photos show the installation of the Mighty River geothermal power station and associated infrastructure and pipelines.

Aerial photographs have shown clear changes in the landscape as the Kawerau area has developed since the first aerial photographs in 1944. One of the most significant changes however was the drainage of the Rangitaiki Plains and the redirection of the Tarawera River. The evidence for this is difficult to observe in aerial photographs due to the 30 year time difference between the completion of these tasks and the first aerial photograph. However, it is clear that there have been significant changes in river depth and vegetation around the edges of the river.

Aerial photograph interpretation made it possible to design field work to target specific features of interest.

Aerial photograph interpretation has identified that there is no apparent difference in the original ground conditions or drainage at Site 1 compared to the surrounding mill area (Figure 27).

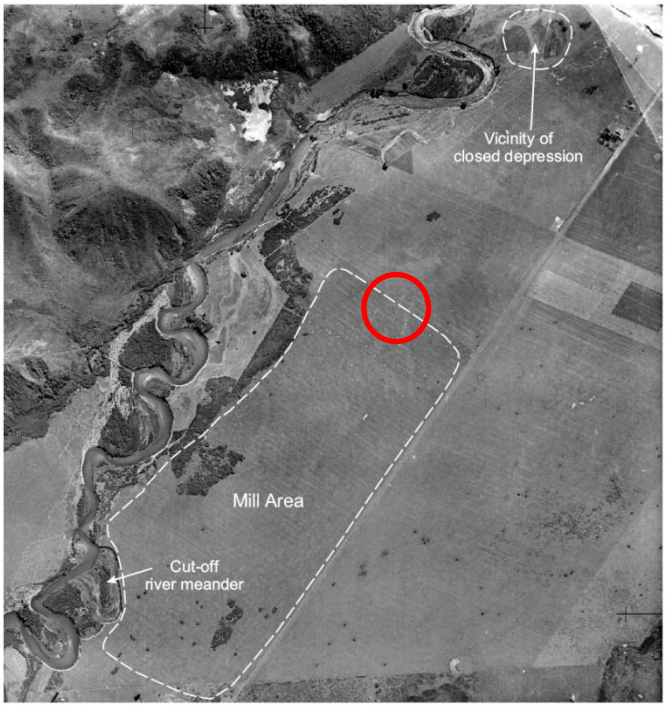

Figure 27: 1945 aerial photograph of mill site. Red circle showing the approximate location of Site 1. Vicinity of closed depression comment is in the southern part of Site 2. Comments by Brock (2006).

Figure 28: 1966 aerial photographs showing mill developments and sites 1 (blue circle) and 2 (red oval).

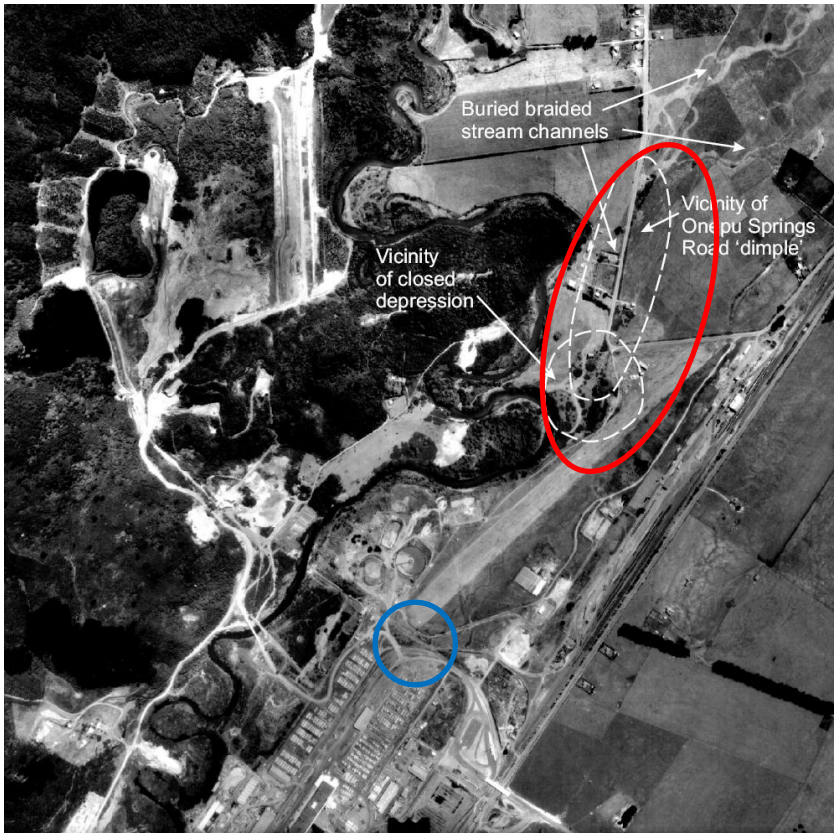

Figure 29: 1987 air photo of the field area, same annotation as above. Comments by Brock (2006).

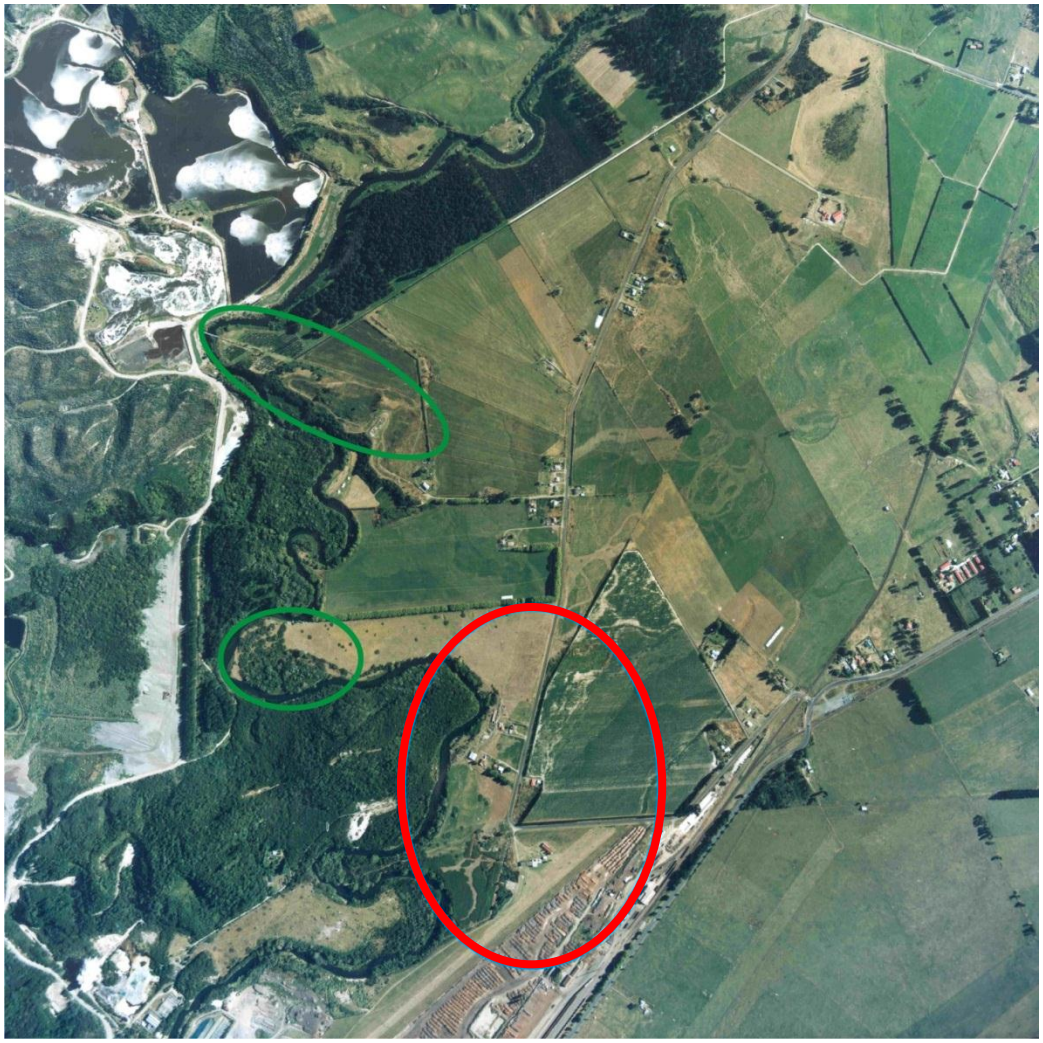

Figure 30: 2000 aerial photo of the field area – Site 2 indicated by red circle. Green circles indicate increases in vegetation. Also obvious in the map are historic braided stream channels to the north and north east of Site 2.

All aerial photographs are appended (Appendix B)

Photographs of the pulp and paper mill before and during construction provide insight into modifications that were made to the site. These photographs have identified that foundations were excavated for the main mill buildings and were likely re-compacted. These photographs have also identified that there is no distinguishable difference between Site 1 and the surrounding ground conditions and that there were no noticeable active or abandoned river channels at Site 1.

Photographs were provided by the Fletcher Trust Archive.

Figure 31: Aerial photograph of the proposed mill site (Photo dated 1951)

Figure 32: Aerial photograph of the mill site during construction (Circa 1955). Site 1 approximately shown by blue circle.

Figure 33: Photograph of mill under construction, this photograph shows considerable ground disturbance and foundation preparation (9 November 1955)

All mill construction photographs are appended (Appendix C)

4.3 Initial site visit

An initial site familiarisation trip was carried out in August 2010. This trip was used to identify and photograph key features in the landscape including:

- Low points in the landscape,
- Tarawera River outcrops,
- Benchmarks,
- Drainage channels, and
- Man-made features.

The initial site visit also provided an opportunity to determine the most suitable geophysical methods for the first phase of sub-surface investigation. This work identified that ground penetrating radar (GPR) and electrical imaging would be the most suitable geophysical investigation techniques. These methods were chosen as they often complement each other, are relatively fast, can cover many lines in limited field time and were generally favourable to the field conditions

(Nobes, pers.comm., 2010). Locations for these investigations were proposed and access to these locations was sought from landowners.

Four GPR lines were identified within the mill grounds, however it was expected that the survey would be disrupted by the many fences, railway lines and steam pipelines causing 'noise' in the results. Sites were identified by evaluating both the most subsidence prone areas and the likelihood of disturbance from surrounding features.

GPR and electrical resistivity lines were chosen at Site 2 based on subsidence features interpreted from levelling surveys, historic river channels visible in the landscape and distance from any farm fences and power lines.

During the initial site visit, conditions were very wet with many parts of Site 1 under water, this provided a good opportunity to observe and photograph the site in different conditions (See figures 34 to 37).

Figure 34: Steam pipeline at Site 1 in drainage channel

Figure 35: Historic railway tracks - create noise on GPR profiles

Figure 36: Steam pipelines, fences and power lines at Site 1. Pipeline foundations in soft, saturated ground.

Figure 37: Historic river channel at Site 2

4.4 Engineering geological mapping

The absence of surface outcrop in the field area restricted geological mapping to a description of site geomorphology which is based on field observations and literature review, LiDAR interpretation and aerial photograph interpretation.

The following engineering geological map (Figure 38) illustrates key features related to this study as well as land use type, field investigation locations, levelling survey benchmarks and the historic location of the Tarawera River. This map developed over time and more data was added as field investigations continued and more data became available.

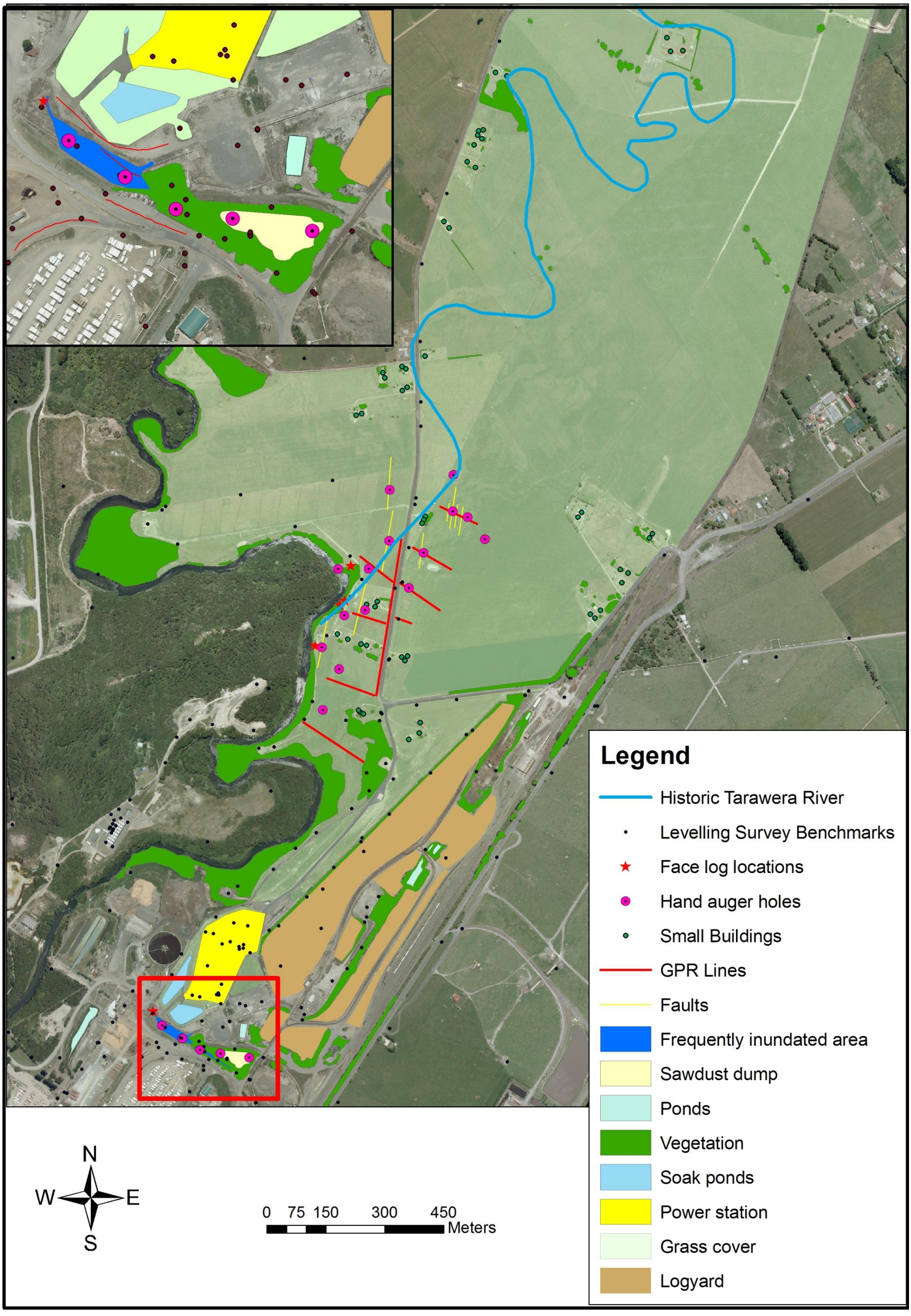

Figure 38: Engineering geological map of the field area including land use and investigation locations

4.4.1 Site geomorphology

Over the past 150 years the most significant influences on the geomorphology of the Kawerau area have been the effects of the rivers of the Rangitaiki Plains and human modification of the plains.

As mentioned in 2.3 the Rangitaiki Plains have been significantly modified as a result of a series of efforts to drain the plains to increase useable land for agriculture. This has resulted in a drop in the water table and has significantly dried out the plains. The outbreak flood from Lake Tarawera covered the Kawerau area in sediment in 1904 (Gibbons, 1990).

Historic river meanders are clear in the landscape where the river has changed course. The Tarawera River had been diverted from its original path to flow towards Lake Rotoitipaku to prevent flooding of farmland following the outbreak flood (Gibbons, 1990). There is evidence in the landscape of historic river meanders. It has however proven difficult to identify the point in the existing Tarawera River where it was diverted as the river cuts through historic river deposits.

Since the 1950's industrial development has seen the Kawerau area rapidly evolve from farmland to a town supporting industry and more recently geothermal power generation. The current landscape is covered with steam pipelines transporting steam from nearby wells to Kawerau for industrial processes or electricity generation. There are also many roads and railways at varying degrees of functionality ranging from old abandoned railway tracks to new roads accessing recent developments such as the geothermal power station.

4.5 Site hydrogeology

Groundwater depths have been taken from monitoring wells around the Kawerau area. Groundwater depths are summarised in Table 6. Section 2.2.6 describes the regional hydrogeology of the Rangitaiki Plains.

Table 6: Groundwater depths in monitored wells – Data valid until 22 April 2010

Drill hole	Well drilled (year)	Hole elevation (m)	Hole depth (m)	Average water table depth (m)	Minimum water table depth(m)	Maximum water table depth(m)
GW1	1991	30	10	6.73	5.65	7.42
GW2	1993	24	35	6.09	5.09	8.25
GW3	1999	21	36	5.58	2.46	8.76
GW4	1999	27	36	8.15	7	9.5
KAM2	1999	34.68	137.6	15.92	13.43	17.85
KAM3	1999	24.61	128.6	6.03	4.7	7.8
KAM4	1999	25.96	109.6	9.60	7.35	11.52
KAM7	2007	17.6	44.5	3.57	3.1	4
KAM8	2007	22.8	44.5	6.48	6.14	6.8
KAM9	2008	28.38	32.1	3.45	3.4	3.5

Data and literature review as well as field investigations indicate that the water table is approximately 6 – 10 m deep and follows the general trend of the landscape. Surface water tends to flow towards the Tarawera River and subsurface water generally flows in a northerly direction (Mighty River Power, 2005). Shallow groundwater operates under conventional hydraulic gradients, rather than the thermal convection cells of the geothermal field and is recharged by excess rainfall (Gordon, 2002); (Mighty River Power, 2005).

Figure 39 shows interpolated depth of water table across the plains around the field area.

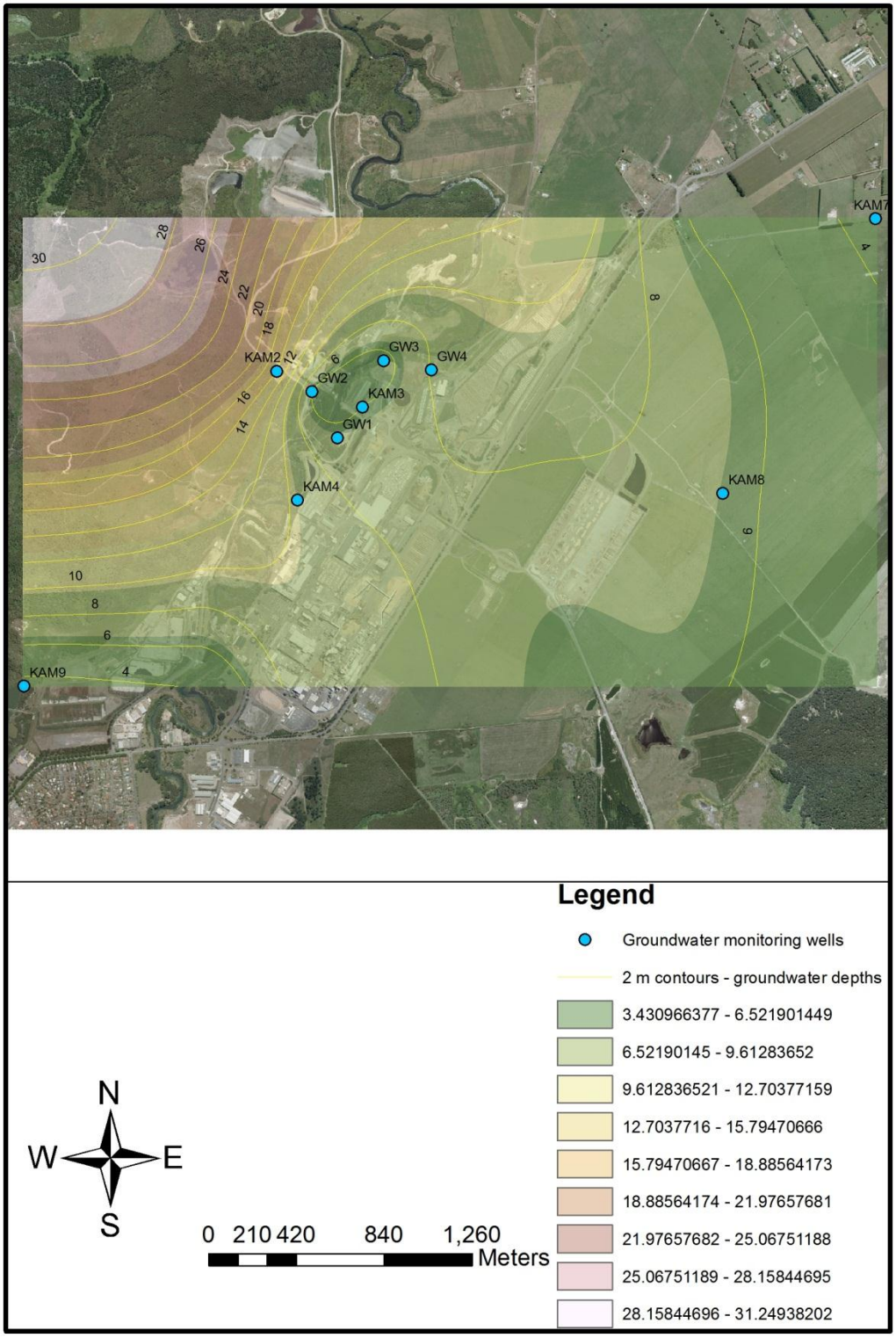

Figure 39: Map of field area showing water table depths calculated by spline interpolation of depths to water table in various groundwater monitoring wells.

Chapter 5: Shallow subsurface investigations

5.1 Introduction

Following the initial site familiarisation trip, two phases of investigation were carried out to further define the subsidence features at Kawerau. The first phase was a geophysical investigation which included ground penetrating radar and electrical imaging, while the second phase was more invasive and included hang augering, face logging and laboratory work.

Objectives of the Kawerau site investigation were:

- To re-characterise the Site 1 and Site 2 subsidence features (see section 2.1) at the surface.
- To define subsurface geology in the area of subsidence.
- To define subsurface structure in the area of subsidence.
- To determine water table depths.

5.2 Geophysical investigation

A geophysical investigation was carried out at Kawerau in December 2010. This section will cover the basics of ground penetrating radar (GPR) and electrical imaging geophysical techniques. This section will also present the results and an interpretation of the findings for both investigation techniques.

The techniques used are discussed below, a background and geophysical principles of ground penetrating radar and electrical imaging are appended (Appendix D)

5.2.1 Ground penetrating radar

Ground penetrating radar is a geophysical investigation method which is used to identify physical property changes within the subsurface by measuring two-way travel time off the reflected radar energy (Godfrey, 2008). Simply, a transceiver sends out electromagnetic waves. These waves reflect from changes in physical properties within the subsurface such as the water table, lithological boundaries or man-made features, and the reflected waves are then detected by a receiver. The

difference in time it takes between sending a wave out from the transceiver and when the receiver picks up the wave forms an image.

This survey was designed to investigate two subsidence zones within the Kawerau Geothermal Field (Figure 40). The local geology comprises of fine grained volcanic sediment, alluvial sediments and flood deposits overlying rhyolite domes, andesite and ignimbrites.

The GPR survey was carried out in December 2010 by Hayden Mackenzie, David Nobes, Ben Pezaro, Georgina Richards and Monika Schneider. Associated data processing and interpretation was carried out by Hayden Mackenzie under the advice of David Nobes.

The survey was acquired using a pulseEKKO 2 100A GPR unit. The unit was set up on a plastic sled with 1.0 m offset 100 MHz bistatic antennae to record GPR traces (sampling rate 0.5 ns) at roughly 0.2 m intervals along 14 lines ranging between 80 and 210 m long. GPR profiles were used to reveal sub-surface structure by crossing subsidence features identified by levelling surveys as well as features identified in the preliminary site investigation (Chapter 4). Profiles were primarily oriented northwest-southeast on either side of Onepu Springs Road as well as one line along the verge of the road (Figure 40).

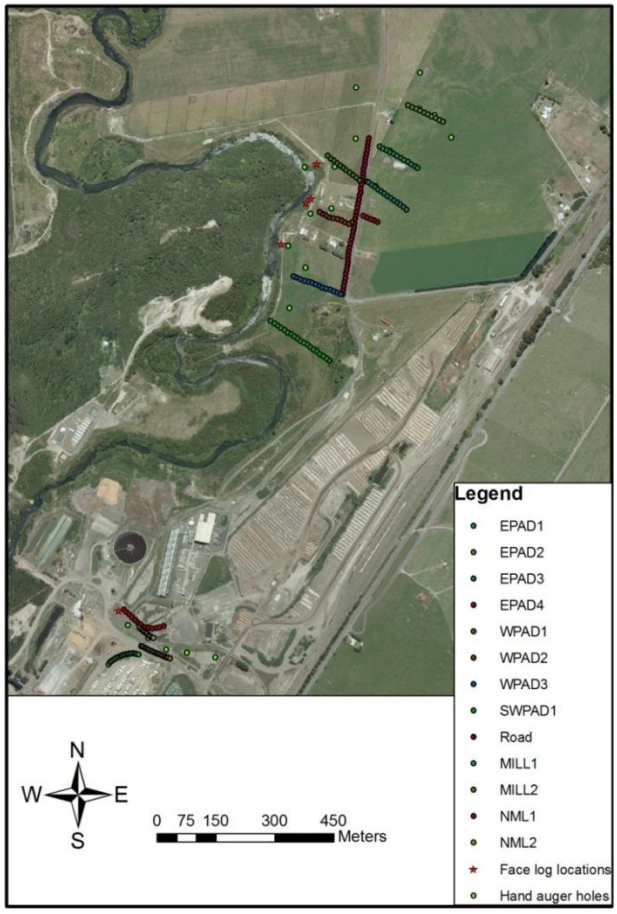

Figure 40: Image showing the location of GPR lines in two main locations – Site 1 to the south and Site 2 to the north

Figure 40 shows the layout of the geophysical investigation. Four resistivity lines were also conducted along the same position as GPR lines. Shared lines were:

- KAWRES1 and EPAD3
- KAWRES2 and EPAD2
- KAWRES1W and WPAD1
- KAWRES5W and WPAD3

5.2.1.1 Test procedure

All of the GPR survey areas were covered using a reflection survey in continuous mode. This was possible due to the relatively flat, open ground, and placement of the antennae on a plastic sled, which was pulled across the ground surface. Lines were run in a direction heading away from Onepu Springs Road. Fiducial markers were sprayed with spray paint every 5 m for surveys within the mill grounds, and every 10 m for the remaining lines. This allows "rubber banding" during processing, which interpolates traces to regular intervals between fiducial markers.

Eight common mid-point (CMP) surveys were conducted along various GPR lines to determine the subsurface velocity which is used in migrating the GPR data and converting travel time to depths.

Figures 41 to 43 show GPR equipment setup and use.

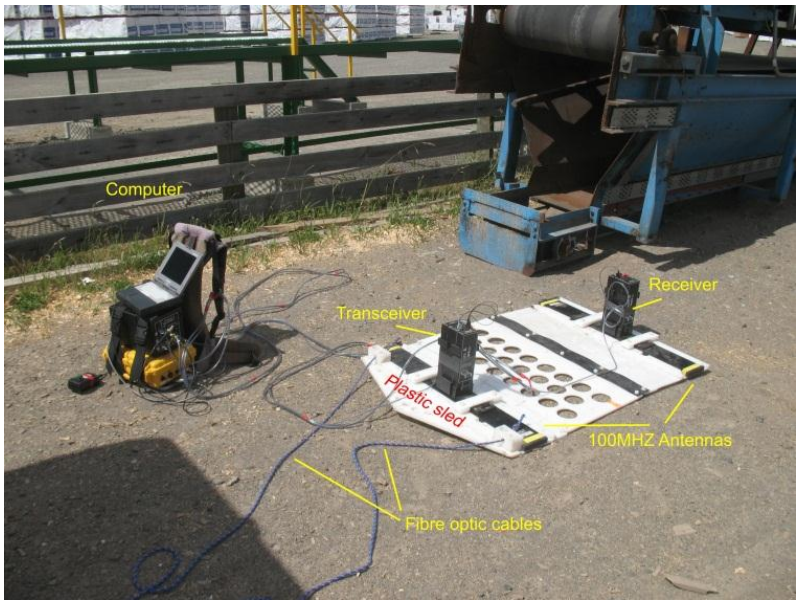

Figure 41: Photograph showing GPR components and set up

Figure 42: Using GPR in the field

Figure 43: CMP survey in progress

5.2.1.2 Processing procedure

GPR data was processed using Sensors & Software EKKO View Deluxe for rubber banding, migrating, filtering and topographic corrections. Appendix E shows the GPR trace lines for raw, processed and interpreted stages of all GPR lines.

5.2.1.2.1 CMP Analysis

The first data set to be processed was the CMP data so that a subsurface velocity could be determined which would then be used in the subsequent migration and depth correction of the GPR profiles. CMP analysis was completed using EKKO View Deluxe version 1.4. Figure 44 shows a semblance analysis of the CMP response where the concentration of velocity response can be seen between 0.10 and 0.12 m/ns.

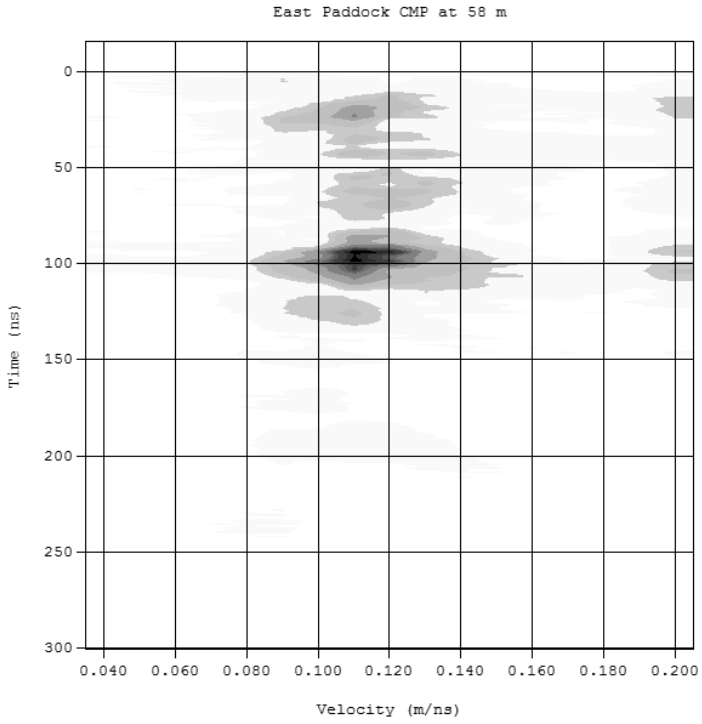

Figure 44: CMP analysis results showing a plot of velocity measurements from within the subsurface of EPAD 3

A mean velocity of 0.11 m/ns was used for the purpose of processing.

5.2.1.2.2 Rubber banding

Because the GPR was set to continuous collection and the sled was being pulled by a person, there are naturally slight variations in the number of collection points between each fiducial marker.

Rubber banding evens out the distance between fiducial markers to make up for variations in walking speed and converts the profiles to regularly spaced traces.

5.2.1.2.3 Migration

Migration was applied to all profiles to collapse diffraction curves and position reflectors correctly within the profile. Dipping reflectors are deeper and steeper than they appear in raw GPR profiles. Migration improves the spatial accuracy of the data. A velocity of 0.11 m/ns, spatial offset of 1.0 m and scale of 0.2 was used for all profiles.

5.2.1.2.4 Filters

Dewow was used to remove unwanted low frequency signals from the profiles, while preserving the high frequency signal. These low frequency signals are superimposed on high frequency reflections by the transmitting signal in some conditions (Sensors & Software, 2003).

5.2.1.2.5 Gain functions

Two types of gain functions were applied to the data sets to correct for loss of signal with depth; these boost the weaker signals at depth and make the profiles easier to interpret. Gains applied were AGC and SEC.

- AGC (Automatic Gain Control) is an exponential gain function which attempts to equalise all signals by applying a gain which is inversely proportional to the signal strength (Sensors & Software, 2003). This means that weak signals, usually at depth, will receive a larger applied gain than strong signals, evening out the signal strengths and making it possible to interpret features to a greater depth. AGC tends to yield an image of all stratigraphy and reflectors.
- SEC (Spreading and Exponential Compensation) is a limited exponential function where a limited gain inverse to signal strength is applied. The limited function allows weaker signals to be amplified, but not to the point where relative signal strength relationships are filtered out. Deeper signals are amplified, but not as much as they are with AGC gain, and weaker signals within the main body of the signal response maintain their relative signal strength (Godfrey, 2008).

AGC appeared to display the profiles from Kawerau the best, so interpreted results are presented with AGC gains. However, SEC processed profiles were used to help identify features, they were just not the primary profiles used.

5.2.1.2.6 Topographic correction

Topographic files were derived from GPS co-ordinates overlying LiDAR data. This made it possible to get very accurate elevation data to correct GPR profiles to accurately represent the landscape.

Once topography was added to the profiles, topography was shifted, which permanently shifts traces up and down, based on the topographic data. The subsurface velocity as determined by CMP is used to shift topography, 0.11 m/ns was used for all profiles.

5.2.1.3 Results

Figures 47 to 49 are representative examples of processed and interpreted profiles. All un-interpreted and interpreted profiles are appended (Appendix E). Blue dotted lines on figures show water table location and red lines show interpreted faults.

Raw profiles of Mill1, NML1 and NML2 showed high levels of noise so were not processed further. This would have been due to the close proximity to fences, pipelines and railway lines. Figure 45 shows GPR line NML2 data collection between pipelines and Figure 46 shows high levels of noise in the processed profile. These profiles were not included in the model.

Figure 45: GPR line NML2 between and under steam pipelines delivered noisy profiles

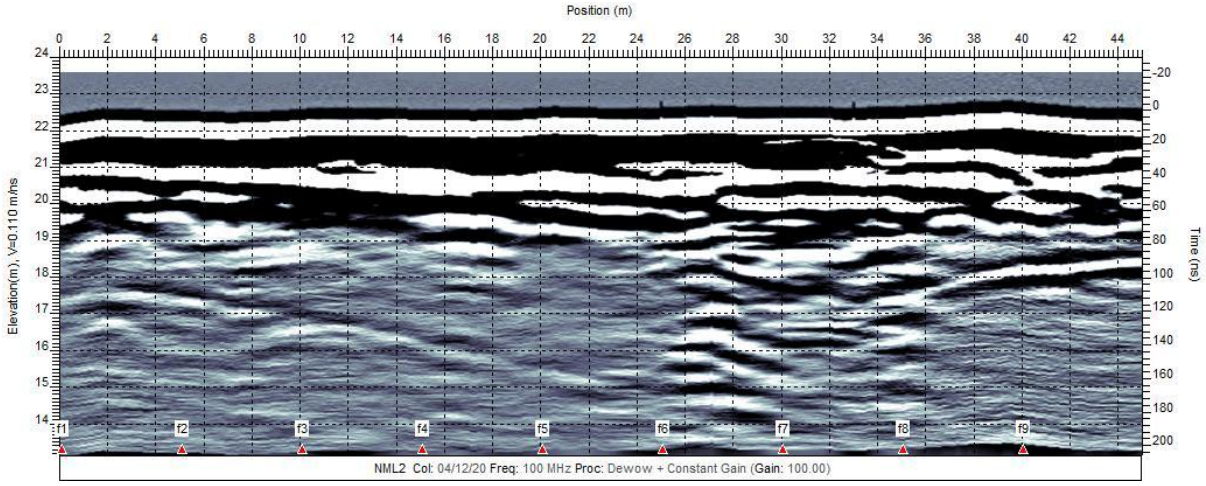

Figure 46: Basic processing of NML2 show high levels of noise and no real structure for interpretation

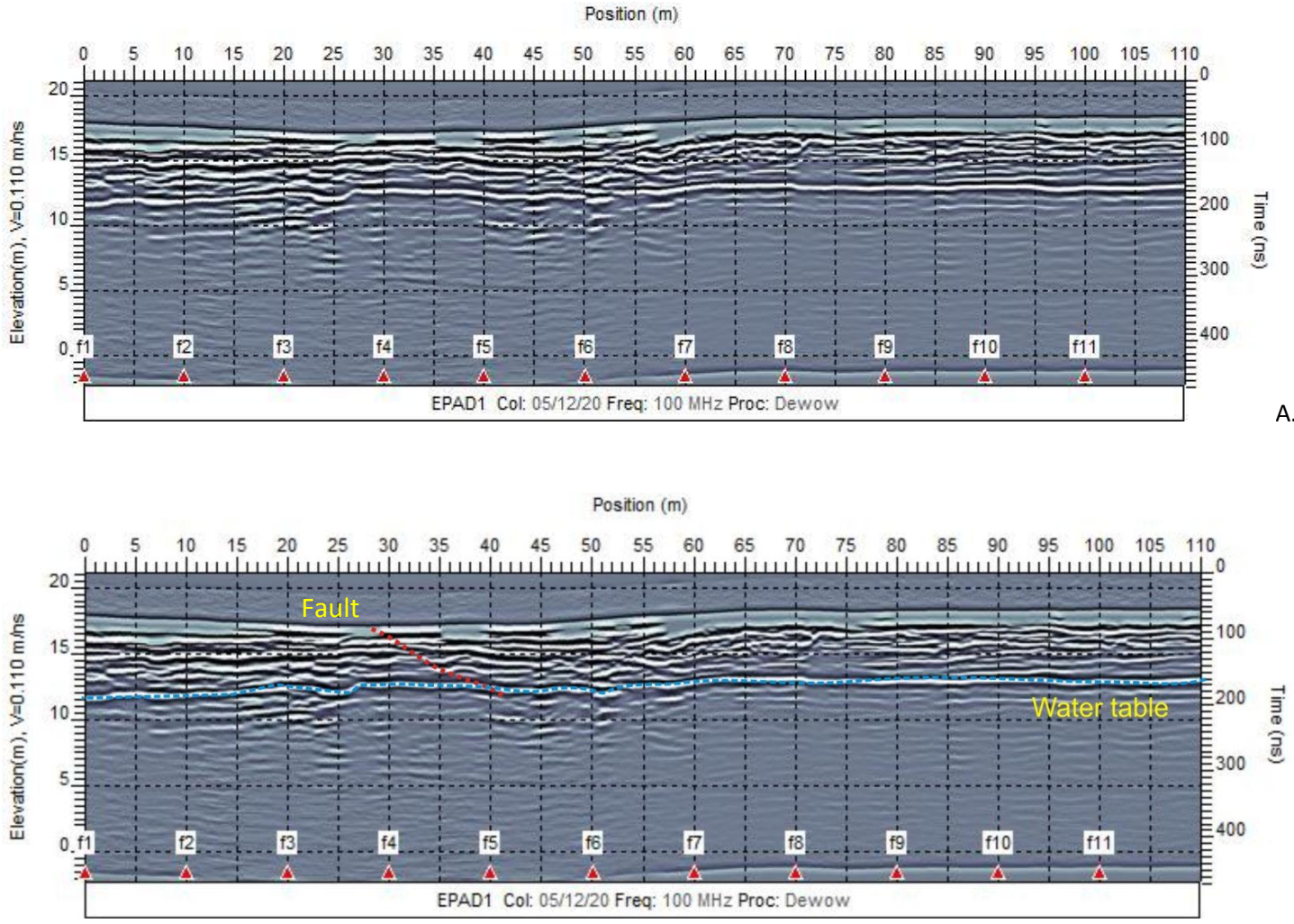

Figure 47: Processed (A.) and interpreted (B.) GPR profiles for EPAD1

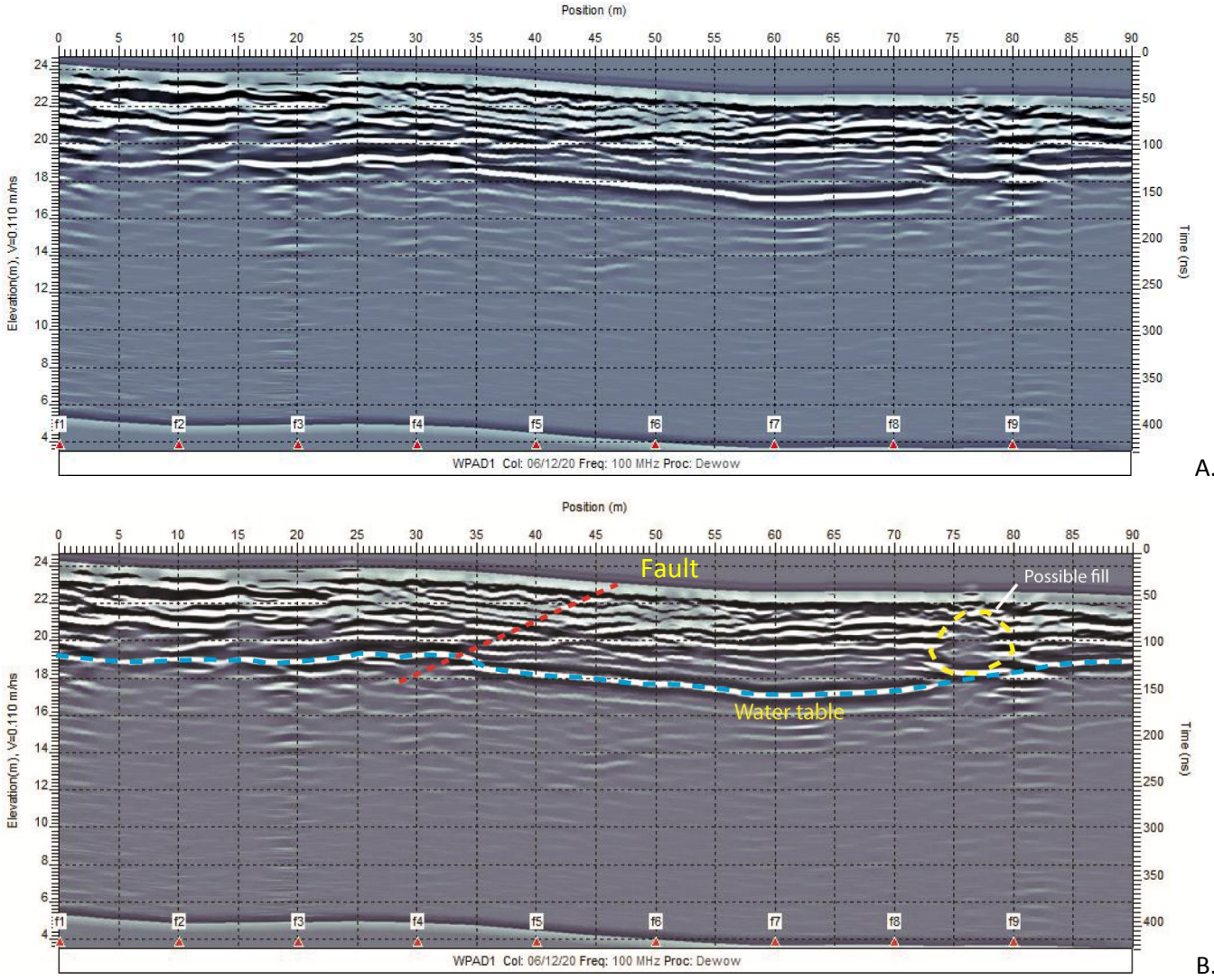

Figure 48: Processed (A.) and interpreted (B.) GPR profiles for WPAD1

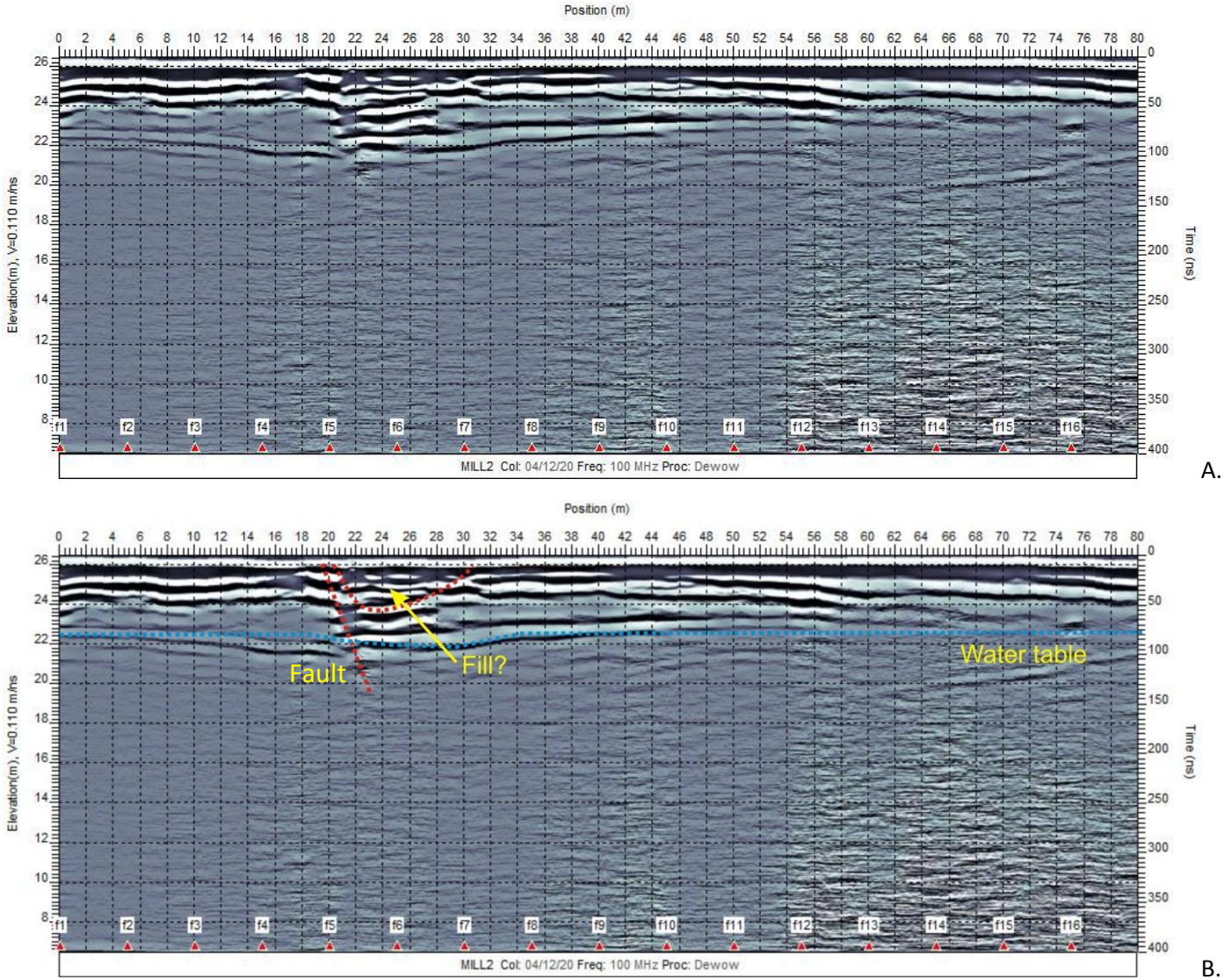

Figure 49: Processed (A.) and interpreted (B.) GPR profiles for Mill2

5.2.1.4 Interpretation

The GPR survey has shown stratigraphy, and in particular identified truncated stratigraphy which has been interpreted as faults. The GPR survey has also identified the depth to water table.

Faults identified have been interpreted as a series of en echelon and overlapping faults which are an extension of the Onepu Fault System – an area which has not been accurately mapped for faults within the field area in the past. The Onepu Fault system has a recurrence interval of approximately 249 years (URS, 2005). Beanland, et al. (1989) have mapped the fault to the edges of the field area and the GPR investigation has made it possible to extend the fault zone through the field area (Figure 52).

Fill was interpreted as areas where there is a zone of no clear bedding surrounded by bedding on either side, or a zone of disturbed and inconsistent looking bedding with offset beds around the edges of the possible fill area. Areas of possible fill were identified in WPAD1 (Figure 48) and Mill2 (Figure 49). The water table was interpreted from laterally continuous, strong reflectors which were visible across the whole profile.

Fault dips have been identified to be between approximately 20° and 35° with one fault within the mill area steepening to 63°. Faults identified by GPR appear to be shallower than those discussed in Beanland et al (1989) which show faults dipping at approximately 55° to within 10 m of the ground surface, then become almost vertical as they approach the surface. Trenching along interpreted fault locations would allow for accurate fault dip measurement. Faults strike between 32° and 38° (ENE). This is similar to the angle of the historic Tarawera River in this location (~40°). This is discussed further in Chapter 6. Faults were interpreted by observing offsets or disruption to bedding. This fault identification technique is well established and has been used in many papers (Yetton & Nobes, 1998); (Wallace, et al., 2010); (Godfrey, 2008). Identification of faults influenced the location of hand auger holes in the second phase of the shallow subsurface investigation (Section 5.4).

All raw, processed and interpreted GPR profiles are appended (Appendix E)

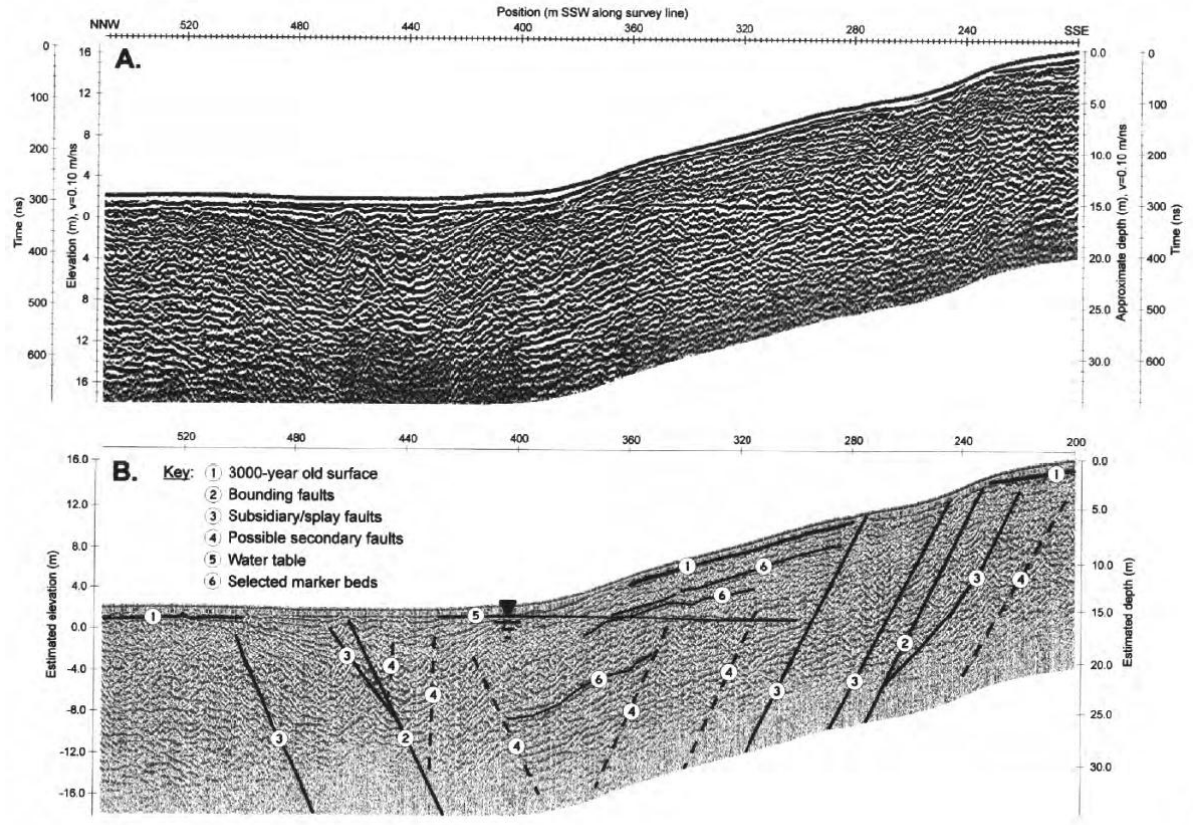

Figure 50: Example of fault identification from Yetton and Nobes (1998)

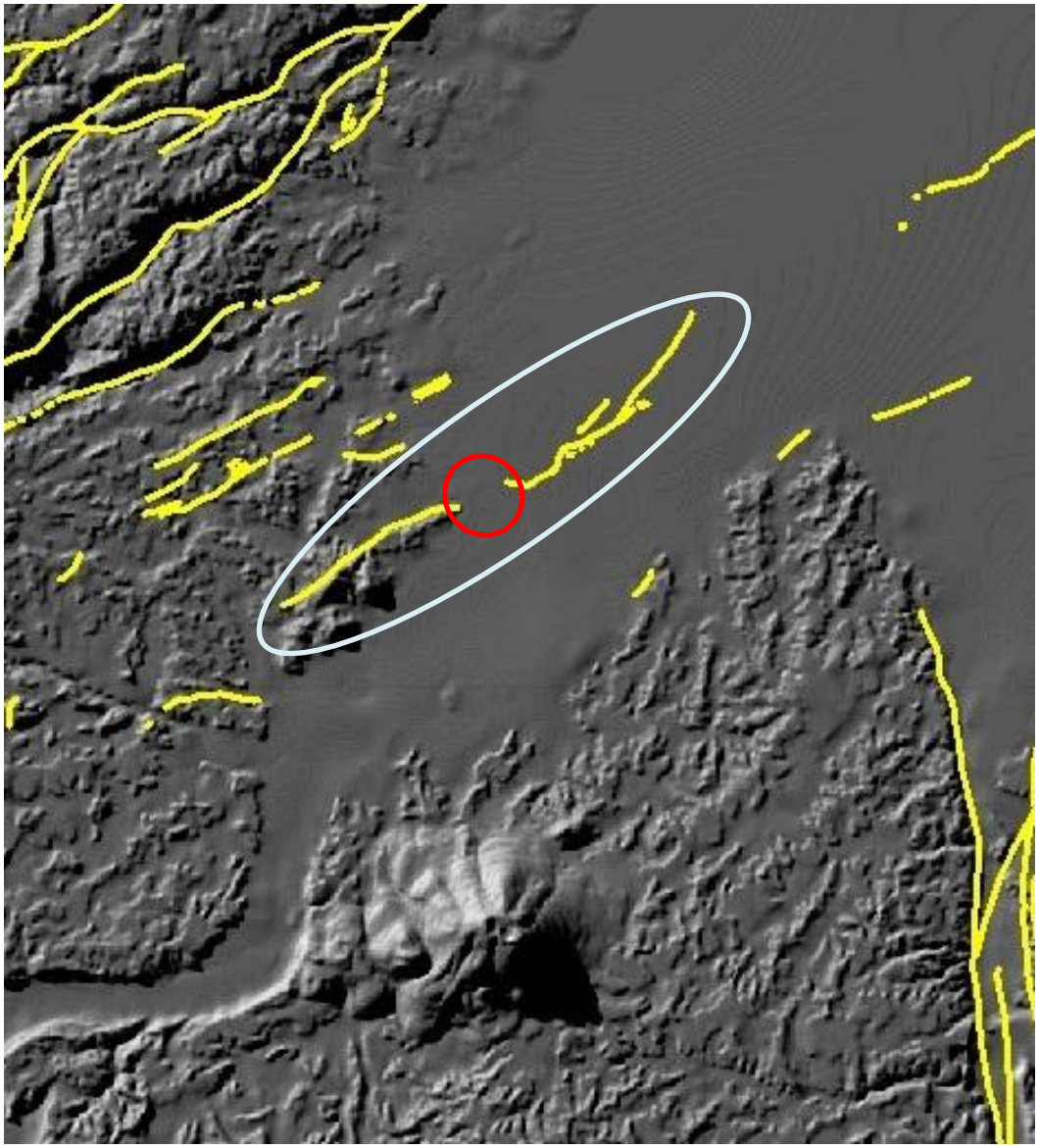

Figure 51: Figure showing active faults in the Kawerau area - Onepu Fault in centre, site 2 within red circle (GNS, 2011) .

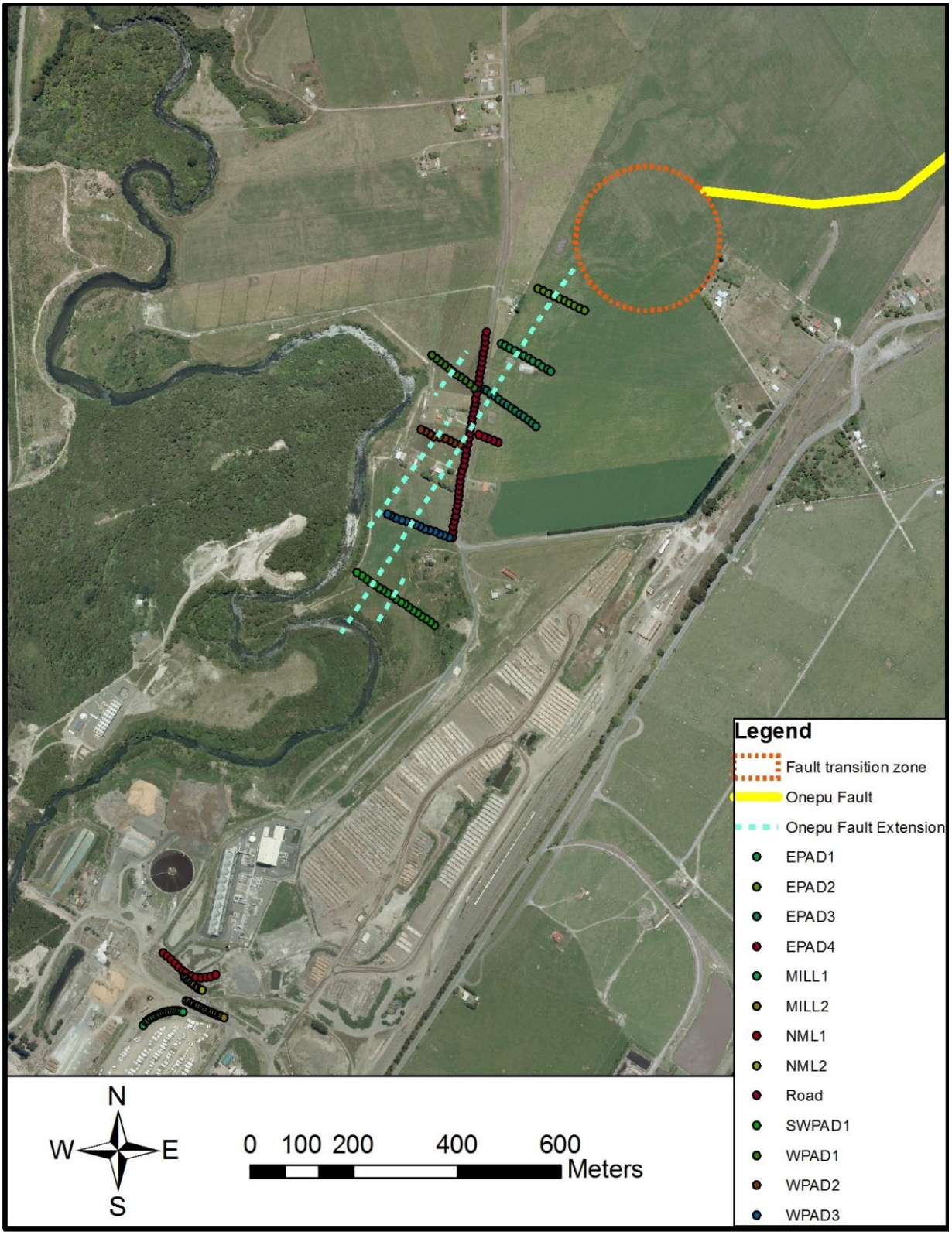

Figure 52: Image showing new mapped location of the Onepu Fault

5.2.2 Electrical imaging

Electrical imaging in the form of resistivity surveys were conducted in four selected locations in Kawerau. The small number of surveys was limited due to time constraints and the duration of tests. Sites chosen for electrical imaging were determined by prior GPR investigation and interesting surface features within subsidence bowls identified by levelling surveys. Electrical imaging was not carried out in Site 1 due to the high chance of interference from the mill, power station, vehicles, fences and pipelines.

The electrical resistivity (ER) method involves the measurement of the apparent resistivity of soils and rock as a function of depth or position. During resistivity surveys, current is injected into the earth through a pair of current electrodes, and the potential difference is measured between a pair of potential electrodes. The current and potential electrodes are generally arranged in a linear way. The apparent resistivity is the bulk average resistivity of all soils and rock influencing the current.

Electrical resistivity can be used to determine depth to bedrock, depth to groundwater, map faults and map paleo-channels (GEOVision, 2010).

Electrical resistivity is non-intrusive and leaves the ground in-tact, is less impacted by subsurface clays or groundwater quality than other methods and direct current ER potentially has depth capabilities greater than GPR, however, it is prone to unique interpretation properties when utilized in urban environments where conductive and/or resistive materials near buildings and other structures are present (Schmidt, 2005).

5.2.2.1 Test procedure

Resistivity data were collected using a Campus Tigre resistivity system and ImagerPro software. All surveys were conducted using the Wenner array configuration using 64 electrodes with 2 m electrode spacing, apart from KAWRES5W which used 32 electrodes and had 3 m electrode spacing. Figure 53 and Figure 54 show images of resistivity data collection.

The resistivity system passes current through multi-channel electrode cables connected to a central control unit (Figure 53). The multi-channel electrode cables allow the initial current and electrical response to be isolated and recorded separate from each other. The electrode cables make contact with the ground through metal spikes planted into the ground and clipped on to the cable (Figure 54). Electrode contact was very good for all surveys conducted.

Figure 53: Campus Tigre resistivity unit and laptop protected within blue box

Figure 54: Photograph of electrode layout and electrode cable

Resistivity data were initially edited to remove any bad data points such as open electrodes and bad connections. Data were then processed by David Nobes and Hayden Mackenzie using the Res2DInv modelling software package.

5.2.2.2 Results

Resistivity results present a model which shows resistivity as a function of position and depth to minimise the misfit between the model resistivity response and the measured apparent resistivity. The uncertainty in the resistivity for each model cell was also obtained as well as the sensitivity of each cell to changes in the measured resistivity.

The results for line KAWRES1 are shown in Figure 55 as an example. All resistivity lines are appended (Appendix F).

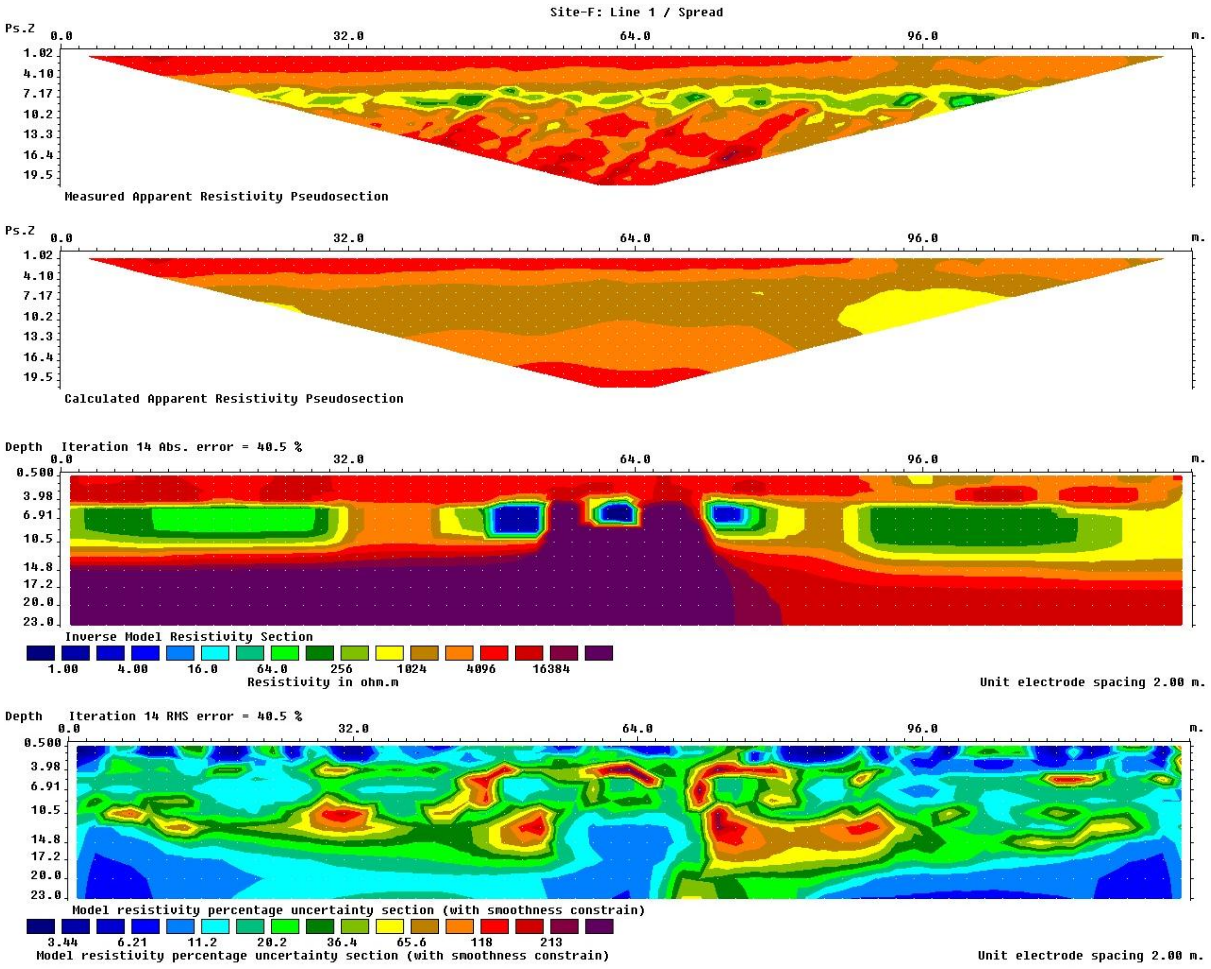

Figure 55: Typical resistivity profile showing various processing forms for resistivity line KAWRES1

5.2.2.3 Interpretation

Resistivity surveys are best interpreted alongside other geophysical data such as GPR. This was done in Kawerau and results identified the location of faults, these agreed well with GPR results, particularly in KAWRES1.
Measured apparent resistivity pseudosection in KAWRES1 show faults dipping in the same direction, angle and location as in the corresponding GPR profile (EPAD3).

5.3 Leapfrog model and LiDAR

Leapfrog 3D is a 3D geological modelling software package which has been developed in Christchurch, New Zealand by ARANZ Geo. Field and existing data were imported in to the Leapfrog Geothermal suite to bring data together in a way which enabled clear visualisation of the subsurface in three dimensions. This software is continuously being developed and a relationship was established with Leapfrog staff which helped develop the software to project what we wanted to see more clearly.

Leapfrog 3D made it possible to import interpreted GPR profiles and build faults into the model. Importing fault data into Leapfrog and having Leapfrog join interpreted locations of faults has highlighted that that the fault system through the field area is most likely en echelon or overlapping in structure and has variations in dip as the fault progresses. Figure 58 shows the two faults Leapfrog has interpreted, this shows a non-linear line with step overs and bends, this image lead to the realisation that this is more likely a series of faults, rather than just one or two main faults.
Adding geophysics profiles to the model allowed clear visualisation for comparison with aerial photographs and LiDAR which brings together different investigation techniques. This allows verification of interpretations of surface expressions as you can see if surface and sub-surface features correlate with each other.
Fault projection in three dimensions assisted planning for the second phase of field investigation as discussed in 5.4. Faults which had been buried by fluvial processes and agriculture were projected to surface and locations for hand auger investigations were planned.

Leapfrog does not currently support modelling of en echelon faults with ease which makes modelling these areas particularly difficult. However, the software quickly and clearly shows data effectively as it is provided. The model of the subsurface which was constructed using drill hole data does not exactly match that as drawn by Milicich, et al, 2011 (Figure 64) as the software does not

automatically take in to consideration the geologic behaviour and typical structures found in various lithologies such as rhyolite. This however is not a flaw in the software, but in the time the operator has to manipulate or modify data to suit the real life situation.

Light detection and ranging (LiDAR) data were added to Leapfrog to help with aerial photograph interpretation and analysis of topography. Adding LiDAR to Leapfrog made it possible to examine the data from every direction and provided realistic surfaces to tie GPR results to.
LiDAR is an airborne method of producing high resolution topographic data. LiDAR was flow over the field area in 2006. The full survey included ~123.25 × 10^6 last return (ground) points with an average separation of ~1.2 m (Begg & Mouslopoulou, 2010). The project was designed to return, for each derived point, vertical and horizontal accuracies of ~0.15 and <0.55 m, respectively (Begg & Mouslopoulou, 2010). Ground truthing of interpolated point data, using conventional survey methods includes a standard error (RMS) altitude accuracy of 0.045 m and an error for the horizontal measurements of 0.05 m (Begg & Mouslopoulou, 2010). LiDAR data were obtained from Environment Bay of Plenty (EBoP) in August 2010 and were examined to help understand the topography of the field area. The LiDAR dataset obtained was only a subset of the full survey and only covered a limited area around Kawerau (Figure 60).

LiDAR data added significantly to interpretation of aerial photographs by making it possible to identify and examine subtle changes in elevation in the landscape. If patterns were identified in the aerial photographs, LiDAR was often used to confirm these patterns (Figure 61).

Figures 56 to 63 show some of the findings from 3D modelling in Leapfrog.

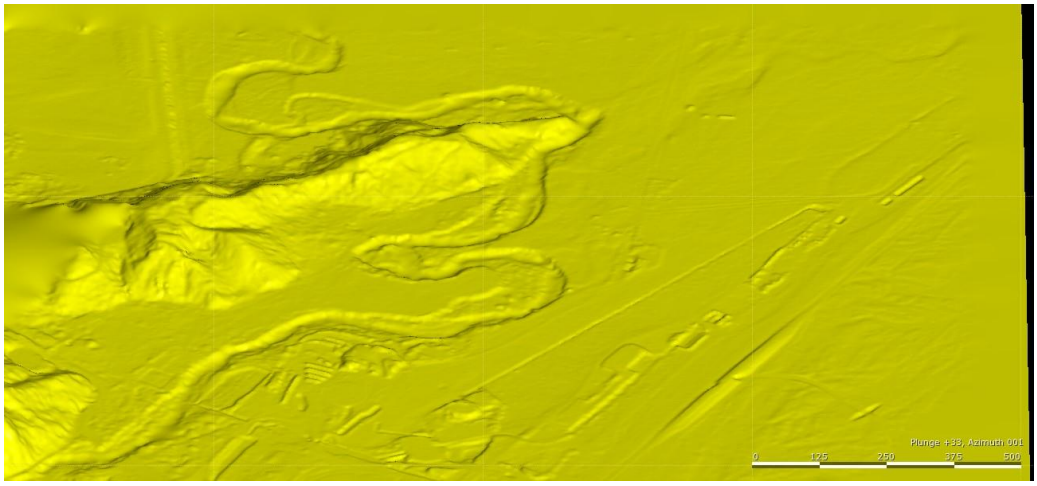

Figure 56: LiDAR image projected in Leapfrog 3D

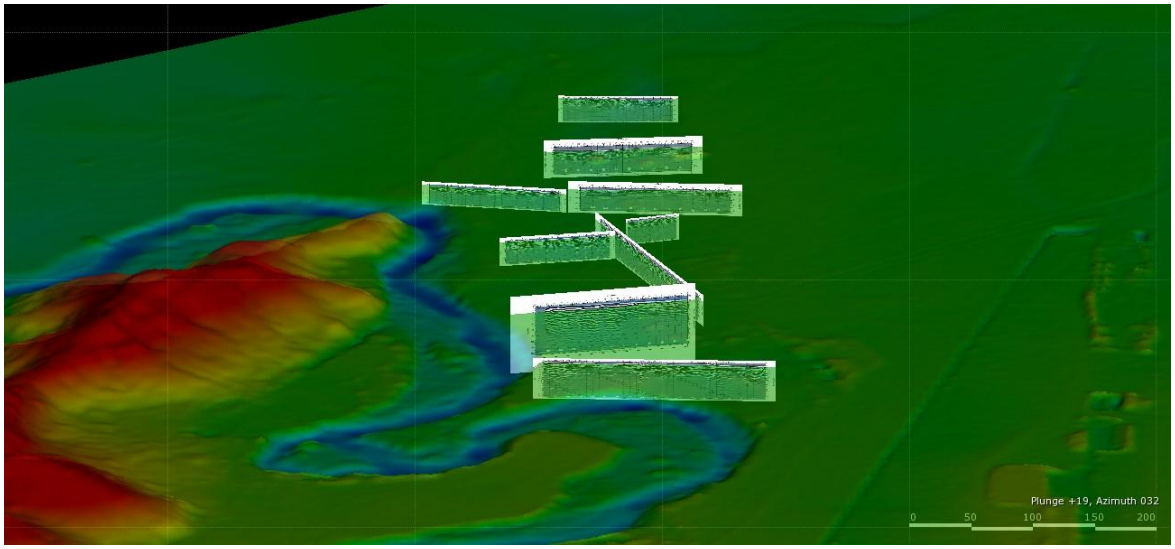

Figure 57: 3D image of LiDAR and GPR profiles, this allows clear visualisation of sub-surface profiles. GPR profiles are appended (Appendix E)

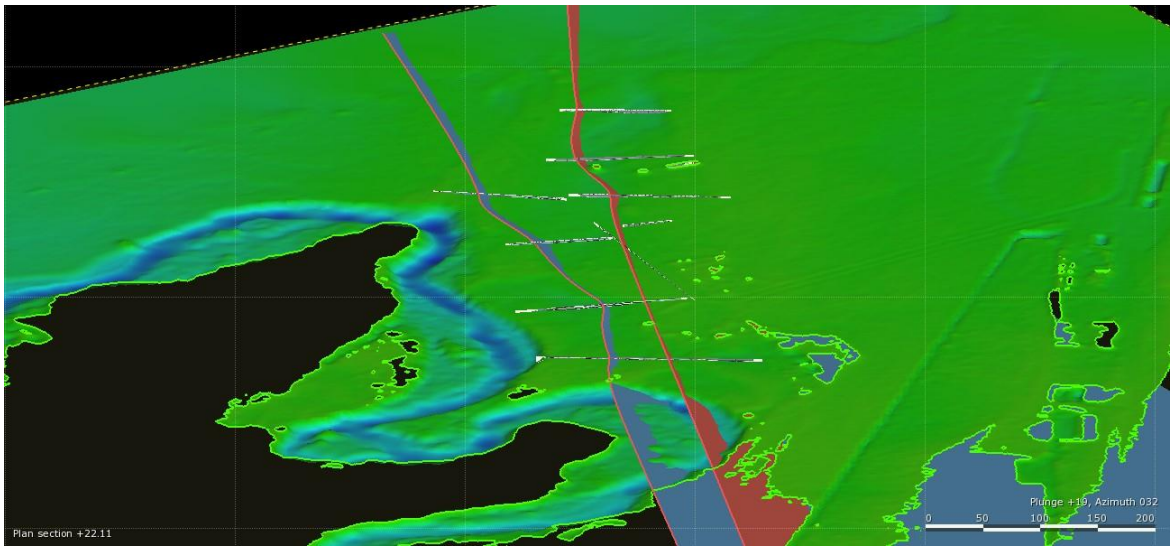

Figure 58: Projection of faults to the surface as extrapolated from GPR profiles. The irregular shape and stepovers suggest en echelon or overlapping faults. GPR profiles are appended (Appendix E). This figure does not show predicted fault location, but was used as a tool to identify fault morphology. With further processing of data, this could show more accurate fault locations.

Figure 59: Adding aerial photographs to LiDAR and GPR profiles allow the viewer to see low points in the landscape and where the potential faults meet the surface

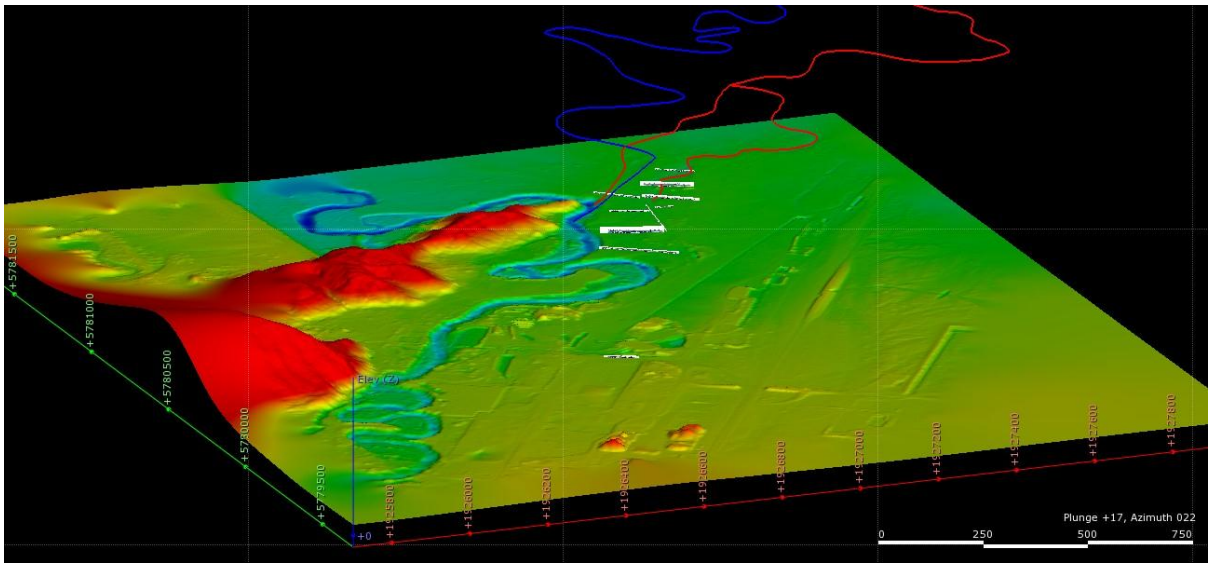

Figure 60: Full view of LiDAR data set and GPR profiles. Leapfrog 3D also allows you to import GIS files such as the ones here which show the pathways of old rivers (Tarawera River is the blue line)

A

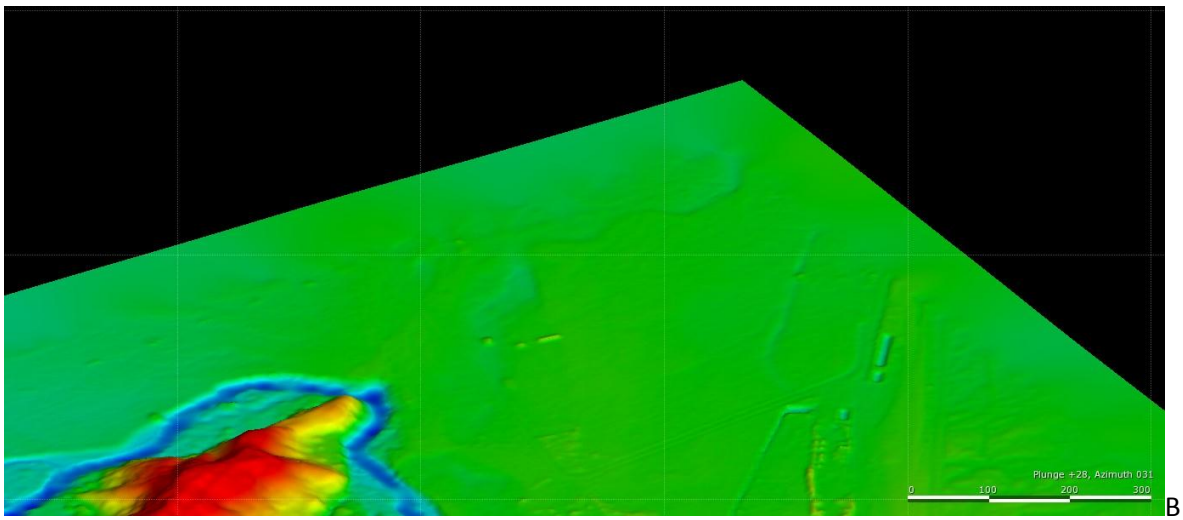

B

Figure 61: Leapfrog images of A: Aerial photograph of suspected river channels (centre of image) and, B: LiDAR image which shows there is a change in elevation around the location of possible river channels

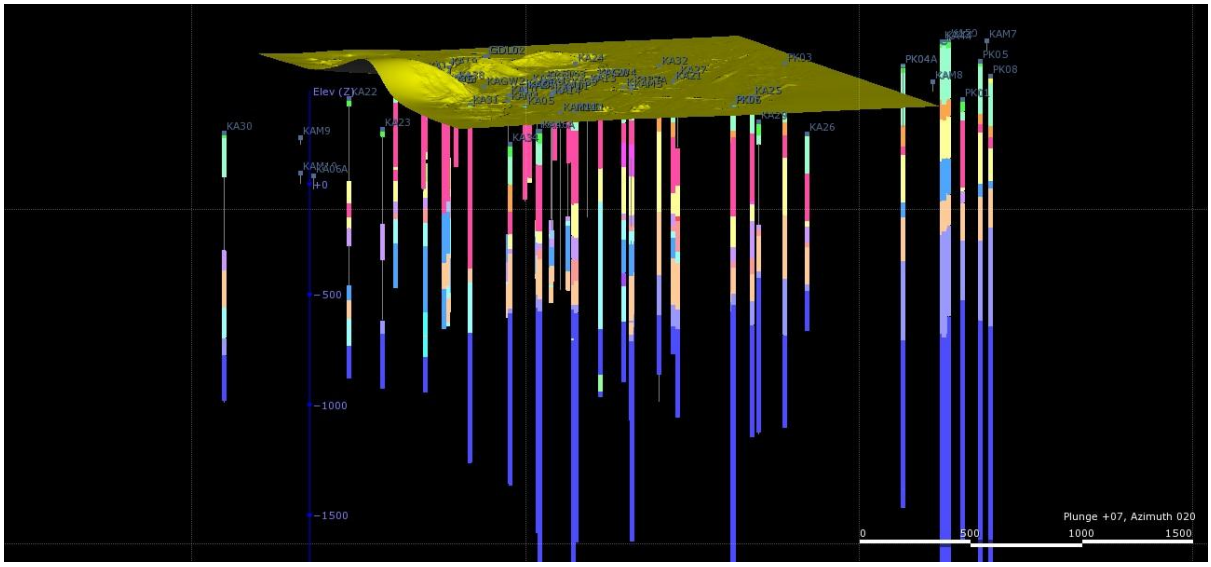

Figure 62: Drill hole data can be imported in to Leapfrog 3D

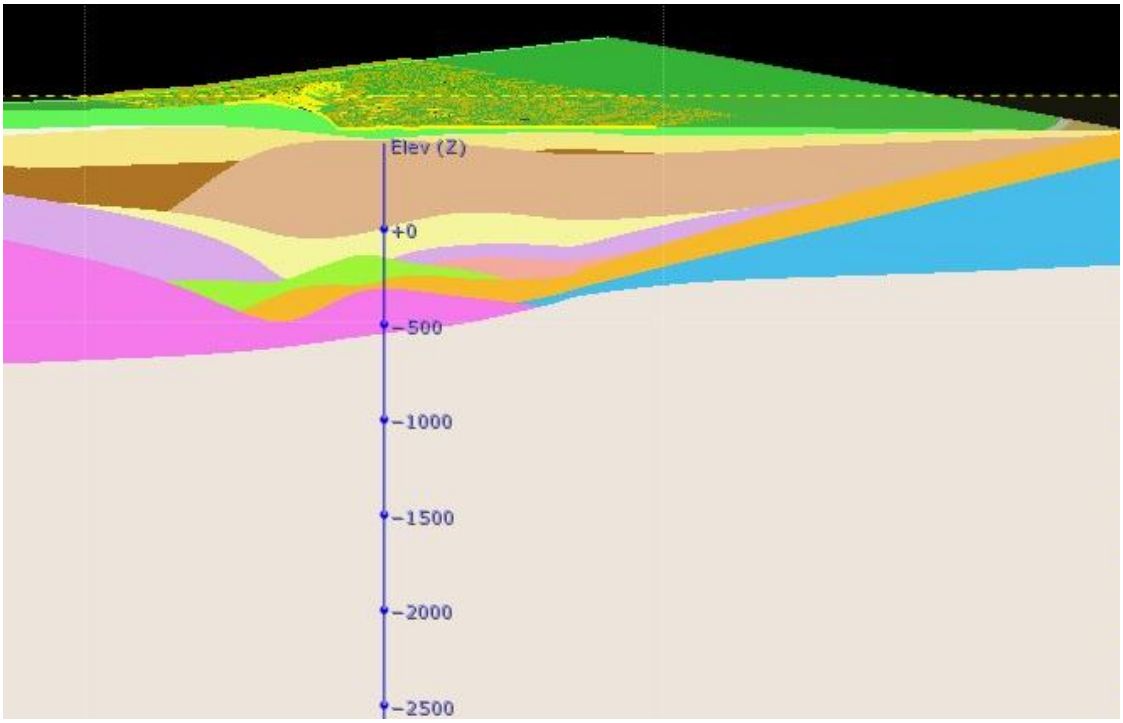

Figure 63: Drill hole data can be interpreted to model features and lithology. This figure shows an unmodified or processed model made purely from drill hole data with no faults added. The figure has close resemblance to the most up to date geological model of the area.

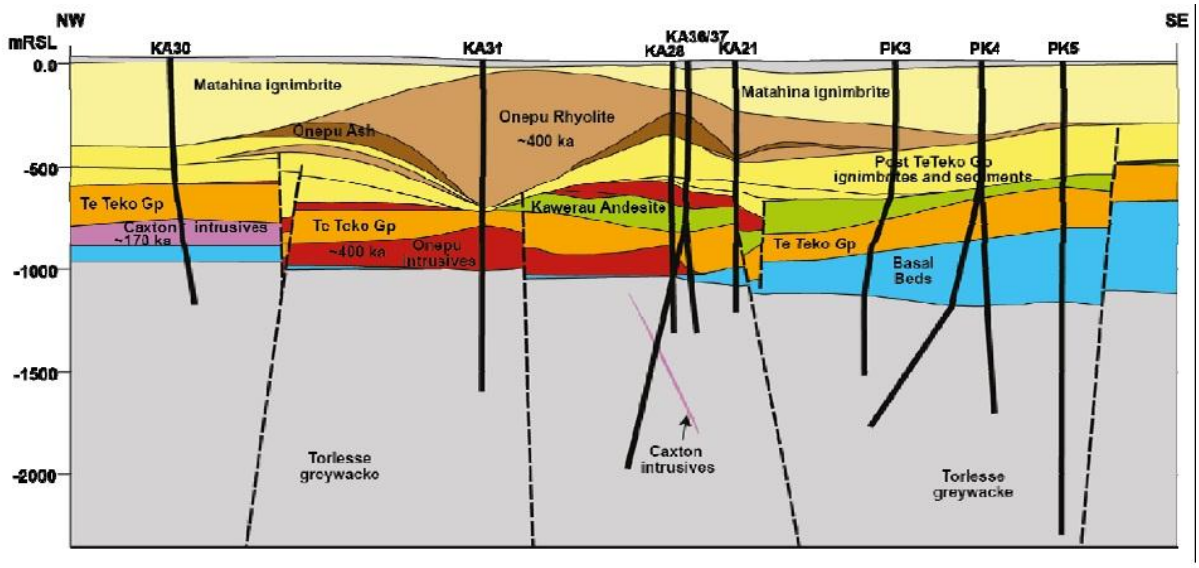

Figure 64: The most recent geological model of the Kawerau Geothermal Field (Milicich, et al., 2011) shows close resemblance to the unprocessed Leapfrog model (Figure 63).

5.4 Invasive investigation

An invasive investigation program was carried out to validate the GPR survey and to collect samples for laboratory testing. The invasive investigation included hand augering and face logging. The field investigation took three days between November 7th and November 9th 2011.

Initially the invasive investigation was to include test pits and a drill hole, but due to land access and time constraints this was not possible.

5.4.1 Hand auger and face logs

Twenty hand auger holes were dug in the field area between November 7th and November 9th 2011 in hot sunny weather. Figure 65 shows the location of auger and face logs. Hand auger holes were arranged along GPR lines, across significant subsidence bowls and in specific areas of interest such as where faults were expected to reach the surface. One calibration hole was dug out of the known subsidence bowls.

Face logging was carried out on five exposures across the field area. These were on the side of the Tarawera River and in stream channels and acted as faster methods than hand augering. Face logs provided clear examination of structure of the deposits in the near surface environment and an opportunity to photograph the deposits structure.

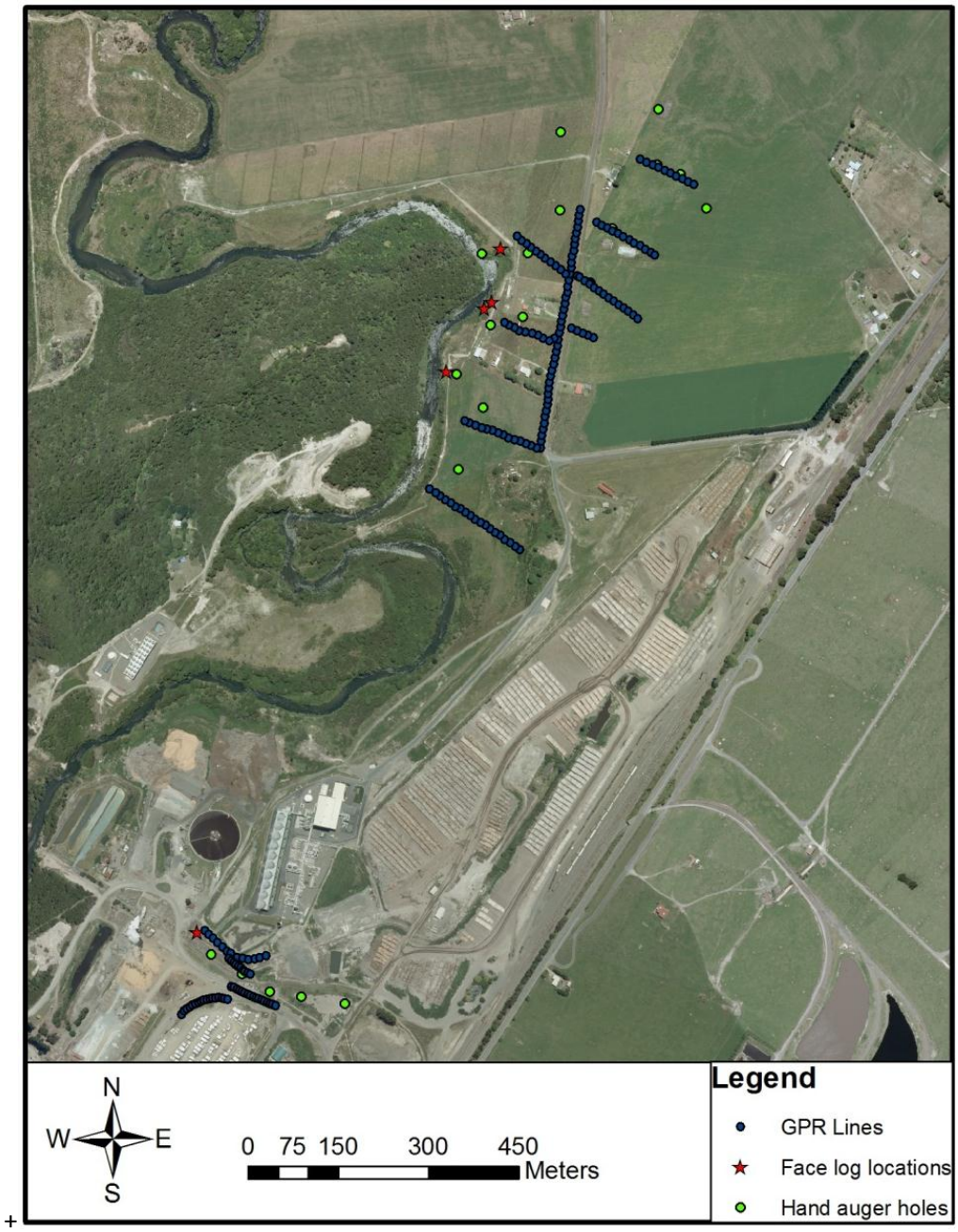

Figure 65: Location of hand auger holes and face logs

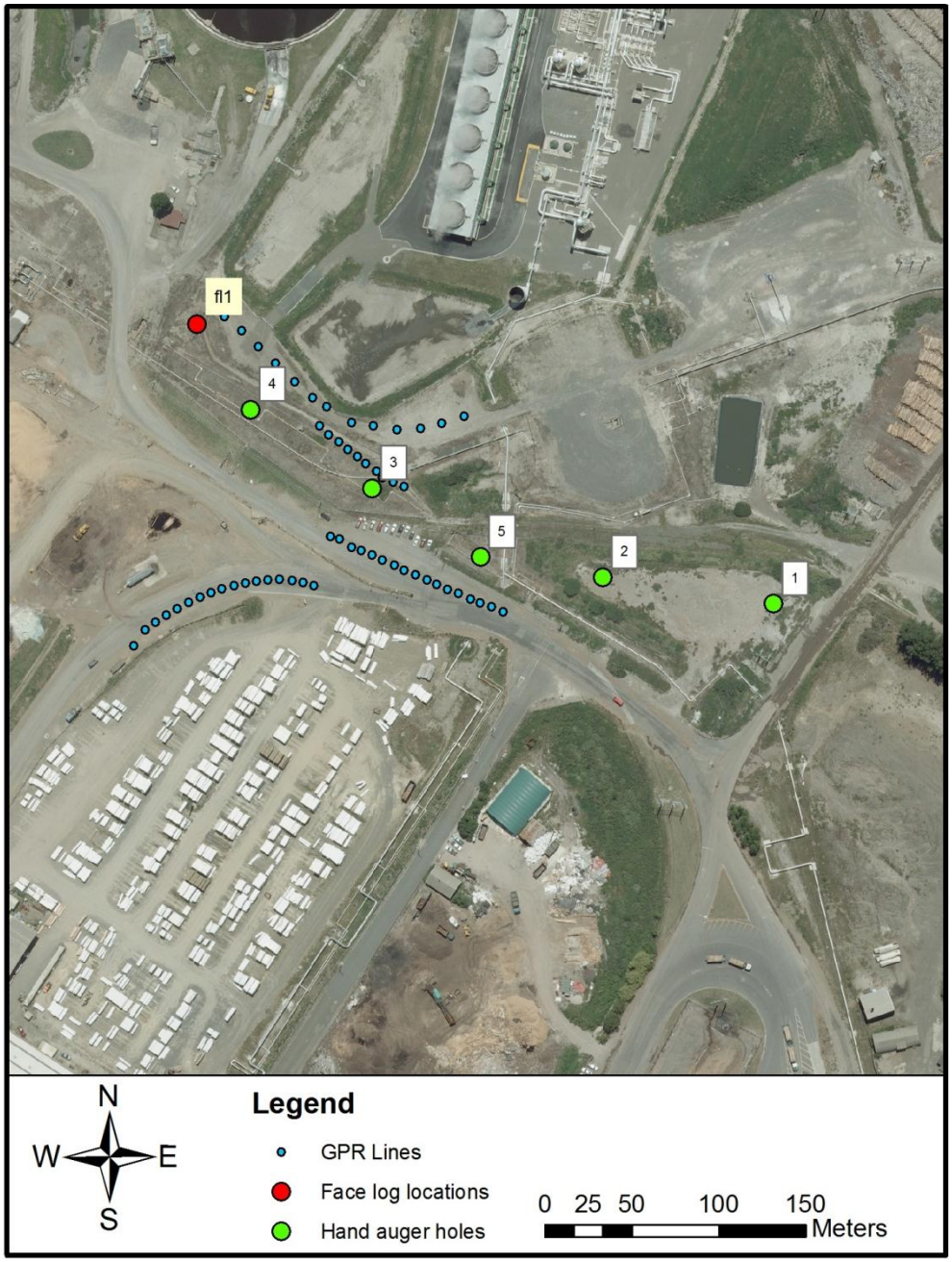

Figure 66: Location of hand auger holes and face logs at Site 1

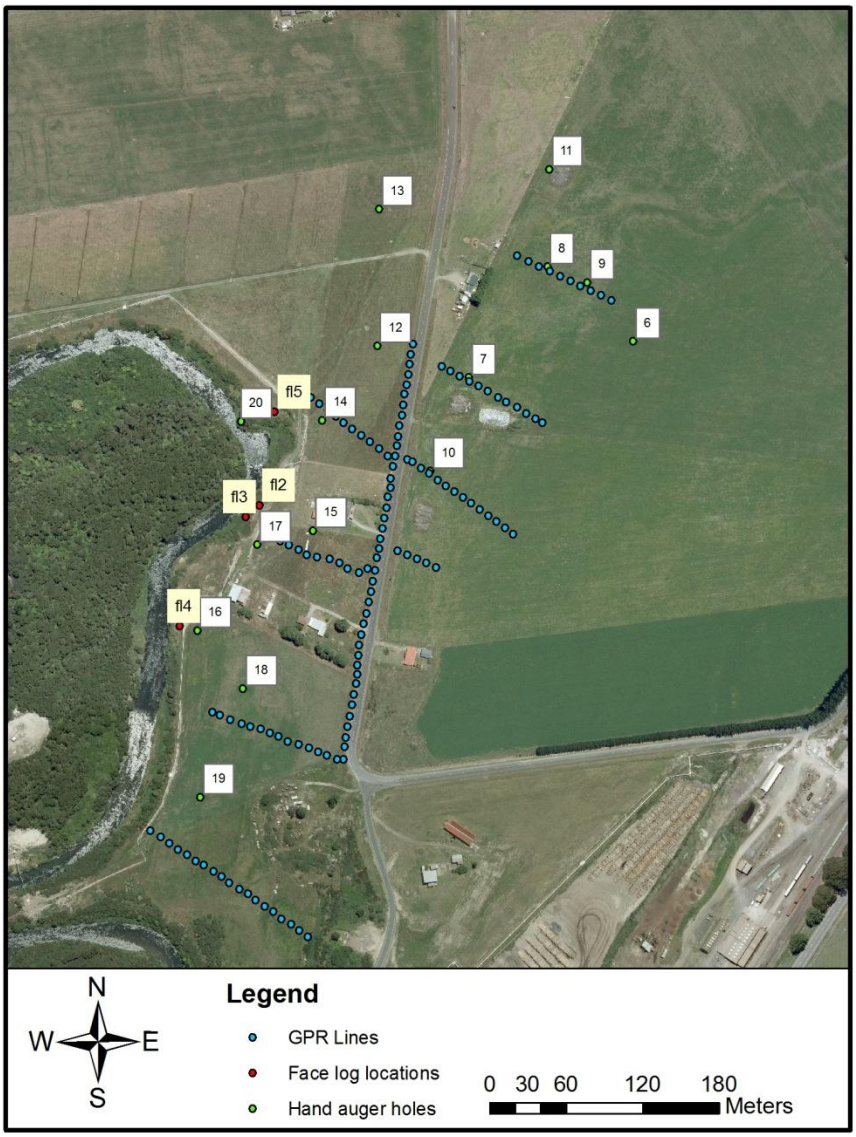

Figure 67: Location of hand auger holes and face logs at Site 2

5.4.1.1 Test procedure

Two hand augers were taken to Kawerau from the University of Canterbury to carry out the hand augering investigation. Hand augers consist of a shaft, handle, and auger head and are manually turned and pushed in to the ground to create a hole and recover a sample. When the shaft runs out of length, additional rods can be added to extend the length of the auger shaft. The auger can only dig approximately 5 to 10 cm at a time and needs to be regularly lifted out of the hole to empty the sample on to a prepared surface.

In Kawerau, sites were chosen on a map and locations were noted and found using GPS. Hole locations were then marked with spray paint and/or a stake in the ground so they were easy to find.

A tarpaulin was laid then down next to the hole for samples to be placed on to give a clean surface for photographing against and making it easy to back fill the holes once augering was complete.

The hole was started with a spade and augering commenced and progressed until either a target depth or lithology was hit, or the hole collapsed in on itself and time constraints did not allow progression.

Once the end of the hole was reached, the hole was measured for depth, a tape measure laid down next to the removed samples and photographed. Removed samples were then logged and sampled. Finally the hole was back filled to restore the original ground cover.

Figure 68: Photograph of hand auger in operation

Figure 68 shows the hand auger in operation – auger head is in the ground, samples are being laid out on a tarpaulin which is being held down by spare rods which are used when the hole becomes deeper.

Figure 69: Image of a soil auger head similar to what was used in Kawerau (AMS, 2011)

Face logs were carried out by clearing the face of existing banks to a depth which removed all topsoil and organic material to expose sediment beneath. Faces were cleared with a shovel to near a vertical angle to provide a clean face to log off and to photograph and provide accurate depths.

A tape measure was placed on the face for reference and the face was photographed and logged with the same descriptions as the hand auger logs (Figure 70).

Once face logs had been described the area was restored as close as possible to its original condition.

Figure 70: Face log 1

5.4.1.2 Results

Most auger holes returned light brown, greyish coarse sandstone with a wide range of grain sizes from mud to cobble. Sand was primarily comprised of quartz, pumice, scoria and volcanic glass, with volcanic glass content increasing in auger holes that were located close to the Tarawera River. All holes were moist and had very loose material which could not support itself and commonly collapsed into the holes.

Perched water tables were encountered in holes 18 and 19 which coincided with very soft layers and an area identified for subsidence in the levelling surveys. Below the perched water table, sand was

encountered which was primarily dry. The hand auger pushed through the soft layer approximately 400 mm with very little effort in these holes.

A distinctive change in colour and lithology separated by a very thin (20 – 100 mm) layer of fine grained, puggy material was identified in holes 8 and 10. These lithology changes coincided with where faults had been interpreted in GPR lines EPAD1 and EPAD2 (see Appendix E). This intersection has been interpreted as the identification of faults; however more work would need to be done to confirm this. Further work is discussed in 7.3.

Occasionally dark, organic horizons were encountered; these usually had granules and pumice within them and were black in colour, occasionally with bark and other organic material.

There was no clear evidence of concrete, metal or large amounts of wood fibre in any of the hand auger holes as expected, although speaking to local farmers, this is expected in other areas outside the field area. All sediment encountered appeared in situ.

Figures 71 to 73 show logs of three typical auger holes. All auger logs are appended (Appendix G).

	Hole 3			
	Depth (m)		Thickness	Description
	From	To		
	0.00	0.03	0.03	Soil: Topsoil and grass
	0.03	0.26	0.23	Clay: Creamy, whiteish, very uniform grain size, chalky feel
	0.26	0.30	0.04	Bark
	0.30	0.43	0.13	Soil: Soil and wood fibre, organic
	0.43	1.07	0.64	Clay: Medium grey clay, clay to silt size grains. Very puggy and soft, chalky feel and occasional pumice grains
	1.07	1.45	0.38	VCSS: Very coarse sandstone, black. Organic layer with very coarse grains throughout. Gradational basal contact.
	1.45	2.16	0.71	CSS: Coarse sandstone, medium grey, brownish. Fine to very coarse grains and occasional cobble sized pumice. Very friable.
	2.16	3.00	0.84	CSS: Coarse sandstone, light brown, greyish. Fine to granule sized grains. Occasional cobble sized pumice. Very loose and friable. Collapsing in to hole.

Figure 71: Hand auger log for Hole 3

	Hole 8			
	Depth (m)		Thickness	Description
	From	To		
	0.00	0.20	0.20	Soil: Topsoil, light brown
	0.20	1.70	1.50	MSS: Medium sandstone, come coarse sand lenses. Light brown, greyish. Moist, loose.
	1.70	1.80	0.10	ZST: Siltstone, sandy, light brown, greyish. Moist to wet. Possibly fault gouge
	1.80	2.10	0.30	CSS: Coarse sandstone, minor granule. Dark grey, brownish. Moist. Sub-rounded to sub-angular. Possibly buried soil horizon.
	2.10	2.12	0.02	ZST: Siltstone, sandy, light brown, greyish. Moist to wet. Possibly fault gouge
	2.12	2.80	0.68	VCSS: Very coarse sandstone. Light brown, firm, moist, sub-angular to rounded.

Figure 72: Hand auger log for Hole 8

	Hole 10			
	Depth (m)		Thickness	Description
	From	To		
	0.00	0.20	0.20	Soil: Topsoil, sandy, light brown
	0.20	0.90	0.70	VCSS: Very coarse sandstone, very coarse sand to granule, light brown, moist, sub-rounded to sub-angular
	0.90	1.00	0.10	ZST: Siltstone, brown, reddish, moist. Possibly fault gouge
	1.00	2.20	1.20	VCSS: Very coarse sandstone, very coarse sand to pebble. Light brown. Lenses of lighter coloured material, moist, firm. Rounded to sub-angular.

Figure 73: Hand auger log for Hole 10

5.4.1.3 Interpretation

The presence of pumice and volcanic glass in sediments clearly identify that the near surface sediment is of volcanic origin, the increase in volcanic glass closer to the Tarawera River suggest that the sediment of the plains near Kawerau is provided from more than one source or that the sediment has been the result of sporadic increases in sediment supply. This agrees with the supply of sediment being from the Tarawera River and the Rangitaiki River and an increase in sediment supply in the catchment due to volcanic eruptions.

The range of grain sizes from mud to cobble indicates variations in depositional environment over short distances, created by systems such as meandering streams or rivers and changes in flow velocity or source. This agrees with the sourcing of sediment from various volcanic events which transport material with both fluvial and aeolian mechanisms. The 1904 outbreak flood which covered the plains in fine silt (Gibbons, 1990); (Hodgson & Nairn, 2003); (White, et al., 1997) will have provided large amounts of volcanic material to the Kawerau area. The range of grain sizes could be explained by change in flow rates in the depositional environment as the field area is near where rivers change from deeply incised channels in steep terrain, to low gradient, meandering rivers on the plains. With a higher water table in the past and occasional situations of lake-like conditions (Gibbons, 1990), the flow rate would drop considerably upon reaching the Kawerau area, allowing fine grained material to settle, larger grains would be supplied by flood and/or eruption events.

Perched water tables which were identified in holes 18 and 19 (see Appendix G) coincided with a silt layer and were underlain by dry, coarse sand. The perched water table is likely to be due to very low permeability in the silt which would prevent meteoric water infiltrating past the silt layer. This is discussed further in 5.5.

The very loose nature of the sand encountered suggests low clay content and limited compaction post-deposition to help bind the sediment. The loose sediment in auger holes agreed with what was seen in face logs and examination of the banks of the Tarawera River (Figure 74 and Figure 75). This indicates that without groundcover, the sands within the field area would readily erode.

Black, scoria rock has been identified as basaltic scoria from the 1886 Tarawera eruption, this has often been reworked into other layers and is common in the top 2 – 3 m of the field area. The main layer encountered across the field area is a light brown, sometimes orangeish sand with grain sizes ranging from silt to cobble, the unit is very loose and friable and consists of quartz, pumice, some basaltic scoria and some volcanic glass. Examination of this unit by Jim Cole and Hayden Mackenzie identified it as eruption material from the 1314 Kaharoa eruption.

Hand auger and face log investigations have helped identify geologic processes and environmental settings associated with the development of the Rangitaiki Plains. Hand auger holes proved interpretation and ground truthed the geophysical investigation. Hand augering provided an opportunity to gather samples for lab testing, identified perched water tables and zones of very soft ground which were also identified in CPT investigations (See 3.4).

Hand auger and face logs provided an opportunity to examine grains for roundness and composition. This showed that most samples were sub-angular to angular for hard minerals such as quartz, while pumice was sub-rounded. This shows variation in distance from the supply source, but also that the supply was generally not too far away. A wide range of grain sizes was identified from hand auger holes which show that there were both fluvial and aeolian transport mechanisms depositing sediment at the site.

Figure 74: Tributary to the Tarawera River - the incised channels show the ready erodability of the material around Kawerau

Figure 75: Photograph of the banks of the Tarawera River showing very loose sand eroding easily into the river

5.5 Laboratory investigation objectives and approach

To support field investigations, laboratory testing was conducted to further define the material properties of near surface lithologies within the field area. Objectives of the laboratory investigations are:

- To characterise materials in terms of their clay mineralogy and particle size distribution
- To determine the plasticity index of non-sand samples
- To test the permeability of materials and relative infiltration rates

Samples tested in the laboratory were collected from various hand auger holes between the 7th and 9th of November 2011. Samples were all collected as disturbed samples.

Material characterisation testing was carried out at in the engineering geology laboratories at the University of Canterbury, Christchurch.

5.5.1 Sample history

Samples between 300 and 500 grams were collected for laboratory analysis. Samples were chosen as representative for each major lithology encountered as well as any areas that were soft or appeared different from surrounding lithologies.

To minimise changes in water content, large samples collected from augering were placed in plastic sample bags, then sealed with a cable tie. All samples were then sealed in a plastic bucket and couriered to Christchurch from Kawerau. Once in Christchurch, the buckets were stored in a dark cupboard until ready to use.

5.5.2 Water content

In-situ water content was determined for a number of samples upon returning to Christchurch. In-situ water content allows comparisons of the plasticity index to field measurements and helps define the material properties of samples.

5.5.2.1Test procedures

Water content is determined by first weighing a container, then filling the container with a wet sample and re-weighing the container, the container is then placed in an oven for 24 hours to allow the sample to dry out, and the container is weighed again. The difference in wet weight and dry weight gives the amount of water in the sample and can be calculated using Equation 1.

$$W = ((M_2 - M_3) \div (M_3 - M_2)) \times 100$$

Equation 1: Water content

Where:

M_1 = mass of container (g)

M_2 = mass of container and wet soil (g)

M_3 = mass of container and dry soil (g).

Tests were carried out in accordance with New Zealand Standard NZS4402: 1986: Test 2.1.

5.5.2.2 Results

Water content for various samples is presented in Table 7.

Table 7: Water content for various samples

Sample	Hole	Depth (m)	Lithology	Water content (%)
1	2	2.6-2.7	Siltstone	25.85
2	3	0.3-0.4	Clay	51.01
3	3	0.5-0.75	Clay	67.28
4	3	2.6-3.0	Coarse sandstone	13.68
5	5	1.2-1.5	Peat	56.23
6	8	1.7-1.73	Siltstone – possible fault gouge	44.61
7	13	0.25-0.4	Very coarse sandstone	10.70
8	13	0.8-0.85	Siltstone – possibly fault gouge	31.57
9	13	1.2-1.4	Medium sandstone	20.05
10	19	0.4-1.0	Siltstone	50.39
11	20	0.4	Clay	26.83
12	FL4	0.4-0.8	Very fine sand	19.11

5.5.2.3 Interpretation

Water content results show that all samples are moist; some samples have as much as 67% water content. This shows that the subsurface at Kawerau is being recharged regularly or stores water well. Water content results show that there is not likely to be a large percentage of clay in samples as clay can often have water contents of 200 – 300 %. Samples described as clay in the field logs are more likely to be silty.

The results of water content are important when put in context with other laboratory results.

Water content in the sediment however does show that there is room for compaction.

5.5.3 Atterberg limits

Atterberg limits test determine the liquid and plastic limits of soils. The liquid and plastic limits define the water content boundary between the non-plastic, plastic and viscous fluid states. This helps describe the properties and possible behaviours of the soil.
Atterberg limits are determined using two tests; the first is the cone penetrometer which determines the water content at the plastic – viscous fluid boundary. The second test is to determine the water content at the non-plastic – plastic boundary.
The Atterberg limits are used to find the plasticity index of fine grained engineering soils by **Error! eference source not found.**).

Plasticity Index (PI) = Liquid Limit (LL) – Plastic Limit (PL)

Equation 2: Plasticity index

5.5.3.1 Rolled threads of soil for plastic limits test

Rolling a thread with a soil sample determines if a soil can behave as a plastic and what the plastic limit of the soil is. This is the first half of the Atterberg Limits test.

5.5.3.1.1 Test procedures

The following section describes the procedures that were undertaken to determine the plastic limit of samples by rolled thread method. This description is simplified; testing was carried out in accordance with New Zealand Standard NZS 4402:1986 Test 2.3.

A soil sample is taken and rolled in to a ball between the fingers, then rolled between the palms of the hands until small cracks appear on the surface of the sample. The sample is then split in half and placed on a glass plate and rolled under the palm of the hand to form a thread about 3 mm in diameter. The sample should shear both longitudinally and transversely as it gets to 3 mm diameter. This is repeated with both samples, then water content of samples is determined as described in 5.5.2.

5.5.3.1.2 Results

Summarised results are shown in Table 8. Full results and calculations are appended (Appendix H).

Figure 76: Rolled thread breaking apart

5.5.3.1.3 Interpretation

Results for the plastic limit test indicate that the soils tested do not have very plastic behaviour which could be due to the inclusion of grains larger than silt sized particles. Rolling a thread proved difficult and great care was required not to break the sample apart before it got to 3 mm diameter.

5.5.2.1 Cone penetrometer test for liquid limit

Cone penetrometer tests were carried out on 7 samples and works by pushing a cone into a prepared sample of soil at various water contents. This determines the water content at which the cone penetrates the soil 20 mm, which is the liquid limit. This is the second half of the Atterberg Limits test.

5.5.3.2.1 Test procedures

The following section describes the procedures that were undertaken to determine the liquid limit of samples by cone penetrometer method. This description is simplified; testing was carried out in accordance with New Zealand Standard NZS 4402:1986 Test 2.5.

1. A sample was placed in a mixing bowl and mixed thoroughly, if originally dry, water was added (Figure 77)
2. The sample was placed in a cone penetrometer cup (Figure 78)
3. The sample was placed under the cone (Figure 79)
4. A release button was pressed which pushed the cone in to the sample for 5 seconds, then clamped the cone in place
5. The distance the cone penetrated the sample was measured to 0.01 mm and recorded (Figure 80)
6. A sample of soil was taken from around where the cone penetrated the soil for water content measurement
7. The sample was removed from the cup and re-mixed and steps 2 – 6 were repeated twice more
8. The sample was returned to the mixing bowl and more water was added and mixed in thoroughly
9. Steps 2 to 8 were repeated three more times until four measurements at different water contents were measured
10. Samples were then measured for water content (5.5.2) and plotted on a graph of penetration vs. water content. The point where the trend line crosses 20 mm of penetration is the liquid limit of the soil.

Figure 77: Soil sample is mixed thoroughly

Figure 78: Sample is placed into cone penetration cup

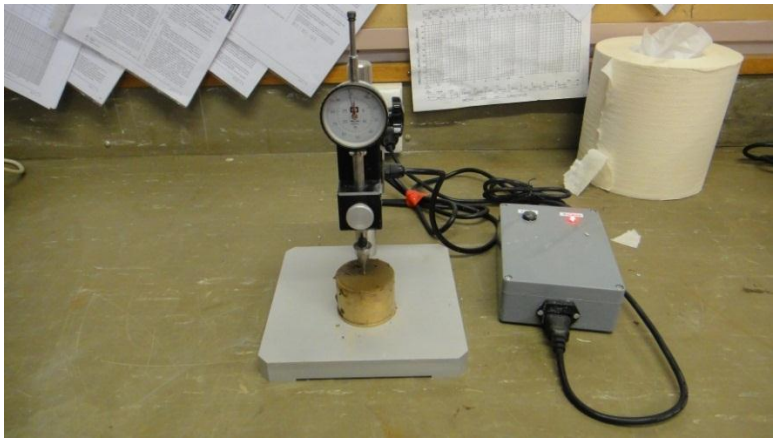

Figure 79: Cup is placed under cone, button on grey box to the right is pressed and cone pushes into sample

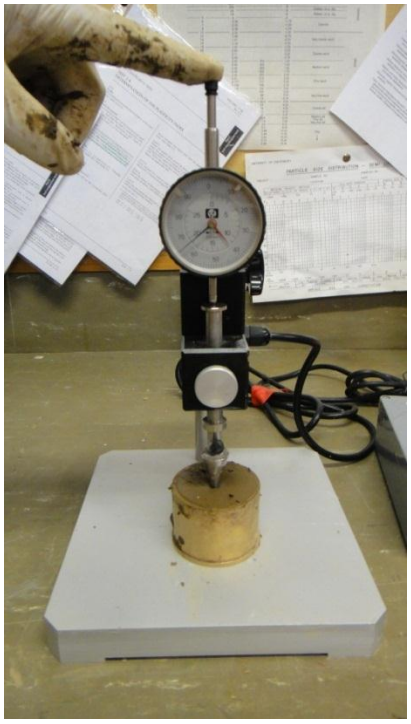

Figure 80: Penetration distance is measured

5.5.3.2.2 Results

Summarised results are shown in Table 8. Full results and calculations are appended (Appendix I).

5.5.3.2.3 Interpretation

Results for cone penetrometer tests showed the liquid limit of the soils have a water content which ranges between 45 and 65 per cent. This is a low value in relation to clays where the liquid limit in bentonites can be upwards of 400%. This is an indication that the samples do not have high clay content, or that the clay sized particles are actually volcanic glass shards (see 5.5.6).

5.5.3.3 Plasticity index

Following tests for plastic and liquid limits, the plasticity index was calculated using Equation 2.

Table 8: Plasticity index for samples tested for Atterberg limits

Sample	*Hole*	*Depth*	*Lithology*	*Liquid Limit*	*Plastic Limit*	*Plasticity Index*
1	3	0.45-1.00	Clay	64.5	53.10	11.40
2	3	0.03-0.25	Clay	52.75	44.60	8.15
3	18	0.9-1.4	Silt	50	41.42	8.58
4	19	0.4-1.0	Silt	52.75	52.60	0.15
6	20	2.8	Clay	48.35	40.84	7.51
7	20	1.8	Clay	45.75	37.77	7.98

Results show that samples are generally non plastic to low plastic indicating that they are most likely to be silt to sand sized grains.

Results have also identified that two thirds of samples have a liquid limit higher than 50%. It is generally accepted that soil materials with liquid limits greater than 50% exhibit high compressibility (Terzaghi, et al., 1996).

5.5.4 Emerson Aggregate Test

The Emerson Aggregate Test (EAT) is a test for dispersivity of soils. If water is added to, or drained from dispersive soils, the soil will readily move, become unstable or flush from the system, leaving more pore space between larger grains and allowing them to consolidate. Dispersive soils are readily erodible and may cause tunnel gullying.

5.5.4.1 Test Procedures

The Emerson Aggregate Test is a simple test where samples of soils are made in to a cube 5 – 10 mm in diameter, dried out, then placed in to a beaker of distilled water (Figure 81) and observed for changes after 2 and then 20 hours. Levels of slaking (Figure 82) and dispersion (Figure 83) are then recorded. A second test may be carried out with un-dried samples as determined by a flow chart (Appendix J). The time and way samples slake or disperse determine its classification number.

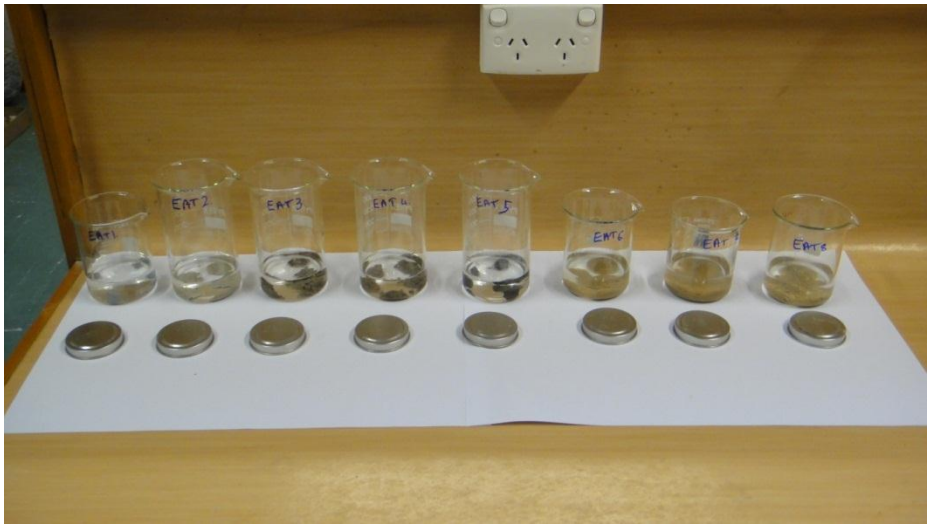

Figure 81: Soil sample cubes in distilled water

Tests were carried out in accordance with test number P9, Department of Sustainable and Natural Resources, Environment New South Wales (Appendix J).

5.5.4.2 Results

Table 9: Emerson Aggregate Test results summary

Sample	*Hole*	*Depth*	*Lithology*	*Class*
1	3	0.45-1.00	**Clay**: Medium grey clay, clay to silt size grains. Very puggy and soft, chalky feel and occasional pumice grains	8
2	3	0.03-0.25	**Clay**: Creamy, whiteish, very uniform grain size, chalky feel	3
3	18	0.9-1.4	**ZST**: Siltstone, medium grey, brownish. Light brown at base. Increase in moisture to base. Puggy in basal 300mm. Very soft - auger pushed through approximately 0.4m with very little effort	3
4	19	0.4-1.0	**ZST**: Siltstone, medium brown, moist, slightly carbonaceous	3
5	5	1.2-1.5	**Peat**: Dark brown, blackish. Soft, saturated, organic peat material	3
6	20	2.8	**Clay**: Clay, silty. Brown. Firm. Grades from moist to wet at 2.3m	3
7	20	1.8	**Clay**: Clay, silty. Brown. Firm. Grades from moist to wet at 2.3m	3
8	20	3.5	**MSS**: Medium sandstone. Mud to granule. Light grey. Soft, occasional granules.	3

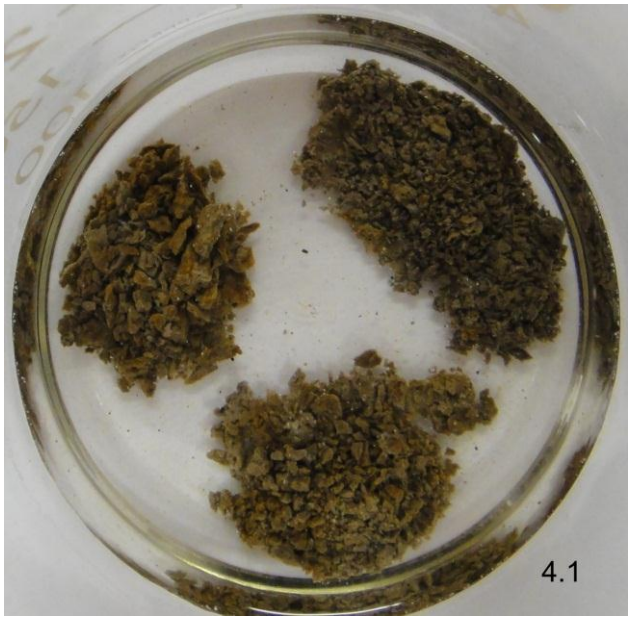

Figure 82: Slaked soil sample

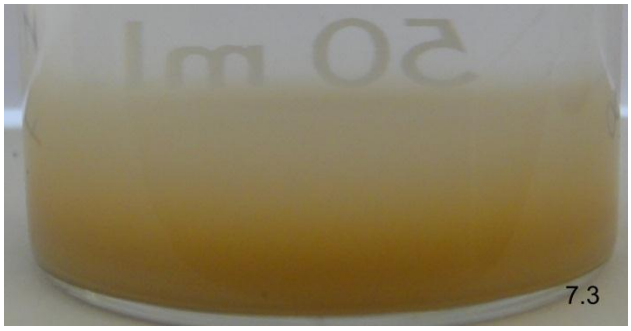

Figure 83: Dispersed soil sample

Full results and photographs are appended (APPENDIX K)

5.5.4.3 Interpretation

Results show that most samples are dispersive, however, samples were only dispersive when already wet and the level of dispersion varied considerably between samples. It is interpreted that samples will disperse and will very likely erode when water is added to the system.

5.5.5 Grain size distribution

Grain size distribution analysis shows percentages of grain sizes within a sample. This was carried out in the sedimentology laboratories at the University of Canterbury and involved dry sieving and laser sizing samples. Grain size distribution can help determine the deposition environment and material properties of samples.

5.5.5.1 Test procedures

The following section describes the processes that were undertaken to determine the grain size distribution of samples.

1. Samples were dried in an oven for 24 hours at 80°C
2. An empty beaker was weighed
3. A sample was placed in the beaker and reweighed
4. The sample was placed in a stack of 4 mm, 2 mm and 1 mm sieves and placed in a sieve shaker for 10 minutes (Figure 84)
5. Each grain size as separated by sieving was weighed again (Figure 85 and Figure 86)
6. A sample was taken from the bottom receiver tray (<1 mm grain size) and put in a vial for later analysis by laser sizer
7. Sodium hexametaphosphate was added to laser sizer samples to assist in separation of grains to allow laser analysis to be more accurate. Laser sizer samples were then shaken to separate grains.
8. Laser sizer samples were added to the laser sizer (Micromeritics Saturn DigiSizer 2 5205) (Figure 87) which processed samples and provided a printed report on grain size distribution (Appendix L).

Sieve sizes were chosen at the boundaries between pebble and granule (4 mm), granule and very coarse sand (2 mm) and very coarse sand and coarse sand (1 mm). The laser sizer can analyse samples up to 3 mm grain size, but to improve accuracy due to the small sample size you put in to the laser sizer, it was decided to sieve the samples to 1 mm first to reduce sample bias.

Figure 84: Sieve shaker

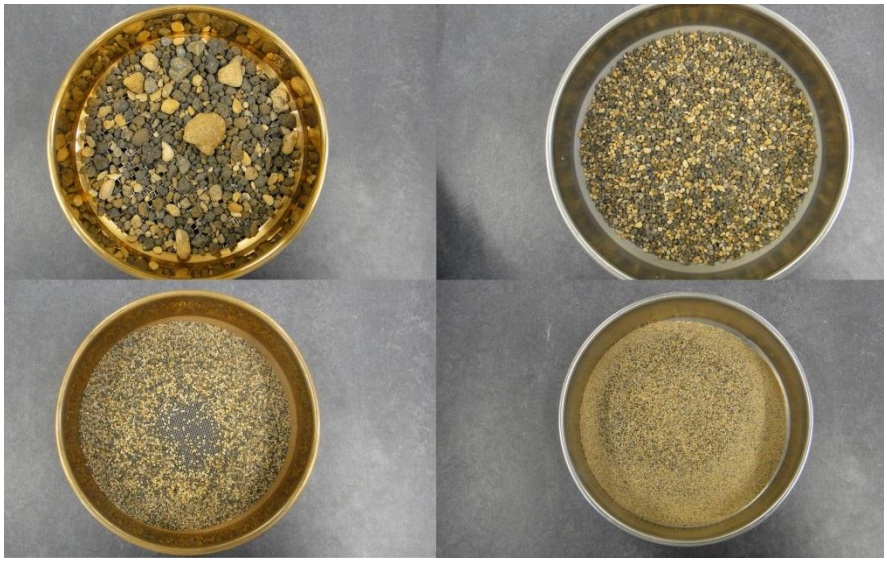

Figure 85: Sample after being in the sieve shaker - grains are sorted in to sieves depending on size

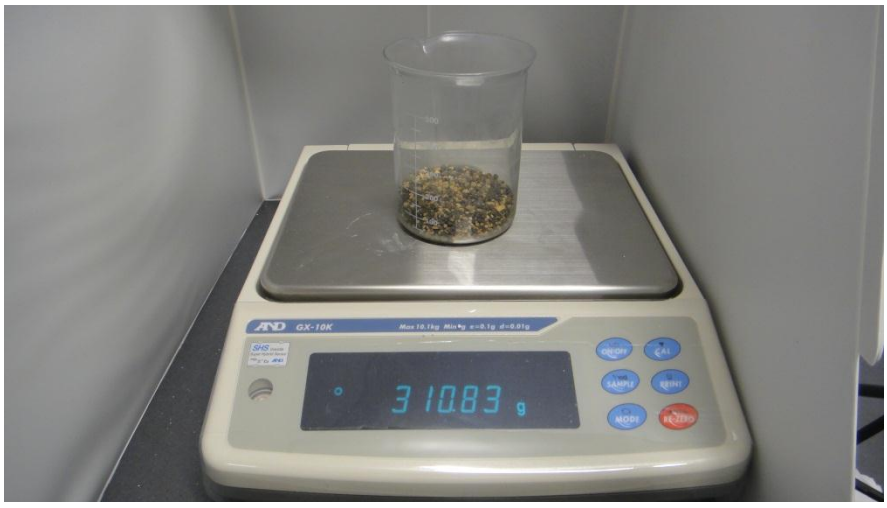

Figure 86: Each grain size is weighed to 0.01 of a gram

Figure 87: A sample of grains <1 mm is processed in the laser sizer

5.5.5.2 Results

Table 11 show the grain size distribution of samples from various hand auger holes in the field area.

Laser sizer graphs and full results are appended (Appendix L)

Table 10: Grain size distribution of samples from hand auger holes by sieving method

Sample	Hole	Depth (m)	Lithology	< 1mm (%)	< 2mm (%)	< 4mm (%)	>4mm (%)	>6mm (%)
1	3	0.45-1.00	**Clay**	**100.00**	0.00	0.00	0.00	0.00
2	3	0.03-0.25	**Clay**	**100.00**	0.00	0.00	0.00	0.00
3	18	0.9-1.4	**ZST**	**100.00**	0.00	0.00	0.00	0.00
4	19	0.4-1.0	**ZST**	**100.00**	0.00	0.00	0.00	0.00
5	5	1.2-1.4	**Peat**	**78.00**	10.85	7.67	3.06	0.00
6	20	2.8	**Clay**	**75.12**	18.81	4.73	1.52	0.00
7	20	1.8	**Clay**	**100.00**	0.00	0.00	0.00	0.00
8	20	3.5	**MSS**	**79.32**	12.24	6.07	1.81	0.00
9	20	0.4	**Clay**	**93.71**	3.74	1.75	0.18	0.00
10	FL4	0.4-0.8	**VFS**	**100.00**	0.00	0.00	0.00	0.00
11	12	0.9-1.2	**GRS**	**35.31**	19.24	18.22	22.08	5.01
12	FL2.2	1.0-1.3	**ZST**	**82.81**	6.41	6.46	4.06	0.00
13	19	2.9-3.1	**VCSS**	**42.07**	21.81	26.31	9.74	0.00
14	3	1.1-1.45	**VCSS**	**44.60**	22.98	20.37	12.24	0.00
15	19	1.3-1.8	CSS	11.44	5.77	0.34	**80.08**	0.00
16	11	0.3-0.5	**MSS**	**58.73**	12.08	12.03	16.90	0.00
17	FL2.1	1.2-1.4	VCSS	23.26	17.80	21.03	**37.66**	0.00

Table 11: Grain size distribution of samples from hand auger holes by laser sizer analysis of samples <1mm diameter

Sample	Hole	Depth (m)	Lithology	Particle diameter (µm)		
				Mean	Median	Mode
1	3	0.45-1.00	**Clay**	40.742	21.867	21.138
2	3	0.03-0.25	**Clay**	25.059	17.426	25.122
3	18	0.9-1.4	**ZST**	84.526	72.02	89.137
4	19	0.4-1.0	**ZST**	57.413	46.46	50.126
5	5	1.2-1.5	**Peat**	98.074	59.745	281.877
6	20	2.8	**Clay**	118.199	89.201	281.877
7	20	1.8	**Clay**	105.128	58.27	316.271
8	20	3.5	**MSS**	88.371	41.009	298.579
9	20	0.4	**Clay**	62.296	38.496	44.674
10	FL4	0.4-0.8	**VFS**	139.361	136.427	177.852
11	12	0.9-1.2	**GRS**	121.447	95.908	237.17
12	FL2.2	1.0-1.3	**ZST**	122.733	122.679	149.644
13	19	2.9-3.1	**VCSS**	111.702	90.897	118.866
14	3	1.1-1.45	**VCSS**	73.035	28.147	251.223
15	19	1.3-1.8	CSS	110.642	85.318	141.273
16	11	0.3-0.5	**MSS**	191.21	185.831	281.877
17	FL2.1	1.2-1.4	VCSS	323.239	287.844	631.044

5.5.5.3 Interpretation

Results from sieving show that the majority of grain sizes are below 1mm.

Laser sizer analysis shows that the majority of samples are in the fine to medium sand range with only four samples showing their mode to be in the silt size range. Grain size distribution has also shown that there is only a small portion of clay sized particles in samples (generally less than 5 %) see Appendix L.

The implications of grain size on the properties at Kawerau are that the soil will not behave in a plastic manner. This agrees with the findings from Atterberg limits which showed very low plasticity index for samples.

Large ranges of grain size may cause local variations in hydraulic conductivity which may lead to perched water tables, ponding and settling.

Grain size distribution showed a wide range of grain sizes which shows there have been various sediment supply and transport mechanisms at work. Grain size has been identified as a potential control of permeability and fluid flow in the subsurface.

5.5.6 Microscopy

Two samples were inspected under a binocular microscope to identify the properties of clay sized particles following grain size analysis.

Sample 1: Hole 20, depth 0.4 m

Sample 2: Hole 3, depth 1.1 – 1.45 m

5.5.6.1 Test procedures

Two samples were selected after grain size analysis by laser sizer technique identified samples with the highest percentage of clay sized particles. Samples were dried out on a petri dish and placed under a binocular microscope and examined under various magnifications ranging from 6.5 to 40 times magnification.

5.5.6.2 Results

The following images have been taken of samples

Figure 88: Microscope photo 10 times magnification Sample 1

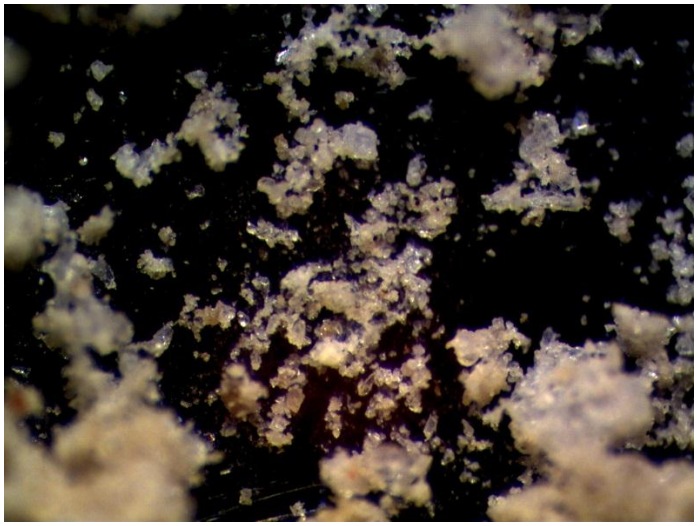

Figure 89: Microscope photograph 40 times magnification Sample 1

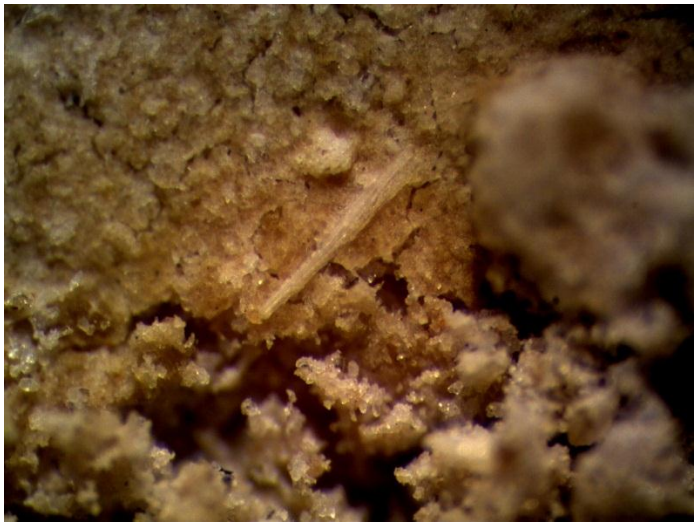

Figure 90: Microscope photograph 40 times magnification Sample 1 showing fibrous pumice shard

Figure 91: Microscope photograph 10 times magnification Sample 2

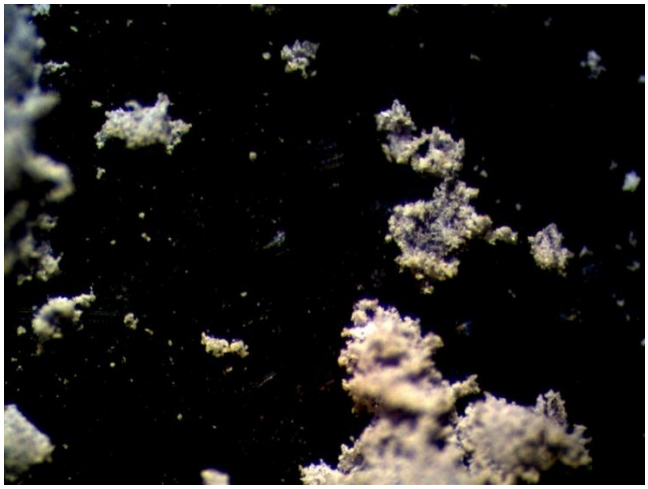

Figure 92: Microscope photograph 40 times magnification Sample 2

5.5.6.3 Interpretation

Microscope photographs have identified that the fine material in Samples 1 and 2 are primarily comprised of broken volcanic glass and quartz rather than clay. This will explain the lack of cohesiveness in the soil and the low plasticity index.

Grains have been identified as angular to sub-angular shape which shows short fluvial transport distance or aeolian transport mechanisms. The composition of sediment identified under the microscope shows quartz, volcanic glass and pumice.

5.5.7 Detection of allophane in soils

Allophane is a common component of weathered volcanic materials in New Zealand (Kelsey, 1986) and can have considerable influence on the behaviour of soils. The allophane detection test was carried out to determine the presence of clays in the near surface around Kawerau.

5.5.7.1 Test procedures

Tests were carried out in accordance with New Zealand Standard NZS 4402:1986 Test 3.4.
Simplified procedures are:

- A small sample of soil was smeared on to indicator paper prepared with phenolphthalein indicator

- A single drop of saturated aqueous sodium fluoride was added to the soil sample and observed for at least 3 minutes to note any colour changes.

The colour change of the indicator paper was recorded and is presented below (Table 12).

5.5.7.2 Results

Table 12: Allophane detection test results

Sample	Hole	Depth	Lithology	Colour	Acid test
1	20	0.4	Clay	No change	
2	3	1.1-1.45	VCSS	Pinkish red	
3	20	0.4	Clay	No change	
4	19	0.4-1.0	ZST	Pinkish red	
5	18	0.9-1.4	ZST	Pinkish red	
6	20	2.8	Clay	No change	
7	3	0.45-1.0	Clay	Bright red	Fizzes
8	3	0.03-0.25	Clay	Red	Fizzes
9	5	1.2-1.5	Peat	Pinkish red	Fizzes
10	FL2.1	1.2-1.4	VCSS	Pinkish red	

The colour the indicator paper changes to represents approximate proportions of allophane in the sample, the colour coding is:

Bright red: more than 7 % allophane

Pink to red: 5 % to 7 % allophane

Colourless: less than 5 % allophane

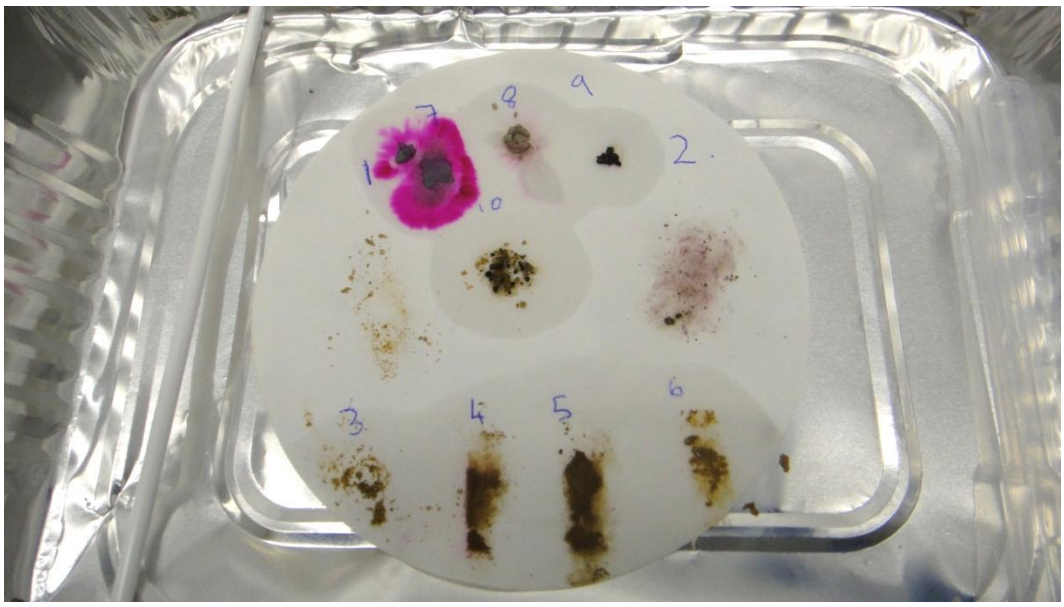

Figure 93: Photograph of samples on indicator paper after adding sodium fluoride

5.5.7.3 Interpretation

Results from the allophane detection test have identified that most samples contain some level of allophane. The following points must be noted when interpreting allophane detection test results:

1. Only clay or very fine sand grained parts of samples were tested, so results only apply to a sub-set of full samples
2. Soils initially high in alkali or containing free calcium carbonate will also turn the indicator paper red. Samples were tested with 10 % hydrochloric acid to determine the presence of carbonate by effervescence; these results are also presented in Table 12 and it can be assumed allophane is not present in samples that fizz.

The lack or low concentration of clays in samples provides an explanation into the material properties of the sub-surface at Kawerau, but also confirms that the top 3 m of sediment is very young and immature and has not had time to weather.

The allophane detection test is limited in the way it only tests for presence of allophane and no other clays. There may be other clays present in the field area which have not been identified.

5.5.8 Falling head permeability test

A falling head test was carried out on one sample at the University of Canterbury Engineering Geology Laboratories.

The falling head test is suitable for fine grained soils such as silts and some clays. The falling head test works by allowing water to percolate through a soil sample over time.

The sample tested was from Hole 18 at a depth of 0.6-1.0 m and is silt to medium grained, loose sand.

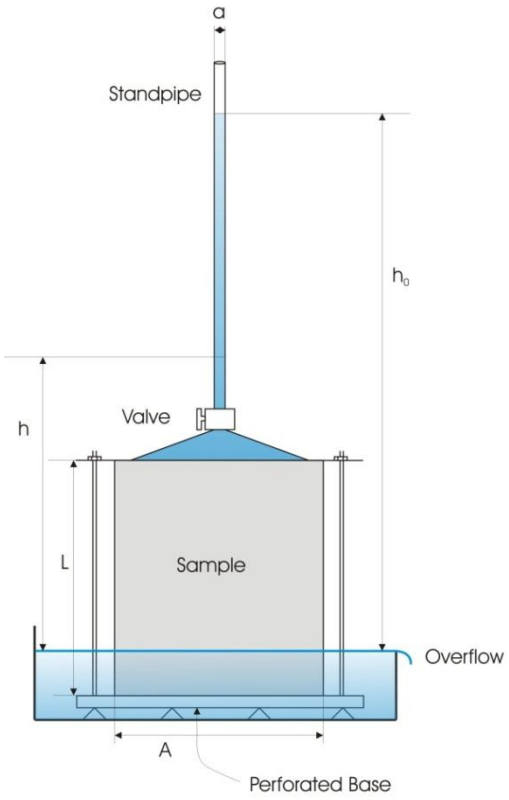

Figure 94: Falling head permeameter

5.5.8.1 Test procedures

A gauze, then sample was loaded into the falling head permeameter, another gauze was added with pea gravel on top. Water was then added to the sample and the standpipe was filled. Water was then allowed to flow through the sample and time was recorded for the standpipe to empty.

By measuring the time the test has been running and the change in head over time, the permeability (K) can be calculated using Equation 3.

$$K = 2.3(a/A).(L/t)/\log_{10}\{h_o/h\}$$

Equation 3: Falling head permeability

Where:

- a = cross-sectional area of standpipe tube (m^2)
- A = cross-sectional area of sample tube (m^2)
- L = Sample length (m)
- t = time from start of test (minutes)
- h_0 = Initial head (m)
- h = final head (m)
- K = hydraulic conductivity (m/s)

Falling head tests were carried out in accordance with British Standard BSS 1377: Part 5: 1990.

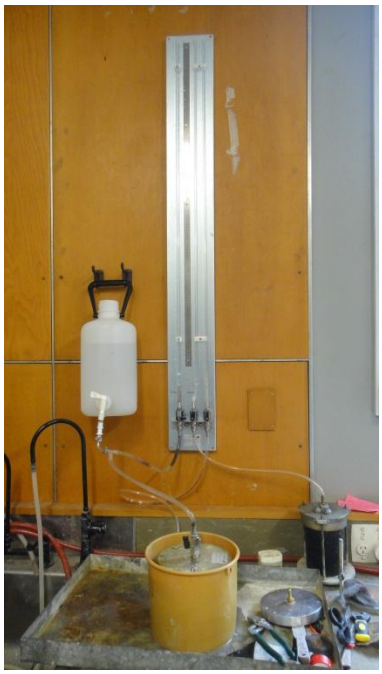

Figure 95: Photograph of falling head permeameter set up

5.5.8.2 Results

Table 13: Falling head permeability results

a (m^2)	A (m^2)	L (m)	t (s)	$h_{0\ (m)}$	h (m)	K (m/s)
0.0058	0.008	0.089	93	0.001	1	2.18E-05

Results show a hydraulic conductivity of $2.18E^{-5}$ for the sample.

5.5.8.3 Interpretation

The hydraulic conductivity of the sample is relatively low for sand but high for silts and clays (see Figure 96), this may be due to the large range of grainsizes found in the sample. It was also not possible to compact the sample to maximum density prior to testing or test un-disturbed samples, this may increase the hydraulic conductivity of the sample.

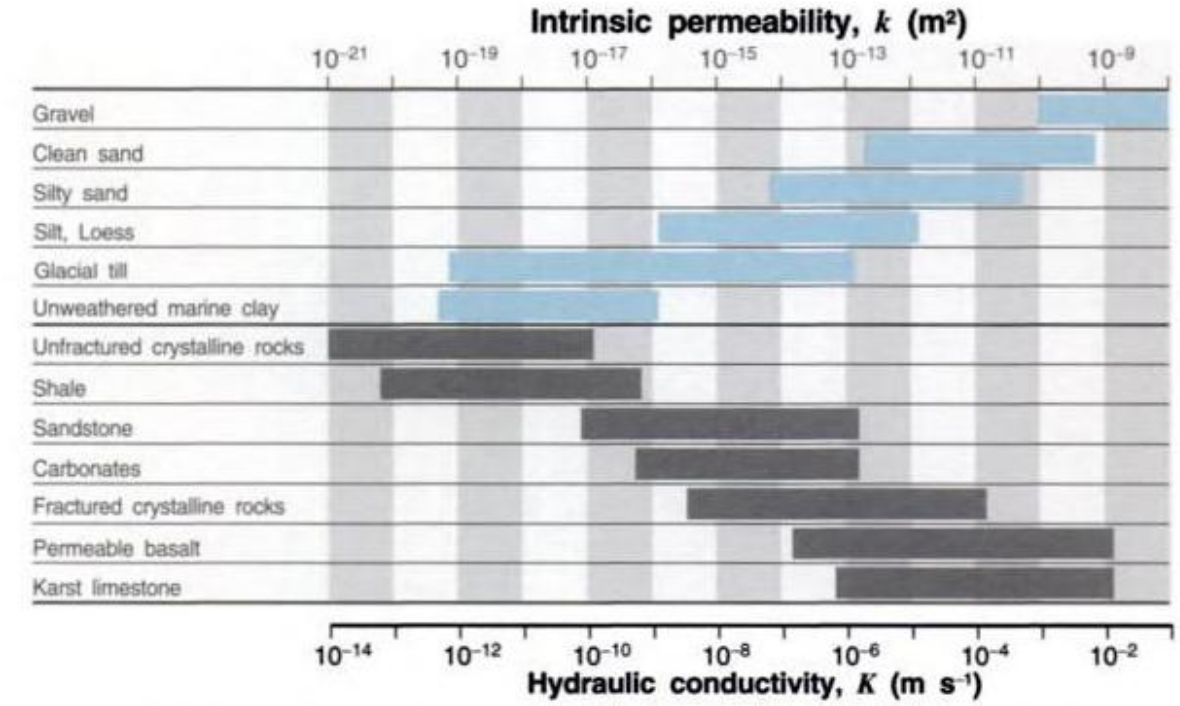

Figure 96: Typical intrinsic and hydraulic conductivity values for a variety of rocks (grey bars) and sediments (blue bars) (Hornberger, et al., 1998).

5.5.9 Constant head permeability test

Constant head tests were carried out on two samples at the University of Canterbury Engineering Geology Laboratories.

The constant head permeameter is used for testing permeability of soils which are not fine grained. The constant head permeameter works by allowing water with constant head to pass through a soil sample. Head is kept constant in a header tank by allowing water to overflow at one point and having a greater input to the header tank than output through the sample. The head loss across the sample is then measured off manometers at distance (L) apart.

Samples tested were:

1. Hole 12, 0.9 – 1.2 m depth (Granules – Kaharoa eruption deposit)
2. Face log 2.1, 1.2-1.4 m depth (very coarse sandstone – Kaharoa eruption deposit)

5.5.9.1 Test procedures

Samples for the constant head test were loaded in to the constant head permeameter on top of pea gravel, separated by gauze. Gauze and more pea gravel were added at the top of the sample and compacted by hand. Water was added to the samples from the bottom up and the water level in the manometers was allowed to stabilise. Water was then allowed to flow through the sample and water flow was measured at three rates. The volume of water passing through the sample over a one minute period was recorded three times for every flow rate.

Permeability (K) for the constant head test can be calculated using Equation 4.

$$K = Q.L/(A.h)$$

Equation 4: Constant head permeability

Where:

- K = hydraulic conductivity (m/s)
- Q = volumetric flow rate (m^3/s)
- L = distance between piezometer (manometer) connections (m)
- A = cross-sectional area of sample (m^2)
- h = head drop between piezometers (manometers) (m)

Constant head tests were carried out in accordance with British Standard BSS 1377: Part 5: 1990.

Figure 97: Photographs of constant head set up (left) and constant head permeameter unit (right)

5.5.9.2 Results

Table 14: Constant head permeability results

Sample	L (m)	A (m^2)	h (m)	Q (m^3/s)	K (m/s)
1	0.145	4.42E-03	8.200E-02	6.91E-06	6.20E-03
2	0.145	4.42E-03	1.87E-01	4.16E-06	1.07E-03

5.5.9.3 Interpretation

The results determined by constant head test show typical hydraulic conductivity values for clean to silty sand (see Figure 96). These samples are typical of near surface granule sands comprised of volcanic detritus in the field area. Constant head tests were initially difficult to carry out due to the presence of fine grained particles blocking manometer outlet pipes, but with the addition of fine mesh, this made it possible to conduct the tests. The difficulties associated with this test confirm the presence of a wide range of grainsizes as identified by grainsize analysis and explain why there may be local variations in hydraulic conductivity.

5.5.10 Permeability summary

Permeability testing has provided broad data on infiltration into the subsurface. Testing has shown that there are clear variations in permeability between coarse grained sediment which was usually intercepted in the top 2 m in hand auger holes, and fine grained silt or ash deposited by either ash fall or flooding events. These changes in permeability have led to the development of perched water tables and soft ground which coincide with areas identified for subsidence by levelling surveys. Figure 98 shows a basic outline of water flow in the subsurface at Kawerau and how perched water tables form above fine grained sediments.

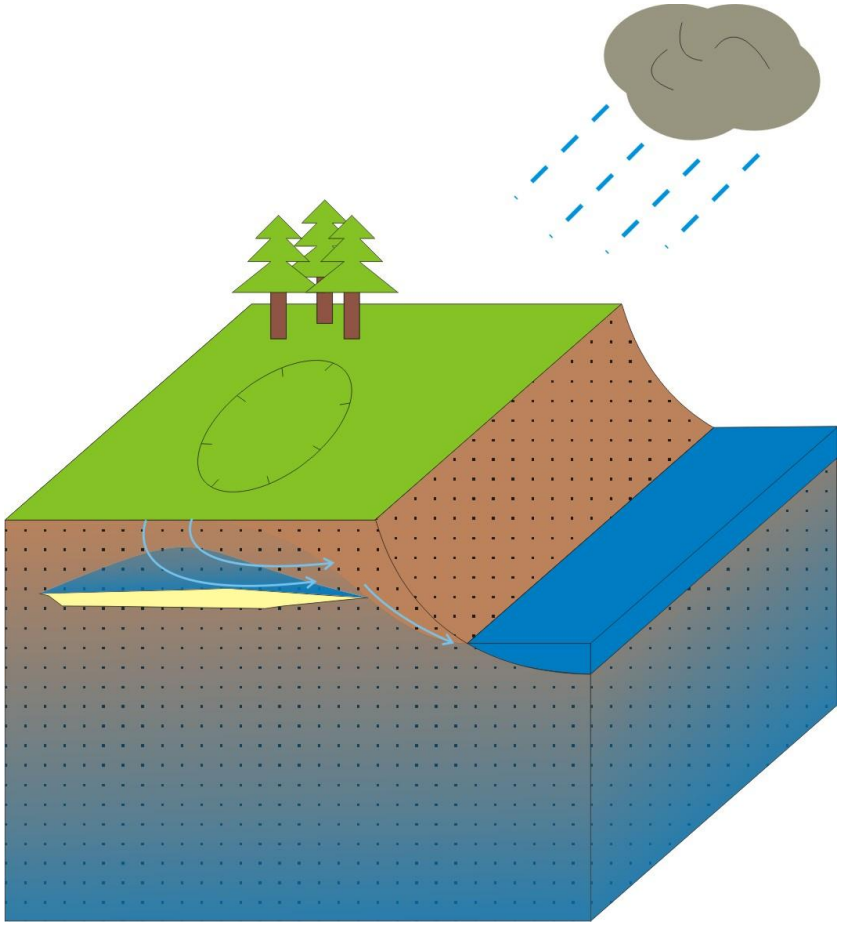

Figure 98: Schematic drawing of infiltration at Kawerau with perched water table

Permeability in coarse grained sediments was not as high as expected due to the high percentage of fine grains mixed through the sediments. Permeability investigations were limited to three samples due to the large size of sample required for the test and limited sample collected while in the field.

5.5.11 Implications of laboratory investigations to subsurface model

All laboratory tests were carried out on disturbed samples collected by hand auger. All samples appeared to be unaffected by geothermal waters.

Laboratory investigations have shown that the sediments at Kawerau show a wide range of grain sizes including low permeability silt layers which inhibit the flow from coarser grained sediments. This results in perched water tables in localised areas which can lead to lower ground strength due to high water content. The wide range of grain size and variations in sample compositions indicates more than one sediment source and transport mechanism as well as changes in the local geomorphology.

Microscope observation of fine grained sediment has identified the fine material is generally volcanic glass shards and quartz, rather than clays, this is supported by the allophane detection test which only identified small amounts of allophane in sub-samples. This means that sediments are not likely to behave in a plastic manner and are unlikely to hold large volumes of water. Testing of samples with hydrochloric acid identified the presence of carbonates in some horizons; the presence of carbonates in the field area is not likely to have formed in a marine environment. Samples to 3 m depth have been identified as 1314 Kaharoa eruption deposits, both by inspection and literature review (Beanland & Berryman, 1992). The location of the coast when the Kaharoa deposits were laid down was in a very similar location to its current position, the last time the coast came close to Kawerau would have been approximately 6.5 ka (Beanland & Berryman, 1992). Carbonates often precipitate from geothermal water (Pezaro, pers.comm., 2011), however the samples were taken in the top 3 m and there are no naturally occurring geothermal waters in this area at this depth. However, the auger holes from which samples that fizzed were taken from, were located at Site 1 which has many steam pipelines running through it. These pipelines often discharge geothermal fluid as shown by Figure 99.

Figure 99: Discharge point on steam pipeline at Site 1

Further to the presence of carbonates from geothermal water, it is possible to get carbonates in soil from magmatic CO_2 degassing at depth and migrating to the surface and building up in soils. Carbon isotopes and CO_2 flux surveys would indicate the amount this would be affecting the field area.

Sediments are generally non-plastic to low plasticity which means that an increase in water content will not cause sediment to expand and flow and means that movement due to water content changes is the result of mechanical processes rather than chemical and will be in response to a change in effective stress. Changes in shear resistance to movement by mechanical processes such as increase in water content are much lower than changes as the result of expansion of clays.

Sediments have been found to readily slake and most are dispersive to some degree suggesting that the material is highly erodible, this is also clear in the landscape when observing river banks and tributaries as they incise easily and are constantly eroding, even in stable, non-flood conditions.

Tests on samples were limited to those collected from hand auger holes in the top three metres. Further testing of samples at greater depth would add considerably to the engineering geological model.

Chapter 6: Subsidence model

The following chapter presents and critically evaluates current theories of subsidence mechanisms at Kawerau followed by a preferred model of subsidence, supported by field and laboratory investigations.

The focus of the subsidence model presented in this chapter is on the localised round and linear subsidence features, and does not attempt to reinterpret data or mechanisms described by Young and White (2006) or Terralog Technologies (2006) which have explained field wide subsidence. Field wide subsidence has been attributed to compaction of the reservoir at depth, whereas the localised subsidence features are distinctly different from the field wide feature and are likely to be controlled by near surface processes.

Before presenting a new subsidence model for Kawerau, it is important to first provide an evaluation of current subsidence models that have been suggested for Kawerau.

6.1 Evaluation of current theories on subsidence mechanisms

From existing information a number of causes have been suggested to explain subsidence in Kawerau. Possible models can be broken into:

1. Those independent from geothermal power generation:
    a. Seismic activity
        i. Direct
        ii. Indirect
    b. Meteoric water percolating down faults and cooling hydrothermally altered rocks and causing them to contract
    c. Compaction of hydrothermally altered rocks
    d. Natural consolidation of alluvial sediment/weak ground
    e. Consolidation of surficial deposits due to changes in groundwater conditions
    f. Consolidation of surficial deposits due to the placement of waste construction material
    g. Direct disturbance by construction
    h. Vibration from factories and road or rail traffic

2. Those related to geothermal power generation
    a. Geothermal fluid extraction and injection
    b. Cooling and contraction of reservoir rocks
3. Apparent subsidence resulting from movement of structures benchmarks are on, giving a false positive result for subsidence, rather than actual subsidence.

A model explaining the cause of subsidence in Kawerau could include any number of the above scenarios.

6.1.1 Seismic activity

6.1.1.1 Direct seismic activity

Direct seismic activity causes part of the ground to drop in relation to its surroundings, this can be localised around surface fault rupture, or regional with movement primarily occurring on deep faults. Both of these mechanisms are taking place in Kawerau as it is in an active rifting environment.

Subsidence caused by seismic activity is generally on a regional scale and is described in the influence of regional factors on the area (2.2). Begg and Mouslopoulou (2010) have identified that due to seismic activity across the Whakatane Graben, the Rangitaiki Plains have had a subsidence rate of approximately 3 mm/yr over the last ~2 kyr between the Edgecumbe and Matata Faults.

Subsidence at Kawerau is likely to be controlled to some extent by localised direct seismic activity by surface fault rupture. Wood et al. (2001) have identified that the closest surface rupture to Kawerau in the 1987 Edgecumbe earthquake was ~1 km to the NE of the town which is near the field area. En echelon faulting has been described by Wood et al. (2001) and was also interpreted from the GPR investigation. Faulting in the area is described as typical of normal faulting in the TVZ with a fault strike of 055 - 065° (Wood, et al., 2001).

6.1.1.1 Indirect seismic activity

Indirect seismic activity causing subsidence occurs when ground shaking either causes the ground to consolidate or spread laterally due to shaking. Lateral spread is particularly likely near rivers, or next to excavated ground. Indirect seismic activity can also modify the environment in a way that causes the ground to consolidate. This could occur when seismic activity raises the ground level, effectively lowering the water table and increasing the effective stress on the soil. Indirect seismic activity can

also modify groundwater flow by formation of fault gouge which could then act as an impermeable barrier, or as a conduit which redirects fluid flow. Field examination of fault gouge suggests permeability would be reduced around fault gouge.

Indirect seismic activity is believed to be one of the contributing factors of subsidence at Kawerau. Seismic activity may also have controlled the location of historic river channels by forming low points in the topography. This will in turn have contributed to the deposition of sediment which is susceptible to compaction, consolidation and liquefaction, all of which are contributing factors to subsidence.

There was considerable subsidence noted following the 1987 Edgecumbe earthquake. This change in elevation is not entirely structural, but may possibly be because this was the first significant seismic event following the draining of the Rangitaiki Plains and seismic shaking would have allowed the slowly compacting sediment to compact more rapidly.

6.1.2 Cooling of hydrothermally altered rocks

Percolation of meteoric water through faults which cool and contract hydrothermally altered rocks is a possible mechanism of subsidence at Kawerau (Pezaro, pers.comm., 2011). This mechanism would likely form depressions within close proximity to the fault and would be expected to form relatively wide, open subsidence bowls. The GPR investigations and a literature review have identified the location of faults in the area; this fault system coincides with part of the subsidence anomaly in Site 2 (Figure 100). Temperature profiles across the field area are however not known exactly and Site 2 has not had holes drilled in it, so the level of hydrothermal alteration in this area is inferred from other boreholes. To validate this theory a drill hole or multiple drill holes would need to be drilled to further define the temperature and alteration properties of the area.

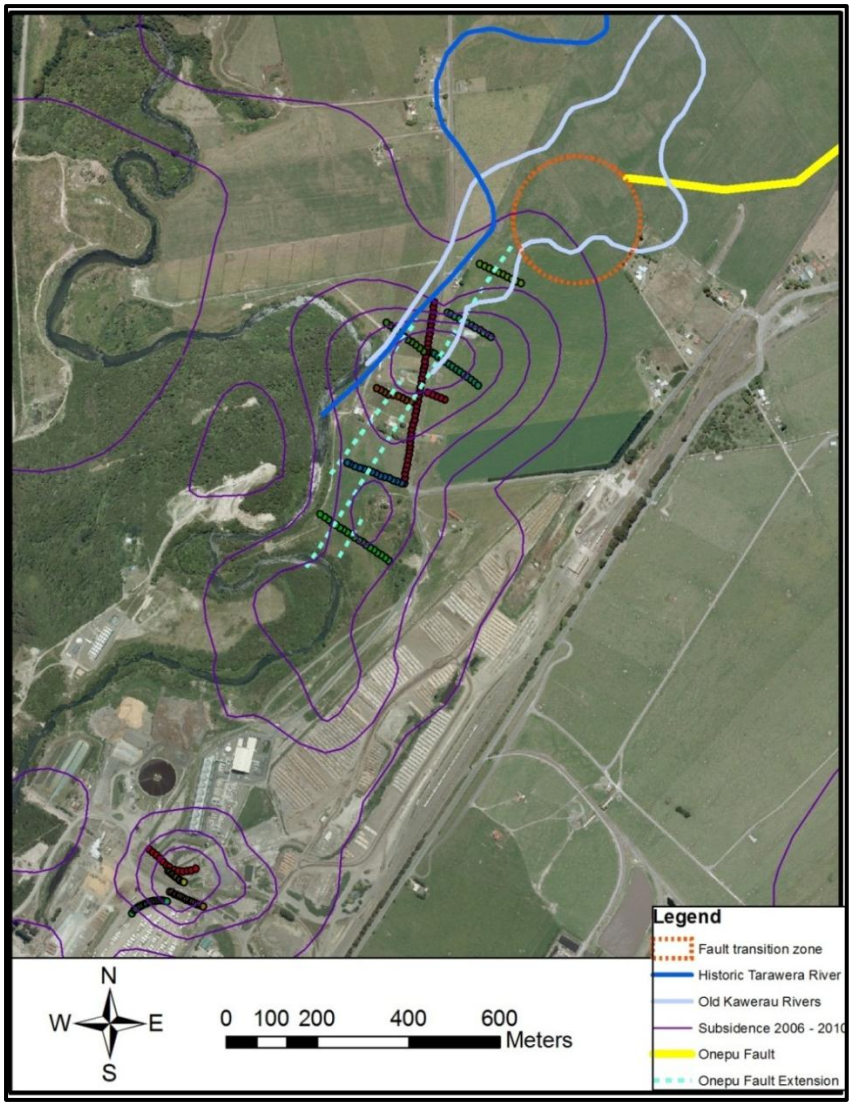

Figure 100: Location of faults as interpreted from GPR and literature review and their spatial relationship with subsidence bowls and river channels

It is likely that fluid flow is possible in the Kawerau Area which would allow cool water to percolate down to hydrothermally altered rocks. Mighty River Power conducted shallow reservoir tracer tests which have shown this fluid movement is possible, fluid chemistry of shallow ground water wells also indicates active fluid flow in the area. These tests show rapid and sometimes very high volume returns from 300 mRL to 30 mRL in areas surrounding Site 1 (Seiga, et al., 2011).

The SKM geotechnical investigation (SKM, 2005) which encountered the Onepu Rhyolite in hole G3 only found occasional hydrothermal alteration. However, hydrothermal alteration can be localised, so may be restricted to Site 2 and may be associated with faulting. Utada (2001) has stated that generally, hydrothermal alteration rarely occurs over wide areas and is more typically localised around zones of circulating solutions. Hydrothermal alteration localised around fault zones has been identified at the Sanzugawa caldera in northern Honshu (Udata, 2001).

6.1.3 Compaction of hydrothermally altered rocks

Compaction of hydrothermally altered rocks and hydrothermal eruption breccias has been identified as the cause of some subsidence features at Tauhara (Bromley, et al., 2010). Hydrothermal eruption breccias have been identified in Kawerau (Nairn & Wiradiradja, 1980). However these are located to the east of the mill site and levelling surveys have not identified any significant subsidence over these areas.

6.1.4 Natural consolidation of surficial deposits

Consolidation of surficial deposits is possible through either drainage of the Rangitaiki Plains or the natural incision of the Tarawera River causing lowering of the water table. Consolidation of flood deposits in old river channels would give relatively linear subsidence patterns; they would also be highly active in the short term following deposition and be heavily influenced by water table depth. Areas that are liquefiable will be susceptible to settlement and collapse during seismic events. There are also alluvial silt and clays which would be susceptible to consolidation, particularly if dewatered (Brock, 2006).

6.1.4.1 Consolidation of surficial deposits due to changes in groundwater conditions

Lowering of the water table in response to continued incision of the Tarawera River, seismic events or drainage will increase the rate of natural consolidation by increasing the effective stress on soils as a result of reduced pore pressure in the ground. The Rangitaiki Plains are a naturally swampy area with many flood deposits and old river channels filled with sediment (Beanland, et al., 1989). The Tarawera River has been incising into loose alluvial sediment, down cutting approximately 3 m between 1920 and 1950 in response to a lowered groundwater table (Bignall & Harvey, 2005). Increased effective stress would cause localised subsidence in areas susceptible to compaction and/or consolidation, which in the case of Kawerau may follow the paths of old river channels. The alluvial sequence at Kawerau may be prone to on-going creep (secondary compression) under the weight of overlying material. Overlying materials are generally relatively permeable and will consolidate rapidly (months or years) as a result of any groundwater change (SKM, 2005).

Changes in groundwater conditions may also be attributed to extraction of water for irrigation, stock and farm water supply or domestic use.

6.1.4.2 Consolidation of surficial deposits due to placement of waste material

Consolidation of surficial deposits due to the placement of waste construction material is a likely cause of subsidence at Kawerau. Discussion with local residents and a literature review has shown that historic river meanders have been filled with a variety of un-engineered waste material around the Kawerau area, including sawdust, bark, waste steel, and broken concrete (Beanland, et al., 1989); (Olsen, pers.comm., 2011). It would be expected that this loose fill would compact over time. It is also possible that adding extra load to localised areas may compact the underlying surficial deposits. Consolidation of waste materials is however not expected to be the main cause of localised subsidence over the field area as locations described by residents do not fall within Sites 1 or 2.

6.1.5 Direct disturbance by construction

Subsidence as a result of direct disturbance by construction is most likely to become a contributing mechanism when lateral support of soils is removed due to excavation, loading, and/or vibrations. Brock (2006) has interpreted CPT results to indicate that shallow soil and groundwater conditions in the field area could give rise to localised subsidence, lateral spreading and compaction. Where clays are present consolidation is possible. These processes are particularly likely when exposed to nearby loading, vibration, groundwater fluctuations or loss of support due to nearby excavation.

6.1.6 Vibration

Vibration from factories and road or rail traffic is a mechanism which could work in one or both of the following ways:

1. Vibrations cause settling of particles in saturated or partially saturated ground, reducing the space between grains and increasing the rate of consolidation.
2. Vibrations cause structures with benchmarks on them (in particular those without engineered foundations) to settle into soft ground, giving the appearance of subsidence (Figure 20).

Vibrations from various sources would cause localised subsidence patterns in areas susceptible to compaction and consolidation or with heavy structures on soft ground with un-engineered foundations. Settling of particles due to vibration works in a similar way to seismic activity where sediment particles are shaken into more tightly compacted configurations resulting in a reduction in soil volume (Atkins, 2011). Sinking of structures into weak ground exaggerated by vibration is not an

uncommon occurrence. This mechanism is the basis behind the coring technique vibracore, where a sampling tube is vibrated into the ground to collect soil samples. Vibration is clearly present at Site 1, but not obvious at Site 2. The remnants of an historic train track are still evident through Site 1, which would have provided considerable amounts of vibration across the site while it was in use.

6.1.7 Geothermal fluid extraction and injection

Geothermal fluid is extracted from depths between 450 m and 3 km in Kawerau. The process of extracting water transfers the weight of overlying sediments from a fluid and rock matrix supported system to a rock matrix supported system due to a drop in pore fluid pressure. This increases the effective stress of the system and can cause the formation to consolidate. Consolidation of the formation will depend on changes in pressure (water extraction) and temperature (addition of cooler injected water).

There have been a number of significant increases in the extraction rates of fluid from the Kawerau Geothermal Field since its beginnings in the 1950's and the pattern of field activities has also changed along with these rates. If geothermal fluid extraction was the cause of subsidence features within the field area, it would be expected that the shape and/or location of these features would change in response to changes in extraction rate and locations. However, there have been no significant changes in surface morphology of these features since levelling surveys began in the 1970's.

Extraction of geothermal fluid is more influential on field-wide subsidence and is not expected to contribute considerably to the localised round and linear subsidence features at Sites 1 and 2.

6.1.8 Cooling and contraction of reservoir rocks

Cooling and contraction of reservoir rocks occurs in response to reinjection of cooler fluid into the reservoir. Terralog Technologies (2006) identified through laboratory testing that the greywacke basement is highly susceptible to thermally induced contraction.

As with geothermal fluid extraction (6.1.7), this mechanism contributes to field-wide subsidence features rather than the localised features at Sites 1 and 2.

6.1.9 Apparent subsidence

Apparent subsidence can also explain subsidence patterns in Kawerau. The benchmarks within Site 1 are often located on structures without engineered foundations in soft ground or areas where the foundations are being eroded by drainage (Figure 20). At Site 2, benchmarks are widely spaced and are primarily placed along the length of Onepu Springs Road which may result in the appearance of an elongated subsidence pattern parallel to sub-parallel to the road (Figure 22). Areas in agricultural land are susceptible to damage by heavy machinery driving over benchmarks such as seen in the 2007 – 2008 survey (Figure 24). Apparent subsidence at Site 1 is likely the product of vibration, consolidation, compaction of weak ground under un-engineered foundations or damage to benchmarks. Apparent subsidence at Site 1 may also be a factor of water content and erosion due to drainage channels through the site. With apparent subsidence, a drop in elevation is being measured, but the whole ground surface may not be dropping. The bottom depth of subsidence may also be very shallow. Further recommendations on identifying the depth to the base of the subsiding layer are discussed in 7.3.

6.2 Key results

Aerial photograph interpretation has identified that there is no apparent difference in surface conditions at Site 1 from its surroundings in original aerial photographs taken before any construction occurred in the area. This suggests that subsidence at Site 1 is likely a product of drainage and/or modification of the ground.

CPT has identified that there are zones of very soft ground (See 3.4). Points where the CPT sampling spoon dropped 300 mm relatively quickly were also identified in hand auger holes, but at much shallower depths. This shows that there is highly compressible ground across the field area. It has been identified that these soft areas are associated with perched water tables, controlled by low permeability silts and ash.

Site investigation identified that wetting and drying sequences at Site 1 are likely to be associated with the discharge of large volumes of water into soak ponds immediately adjacent to the site.

6.3 Preferred subsidence model

There is not likely to be a single cause of subsidence in Kawerau, but more likely a combination of the scenarios described in 6.1. The large, field wide subsidence bowl which is tilting to the north-west is likely to be directly related to the extraction of geothermal fluid resulting in consolidation of the volcanic deposits between 450 m and 800 m, and contraction of greywacke between 800 m and 3 km depth due to a drop in reservoir temperature. It is not however expected that geothermal fluid extraction is responsible for the creation of the localised, linear or circular subsidence features. This is thought to be controlled by shallower mechanisms. Subsidence mechanisms at Sites 1 and 2 at Kawerau are likely to be independent of each other. The following section describes the preferred subsidence model for each site.

6.3.1 Site 1

The main mechanisms contributing towards subsidence at Site 1 are: indirect seismic activity, direct disturbance by construction, vibration, apparent subsidence, the influence of drainage through the site, and wetting and drying sequences associated with rainfall and the soak ponds immediately adjacent to Site 1.

In aerial photographs, Site 1 showed no obvious difference in surface conditions compared to the rest of the mill site prior to construction in 1945. Aerial photographs identified that the site developed with the mill and became a drainage channel. Waste material was dumped in and around Site 1 (Figure 101), whereas foundations of buildings at the mill will have been excavated and compacted (see 4.2). Steam pipelines, supported by concrete pads were constructed through the site.

Figure 101: Buried waste material found at Site 1

Drainage through the site has added considerable amounts of water which varies rapidly in response to rainfall events. Excavation of the drainage channel has removed lateral support for sediment which can lead to lateral spreading during seismic events. Vibration from train tracks through the site (Figure 35), then from heavy machinery and industrial processes along with increased water content from drainage and indirect seismic activity will increase the rate of consolidation at the site. Apparent subsidence is also very likely at Site 1 with the erosion of foundations below structures holding benchmarks (Figure 20), and the sinking of heavy foundations in to soft, saturated ground (Figure 25). A number of methods to test the depth to the base of subsidence and the presence of apparent subsidence at Site 1 are discussed in 7.3.

Soak ponds are located directly adjacent to Site 1. These ponds are regularly filled with water from the power station and allowed to drain. The site is also heavily influenced by rainfall events, so is regularly exposed to wetting and drying sequences. Wetting and drying sequences increase the rate of weathering and will cause sediment to disperse as discussed in 5.5.4.

6.3.2 Site 2

The main mechanisms contributing towards subsidence at Site 2 are: direct seismic activity, indirect seismic activity, consolidation of sediment due to changes in the groundwater table, and the influence of perched water tables. It has been suggested that cooling of hydrothermally altered rocks at depths of 100 – 200 m could contribute to the subsidence features, however there is no drill hole or temperature data to confirm this.

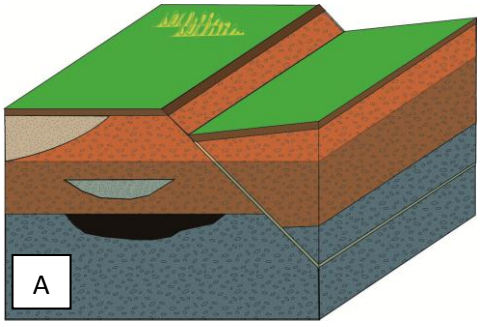

Direct seismic activity at Site 2 has resulted in surface rupture and the direct displacement of the ground surface by up to 1.7 m (Beanland, et al., 1989).

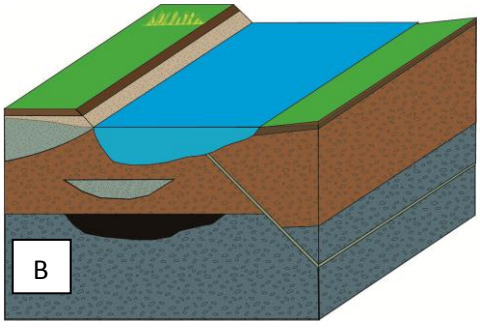

Direct seismic activity in the past will have led to the creation of low points in the topography which developed into river channels. This has been identified in aerial photographs and LiDAR data (See Figure 61).

Following the 1904 outbreak flood, the plains were blanketed in fine grained sediment and the river was diverted.

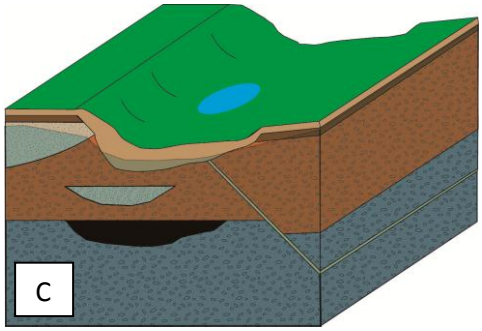

Following redirection of the Tarawera River and drainage of the Rangitaiki Plains, the Tarawera River incised into the plains at a high rate and the water table dropped in response to the diversion and new drainage channels.

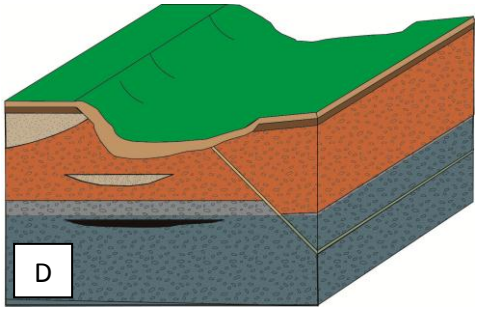

Dewatering of the plains has led to consolidation of loose sediment. Seismic activity following the dewatering of the plains has increased the rate of consolidation of sediment, particularly in the recently diverted river channel due to the presence of large amounts of unconsolidated material.

Figure 102: Progression of conditions at Site 2. A: Fault rupture causes low point in topography, B: River forms in low point in topography, C: Tarawera River is diverted and original river channel dries up, D: Rangitaiki Plains are drained, water table drops and sediment compacts.

Figure 102 shows the progression of conditions at Kawerau starting with active faulting causing a low point in topography (A). This is followed by the establishment of a river in low points, which erodes into the loose sands of the plains (B). The outbreak flood occurs in 1904, blanketing the plains in fine grained sediment and the Tarawera is diverted to flow towards Lake Rotoitipakau (C). The plains are then dewatered to create more useable land for farming, the water table drops and sediment consolidates (D).

Field and laboratory investigations have identified that the ground in the top 3 m varies over short distances and some areas have perched water tables with very soft and saturated zones. The saturated zones above perched water tables are likely to be susceptible to subsidence. This was identified in both CPT results (See 3.4) and hand auger holes 18 and 19 (See 5.4.1). Localised variations in lithology are common on the Rangitaiki Plains in response to flooding events as shown by Figures 103 and 104.

Figure 103: Waikamihi Stream on Rangitaiki Plains following a flood (February 2011)

Figure 104: Flood deposits on the banks of Waikamihi Stream on the Rangitaiki Plains (February 2011)

Subsidence as a result of cool meteoric water percolating down faults and cooling hydrothermally altered volcanic material, causing it to contract is a likely contributor to subsidence in Kawerau. This

method of subsidence would likely induce elongated features along similar strike to faults (Figure 100).

Consolidation of sediment and historic river channels due to changes in groundwater conditions and indirect response to seismic activity is suggested as the most significant driver of subsidence at Site 2.

6.4 Explanation of patterns identified in levelling surveys

Subsidence rates at Kawerau have not been consistent and often increase and decrease on a yearly basis. These fluctuations in subsidence rate may at least in part be related to rainfall events.

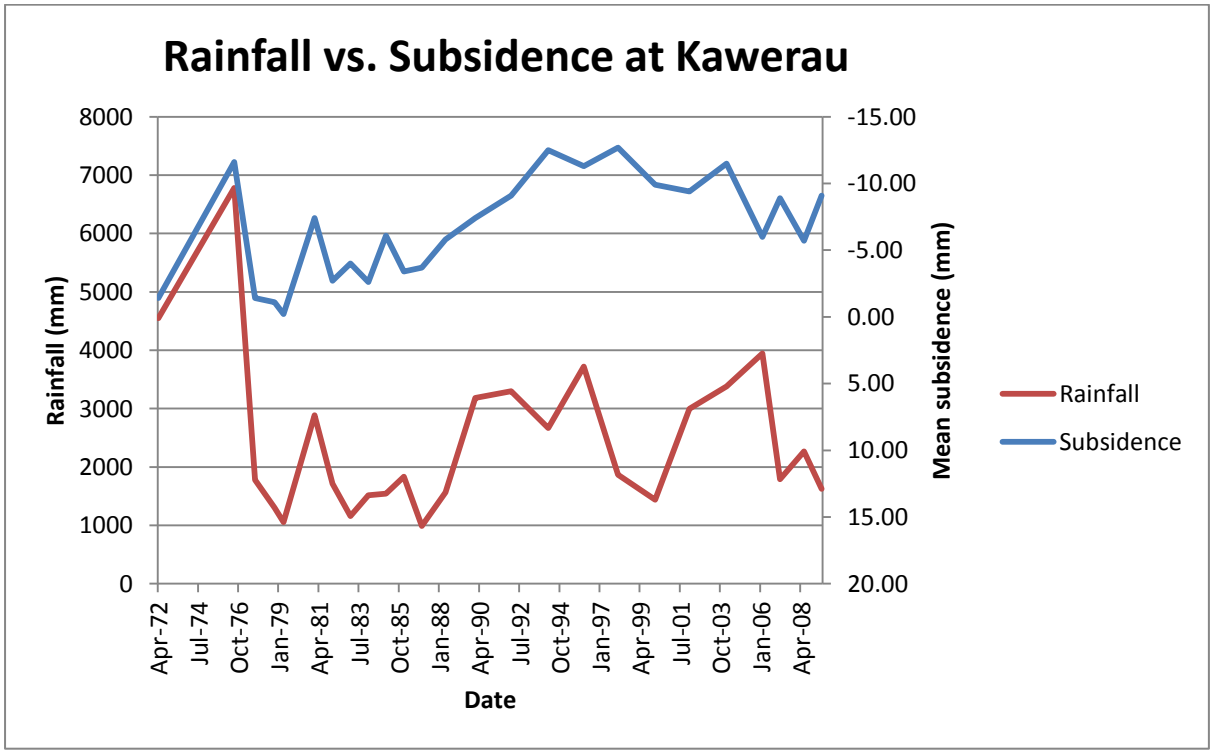

Figure 105: Graph of rainfall vs. subsidence rates at Kawerau. 1987 earthquake data removed

Figure 105 shows that there are generally increased rates of subsidence with periods of increased rainfall. Rainfall data were only available until 2010 before bi-monthly levelling surveys were undertaken. The relationship between rainfall and subsidence shows that water has a clear influence on subsidence rates. Increased rainfall may increase the rates of percolation of fluid down faults into hydrothermally altered rock, soften ground increasing the chance of structures settling or decrease the depth to groundwater, increasing the rate of wetting and drying sequences.

6.5 Predictions for future evolution of subsidence and assumptions

It is not expected that subsidence patterns will change considerably or move towards the mill and cause significant damage to sensitive equipment. Further investigations as discussed in 7.3 will identify if levelling surveys are providing accurate results at Site 1. Subsidence at Site 2 should continue at similar rates or reduce over time as sediment settles and adjusts to changes in the depth to water table.

6.6 Kawerau in relation to other settings

Kawerau is similar in many ways to other geothermal fields within the TVZ. It has similar lithologic units, production depths and has a similar power generation age to other fields such as Wairakei. However, it has local variations of geologic units which exhibit different material characteristics and extraction of geothermal fluid has recently moved to greywacke basement, a target that has not been used for fluid extraction in any other geothermal field in New Zealand. After thorough investigation, Kawerau is actually quite different from other geothermal fields in New Zealand. One of the significant differences is that it is not located within or on the faulted margins of a caldera.

Kawerau has had vastly different rates of subsidence than that at Wairakei where subsidence has been attributed to compaction of the Huka Falls Formation due to pressure decline in the reservoir. Subsidence rates in Wairakei have been as high as 450 mm/year during the 1970's (Allis, et al., 2009); rates are currently around 58 mm/year (O'Sullivan, et al., 2010). Subsidence patterns are similar to Kawerau; however, the localised subsidence bowls at Wairakei are much larger than the small features at Kawerau (Figure 106). By comparison to Wairakei, the localised round and linear subsidence features at Kawerau are very likely to be attributed to a different subsidence mechanism.

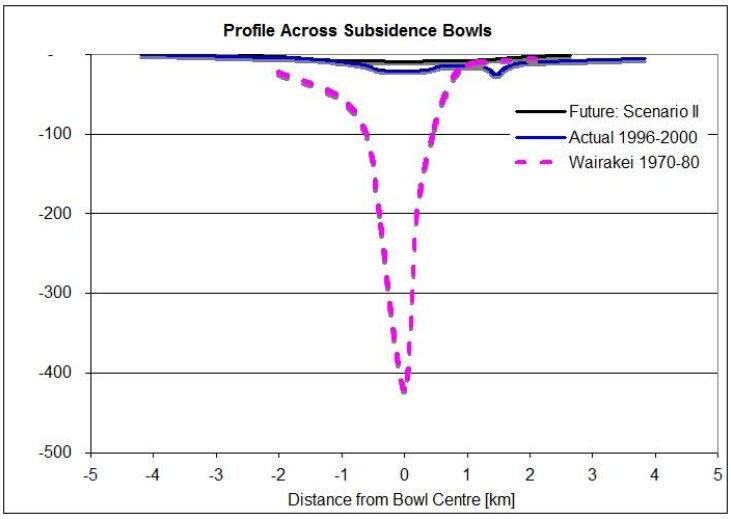

Figure 106: Cumulative subsidence, Kawerau vs. Wairakei (Spinks, et al., 2007). Blue and black lines refer to Kawerau, future scenario is predicted basin-wide subsidence as calculated by computer modelling, and actual subsidence is measured by levelling surveys. Purple dashed line refers to Wairakei.

Kawerau shows similar subsidence rates to The Geysers Geothermal field in the Mayacamas Mountains in Northern California. However the subsidence bowls at The Geysers are much larger than at Kawerau, with most bowls being larger than 5 km in diameter (Mossop & Segall, 1997). Subsidence rates at The Geysers are 10 – 30 mm/year (Floys, et al., 2010) and have been attributed to the extraction of water (Mossop & Segall, 1997). Kawerau has similar geology (see 1.2), however the extraction rates are very different and the large size of the subsidence bowls at The Geysers suggests a different mechanism to the localised, linear features at Kawerau.

Kawerau also shows similar patterns of subsidence to those seen at the Wilmington Oil Field in Long Beach, California, but these have been attributed to the extraction of oil in a very sensitive environment which is affected by the nearby harbour. Kawerau does not have a similar ground water system to the Wilmington Oil Field, so is therefore not a good analogy of subsidence mechanisms. However, the setting of the Wilmington Oil field is beneath an area of very high value real estate, and sensitive buildings in the Long Beach area. This shows that it is possible to have subsidence in areas beneath sensitive buildings with no adverse effects. As of 2006 there had been no report of damage to buildings as the result of subsidence within the Kawerau field (Terralog Technologies, 2006).

Possibly the most representative analogue of the subsidence at Kawerau is the drainage of land in locations such as the Netherlands. Subsidence in the Netherlands has occurred following the dewatering of large amounts of peat swamp and water logged ground to increase useable land for

agriculture and the expansion of cities. Subsidence rates in the Netherlands are approximately 10-20 mm/year (Andriesse, 1988) and form patterns depending on the location and thickness of the underlying peat, creating small, localised features like those seen in Kawerau, as well as much larger wide bowls.

Chapter 7: Conclusions and Recommendations

7.1 Project methods

This thesis has approached the subsidence investigation in Kawerau through a progressive technique which developed on existing knowledge, proposed new phases of work from this knowledge, then re-evaluated the model and proposed further work based on continuing field and laboratory investigations. The investigation began by identifying that subsidence exists in Kawerau, reviewing available literature on the subsidence in Kawerau and in other areas around the world and identifying if subsidence mechanisms in other settings may apply to the Kawerau Geothermal Field.

After examination of the localised subsidence features and a literature review, it became apparent that the localised subsidence features are likely to be attributed to near-surface processes rather than geothermal fluid extraction. This led to the development of a near surface investigation program, initially with a geophysical investigation that informed an invasive investigation. Laboratory testing followed the invasive investigation which allowed further testing and validation of theories into subsidence mechanisms.

This work has identified potential mechanisms for subsidence and given results which have been useful in describing the behaviour of the Kawerau area and determining the origin of the localised subsidence features.

7.2 Summary of results

7.2.1 Regional factors influencing subsidence

Region wide features which are considered to have contributed to subsidence in Kawerau include the extension and subsidence of the Whakatane Graben, and active volcanism. Extension and subsidence of the Whakatane Graben have resulted in seismic activity and faulting on the Rangitaiki Plains (Begg & Mouslopoulou, 2010). These faults have contributed to the geomorphology of the Rangitaiki Plains not only by structural changes, but by altering relief to create low points in the topography which have in turn provided channels for rivers to form. The Onepu Fault runs through the field area and may have been an initial influence for the location of the Tarawera River. The

elongated and sinuous pattern of subsidence which has been identified by levelling surveys is similar in appearance to the current morphology of the Tarawera River, suggesting that the localised subsidence bowls in Kawerau are associated with historic river channels.

Active volcanism has affected the geomorphology and structure of the Kawerau area considerably. Not only does volcanism provide the heat source for geothermal energy, but it has also contributed the majority of sediment that has built up the Rangitaiki Plains, both from proximal and distal sources. Mt Putauaki is a significant landmark in the Kawerau area (Figure 2) and provides the heat source for the Kawerau Geothermal Field. The Okataina and Taupo volcanic complexes have contributed significant amounts of sediment to the Kawerau area. The shallow subsurface beneath Kawerau is comprised of volcanic material from these sources that has been transported to the area primarily by fluvial mechanisms. The variation in fluid transport means a wide range of grain sizes have been deposited across the Kawerau area which affects localised variations in groundwater content and flow. With sediment supply being controlled by volcanism, the rate and duration of supply varies considerably with large volcanic events depositing large amounts of sediment to various catchments which is then transported to the plains and coastline during heavy rainfall and flooding events. In the case of the 1886 Tarawera Eruption, a dam formed at the outlet of Lake Tarawera, resulting in the level of the lake increasing by 12 metres until the dam failed in 1904, flooding the Kawerau area and transporting large amounts of sediment to the plains. Since 1904, the main influence on the morphology of the Kawerau area has been due to anthropogenic mechanisms.

7.2.2 History and location of Kawerau subsidence

Kawerau subsidence has been monitored since the 1970's using levelling benchmark surveys. Subsidence rates have generally increased in the Kawerau area since the levelling survey began (Table 3). Subsidence rates have not increased significantly in the Kawerau Geothermal Field, even though water extraction and production rates and patterns have increased substantially since the commissioning of the field in the 1950's.

Kawerau has two patterns of subsidence features, the first is a large, wide subsidence bowl which extends across the whole geothermal field and is tilting towards the north-west. This subsidence bowl is typical for the shape of subsidence features in geothermal fields around the world and is likely to be due to contraction of reservoir rocks at depth due to geothermal water extraction and/or drops in reservoir temperature. The second subsidence pattern is small (20-200 m wide), localised bowls, one of which is long and sinuous and is similar in appearance to historic river channels found

in the field area. Localised subsidence bowls identified by levelling surveys are often interpreted as anomalies in the survey; however, the two localised bowls which this thesis is focusing on appear in each survey and an increase in benchmarks in areas of interest have increased confidence that these features exist and have made it possible to narrow down the extent of these subsidence bowls.

7.2.3 Principal conclusions

Geothermal fluid extraction is not the primary driver of subsidence at Kawerau. It is likely to be controlling field wide subsidence at low rates, but not the localised, sinuous or round features found at Sites 1 and 2.

Subsidence at Site 1 within the mill grounds is likely to be caused by indirect seismic activity, direct disturbance by construction, vibration, apparent subsidence, the influence of drainage through the site, and wetting and drying sequences associated with rainfall and the soak ponds immediately adjacent to Site 1.

Subsidence at Site 2 is likely to be caused by direct seismic activity, indirect seismic activity, consolidation of sediment due to changes in the groundwater table, and the influence of perched water tables. Subsidence at Site 2 is likely to appear in a linear pattern due to the layout of benchmarks along the length of Onepu Springs Road. It has been suggested that cooling of hydrothermally altered rocks by infiltration of cool surface water down faults is causing subsidence originating at depths of 100 – 200 m at Site 2 (Pezaro, pers.comm., 2011). Fluid flow in the area is possible as shown by tracer tests (see 6.1.2), however, temperature profiles and drill hole data on hydrothermal alteration is not available for the field area. Faults have been identified in the field area and mapped; these faults had not previously been mapped in this area. It is likely that faults play a large part in controlling subsidence features in the Kawerau area, both directly and indirectly. The faults running through Site 2 are thought to have caused low points in the topography, which have in turn controlled the location of the historic Tarawera River, facilitating the deposition of fine grained material in the area. The Tarawera River was diverted following the 1904 Lake Tarawera outbreak flood, this diversion aided draining of the plains and the lowering of the water table in the field area. Subsequent seismic activity has shaken the loose sediment deposited by rivers and aided compaction post-draining of the plains causing localised variations in subsidence rate.

7.3 Further Work

This section provides suggestions for future work to further constrain the mechanisms that cause subsidence in Kawerau.

1. Install of water monitoring wells and piezometers in increasing increments away from the soak ponds at the power station to monitor the influence of soak ponds on wetting and drying sequences at Site 1.
2. Drill holes into the top 200 m in subsidence bowls and the installation of borehole extensometers to measure subsidence at various depths throughout the hole. This will further constrain the compacting layer and provide temperature profiles and alteration data to test the idea of cool surface water causing hydrothermally altered rocks to contract.
3. Install 'floating' benchmarks at Site 1 – this would be achieved by creating benchmarks out of very light material such as a light aluminium plate and fixing it lightly to the ground with pegs. This would prove or disprove the theory that benchmark structures are sinking into soft ground, giving the false appearance of subsidence.
4. Install a benchmark on a light peg in the ground immediately adjacent to benchmark K0669 and measure the subsidence on this and see if there is any difference between benchmark K0669 and the peg after 1 year.
5. Install benchmarks in the farmland on the eastern side of Onepu Springs Road to remove any linear bias in the levelling survey in this area and to further constrain the extent of the subsidence features at Site 2.
6. Install shallow wells at Sites 1 and 2 to determine the depth to the base of subsidence by casing small wells to 10 m and measure subsidence at the base of these small wells. Case these wells with PVC pipe.
7. Carry out XRD analysis on samples to determine clay presence and type.
8. Deeper drilling/vibracore to 30 m to thoroughly characterise the shallow surface below the top 3 m.
9. Consolidation test soils using an oedometer.
10. Carry out further ground penetrating radar investigations using both 50 MHZ and 200 MHZ antennas to further define subsidence at Site 2 and further constrain the location of faults within the field area.
11. Carry out further hand augering to determine lateral distribution of units across the field and tie units in different holes together. Further augering would also prove fault presence by augering 3 to 6 holes in close proximity to each other around interpreted fault locations. If faults are present, then the depth to lithology changes should be different in each hole. The difference in depth between units and distance between holes would make it possible to calculate the fault dip.
12. Trench along areas where faults have been identified by both GPR and hand auger to prove presence of faults and accurately determine fault dip.
13. Carry out a CO_2 flux survey to determine the concentration of CO_2 in the soil and the rate at which it is passing through the soil. This will provide an indication as to whether degassing is the source of carbonate in the field area, as well as a possible link to faults (i.e. permeable structures.

7.4 Implications for Future Development and Land Use in the Kawerau Area

It is not expected that localised subsidence features at Kawerau will adversely affect future development in the Kawerau area. Future development of any structures should always have adequately designed foundations which are excavated and compacted appropriately. With well-formed foundations it is not expected that localised subsidence features will damage structures. However, it may be appropriate to avoid construction over areas noted for high subsidence if other, less subsiding areas are readily available.

References

ADSE, 2010. *Subsidence investigation, remedial design and control.* [Online]
Available at: www.andrewdust.co.uk
[Accessed 20 June 2010].

Allis, R., 1982. *Comparison of subsidence at Wairakei, Broadlands and Kawerau fields, New Zealand.* Stanford, Eighth Workshop Geothermal Reservoir Engineering.

Allis, R., Bromley, C. & Currie, S., 2009. Update on subsidence at the Wairakei - Tauhara geothermal system, New Zealand. *Geothermics,* pp. 169-180.

Allis, R. et al., 1993. *The Natural State of Kawerau Geothermal Field.* Auckland, NZ Geothermal Workshop.

Allis, R. & Zhan, X., 2000. Predicting subsidence at Wairakei and Ohaaki geothermal fields, New Zealand. *Geothermics,* pp. 479-497.

AMS, 2011. *Dutch Augers.* [Online]
Available at: http://www.ams-samplers.com/itemgroup.cfm?CNum=7&catCNum=6
[Accessed 1 December 2011].

Andriesse, J., 1988. *Nature and management of tropical peat soils.* Rome: Food and Agriculture Organization of the United Nations.

Armstrong, M., 2000. *Geomorphological and Geophysical Investigation of the Effects of Active Tectonic Deformation on the Hydrogeology of North Culverden Basin, North Canterbury,* Christchurch: University of Canterbury.

Atkins, 2011. *Beach and Ellis Mixed-Use Project Environmental Impact Report,* Los Angeles: City of Huntington Beach.

Bacon, C., Amimoto, P., Sherburne, R. & Slosson, J., 1974. *Engineering geology of The Geysers geothermal resource area Lake, Mendocino, and Sonoma Counties, California,* Sacramento: California Division of Mines and Geology.

Beanland, S. & Berryman, K., 1992. Holocene coastal evolution in a continental rift setting; Bay of Plenty, New Zealand. *Quaternary International,* Volume 15-16, pp. 151-158.

Beanland, S., Berryman, K. & Blick, G., 1989. Geological investigations of the 1987 Edgecumbe earthquake, New Zealand. *New Zealand Journal of Geology and Geophysics,* Volume 32, pp. 73-91.

Begg, J. G. & Mouslopoulou, V., 2010. Analysis of late Holocene faulting within an active rift using lidar, Taupo Rift, New Zealand. *Journal of Volcanology and Geothermal Research,* pp. 152-167.

Bignall, G. & Harvey, C., 2005. *Geoscientific Review of the Kawerau Geothermal Field,* Lower Hutt: GNS.

Bixley, P., 1984. Case History No. 9.9. The Wairakei Geothermal Field, New Zealand, by Paul F. Bixley, Ministry of Works and Development, Wairakei, New Zealand. In: J. Poland, ed. *Guidebook to studies of land subsidence due to ground-water withdrawl.* s.l.:UNESCO, pp. 233-240.

Bloomer, A., 1998. Kawerau Geothermal Development: A Case Study. *GHC Bulletin,* pp. 15-18.

Bloomer, A., 2005. *Kawerau Subsidence Interpretation,* Taupo: Geothermal Engineering Ltd.

Bohidar, R. & Hermance, J., 2002. The GPR refraction method. *Geophysics,* 57(5), pp. 1474-1485.

Bristow, C. & Jol, H., 2003. *Ground Penetrating Radar in Sediments.* London: Geological Socitey.

Brock, D., 2006. *Statement of Evidence of Dana Brock.* s.l.:s.n.

Bromley, C. et al., 2010. *Tauhara Stage 2 Geothermal Project Subsidence Report,* s.l.: GNS Science Consultancy Report 2010/151.

Brouwer, J., 2007. *In-Situ Soil Testing.* s.l.:Lankelma.

Carter, A. C. & Hotson, G. W., 1992. Industrial use of geothermal energy at the Tasman Pulp and Paper Co. Ltd's Mill, Kawerau, New Zealand. *Geothermics,* pp. 689-700.

City of Long Beach, 2011. *Wilmington Oil Field.* [Online]
Available at: http://www.longbeach.gov/oil/about/historical.asp
[Accessed 20 November 2011].

Cole, J. et al., 2010. Volcanic and structural evolution of the Okataina Volcanic centre; dominantly silic volcanism associated with the Taupo Rift, New Zealand. *Journal of Volcanology and Geothermal Research,* pp. 123-135.

Concrete Catalog, n.d. *Soil Compaction Handbook.* [Online]
Available at: http://www.concrete-catalog.com/soil_compaction.html
[Accessed 19 June 2010].

Cowen, R., 2003. *Man-Made Subsidence.* Davis: University of California, Davis.

Cuenca, M., Hanssen, R. & van Leijen, F., 2007. *Subsidence due to peat decomposition in the Netherlands.* Frascati, Delft University of Technology.

Curie, S., 2011a. *Kawerau Geothermal Field - Brief report on the March 2011 Subsidence Levelling Survery near the MRP Station,* s.l.: Energy Surveys.

Curie, S., 2011b. *Kawerau Geothermal Field - Bried Report on the 3-4th May 2011 Subsidence Levelling Survey near the MRP Station,* Taupo: Energy Surveys.

Daniels, J., 2000. *Ground Penetrating Radar Fundamentals,* Columbus: The Ohio State University.

Davis, G. & Annan, A., 1989. Ground-penetrating radar for high-resolution mapping of soil and rock stratigraphy. *Geophysical Prospecting,* Volume 37, pp. 531-551.

DiPippo, R., 2008. *Geothermal Power Plants.* 2nd ed. Oxford: Butterworth-Heinemann.

DWR, 2010. *Methods Used to Measure Subsidence.* [Online]
Available at: www.nd.water.ca.gov
[Accessed 10 June 2010].

Energy Surveys, 2009. *Kawerau Geothermal Field - Report on the June 2009 Subsidence Levelling Survey,* Taupo: Energy Surveys.

Energy Surveys, 2010. *Kawerau Geothermal Field - Report on the June 2010 Subsidence Levelling Survey,* Taupo: Energy Surveys.

Fielding, E., Blom, R. & Goldstien, R., 1998. Rapid subsidence over oil fields measured by SAR interferometry. *Geophysical Research Letters,* 25(17), pp. 3215-3218.

Fletcher Trust Archive, 2011. *Tasman Pulp and Paper Co Ltd - Series 9106P,* s.l.: The Fletcher Trust Archive.

Floys, M., Funning, G., Lipovsky, B. & Gettings, P., 2010. *A reduction in the rate of subsidence observed at The Geysers Geothermal Field, Northern California, between 1994 and 2010.* s.l., American Geophysical Union.

GEOVision, 2010. *Geophysical Methods,* Corona: GeoVision.

Gibbons, W. H., 1990. *The Rangitaiki 1890-1990.* Whakatane: Whakatane and District Historical Society.

Gkowacka, E., Gonzalez, J. & Nava, A., 2000. *Subsidence in Cerro Prieto Geothermal Field, Baja California, Mexico.* Kyushu, World Geothermal Congress.

GNS, 2011. *New Zealand Active Faults Database,* Lower Hutt: Institute of Geological and Nuclear Sciences.

Godfrey, M., 2008. *2D and 3D Geophysical Imaging of Polygonal Patterned Ground in the McMurdo Dry Valleys, Antarctica.* Christchurch: University of Canterbury.

Gordon, D., 2002. *Groundwater Resources of the Bay of Plenty,* Whakatane: Environment Bay of Plenty.

Grindley, G., 1986. Subsurface geology and structure of the Kawerau geothermal field. In: *Geothermal Report.* Lower Hutt: NZ Geological Survey, pp. 49-65.

Gross, R., 2002. *3-D Georadar Surveying Of Active Faults.* Munster: Swiss Federal Institute of Technology Zurich.

Hodgson, K. A. & Nairn, I. A., 2003. *The Sedimentation and Drainage History of Haroharo Caldera and The Tarawera River System, Taupo Volcanic Zone, New Zealand ,* Tauranga: Environment Bay of Plenty.

Hole, J., Bromley, C., Stevels, N. & Wadge, G., 2007. Subsidence in the geothermal fields of the Taupo Volcanic Zone, New Zealand from 1996 to 2005 measured by InSAR. *Journal of Volcanology and Geothermal Research,* pp. 125-146.

Hornberger, G., Raffensperger, J., Wilberg, P. & Eshleman, K., 1998. *Elements of Physical Hydrology.* Baltimore: John Hopkins University Press.

Hornblow, S., 2010. *Climatic Controls on the Physical Properties of the Ruataniwha Fault, Ostler Fault Zone, New Zealand,* Christchurch: University of Canterbury.

Hunt, T., Sugihara, M., Sato, T. & Takemura, T., 2002. Measurement and use of the vertical gravity gradient in correcting repeat microgravity measurements for the effects of ground subsidence in geothermal systems. *Geothermics,* pp. 525-543.

I.S.R.M, 1975. *Recommendations on Site Investigation Techniques,* s.l.: International Society of Rock Mechanics.

Jaksa, M. B., 1990. *A Data Acquisition System for the Cone Penetration Test.* Adelaide, The University of Adelaide, pp. 22-31.

Jol, H., 2009. *Ground Penetrating Radar: Theory and Applications.* 1st ed. Oxford: Elsevier Science.

Kahn, M., 2007. *The Geysers Geothermal Field, an Injection Success Story.* Santa Rosa: Division of Oil, Gas and Geothermal Resources.

Kelsey, P., 1986. *An Engineering Geological Investigation of Ground Subsidence above the Huntly East Mine Area.* Christchurch: University of Canterbury.

Kosloff, D., Scott, R. & Scranton, J., 1980. Finite Element Simulation of Wilmington Oil Field Subsidence: 1. Linear Modelling. *Tectonophysics,* Volume 65, pp. 339-368.

Lankelma, 2010. *Guide to CPT.* [Online]
Available at: www.lankelma.co.uk
[Accessed 20 June 2010].

Lawless, J. et al., 2003. *Two dimensional subsidence modelling at Wairakei-Tauhara, New Zealand.* Reykjavik, International Geothermal Conference.

Lowenstern, J. & Janik, C., 2002. *The Origins of Reservoir Liquids and Vapors from The Geysers Geothermal Field, California (USA),* Menlo Park: U.S.G.S.

Lund, J., Bloomquist, G., Boyd, T. & Renner, J., 2005. *The United States of America Country Update.* Antalya, Proceedings World Geothermics Congress.

Massarsch, D. K. R., 1999. *Deep compaction of granular soils.* Zhejiang University, Zhejiang University.

McKenzie, S. & McLeod, M., 2004. *Subsidence rates of peat since 1925 in the Moanatuatua Swamp area,* Hamilton: Landcare Research.

Mighty River Power, 2005. *Kawerau Geothermal Power Station - Assessment of Environmental Effects,* s.l.: Mighty River Power.

Milicich, S. et al., 2010. *Stratigraphic Correlation Study of the Kawerau Geothermal Field,* Lower Hutt: GNS.

Milicich, S. et al., 2011. *Buried rhyolite in the Kawerau Geothermal Field, Taupo Volcanic Zone, New Zealand: sources of a rejuvenated geothermal system.* Auckland, New Zealand Geothermal Workshop 2011 Proceedings.

Mossop, A. & Segall, P., 1997. Subsidence at The Geysers geothermal field, N. California from a comparison of GPS and levelling surveys. *Geophysical Research Letters,* 24(14), pp. 1839-1842.

Nairn, I. & Beanland, S., 1989. Geological setting of the 1987 Edgecumbe earthquake, New Zealand. *New Zealand Journal of Geology and Geophysics,* Volume 32, pp. 1-13.

Nairn, I. & Wiradiradja, S., 1980. Late Quaternary Hydrothemal Explosion Breccias at Kawerau Geothemal Field, New Zealand. *Volcanol,* 43(1).

NEES, n.d. *Cone Penetration Testing,* Los Angeles: UCLA.

NZGA, 2011. *New Zealand Geothermal Fields.* [Online]
Available at: www.nzgeothermal.org.nz
[Accessed 18 September 2011].

O'Sullivan, M., Yeh, A. & Clearwater, E., 2010. *Three-dimensional model of subsidence at Wairakei-Tauhara,* Auckland: The University of Auckland.

Otott, G. & Clarke, D., 2007. *Histoy of the Wilmington Field - 1986-1996,* s.l.: AAPG Pacific Section, 2007.

Powell, T., 2011. *Natural Subsidence at the Rotokawa Geothermal Field and implications for permeability development.* San Diego: s.n.

Quijano-Leon, J. & Gutierrez-Negrin, L., 2003. An Unfinished Journey - 30 years of Geothermal-Electric Generation in Mexico. *Geothermal Resources Council*, September/October, pp. 198-203.

Reynolds, J. M., 2011. *An Introduction to Applied and Environmental Geophysics - 2nd Edition.* Oxford: Wiley-Blackwell.

Rietveld, H., 1983. *Land Subsidence in the Netherlands.* Venice, The Third International Imposium on Land Subsidence.

Rissman, C. et al., 2010. A model to explain the spatial variation in the magnitude of pressure-induced ground subsidence - Ohaaki hydrothermal field, New Zealand. In: *Using Surface Methods to Understand the Ohaaki Hydrothermal Field, New Zealand.* Christchurch: University of Canterbury, pp. 89-132.

Ryan, R. & Fraser, B., 2010. *Field Guide for Geoscientists and Technicians.* 3rd ed. Burwood: The Australasian Institute of Mining and Metallurgy.

Samsonov, S. & Tiampo, K., 2010. Time series analusis of subsidence at Tauhara and Ohaaki geothermal fields, New Zealand, observed by ALOS PALSAR interferometry during 2007-2009. *Canadian Journal of Remote Sensing,* Volume 36, pp. S327-S334.

Schmidt, W., 2005. *Geological and Geotechnical Investigation Procedures For Evaluation of the Causes of Subsidence Damage In Florida,* Tallahassee: Florida Geological Survey.

Seiga, C., Seiga, F., Pezaro, B. & Wallis, I., 2011. *Kawerau Geothermal Limited (KGL) Annual Report,* s.l.: Mighty River Power.

Sensors & Software, 2003. *EKKO_View Enhanced & EKKO_View Deluxe User's Guide.* Mississauga: Sensors & Software.

SKM, 2005. *Kawerau Subsidence Review - Geotechnical Investigation Report,* Auckland: Sinclair Knight Merz.

Spinks, K., Cumming, B. & Currie, S., 2007. *Subsidence at the Kawerau Geothermal Field to 2006.* s.l., NZGA.

Summers, M., Hikuroa, D. & Gravley, D., 2008. *Ground Penetrating Radar as an Investigative Tool: Human-Modified to Natural Environments,* Stanford: Stanford University Geological and Environmental Sciences.

Terralog Technologies, 2006. *Summary of Rock Property Measurements and Implications for Subsidence at the Kawerau Field,* Arcadia: Terralog Technologies.

Terralog Technologies, 2006. *Summary of Subsidence Risks and Recommendations for Geothermal Operations at the Kawerau Field,* Arcadia: Terralog Technologies.

Terzaghi, K., Peck, R. & Gholamreza, M., 1996. *Soil mechanics in engineering practice.* 3rd ed. New York: Wiley.

Udata, M., 2001. Zeolites in Hydrothermally Altered Rocks. *Reviews in Mineralogy and Geochemistry,* 45(1), pp. 305-322.

URS, 2005. *Kawerau Geothermal Power Station Factual Report,* Hamilton: URS.

USGS, 2005. *Measuring Human-Induced Land Subsidence from Space.* [Online]
Available at: http://pubs.usgs.gov/fs/fs06903/
[Accessed 10 June 2010].

USGS, 2009. *Volcanic Ash: Effects and Mitigation Strategies.* [Online]
Available at: http://volcanoes.usgs.gov/ash/water/index.html
[Accessed 16 March 2010].

Wallace, S. et al., 2010. Three-dimensional GPR imaging of the Benmore anticline and step-over of the Ostler Fault, South Island, New Zealand. *Geophysical Journal International,* pp. 465-474.

White, J., Houghton, B., Hodgson, K. & Wilson, C., 1997. Delayed sedimentary response to the A.D. 1886 eruption of Tarawera, New Zealand. *Geology,* pp. 459-462.

Wigley, D., 1993. *Developments in Kawerau Geothermal Field.* Wairakei, WORKS Geothermal, pp. 47-53.

Wood, P. C., Braithwaite, R. L. & Rosenberg, M. D., 2001. Basement structure, lithology and permeability at Kawerau and Ohaaki geothermal fields, New Zealand. *Geothermics,* pp. 461-481.

Xia, J. & Miller, R. D., 2007. Integrated geophysical survey in defining subsidence features on a golf course. *Journal of Geophysics and Engineeringq,* pp. 443-451.

Yetton, M. & Nobes, D., 1998. Recent vertical offset and near-surface structure of the Alpine Fault in Westland, New Zealand, from ground penetrating radar profiling. *New Zealand Journal of Geology and Geophysics,* Volume 41, pp. 485-492.

Young, R. & White, S., 2005. *Consent Scenarios for the Kawerau Geothermal Field,* Lower Hutt: Industrial Research Limited.

Appendices

Appendix A: Results from compressibility and thermal expansion tests

Results from compressibility tests

Formation	Sample ID	Depth (m)	Estimated In-Situ Reservoir Pressure (psi)	Grain Compressibility (10^{-6}/psi)	In-Situ Porosity (%)	Inferred Reservoir Pressure Range[1] (psi)	Bulk Compressibility[2] (10^{-6}/psi)	Pore Volume Compressibility (10^{-6}/psi)	Porosity (%)
Onepu Ash	MR-63	245	355	0.2	44.06	350 to 280	23.45	53.071	44.02
						195 to 125	132.4	305.402	43.32
						100 to 30	136.5	321.1	42.48
	MR-7	245	355	0.2	42.65	355 to 280	1.957	4.39	42.64
						230 to 160	2.371	5.362	42.62
						125 to 55	2.543	5.768	42.61
Rangitaiki Ignimbrite	MR-1	427	620	0.2	40.41	560 to 400	2.049	4.873	40.39
						355 to 225	2.25	5.374	40.37
						175 to 40	2.399	5.747	40.34
	MR-2	427	620	0.2	40.52	585 to 480	2.011	4.764	40.51
						375 to 255	3.201	7.708	40.48
						155 to 35	4.316	10.475	40.43
Onepu Rhyolite	MR-12	514	745	0.2	27.84	675 to 540	1.402	4.84	27.82
						430 to 295	1.334	4.6	27.79
						180 to 70	1.181	4.052	27.77
	MR-13	514	745	0.2	21.16	750 to 610	4.216	19.749	21.13
						455 to 295	2.193	10.21	21.07
						160 to 45	1.785	8.291	21.02
Huka Falls Formation	MR-16	594	860	0.2	27.5	790 to 570	2.041	7.228	27.48
						455 to 300	1.959	6.941	27.43
						235 to 75	1.934	6.858	27.4
	MR-17	594	860	0.2	28.18	780 to 550	2.05	7.084	28.15
						445 to 280	1.931	6.671	28.1
						215 to 60	1.869	6.458	28.07
Greywacke	MR-26	1616	2345	0.2	11.34	1985 to 1535	0.356	2.947	11.31
						1265 to 770	0.319	2.621	11.29
						550 to 135	0.305	2.509	11.27
	MR-27	1272	1845	0.2	7.69	1770 to 1350	0.24	2.915	7.69
						1170 to 750	0.25	3.061	7.68
						565 to 145	0.335	4.172	7.66

Results from axial thermal expansion tests

Litho-Type	Depth (m)	Confining Pressure (psi)	Sample ID	α axial ~45 to ~88°C (10^{-6} /°C)	α axial ~88 to ~128°C (10^{-6} /°C)	α axial ~128 to ~167°C (10^{-6} /°C)	α axial ~167 to ~128°C (10^{-6} /°C)	α axial ~128 to ~88°C (10^{-6} /°C)	α axial ~88 to ~45°C (10^{-6} /°C)
Rangitaiki Ignimbrite	427	740	MR-3	8.42	15.87	19.76	15.42	15.9	11.79
				Average Over Entire Range = 14.68			Average Over Entire Range = 14.37		
			MR-4	9.98	11.62	12.28	10.83	10.36	12.58
				Average Over Entire Range = 11.29			Average Over Entire Range = 11.25		
Onepu Ash	245	425	MR-8	9.8	17.21	17.45	12.99	18.22	13.13
				Average Over Entire Range = 14.82			Average Over Entire Range = 14.78		
			MR-9	4.28	8.85	9.27	7.16	6.45	6.69
				Average Over Entire Range = 7.47			Average Over Entire Range = 6.77		
Onepu Rhyolite	514	895	MR-14	13.73	23.91	28.61	26.7	20.81	24.53
				Average Over Entire Range = 22.08			Average Over Entire Range = 24.01		
			MR-15	16.04	29.53	29.64	18.39	29.75	24.92
				Average Over Entire Range = 25.07			Average Over Entire Range = 24.35		
Huka Falls Formation	594	1035	MR-18	3.56	8.76	9.23	8.48	7.27	5.4
				Average Over Entire Range = 7.18			Average Over Entire Range = 7.05		
			MR-19	8.09	9.22	9.69	8.91	9.99	11.26
				Average Over Entire Range = 9.00			Average Over Entire Range = 10.05		
Greywacke	1616	2810	MR-25	9.24	13.6	13.72	14.59	13.11	8.49
				Average Over Entire Range = 12.19			Average Over Entire Range = 12.06		
	1272	2210	MR-27	3.79	8.89	12.98	9.97	8.69	6.32
				Average Over Entire Range = 8.55			Average Over Entire Range = 8.33		

Results from radial thermal expansion tests

Litho-Type	Depth (m)	Confining Pressure (psi)	Sample ID	α axial ~45 to ~88°C (10^{-6} /°C)	α axial ~88 to ~128°C (10^{-6} /°C)	α axial ~128 to ~167°C (10^{-6} /°C)	α axial ~167 to ~128°C (10^{-6} /°C)	α axial ~128 to ~88°C (10^{-6} /°C)	α axial ~88 to ~45°C (10^{-6} /°C)
Rangitaiki Ignimbrite	427	740	MR-3	18.14	21.14	22.99	30.38	17.82	12.7
				Average Over Entire Range = 20.76			Average Over Entire Range = 20.30		
			MR-4	14.05	14.26	18.86	15.29	15.77	14.12
				Average Over Entire Range = 15.72			Average Over Entire Range = 15.06		
Onepu Ash	245	425	MR-8	15.07	17.45	20.57	20.92	16.25	13.98
				Average Over Entire Range = 17.70			Average Over Entire Range = 17.05		
			MR-9	11.16	11.15	14.59	9.84	11.85	12.58
				Average Over Entire Range = 12.30			Average Over Entire Range = 11.42		
Onepu Rhyolite	514	895	MR-14	23.91	22.95	28.89	27.24	23.71	23.61
				Average Over Entire Range = 25.25			Average Over Entire Range = 24.85		
			MR-15	22.61	24.51	27.39	26.84	24.71	22.08
				Average Over Entire Range = 24.27			Average Over Entire Range = 22.42		
Huka Falls Formation	594	1035	MR-18	13.4	15.41	20.13	18.29	13.28	12.73
				Average Over Entire Range = 16.31			Average Over Entire Range = 14.68		
			MR-19	12.59	13.81	17.13	18.88	12.61	12.49
				Average Over Entire Range = 14.51			Average Over Entire Range = 14.66		
Greywacke	1616	2810	MR-25	13.2	14.24	15.1	16.41	12.82	12.07
				Average Over Entire Range = 14.18			Average Over Entire Range = 13.77		
	1272	2210	MR-27	15.49	14.63	18.71	23.31	13.15	12.07
				Average Over Entire Range = 16.28			Average Over Entire Range = 16.18		

Appendix B: Aerial photographs

1944

1944

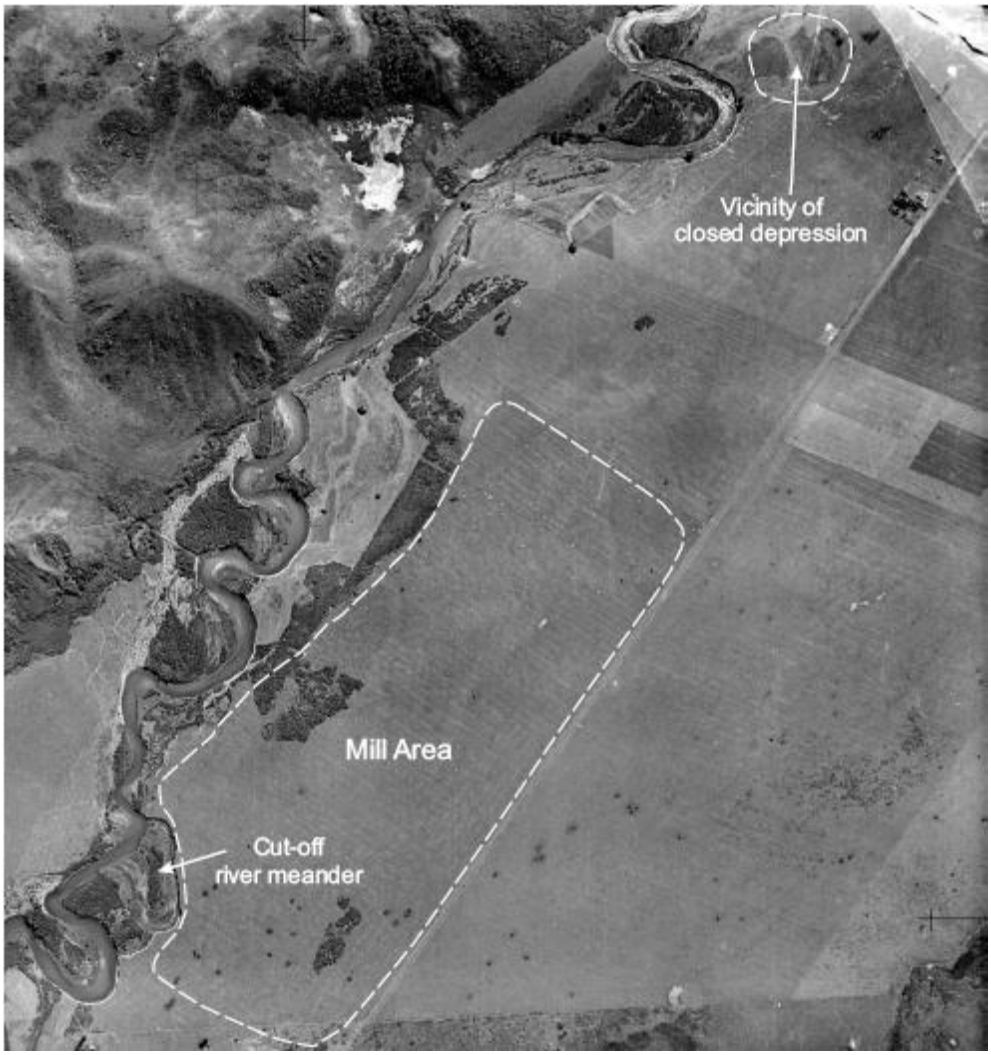

1945 from Brock (Brock, 2006).

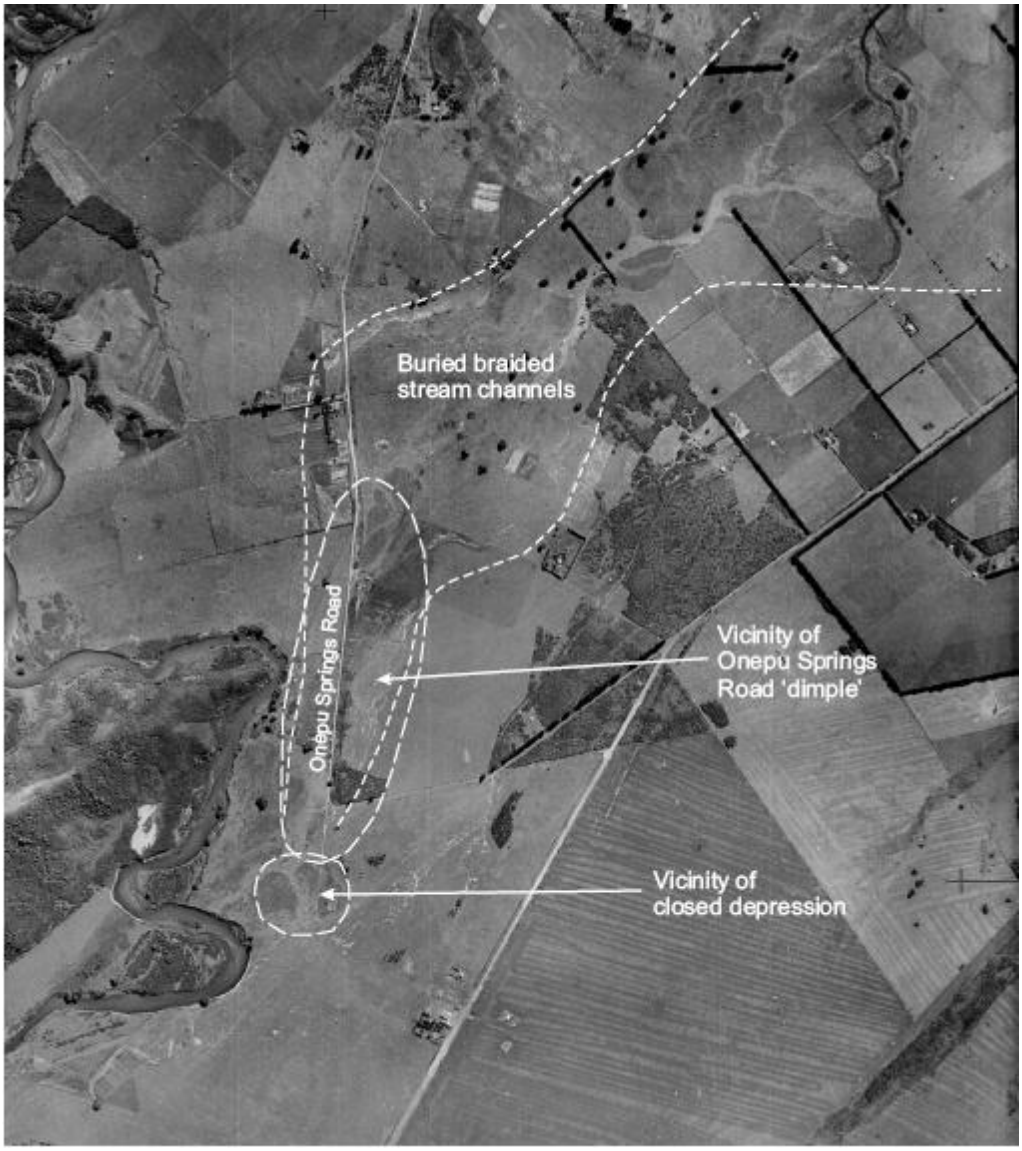

1945 from Brock (Brock, 2006).

1950’s from Brock (Brock, 2006).

30/10/1965

1966

1966

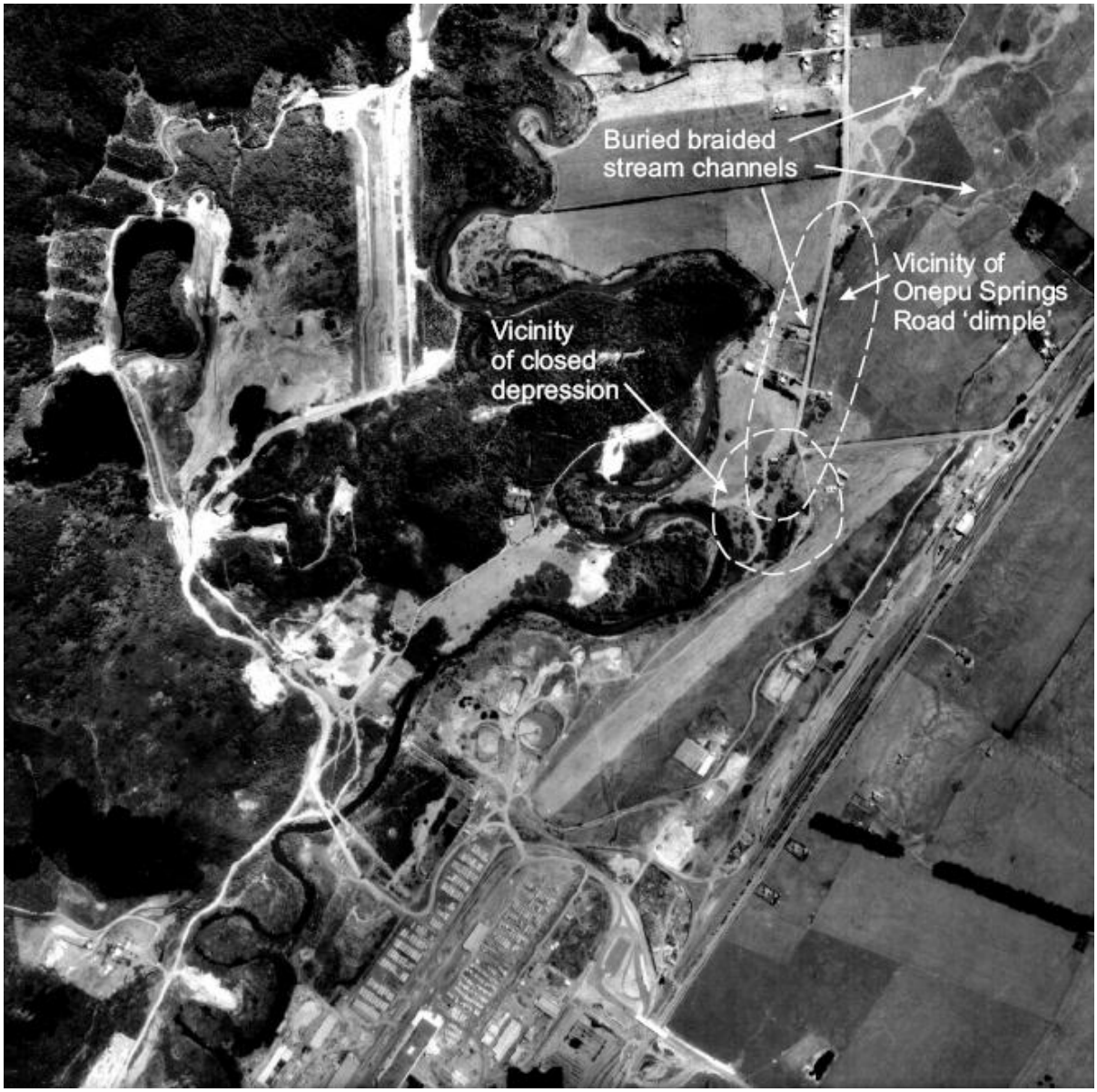

1987 from Brock (Brock, 2006).


REGIONAL
UNCIL
NEGATIVE No.
165369
APPROX.
SCALE
1 : 25,000
FLOWN
22-6-92
PHOTOGRAPHY BY
AIR-MAPS
Ph & FAX (07)5788929

22/6/1992


.P. REGIONAL
COUNCIL
2 -WESTERN
OF PLENTY
NEGATIVE NO
170535
APPROX.
SCALE
1:25,000
FLOWN
1-1-93
AIR-MAPS
PHONE (07) 5788929
FAX (07) 5788029
CELL 025 960361

1/1/1993


NEGATIVE NUMBER
183290
APPROX SCALE
1:15.000
DATE FLOWN
18·10·95
AIR MAPS
PHONE 07 57
FAX 07 57880
CELL 025 960

18/10/1995


ONMENT BOP
T15, U15, V15
NEGATIVE
191536
APPROX
SCALE
1:15,000
FLOWN
17-4-97
AIR MAPS
Ph 07 5788929
Fax 07 5788029
Cell 025 960361

17/4/1997


RONMENT BOP
T15, U15, V15
NEGATIVE
19497/
APPROX
SCALE
1:15,000
FLOWN
13-12-97
AIR MAPS
Ph 07 5788929
Fax 07 5788029
Cell 025 960361

13/12/1997

ENVIRONMENT BOP
NEGATIVE NUMBER
2083Q4
APPROX SCALE
1:15,000
FLOWN
18 3 00
AIRMAPS
Ph 07 578892
Fax 07 57880

18/3/2000

2001

1/12/2002

23/1/2004

August 2009

Appendix C: Mill construction photographs

1951 aerial photograph of proposed mill site, this shows the presence of many active and abandoned river channels

1951 aerial photograph of proposed mill site

1953 photograph of proposed mill site

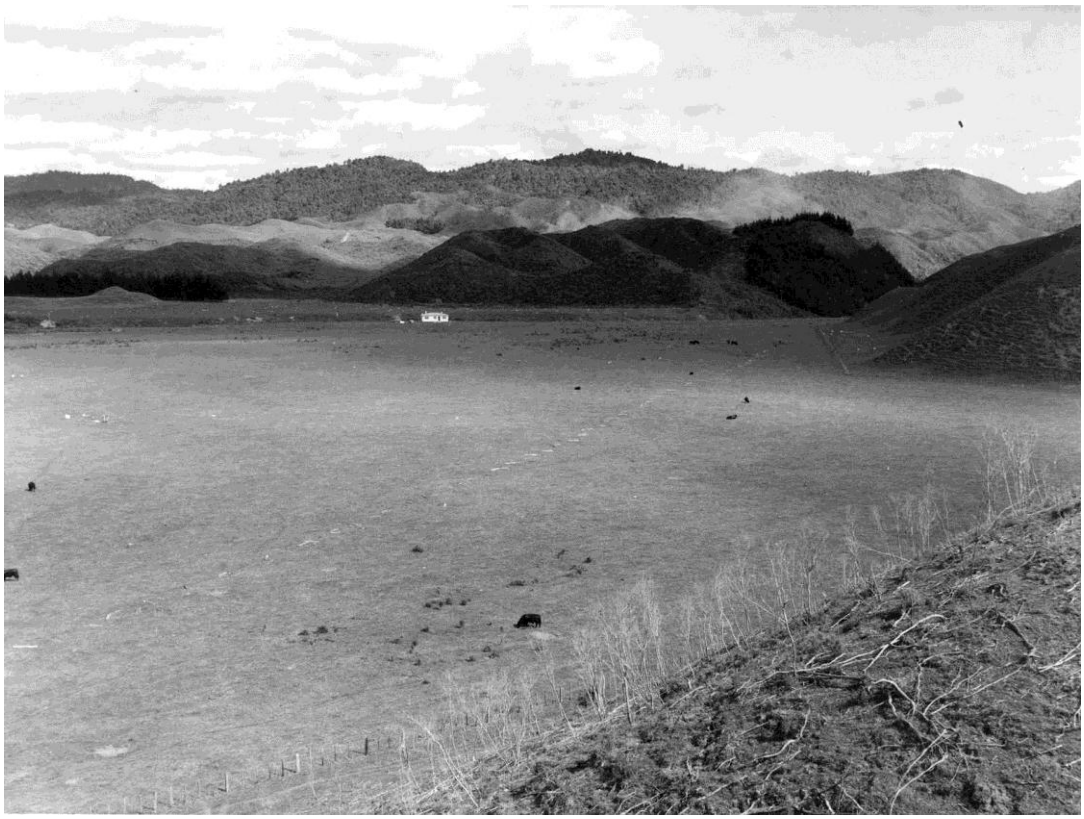

1953 photograph of proposed mill site

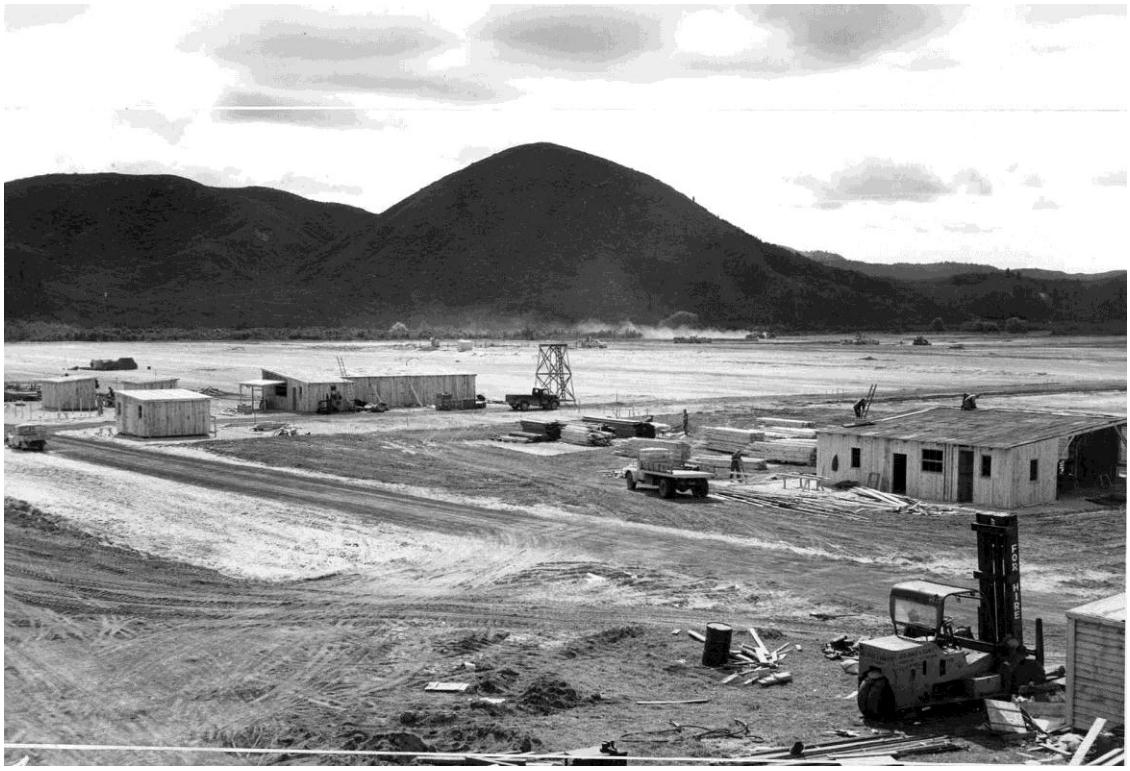

1953 photograph of mill construction beginning

1953 photograph of mill area

8 April 1955 – start of construction of the pulp and paper mill

8 September 1955, pulp and paper mill site

9 November 1955 – pulp and paper mill site

Circa 1955 aerial photograph of mill site

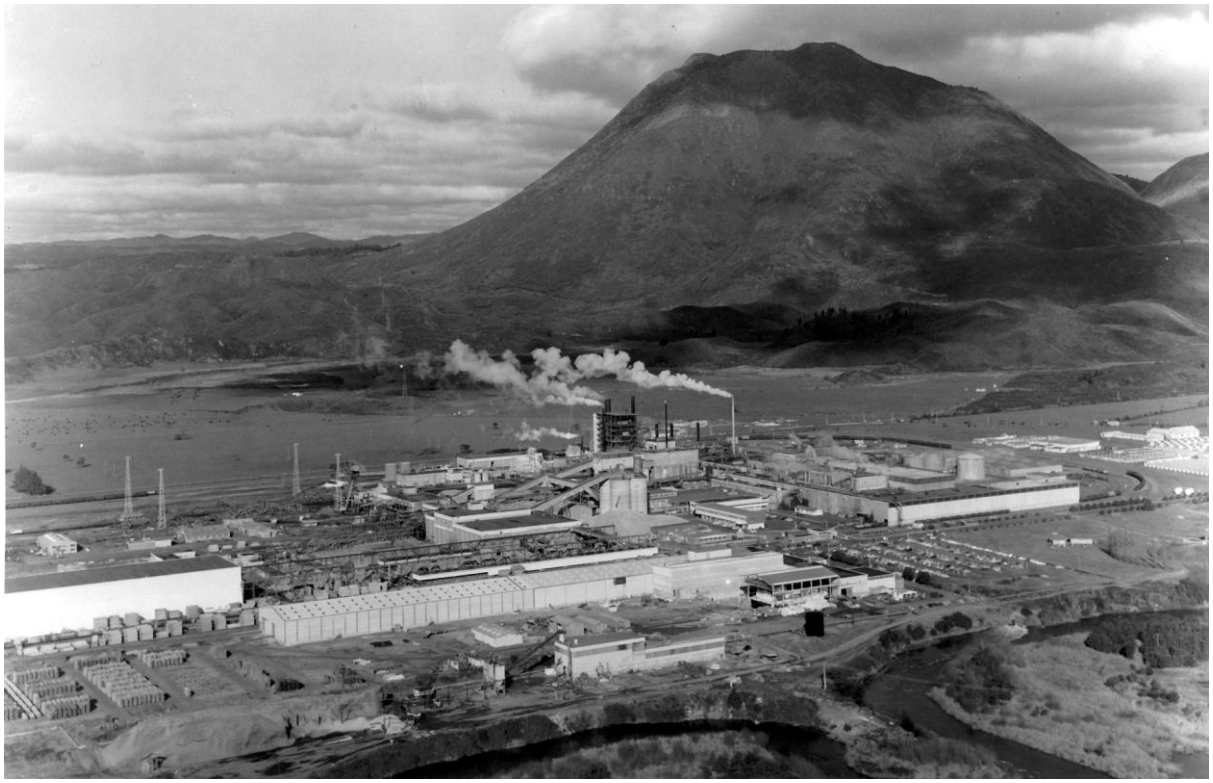

Circa 1955 aerial photograph of mill site

Circa 1955 aerial photograph of mill site

Circa 1955 aerial photograph of mill site

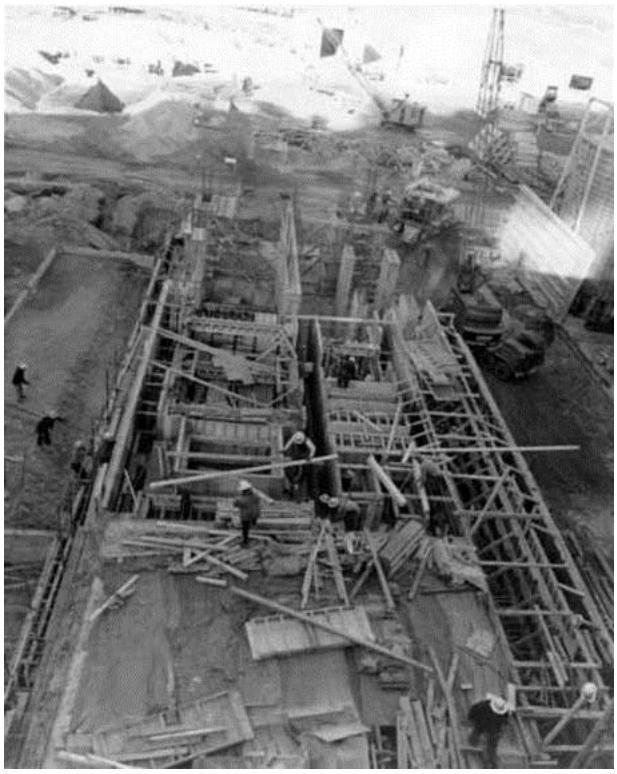

1962 photograph showing excavation of foundations for extensions

Appendix D: Geophysical principles

D.1. Ground penetrating radar

D.1.1 Background

Ground penetrating radar (GPR) is a near surface geophysical investigation technique which can be used in a range of settings to help detect subsurface bedding, structure, the water table, voids, buried objects and foreign material. GPR usually consists of a signal generator, a transmitting and receiving antenna, and a control console for managing the signal generation and recording (Reynolds, 2011). GPR has become a popular geophysical technique that is frequently used to image sedimentary structures (Bristow & Jol, 2003); (Jol, 2009); (Reynolds, 2011). GPR can be conducted at a range of frequencies depending on the desired resolution and can detect features from centimetre to metre scale (Davis & Annan, 1989). GPR uses high frequency electromagnetic energy in the form of radio waves, typically between 10 and 1000 MHZ to transmit a signal into the ground. The waves reflect and refract when they travel through a boundary of two media with differing physical properties, the waves are then detected by a receiver at the surface which records the time from when the wave was transmitted to when the wave was received (Davis & Annan, 1989). The transmitter and receiver are usually assembled in a fixed geometry, which is then moved over the surface to detect reflections from subsurface features (Jol, 2009); this was the case in Kawerau (see Figure 41). An image is formed from reflected waves as a series of wiggle traces with positive signal returns shaded and negative signal returns unshaded and looks similar to a geological cross-section (Armstrong, 2000); (Reynolds, 2011).

As with all geophysics, the higher the resolution of the survey, the lower the depth of penetration; resolution and depth of penetration depend on the frequency of the antennae used in the survey as well as the properties of the material being surveyed. The greatest control on depth of penetration is the conductivity of the material. As the conductivity increases, the depth of penetration of the electromagnetic waves decreases. This means that penetration decreases in areas of high clay content, silts and soils with saline or contaminated pore water (Davis & Annan, 1989); (Jol, 2009).

GPR is a non-invasive investigation technique; this means the ground that is being surveyed remains intact and undisturbed. This can be important in areas where ground excavation is not possible or unwanted as in Kawerau where excavation would have disturbed ground used for grazing. The non-invasive properties of GPR make it useful for detection of buried services such as pipelines and

buried cables where excavation may damage the services. It is often good practice to ground truth a large GPR survey where possible by hand augering, trenching or a test pit.

GPR is a useful technique for identifying faults and producing high-resolution images of young (Quaternary) sediments in the near surface through both 2-D and 3-D GPR surveys (Jol, 2009); (Reynolds, 2011).

D.1.2 Geophysical principles

Electromagnetic energy is transmitted as a pulse. When this energy is transmitted into the ground it also travels to the receiving antenna through the air (A) and along the surface of the ground (G) directly from one antenna to the other as shown in Figure 107 (Jol, 2009). The reflected ground wave (R) is the most important as its arrival time gives information on the distance to various reflective boundaries in the subsurface, the time taken for the pulse to get from the transmitter to the receiver via the reflective surface is known as the two way travel time (TWT).

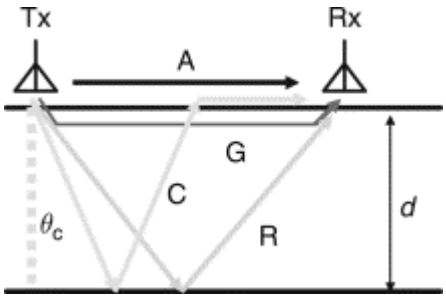

Figure 107: Signal paths between a transmitter and a receiver on the surface. A is the direct airwave, G is the direct ground wave, R is the reflected wave, and C is the critically refracted wave. From Jol, (2009).

The propagation of waves through the ground is primarily dependent on the dielectric permittivity and electrical conductivity properties of the subsurface; however the presence or absence of water in the material dominates the behaviour of the waves (Jol, 2009). The contrast in physical properties (such as dielectric permittivity or electrical conductivity) between two media is the reason why features are distinguishable in the profiles. GPR methods normally depend on detection of reflected or scattered signal. As the wave crosses an interface between two materials the direction of travel changes (is refracted) in accordance with Snell's law (Jol, 2009).

$$\frac{v1}{v2} = \frac{\sin\theta 1}{\sin\theta 2}$$

Equation 5: Snell's law

Where v1 and v2 are the velocities of the wave through the upper and lower materials, and Θ1 and Θ2 are the angles of the incident and refracted raypaths (Daniels, 2000).

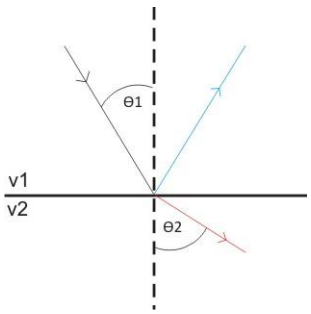

Figure 108: Simple reflection at a geological boundary showing incident wave raypath (black line), reflected wave (blue line) and, refracted wave (red line). Layer 1 velocity (v1) < Layer 2 velocity (v2).

Figure 108 shows the relationship between the angle of propagation, reflection and refraction of a wave. Subsurface refraction occurs when layer 2 has a higher velocity than layer 1 (Bohidar & Hermance, 2002). Velocity tends to decrease with increasing layer density as velocity is proportional to relative permittivity which is, in turn, proportional to density. If the velocity decreases across a boundary, the refracted wave will be bent further towards the normal (Reynolds, 2011). This is often seen when the water table is reached as water has a much higher dielectric permittivity relative to air (Reynolds, 2011).

GPR works by receiving small electrical signals through its receiving antenna. The antenna cannot distinguish between electrical signals intentionally generated by the GPR unit and electrical signals from the surrounding environment. This leaves the GPR unit exposed to 'noise' from other sources as shown in Figure 109.

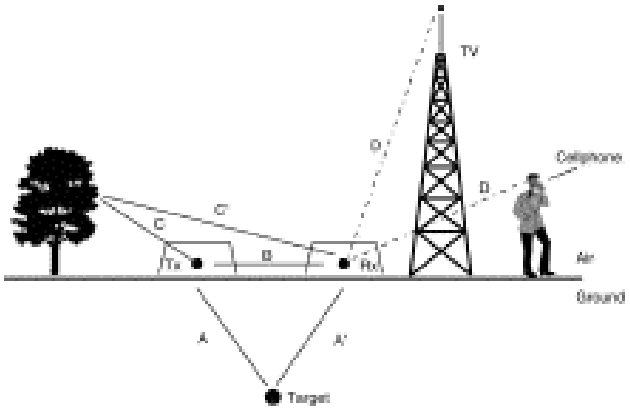

Figure 109: GPR noise sources. From Jol, (2009).

There are many possible signals and paths, the objective is to maximise the target response and minimise others.

D.2. Electrical Imaging

D.2.1. Background

Electrical imaging is the tomographic reconstruction of automated electrical resistivity data acquisition and has been used extensively since the 1970's and has proven capabilities in identifying water sources and also monitoring groundwater pollution, locating sub-surface cavities, faults and fissures as well as mapping of archaeological features (Reynolds, 2011). Electrical resistivity is a useful technique to be used alongside GPR, the resistivity method measures the electrical resistivity of the subsurface by placing electrodes into the ground and transmitting pulses of current into the ground, the system can determine the chargeability of the subsurface by measuring the time-decay of the electrical polarisation induced by the pulse. Minerals that allow electric current to pass through them have low electrical resistivity and include minerals such as iron. High resistivity minerals do not let electricity pass through them easily and include minerals such as quartz and feldspar (Ryan & Fraser, 2010).

Electrical imaging systems typically use either 64, 128 or 256 electrodes for detailed cross sections of ground properties. The arrangement of the transmitting and receiving electrodes (the electrode array), on the ground controls the resolution of the measured electrical properties, depth of investigation, and the geometrical and lateral resolution of specific geologic targets (Ryan & Fraser, 2010).

D.2.2. Geophysical principles

Electrical imaging requires a source of electrical energy to excite the subsurface. Electrodes are placed at even intervals along a survey line and set to run through a series of different voltage and current measurements, the current entering and exiting the ground at different points for each measurement. The current is 'injected' into the ground at one electrode and a second current electrode will complete the circuit, while two electrodes in the middle measure the potential difference across the ground in the centre of this circuit (Reynolds, 2011).

Once data are collected, they are typically processed through a tomographic modelling and reconstruction program as discussed in 5.2.2.

Appendix E: Ground penetrating radar profiles

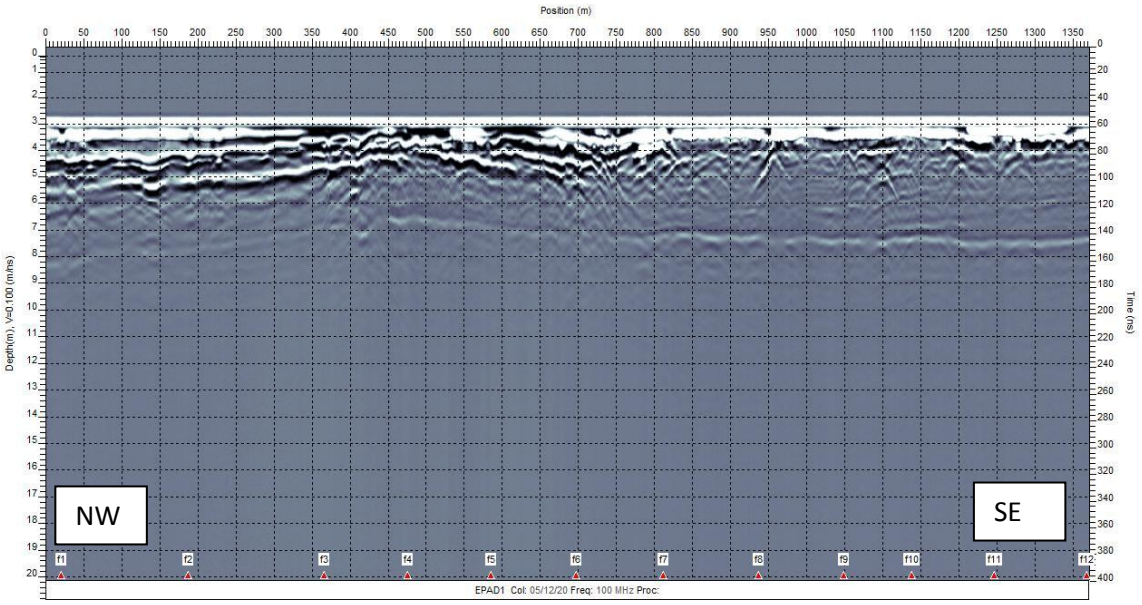
Position (m)
Depth(m), V=0.100 m/ns
Time (ns)
NW
SE
f1
f2
f3
f4
f5
f6
f7
f8
f9
f10
f11
f12
EPAD1 Col: 05/12/20 Freq: 100 MHz Proc:

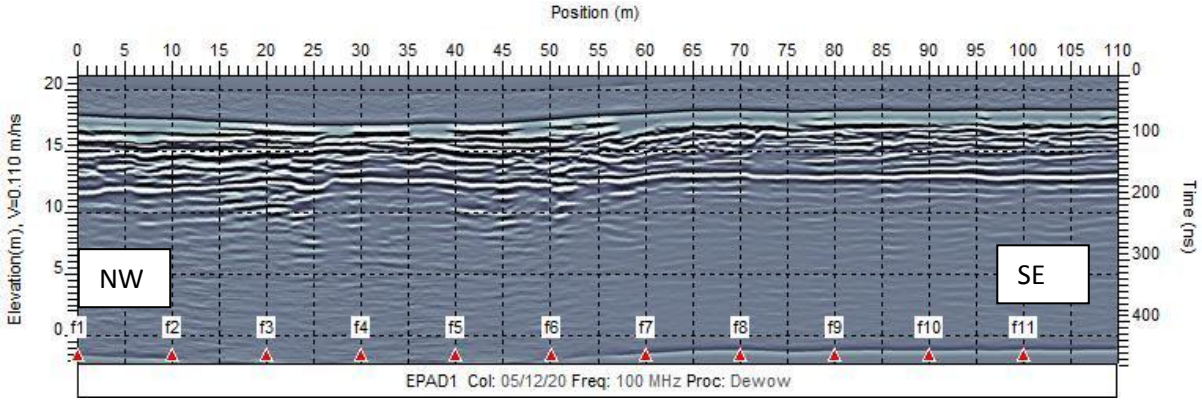
Position (m)
Elevation(m), V=0.110 m/ns
Time (ns)
NW
SE
f1
f2
f3
f4
f5
f6
f7
f8
f9
f10
f11
EPAD1 Col: 05/12/20 Freq: 100 MHz Proc: Dewow

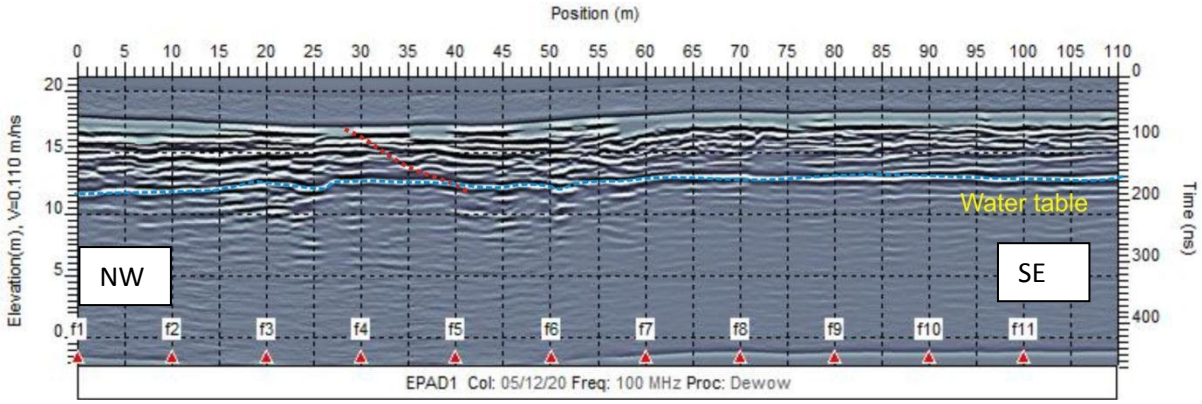
Position (m)
Elevation(m), V=0.110 m/ns
Time (ns)
Water table
NW
SE
f1
f2
f3
f4
f5
f6
f7
f8
f9
f10
f11
EPAD1 Col: 05/12/20 Freq: 100 MHz Proc: Dewow

EPAD1

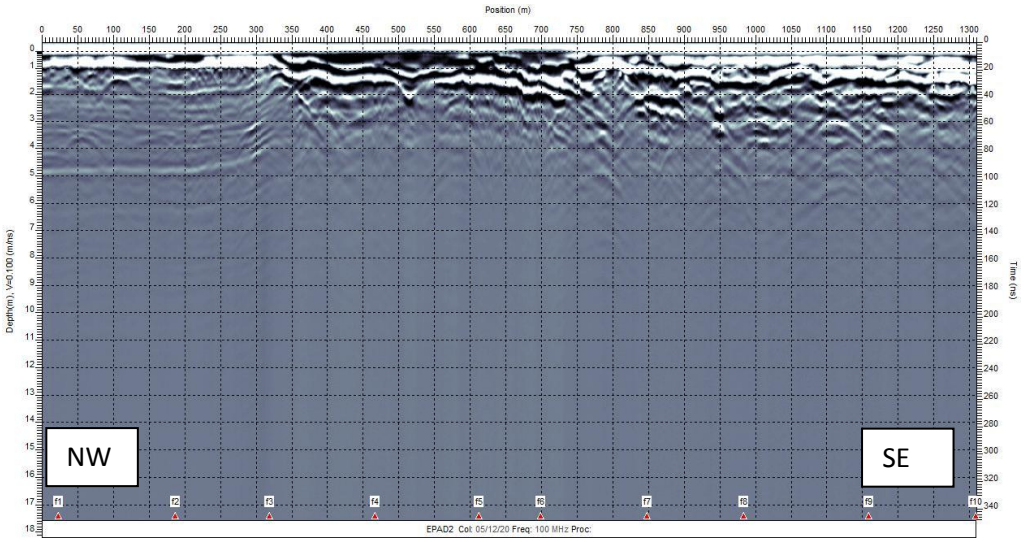
Position (m)
Depth(m), V=0.100 m/ns
Time (ns)
NW
SE
EPAD2 Col: 05/12/20 Freq: 100 MHz Proc:

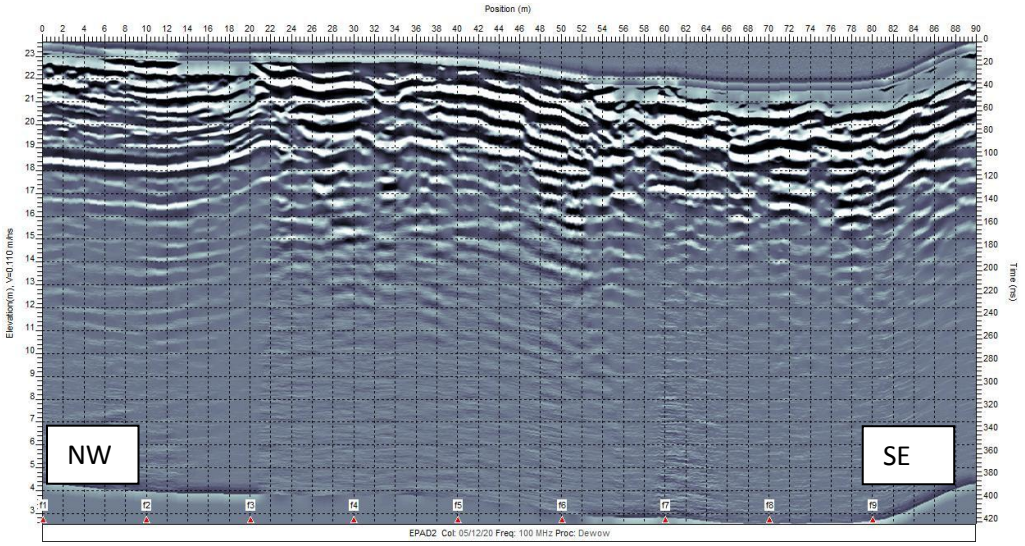
Position (m)
Elevation(m), V=0.110 m/ns
Time (ns)
NW
SE
EPAD2 Col: 05/12/20 Freq: 100 MHz Proc: Dewow

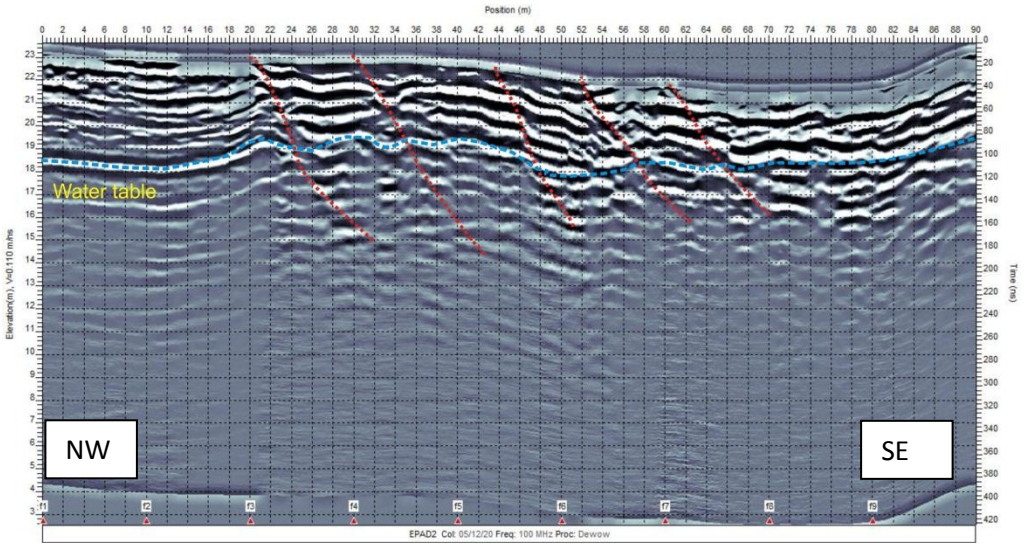
Position (m)
Water table
Elevation(m), V=0.110 m/ns
Time (ns)
NW
SE
EPAD2 Col: 05/12/20 Freq: 100 MHz Proc: Dewow

EPAD2

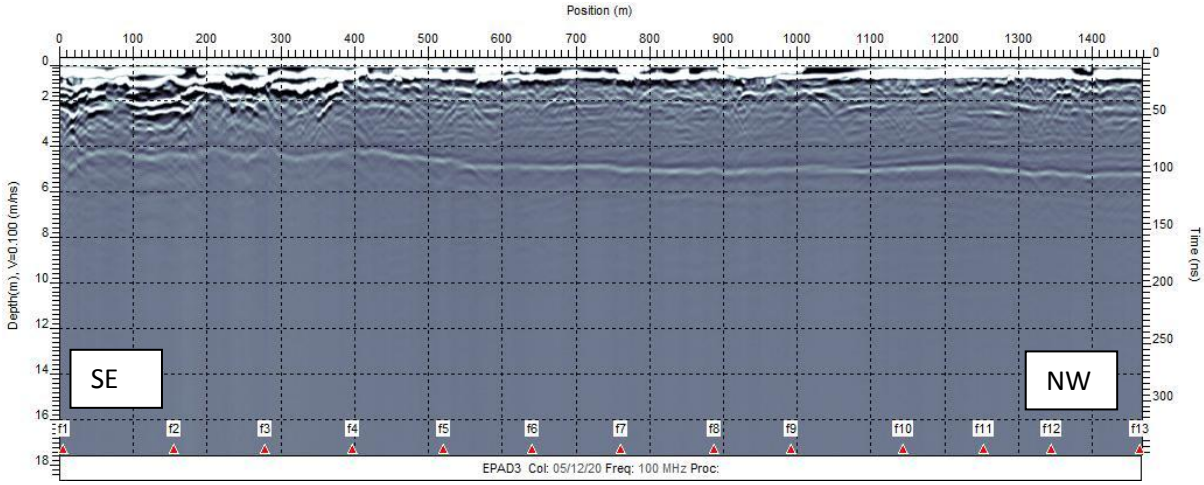
Position (m)
Depth(m), V=0.100 (m/ns)
Time (ns)
SE
NW
f1 f2 f3 f4 f5 f6 f7 f8 f9 f10 f11 f12 f13
EPAD3 Col: 05/12/20 Freq: 100 MHz Proc:

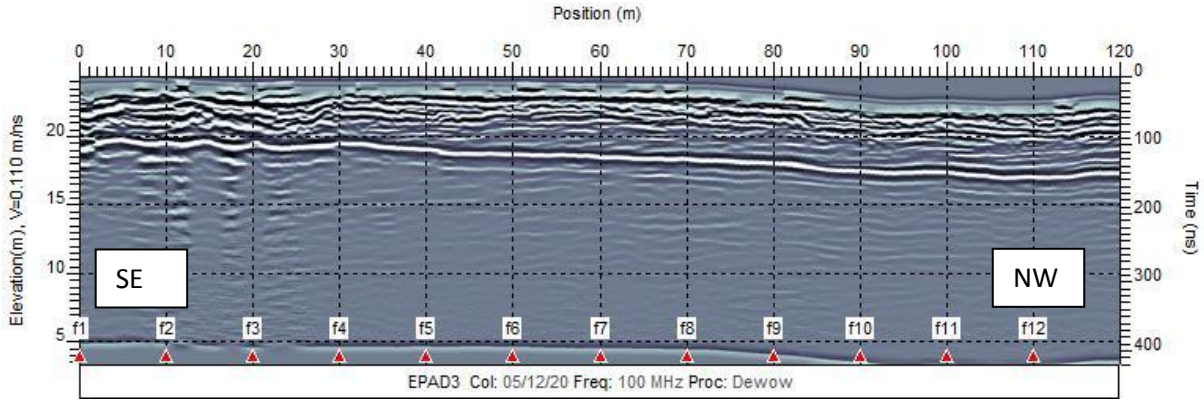
Position (m)
Elevation(m), V=0.110 m/ns
Time (ns)
SE
NW
f1 f2 f3 f4 f5 f6 f7 f8 f9 f10 f11 f12
EPAD3 Col: 05/12/20 Freq: 100 MHz Proc: Dewow

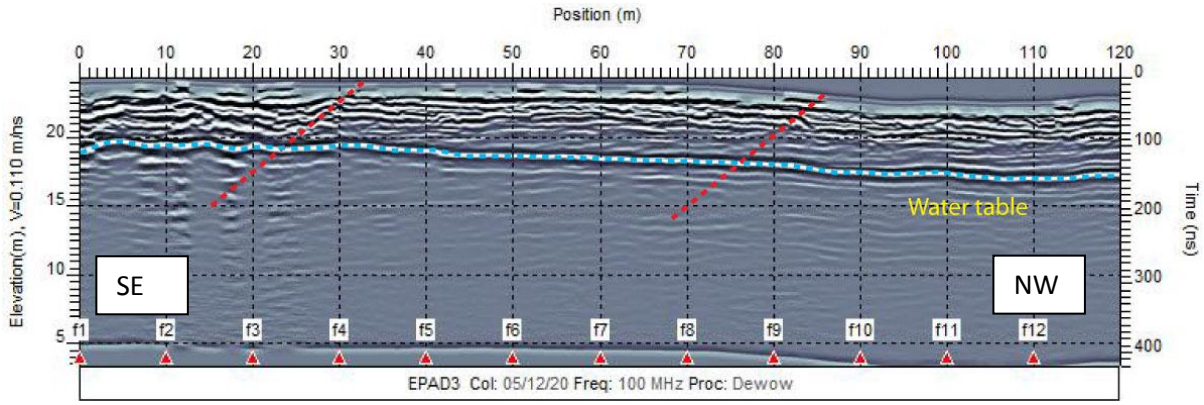
Position (m)
Elevation(m), V=0.110 m/ns
Time (ns)
Water table
SE
NW
f1 f2 f3 f4 f5 f6 f7 f8 f9 f10 f11 f12
EPAD3 Col: 05/12/20 Freq: 100 MHz Proc: Dewow

EPAD3

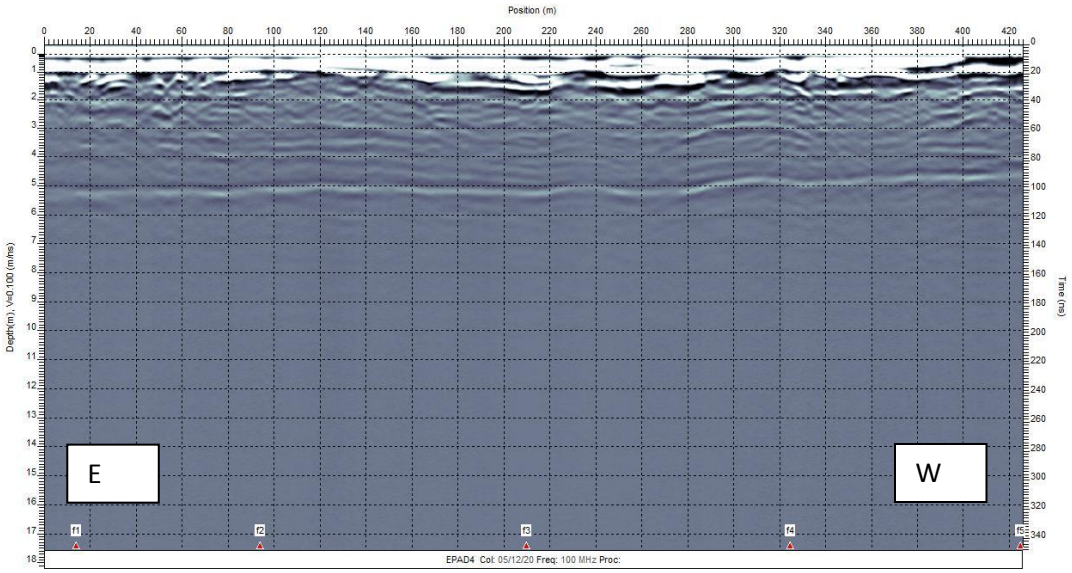
Position (m)
Depth(m), V=0.100 (m/ns)
Time (ns)
E
W
EPAD4 Col: 05/12/20 Freq: 100 MHz Proc:

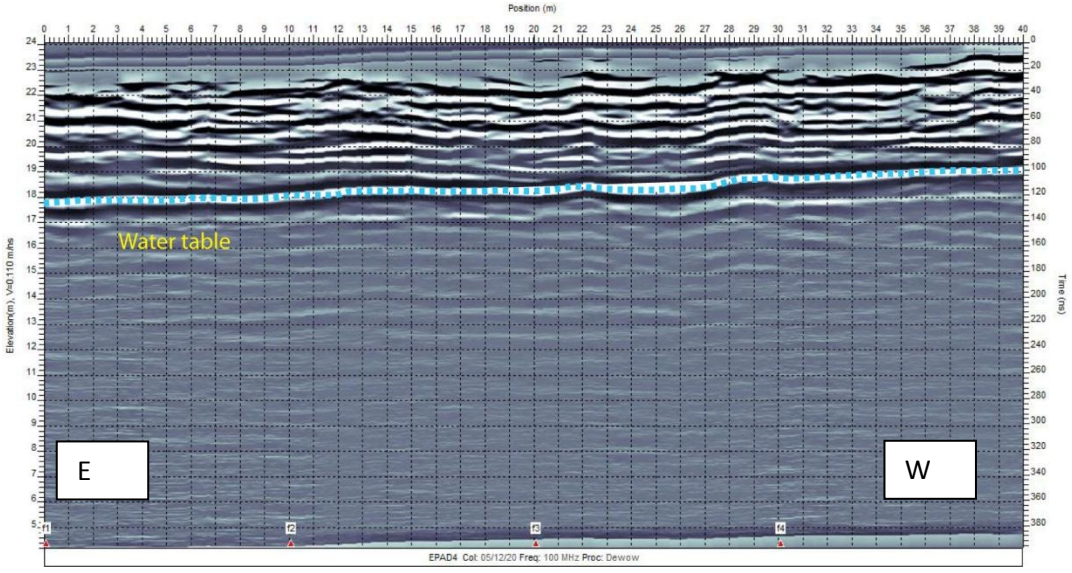
Position (m)
Elevation(m), V=0.110 m/ns
Time (ns)
Water table
E
W
EPAD4 Col: 05/12/20 Freq: 100 MHz Proc: Dewow

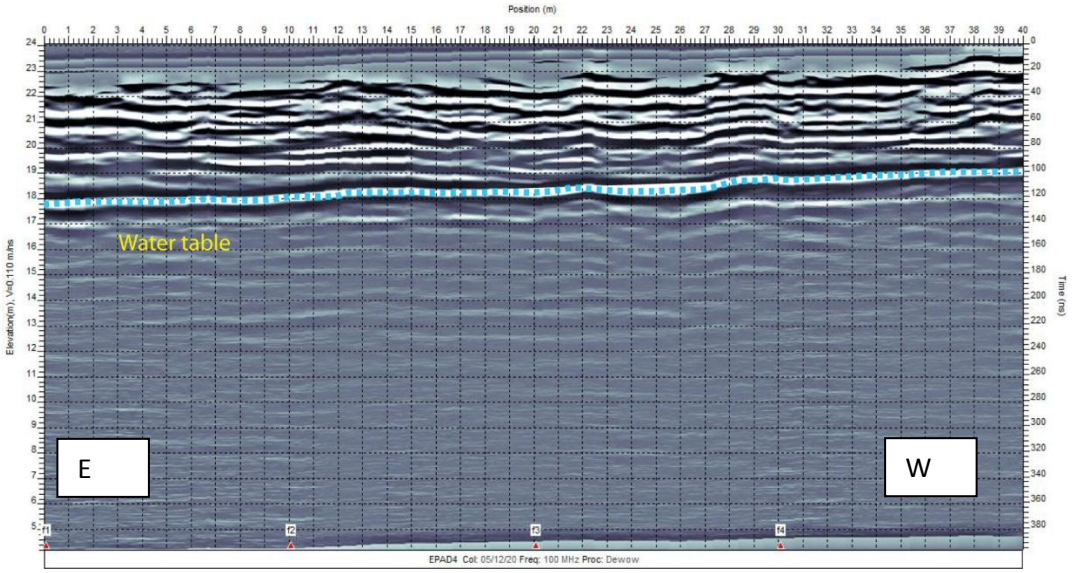
Position (m)
Elevation(m), V=0.110 m/ns
Time (ns)
Water table
E
W
EPAD4 Col: 05/12/20 Freq: 100 MHz Proc: Dewow

EPAD4

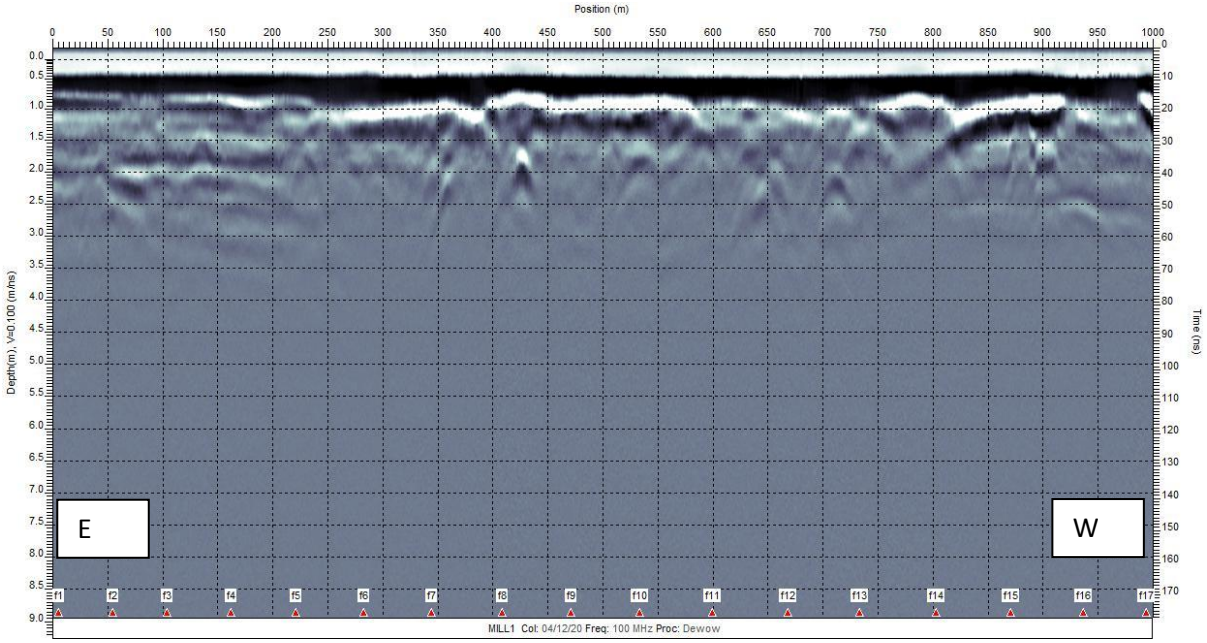
Position (m)
0 50 100 150 200 250 300 350 400 450 500 550 600 650 700 750 800 850 900 950 1000
Depth(m), V=0.100 (m/ns)
0.0 0.5 1.0 1.5 2.0 2.5 3.0 3.5 4.0 4.5 5.0 5.5 6.0 6.5 7.0 7.5 8.0 8.5 9.0
Time (ns)
0 10 20 30 40 50 60 70 80 90 100 110 120 130 140 150 160 170
E
W
f1 f2 f3 f4 f5 f6 f7 f8 f9 f10 f11 f12 f13 f14 f15 f16 f17
MILL1 Col: 04/12/20 Freq: 100 MHz Proc: Dewow

MILL1

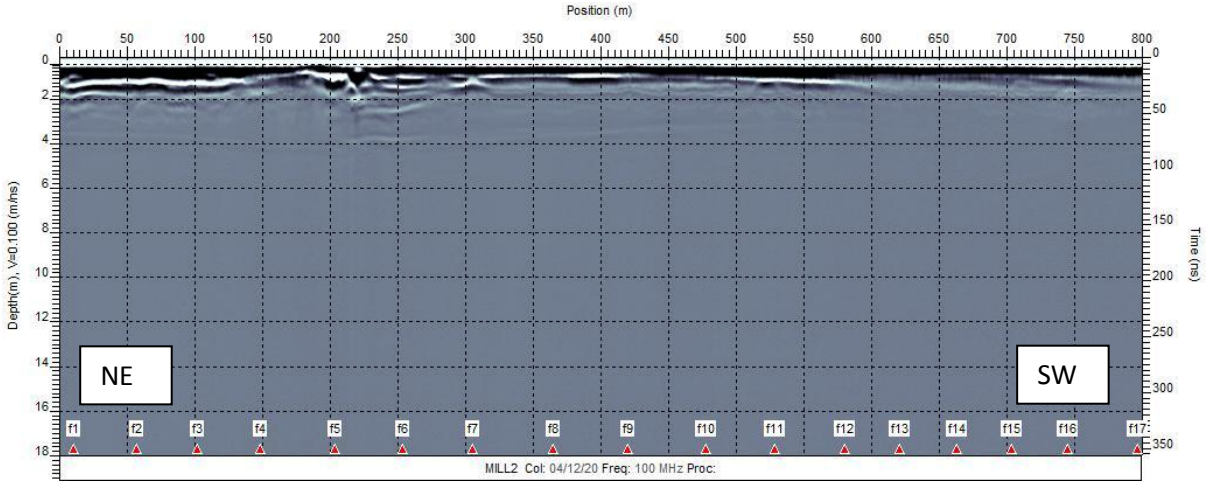
Position (m)
Depth(m), V=0.100 (m/ns)
Time (ns)
NE
SW
MILL2 Col: 04/12/20 Freq: 100 MHz Proc:

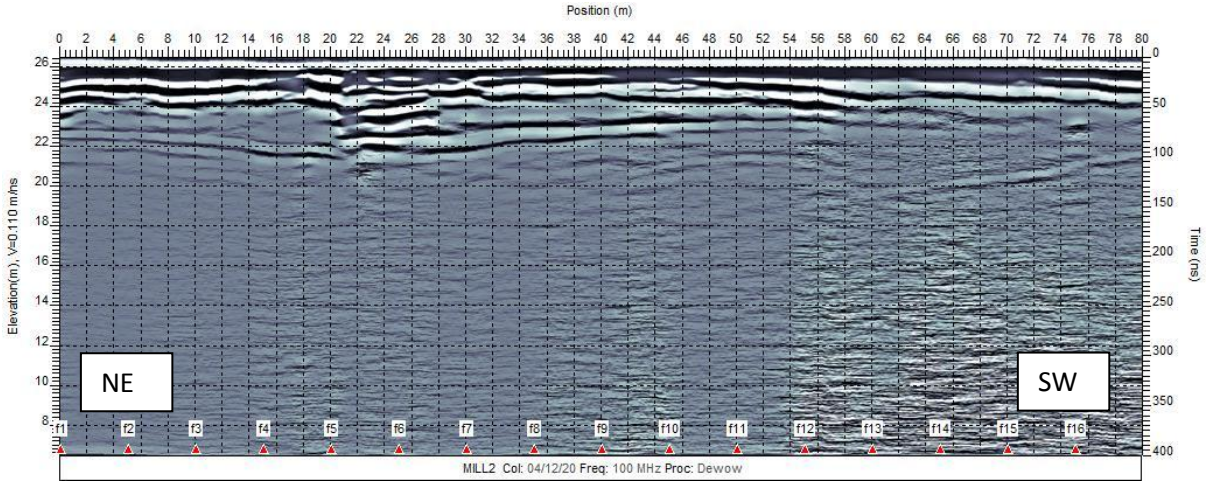
Position (m)
Elevation(m), V=0.110 m/ns
Time (ns)
NE
SW
MILL2 Col: 04/12/20 Freq: 100 MHz Proc: Dewow

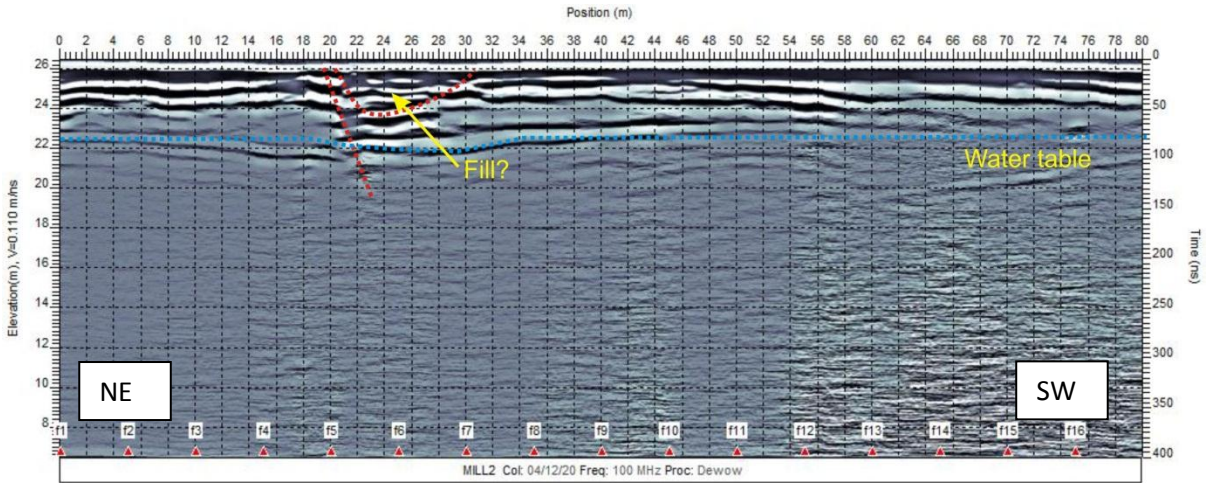
Position (m)
Fill?
Water table
Elevation(m), V=0.110 m/ns
Time (ns)
NE
SW
MILL2 Col: 04/12/20 Freq: 100 MHz Proc: Dewow

MILL2

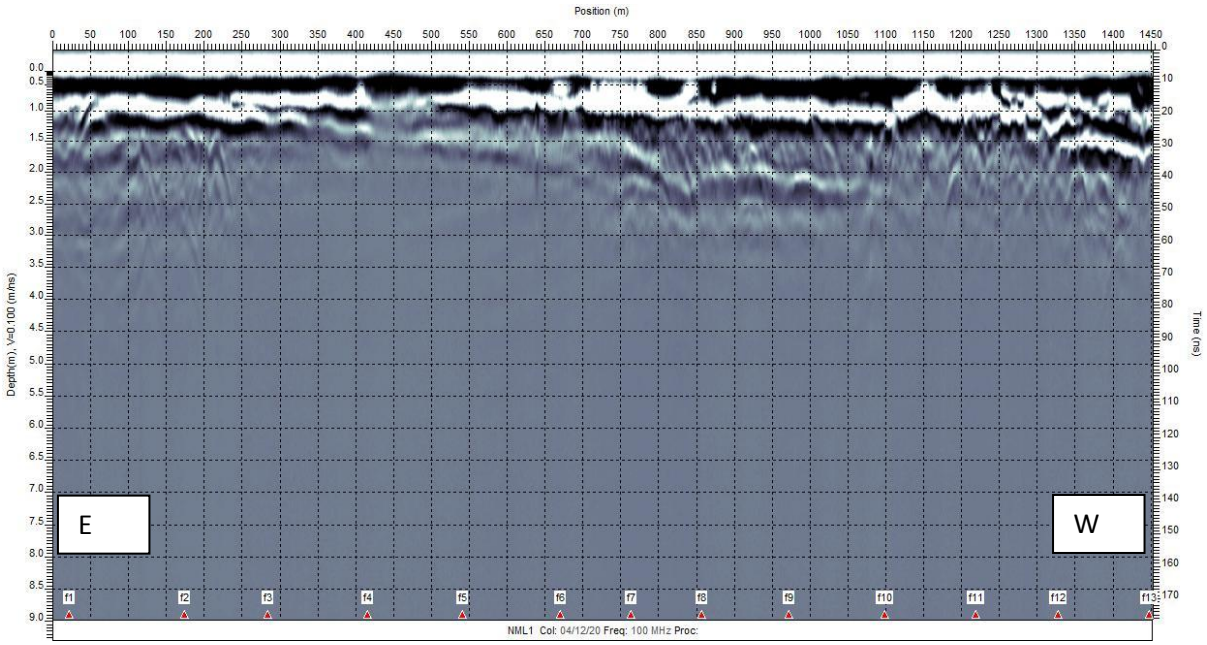
Position (m)
Depth(m), V=0.100 (m/ns)
Time (ns)
E
W
f1
f2
f3
f4
f5
f6
f7
f8
f9
f10
f11
f12
f13
NML1 Col: 04/12/20 Freq: 100 MHz Proc:

NML1

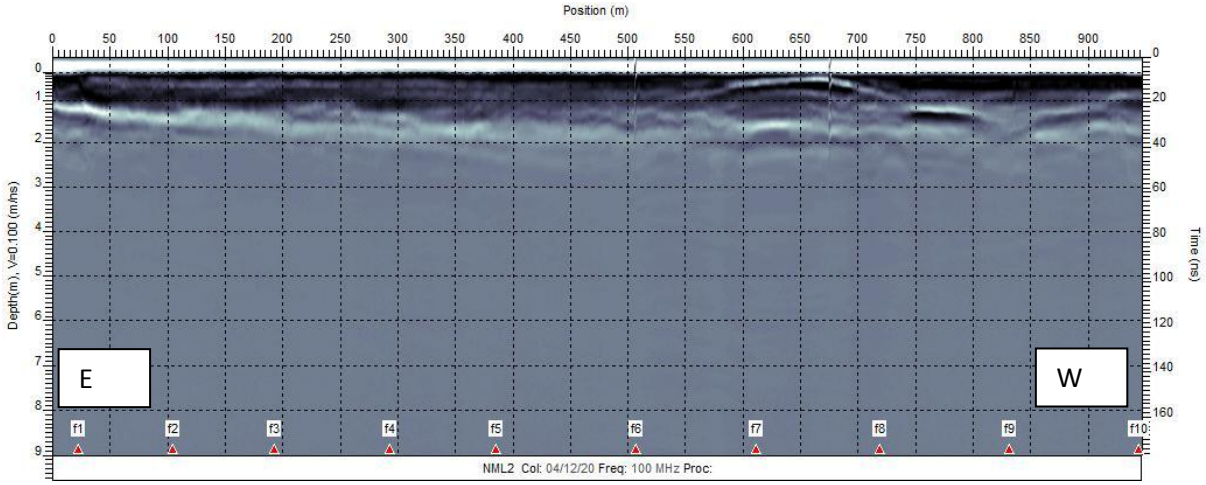
Position (m)
Depth(m), V=0.100 (m/ns)
Time (ns)
E
W
f1
f2
f3
f4
f5
f6
f7
f8
f9
f10
NML2 Col: 04/12/20 Freq: 100 MHz Proc:

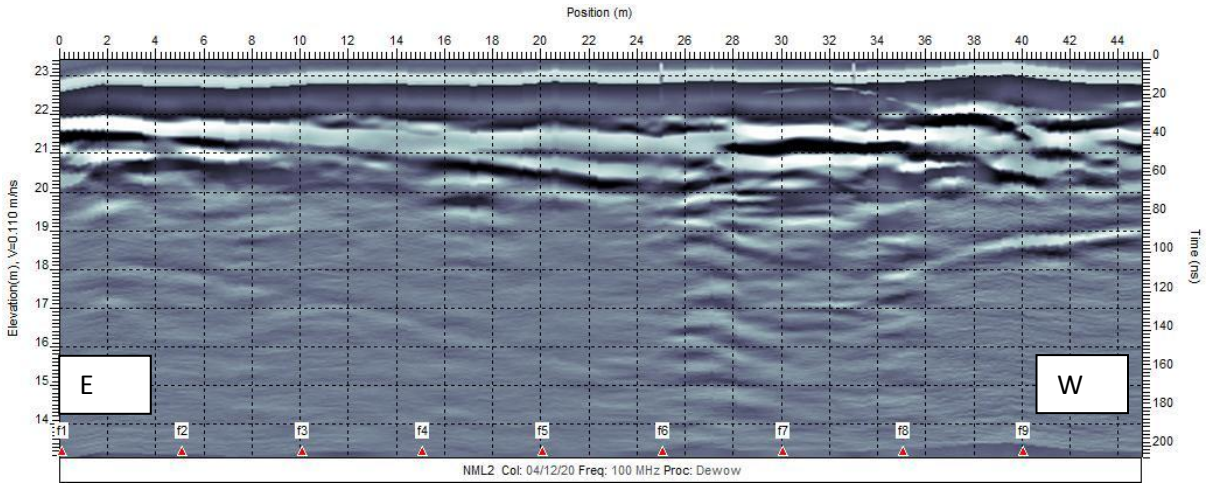
Position (m)
Elevation(m), V=0.110 m/ns
Time (ns)
E
W
f1
f2
f3
f4
f5
f6
f7
f8
f9
NML2 Col: 04/12/20 Freq: 100 MHz Proc: Dewow

NML2

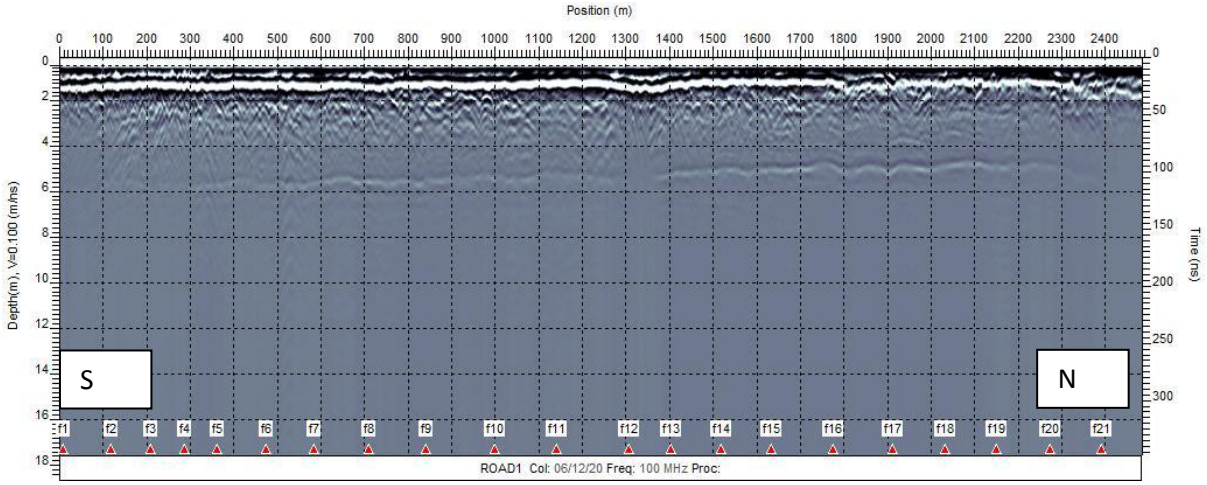
Position (m)
Depth(m), V=0.100 (m/ns)
Time (ns)
S
N
ROAD1 Col: 06/12/20 Freq: 100 MHz Proc:

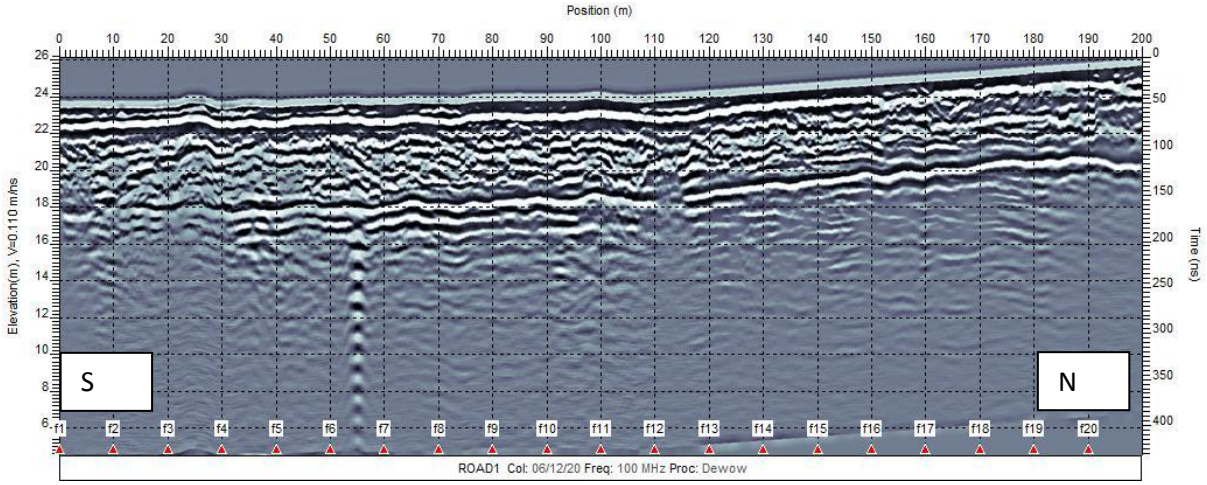
Position (m)
Elevation(m), V=0.110 m/ns
Time (ns)
S
N
ROAD1 Col: 06/12/20 Freq: 100 MHz Proc: Dewow

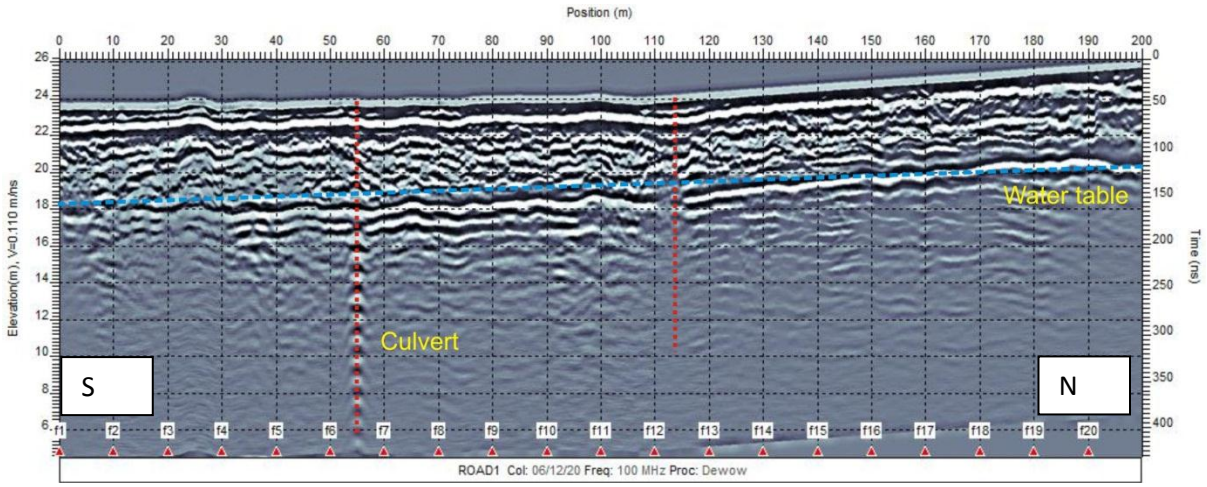
Position (m)
Elevation(m), V=0.110 m/ns
Time (ns)
Water table
Culvert
S
N
ROAD1 Col: 06/12/20 Freq: 100 MHz Proc: Dewow

ROAD1

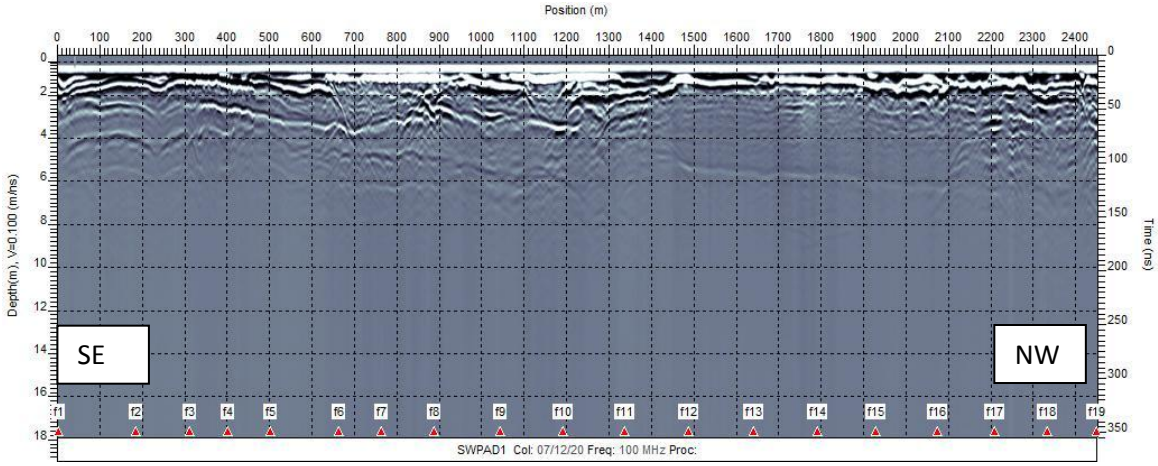
Position (m)
Depth(m), V=0.100 (m/ns)
Time (ns)
SE
NW
SWPAD1 Col: 07/12/20 Freq: 100 MHz Proc:

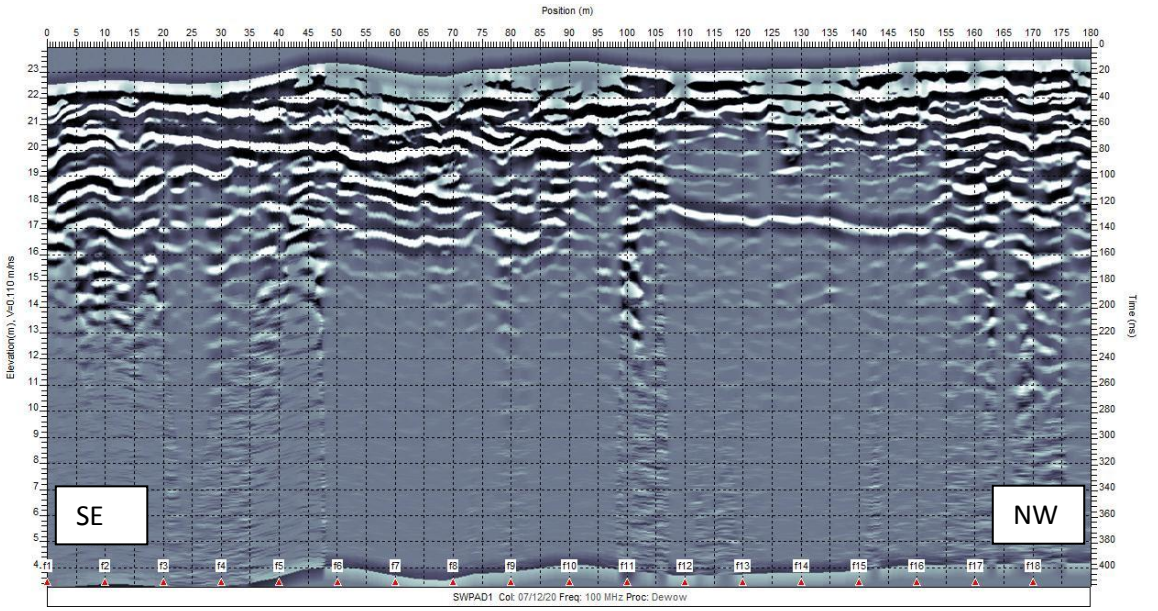
Position (m)
Elevation(m), V=0.110 m/ns
Time (ns)
SE
NW
SWPAD1 Col: 07/12/20 Freq: 100 MHz Proc: Dewow

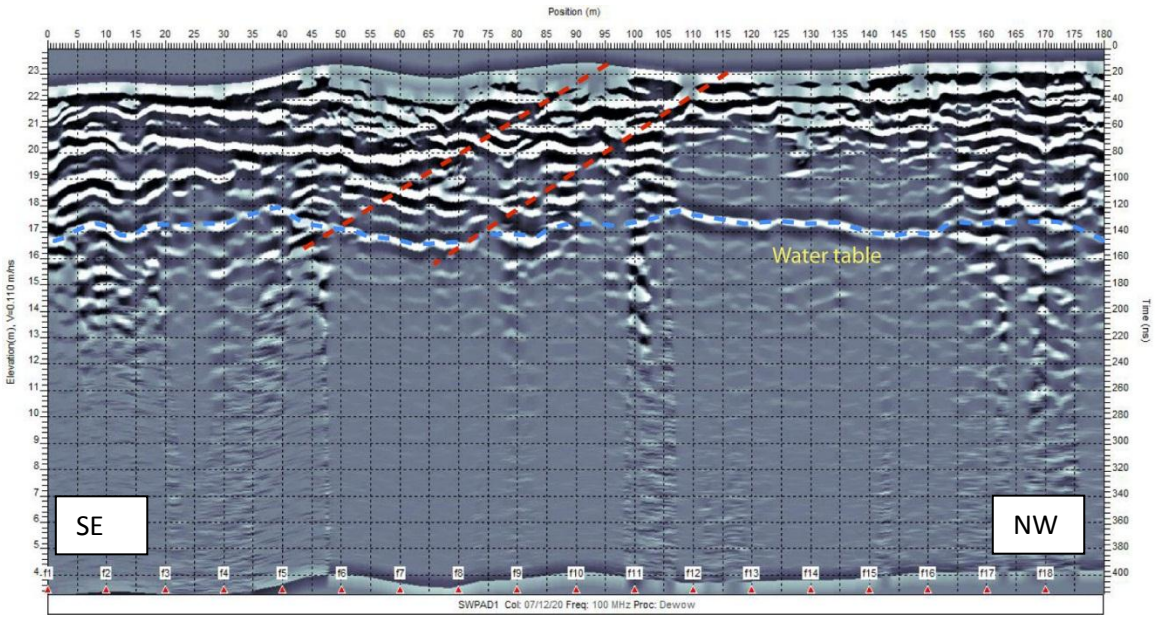
Position (m)
Elevation(m), V=0.110 m/ns
Time (ns)
Water table
SE
NW
SWPAD1 Col: 07/12/20 Freq: 100 MHz Proc: Dewow

SWPAD1

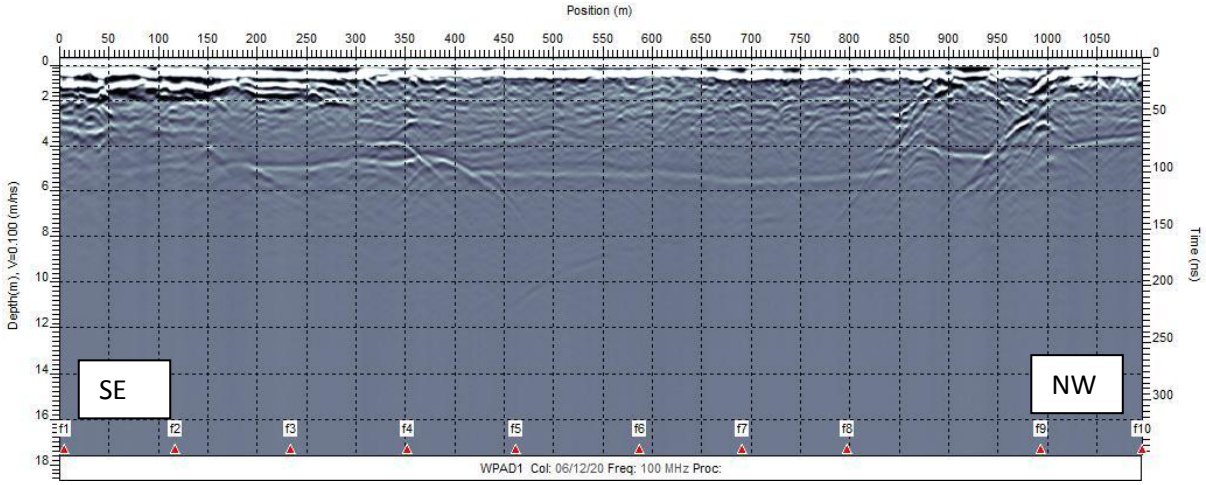
Position (m)
Depth(m), V=0.100 (m/ns)
Time (ns)
SE
NW
WPAD1 Col: 06/12/20 Freq: 100 MHz Proc:

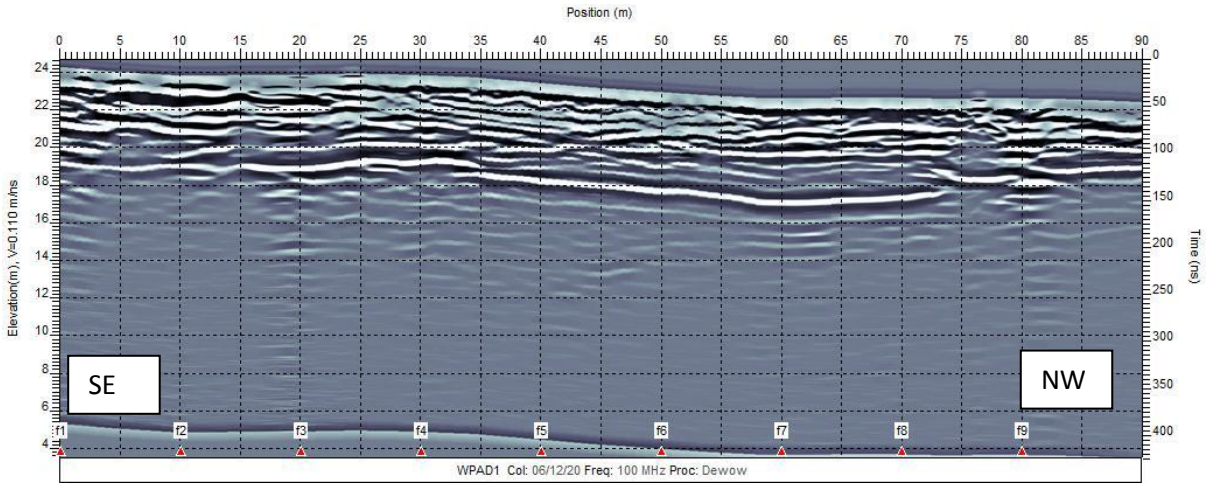
Position (m)
Elevation(m), V=0.110 m/ns
Time (ns)
SE
NW
WPAD1 Col: 06/12/20 Freq: 100 MHz Proc: Dewow

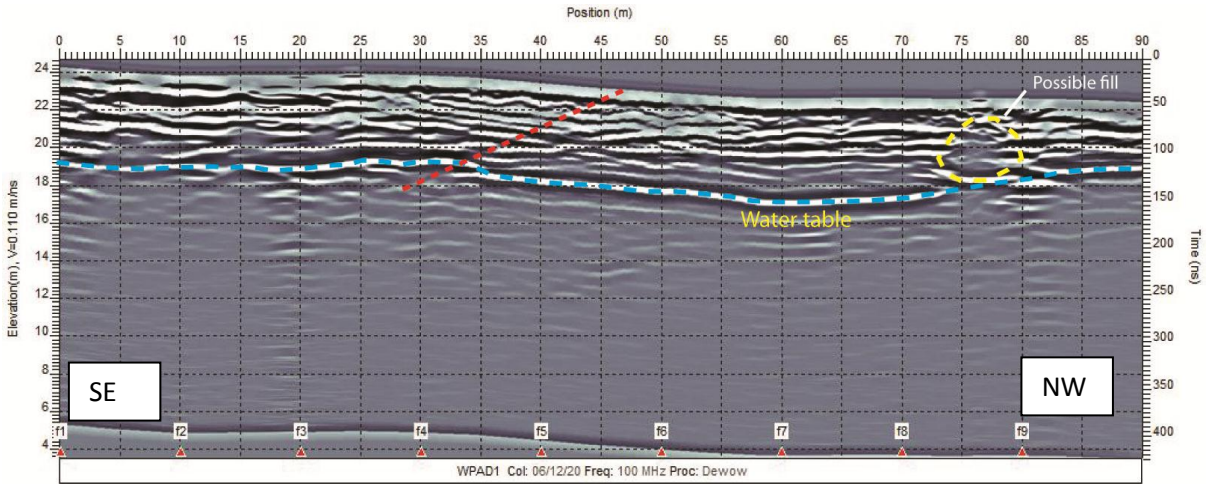
Position (m)
Possible fill
Water table
Elevation(m), V=0.110 m/ns
Time (ns)
SE
NW
WPAD1 Col: 06/12/20 Freq: 100 MHz Proc: Dewow

WPAD1

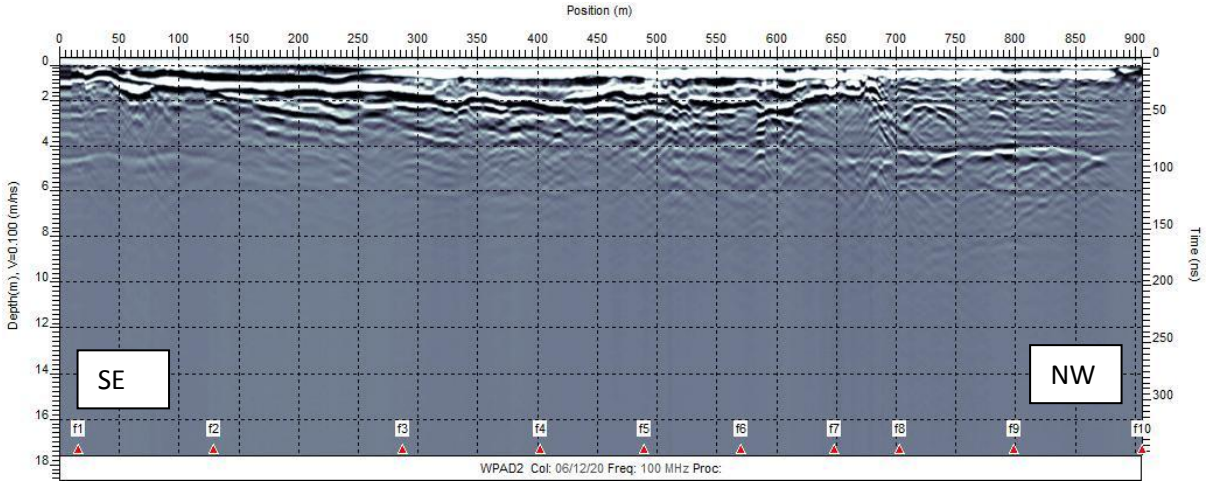
Position (m)
Depth(m), V=0.100 (m/ns)
Time (ns)
SE
NW
f1
f2
f3
f4
f5
f6
f7
f8
f9
f10
WPAD2 Col: 06/12/20 Freq: 100 MHz Proc:

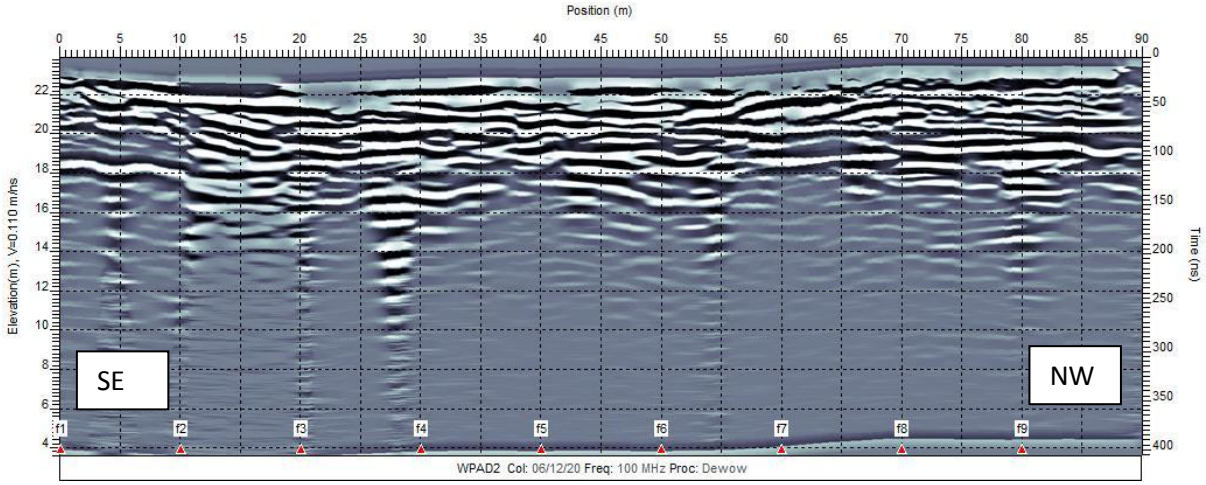
Position (m)
Elevation(m), V=0.110 m/ns
Time (ns)
SE
NW
f1
f2
f3
f4
f5
f6
f7
f8
f9
WPAD2 Col: 06/12/20 Freq: 100 MHz Proc: Dewow

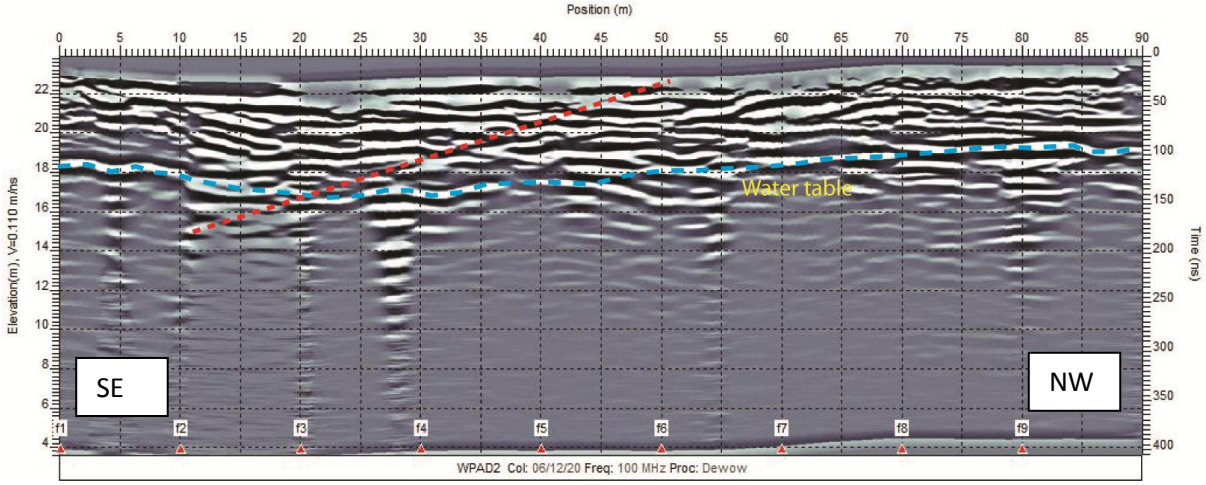
Position (m)
Elevation(m), V=0.110 m/ns
Time (ns)
Water table
SE
NW
f1
f2
f3
f4
f5
f6
f7
f8
f9
WPAD2 Col: 06/12/20 Freq: 100 MHz Proc: Dewow

WPAD2

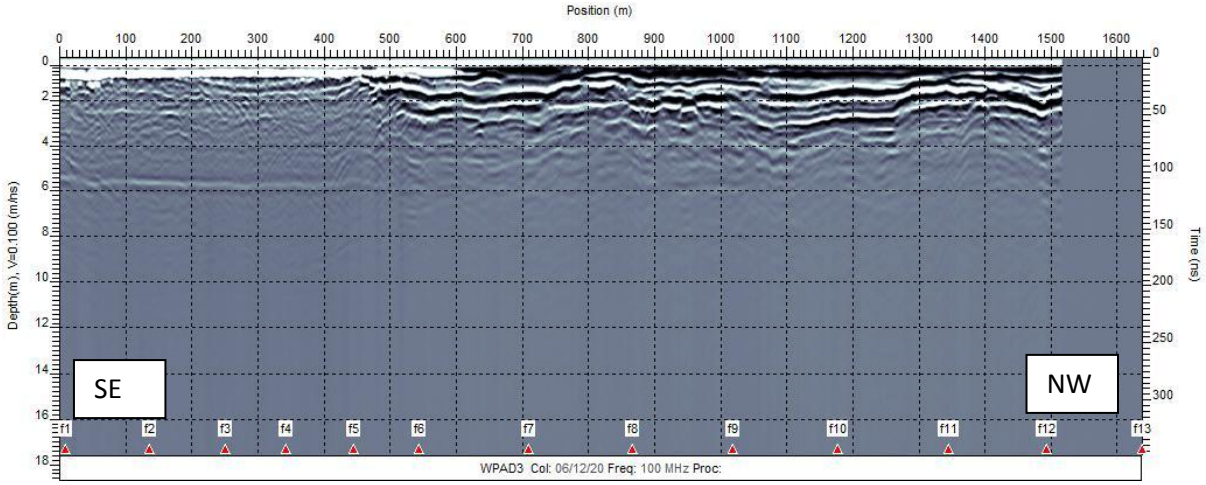
Position (m)
Depth(m), V=0.100 (m/ns)
Time (ns)
SE
NW
WPAD3 Col: 06/12/20 Freq: 100 MHz Proc:

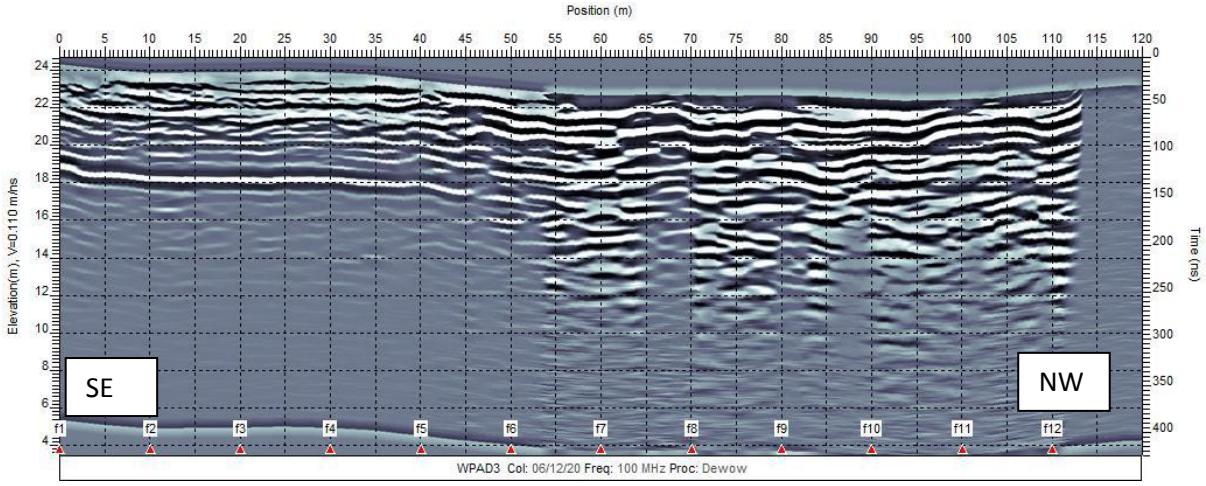
Position (m)
Elevation(m), V=0.110 m/ns
Time (ns)
SE
NW
WPAD3 Col: 06/12/20 Freq: 100 MHz Proc: Dewow

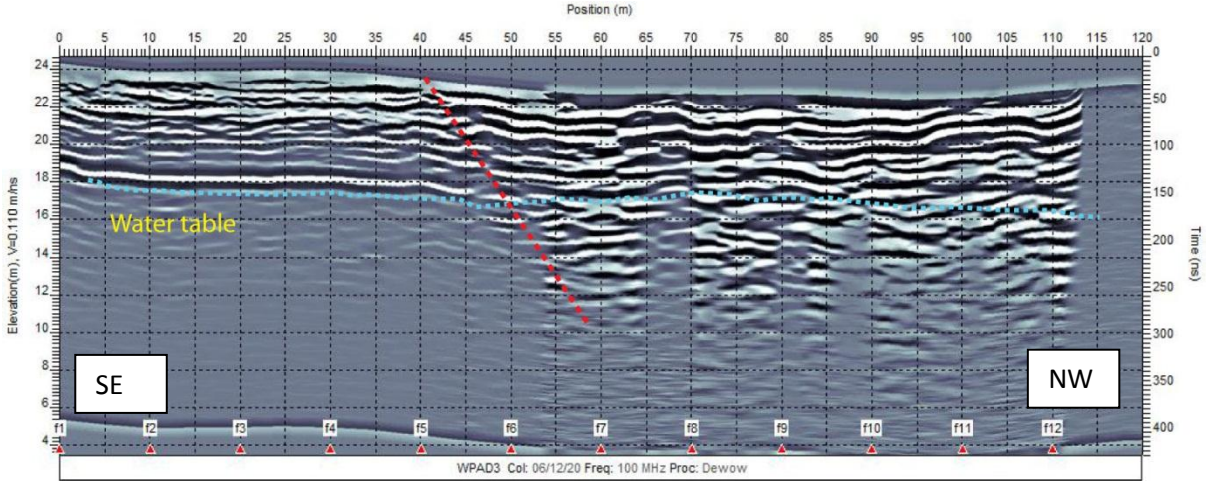
Position (m)
Elevation(m), V=0.110 m/ns
Time (ns)
Water table
SE
NW
WPAD3 Col: 06/12/20 Freq: 100 MHz Proc: Dewow

WPAD3

Appendix F: Electrical imaging profiles

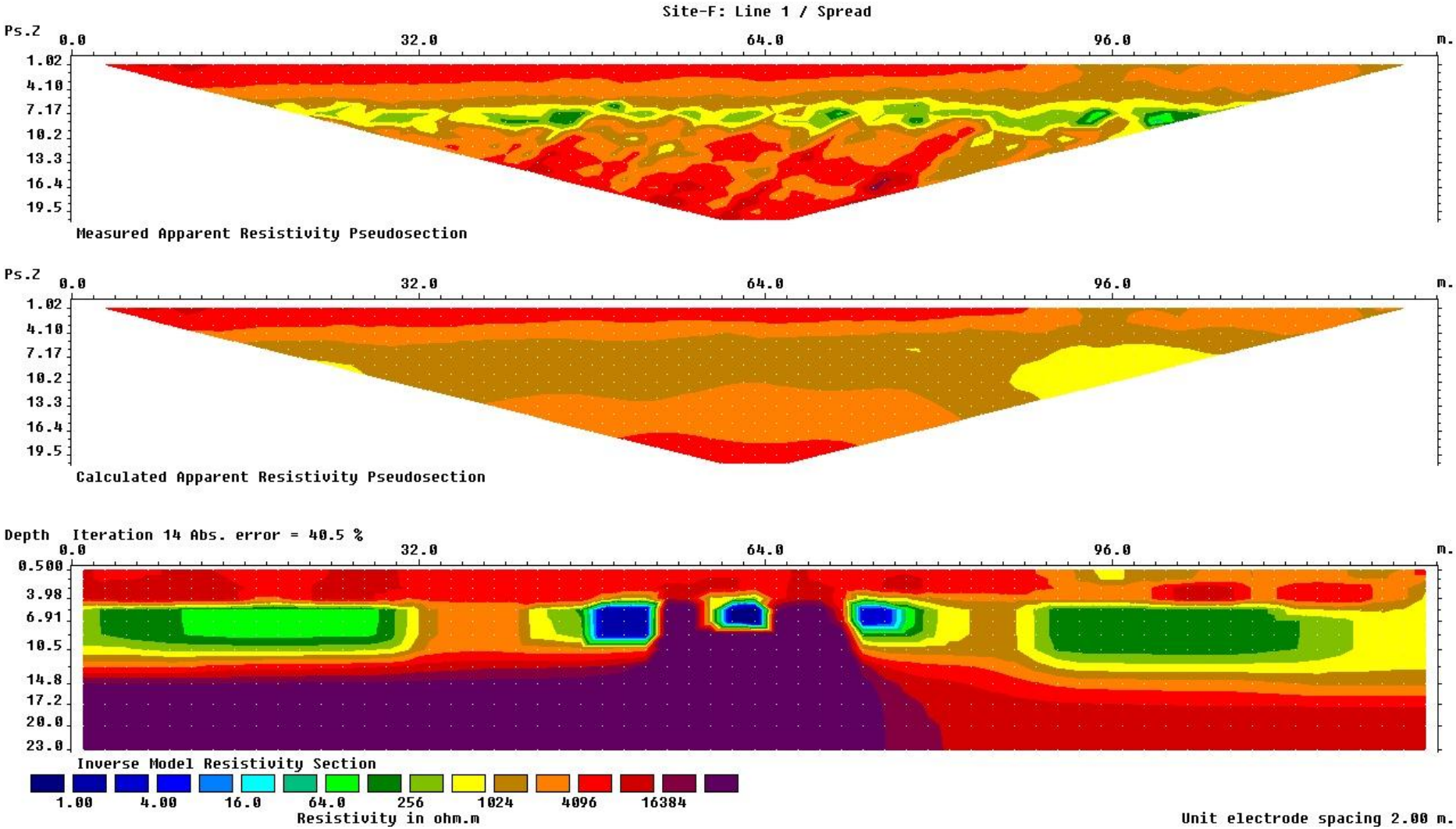
Site-F: Line 1 / Spread
Ps.Z
0.0
32.0
64.0
96.0
m.
1.02
4.10
7.17
10.2
13.3
16.4
19.5
Measured Apparent Resistivity Pseudosection
Ps.Z
0.0
32.0
64.0
96.0
m.
1.02
4.10
7.17
10.2
13.3
16.4
19.5
Calculated Apparent Resistivity Pseudosection
Depth
Iteration 14 Abs. error = 40.5 %
0.0
32.0
64.0
96.0
m.
0.500
3.98
6.91
10.5
14.8
17.2
20.0
23.0
Inverse Model Resistivity Section
1.00
4.00
16.0
64.0
256
1024
4096
16384
Resistivity in ohm.m
Unit electrode spacing 2.00 m.

KAWRES1

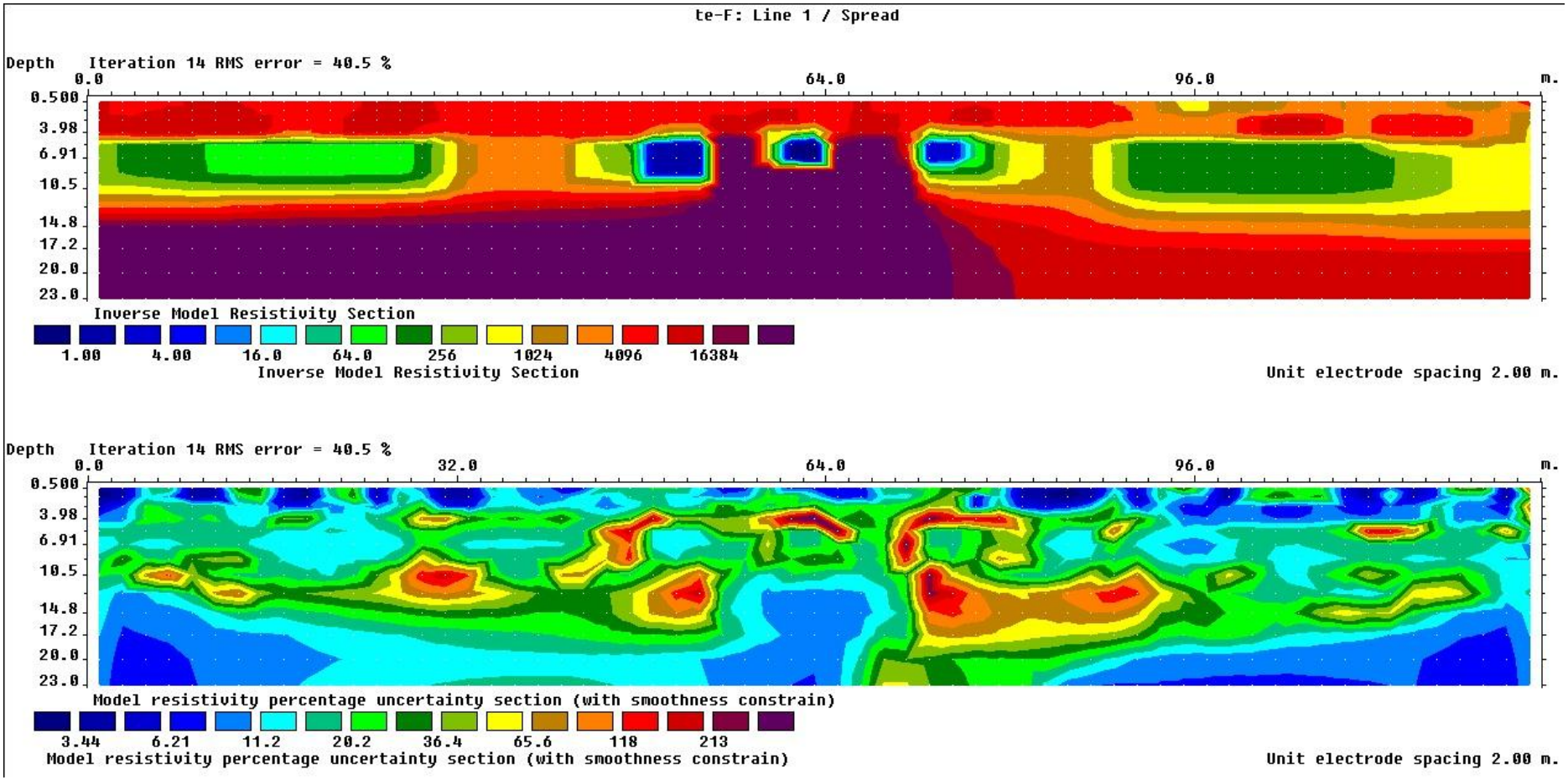

KAWRES1 – Smoothed and uncertainty

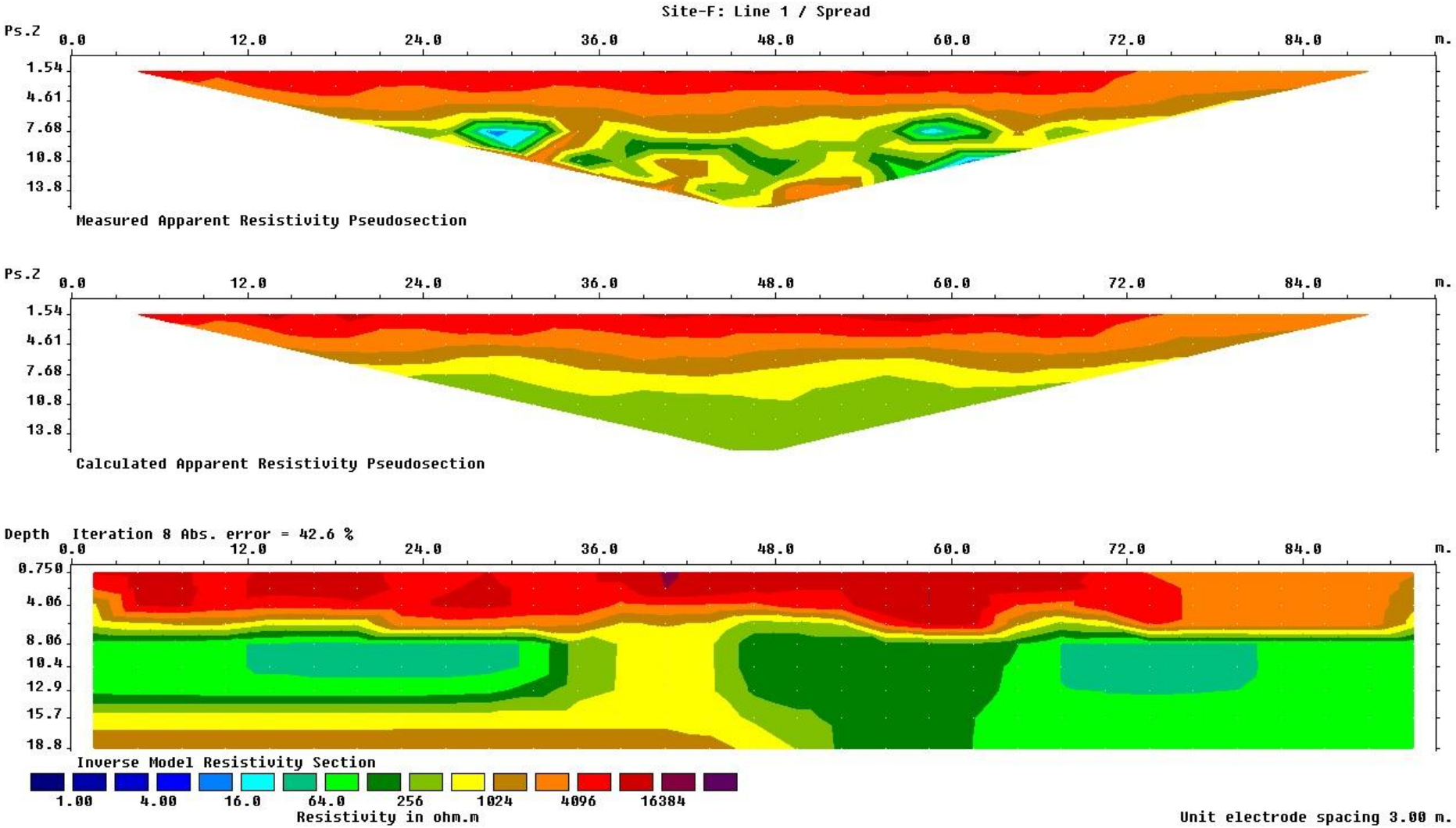
Site-F: Line 1 / Spread
Ps.Z
0.0
12.0
24.0
36.0
48.0
60.0
72.0
84.0
m.
1.54
4.61
7.68
10.8
13.8
Measured Apparent Resistivity Pseudosection
Ps.Z
0.0
12.0
24.0
36.0
48.0
60.0
72.0
84.0
m.
1.54
4.61
7.68
10.8
13.8
Calculated Apparent Resistivity Pseudosection
Depth
Iteration 8 Abs. error = 42.6 %
0.0
12.0
24.0
36.0
48.0
60.0
72.0
84.0
m.
0.750
4.06
8.06
10.4
12.9
15.7
18.8
Inverse Model Resistivity Section
1.00
4.00
16.0
64.0
256
1024
4096
16384
Resistivity in ohm.m
Unit electrode spacing 3.00 m.

KAWRES1W

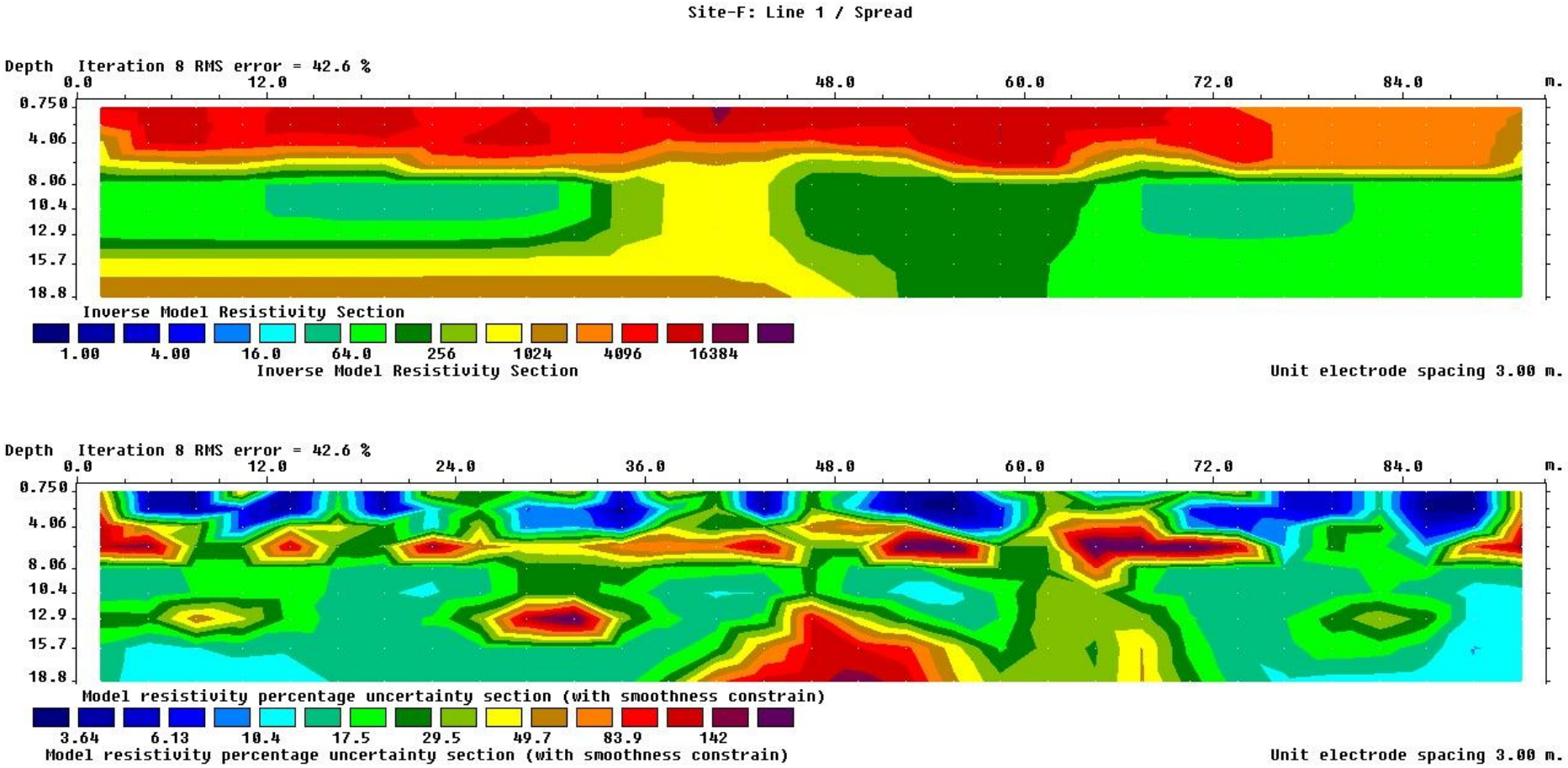

KAWRES1 – Smoothed and uncertainty

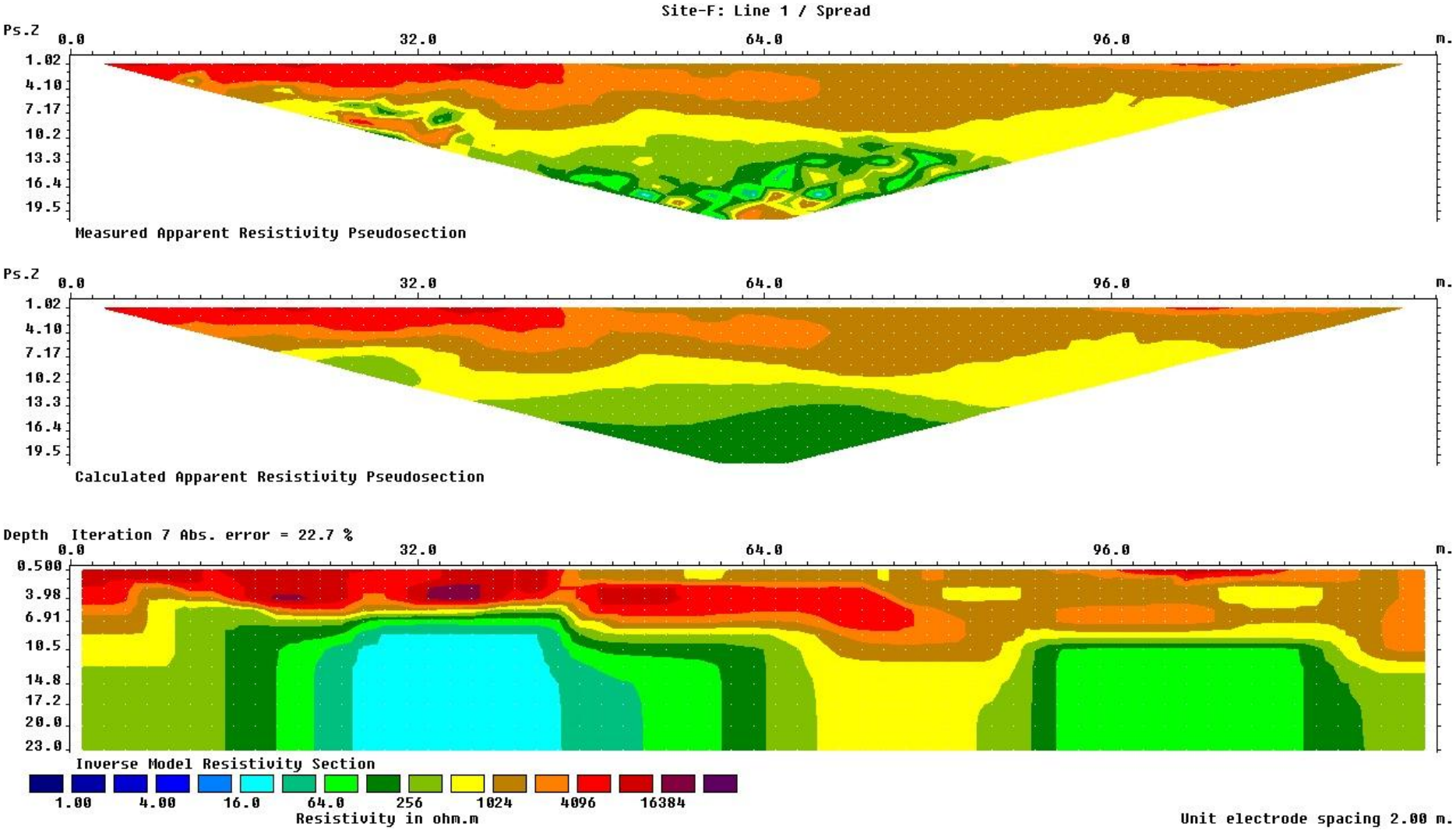
Site-F: Line 1 / Spread
Ps.Z
0.0
32.0
64.0
96.0
m.
1.02
4.10
7.17
10.2
13.3
16.4
19.5
Measured Apparent Resistivity Pseudosection
Ps.Z
0.0
32.0
64.0
96.0
m.
1.02
4.10
7.17
10.2
13.3
16.4
19.5
Calculated Apparent Resistivity Pseudosection
Depth
Iteration 7 Abs. error = 22.7 %
0.0
32.0
64.0
96.0
m.
0.500
3.98
6.91
10.5
14.8
17.2
20.0
23.0
Inverse Model Resistivity Section
1.00
4.00
16.0
64.0
256
1024
4096
16384
Resistivity in ohm.m
Unit electrode spacing 2.00 m.

KAWRES2

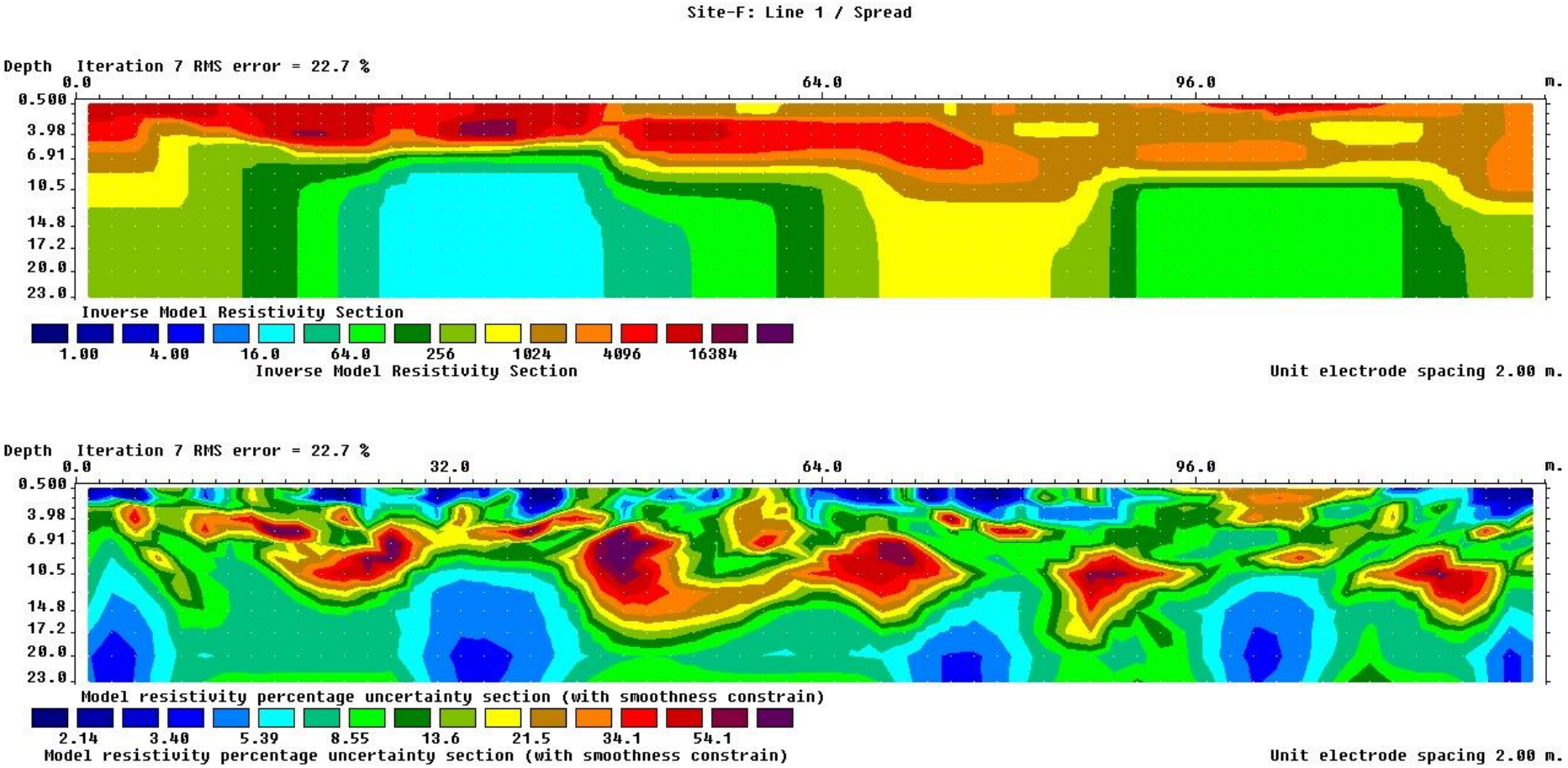

KAWRES2 – Smoothed and uncertainty

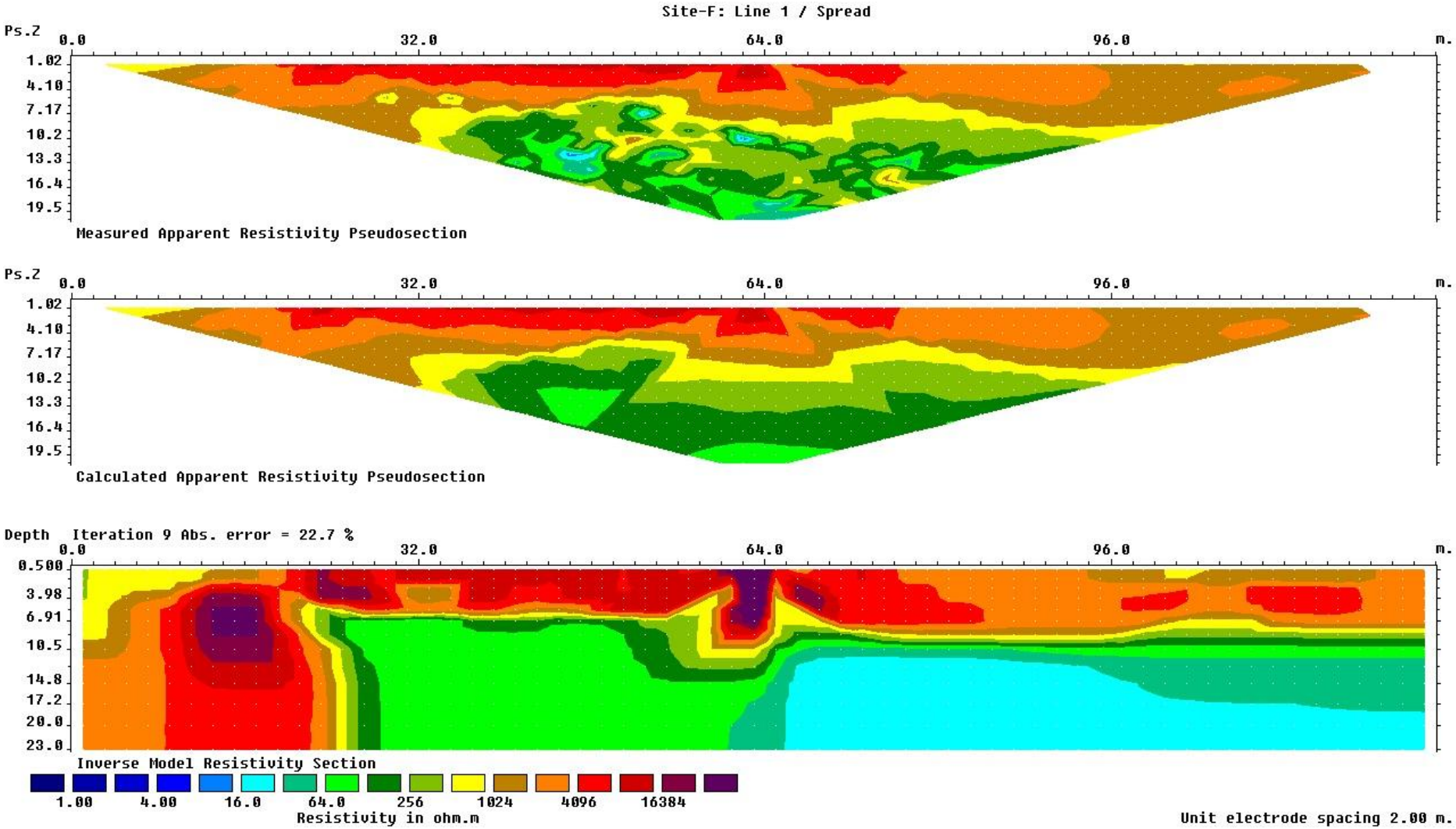
Site-F: Line 1 / Spread
Ps.Z
0.0
32.0
64.0
96.0
m.
1.02
4.10
7.17
10.2
13.3
16.4
19.5
Measured Apparent Resistivity Pseudosection
Ps.Z
0.0
32.0
64.0
96.0
m.
1.02
4.10
7.17
10.2
13.3
16.4
19.5
Calculated Apparent Resistivity Pseudosection
Depth
Iteration 9 Abs. error = 22.7 %
0.0
32.0
64.0
96.0
m.
0.500
3.98
6.91
10.5
14.8
17.2
20.0
23.0
Inverse Model Resistivity Section
1.00
4.00
16.0
64.0
256
1024
4096
16384
Resistivity in ohm.m
Unit electrode spacing 2.00 m.

KAWRES5

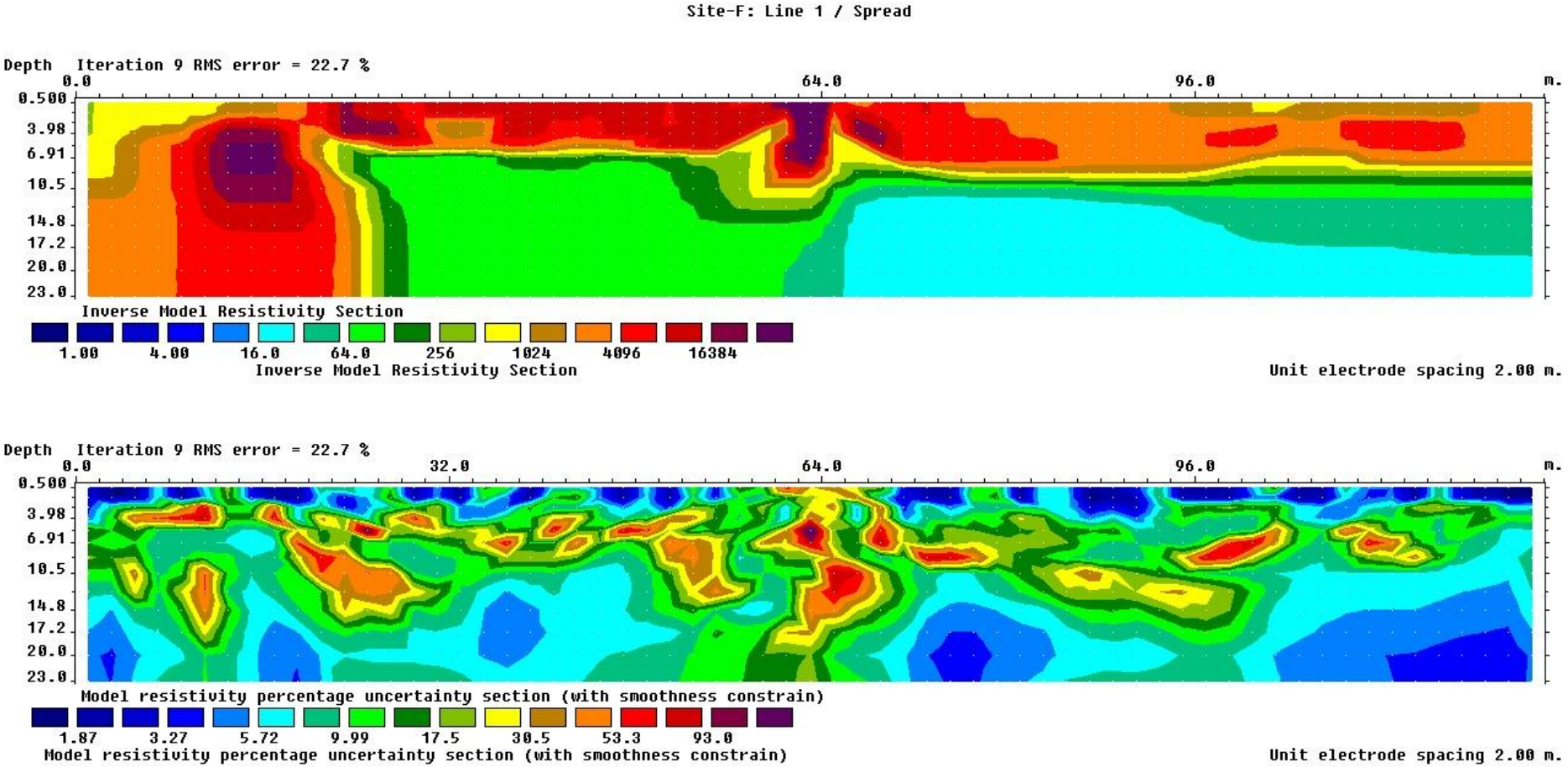

KAWRES5 – Smoothed and uncertainty

Appendix G: Auger logs

Hole 1

Depth (m) From	Depth (m) To	Thickness	Description
0	0.1	0.1	Soil: Topsoil. Some cobbles and coarse gravel (Max 50mm)
0.1	0.2	0.1	CSS: Coarse sandstone, light brown. Loose
0.2	1.1	0.9	CSS: Coarse sandstone, brown, greyish. Silt to pebble. Loose, moist. Silt brownish. Grains sub-angular to rounded
1.1	3.3	2.2	CSS: Coarse sandstone, light brown. Loose, moist. Grades to firm. Occasional pebbles - rounded to sub-angular.

Hole 2

Depth (m) From	Depth (m) To	Thickness	Description
0	0.1	0.1	Grass and sawdust fill
0.1	0.13	0.03	Clay: Creamy, whiteish, very uniform grainsize, chalky feel
0.13	2.5	2.37	CSS: Coarse sandstone, light brown, greyish. Fine to very coarse grains with occasional pebble to cobble sized stones. Pebbles rounded, sand angular to sub-angular. Common pumice
2.5	2.9	0.4	ZST: Siltstone, dark brown, blackish. Silt with some coarse sand and occasional granule size grains. Moderately to highly carbonaceous. Moist. Some reddish orange grains.
2.9	3.1	0.2	FSS: Fine sandstone, light brown, orangeish. Very fine to medium grains. Friable

Hole 3

Depth (m) From	Depth (m) To	Thickness	Description
0.00	0.03	0.03	Soil: Topsoil and grass
0.03	0.26	0.23	Clay: Creamy, whiteish, very uniform grainsize, chalky feel
0.26	0.30	0.04	Bark
0.30	0.43	0.13	Soil: Soil and wood fibre, organic
0.43	1.07	0.64	Clay: Medium grey clay, clay to silt size grains. Very puggy and soft, chalky feel and occasional pumice grains
1.07	1.45	0.38	VCSS: Very coarse sandstone, black. Organic layer with very coarse grains throughout. Gradational basal contact.
1.45	2.16	0.71	CSS: Coarse sandstone, medium grey, brownish. Fine to very coarse grains and occasional cobble sized pumice. Very friable.
2.16	3.00	0.84	CSS: Coarse sandstone, light brown, greyish. Fine to granule sized grains. Occasional cobble sized pumice. Very loose and friable. Collapsing in to hole.

Hole 4

Depth (m) From	Depth (m) To	Thickness	Description
0.00	0.20	0.20	Soil: Topsoil
0.20	2.15	1.95	GRS: Granules, coarse sand to pebble. Light brown. Moist, loose granules grading in to coarse sand. Round to sub-angular grains

Hole 5

Depth (m) From	Depth (m) To	Thickness	Description
0.00	0.80	0.80	GRS: Granule, silt to pebble sized grains. Grey. Small silt lens at 0.2m. Saturated, loose, rouded to sub-angular
0.80	1.20	0.40	Auger drilled straight through, no sample extracted
1.20	1.40	0.20	Peat: Dark brown, blackish. Soft, saturated, organic peat material
1.40	1.50	0.10	CSS: Coarse sand, dark grey. Saturated, loose. Occasional wood and peat chips
1.50	1.55	0.05	CSS: Coarse sand, light brown. Firm

Hole 6

Depth (m) From	Depth (m) To	Thickness	Description
0.00	0.20	0.20	Soil: Topsoil, gradational basal contact
0.20	1.10	0.90	CSS: Coarse sandstone, coarse sand to pebble grainsize. Brown, loose, slightly moist. Sub-rounded to sub-angular
1.10	1.90	0.80	CSS: Coarse sandstone, coarse sand to pebble grainsize. Light brown, loose, slightly moist. Sub-rounded to sub-angular

Hole 7

Depth (m) From	Depth (m) To	Thickness	Description
0.00	0.25	0.25	Soil: Topsoil, some pumice
0.25	0.35	0.10	Clay: Clay, medium brown. Some iron staining
0.35	1.15	0.80	CSS: Coarse sandstone, medium to granule size. Light grey, some orange stained zines and some very light grey, whiteish pumice lenses. Lots of pumice. Sub-rounded to sub-angular grains.
1.15	1.25	0.10	ZST: Siltstone, light grey, orangeish. Fault gouge
1.25	2.80	1.55	CSS: Coarse sandstone, medium to granule size. Grey, some orange stained zines and some very light grey, whiteish pumice lenses. Lots of pumice. Sub-rounded to sub-angular grains. Occasional blackish grains.

Hole 8

Depth (m) From	Depth (m) To	Thickness	Description
0.00	0.20	0.20	Soil: Topsoil, light brown
0.20	1.70	1.50	MSS: Medium sandstone, come coarse sand lenses. Light brown, greyish. Moist, loose.
1.70	1.80	0.10	ZST: Siltstone, sandy, light brown, greyish. Moist to wet. Possibly fault gouge
1.80	2.10	0.30	CSS: Coarse sandstone, minor granule. Dark grey, brownish. Moist. Sub-rounded to sub-angular. Possibly buried soil horizon.
2.10	2.12	0.02	ZST: Siltstone, sandy, light brown, greyish. Moist to wet. Possibly fault gouge
2.12	2.80	0.68	VCSS: Very coarse sandstone. Light brown, firm, moist, sub-angular to rounded.

Hole 9

Depth (m) From	Depth (m) To	Thickness	Description
0.00	0.34	0.34	Soil: Topsoil. Grading in to iron stained clay.
0.34	0.77	0.43	Soil: New soil horizon, black, organic, grading in to dark brown, orangeish coarse sandstone and pumice granules
0.77	2.10	1.33	CSS: Coarse sandstone, Grey, brownish, with light grey lenses and orange stained lenses. Grains from fine sand to granule.

Hole 10

Depth (m) From	Depth (m) To	Thickness	Description
0.00	0.20	0.20	Soil: Topsoil, sandy, light brown
0.20	0.90	0.70	VCSS: Very coarse sandstone, very coarse sand to granule, light brown, moist, sub-rounded to sub-angular
0.90	1.00	0.10	ZST: Siltstone, brown, reddish, moist. Possibly fault gouge
1.00	2.20	1.20	VCSS: Very coarse sandstone, very coarse sand to pebble. Light brown. Lenses of lighter coloured material, moist, firm. Rounded to sub-angular.

Hole 11

Depth (m) From	Depth (m) To	Thickness	Description
0.00	0.30	0.30	Soil: Topsoil, light to medium brown
0.30	0.58	0.28	MSS: Medium sandstone, fine sand to granule grains. Light brown, greyish. Some orangeish lenses. Grains mainly angular. Abundant pumice and obsidian
0.58	0.62	0.04	MSS: Medium sandstone, fine sand to granule grains. Light brown, greyish. Some orangeish lenses. Grains mainly angular. Abundant pumice and obsidian. Many rounded pebbles of volcanic origin
0.62	1.30	0.68	MSS: Medium sandstone, fine to very coarse grains. Grey. Abundant pumice up to cobble size and occasional volcanic glass. Grains generally angular

Hole 12

Depth (m) From	Depth (m) To	Thickness	Description
0.00	0.18	0.18	Soil: Topsoil, dark brown
0.18	1.30	1.12	GRS: Granules, fine sand to pebble sized grains, occasional cobbles of pumice. Light brown, orangeish. Abundant volcanic glass and pumice. Generally angular grains, pumice rounded. Possible blackish scoria. Very loose and friable. Hole abandoned at 1.3m as hole collapsing

Hole 13

Depth (m) From	Depth (m) To	Thickness	Description
0.00	0.20	0.20	Soil: Topsoil with some pebbles. Dark brown, greyish
0.20	0.80	0.60	VCSS: Very coarse sandstone, coarse sand to pebble. Brown, orangeish. Sub-rounded to sub-angular. Loose, moist.
0.80	0.85	0.05	ZST: Silt, clay to silt, brown, soft, moist. Possibly fault gouge
0.85	1.40	0.55	MSS: Medium sandstone, light grey. Loose, moist. Gradational basal contact
1.40	1.50	0.10	ZST: Silt, grey, wet, loose, sandy. Grey. Gradational upper contact
1.50	2.00	0.50	CSS: Coarse sandstone, coarse sand to pebble. Dark grey, brownish. Loose, sub-angular to sub-rounded.
2.00	2.30	0.30	CSS: Coarse sandstone, coarse sand to pebble. Light brown. Loose, sub-angular to rounded. Moist, firm.

Hole 14

Depth (m) From	Depth (m) To	Thickness	Description
0.00	0.20	0.20	Soil: Topsoil, brown, sandy with some pebbles
0.20	1.20	1.00	GRS: Granules, coarse sand to pebble. Light grey, brownish. Sub-rounded to sub-angular. Moist, loose - grading to firm. Obsidian present.

Hole 15

Depth (m) From	Depth (m) To	Thickness	Description
0.00	0.20	0.20	Soil: Topsoil, sandy, brown. Moist, loose, some pebbles
0.20	2.00	1.80	GRS: Granules, coarse sand to pebble. Light grey, brownish. Sub-rounded to angular. Moist, loose - grading to firm. Scoria and obsidian present.

Hole 16

Depth (m) From	Depth (m) To	Thickness	Description
0.00	0.16	0.16	Soil: Topsoil
0.16	0.58	0.42	ZST: Siltstone, medium brown, greyish. Some iron staining. Moist
0.58	0.90	0.32	CSS: Coarse sandstone, medium to very coarse sand grains. Light grey. Many black, pumice like pebbles. Occasional volcanic glass. Hole abandoned as it matched river bank outcrop near by

Hole 17

Depth (m) From	Depth (m) To	Thickness	Description
0.00	0.20	0.20	Soil: Topsoil, brown. Some pebbles, gradational basal contact
0.20	1.90	1.70	CSS: Coarse sandstone, grading from silty at top to very coarse at base. Brown, grades from dark brown at top to medium brown at base. Moist, sub-rounded to sub-angular. Scoria and obsidian present. Loose, grading to firm at base.

Hole 18

Depth (m) From	Depth (m) To	Thickness	Description
0.00	0.20	0.20	Soil: Topsoil, dark brown
0.20	0.40	0.20	Soil: Medium brown soil, silty, some iron staining
0.40	1.40	1.00	ZST: Siltsone, medium grey, brownish. Light brown at base. Increase in moisture to base. Puggy in basal 300mm. Very soft - auger pushed through approximately 0.4m with very little effort
1.40	1.95	0.55	CSS: Coarse sandstone, medium sand to granule grains. Light grey, orangeish. Some pumice, many black scoria-like rocks. Rare volcanic glass. Dry

Hole 19

Depth (m) From	Depth (m) To	Thickness	Description
0.00	0.15	0.15	Soil: Topsoil, dark brown
0.15	0.35	0.20	ZST: Siltstone, light brown, greyish, some iron staining
0.35	1.15	0.80	ZST: Siltstone, medium brown, moist, slightly carbonaceous
1.15	2.85	1.70	CSS: Coarse sandstone, silt to very coarse sand. Medium brown. Slightly carbonaceous. Moist. Some light grey CSS bands
2.85	3.10	0.25	VCSS: Very coarse sandstone, very fine sand to granule grains. Dark brown. Slightly carbonaceous. Scoria-like black grains
3.10	3.30	0.20	VCSS: Very coarse sandstone, medium sand to granule. Light grey. Some pumice and volcanic glass

Hole 20

Depth (m) From	Depth (m) To	Thickness	Description
0.00	2.90	2.90	Clay: Clay, silty. Brown. Firm. Grades from moist to wet at 2.3m
2.90	4.30	1.40	MSS: Medium sandstone. Mud to granule. Light grey. Soft, occasional granules.

Face Log 1

Depth (m) From	Depth (m) To	Thickness	Description
0.00	0.40	0.40	CSS: Coarse sandstone, silt to very coarse sand. Brown, organic. Rounded sst grains. Hard to determine if it is fill or fluvial deposit, not apparent bedding
0.40	0.43	0.03	Soil: Buried topsoil, black, historic soil level.
0.43	0.70	0.27	VCSS: Very coarse sandstone, brown, many pumice pieces up to large pebble size
0.70	1.40	0.70	VCSS: Very coarse sandstone, grey, brownish with some lenses of orange sst. Medium sand to granule with occasional large pumic pebbles. All rounded indicating alluvial setting.

Face Log 2.1

Depth (m) From	Depth (m) To	Thickness	Description
0.00	0.30	0.30	Soil: Topsoil, medium brown
0.30	1.80	1.50	VCSS: Very coarse sandstone, medium sand to pebble size grains. Light grey, with occasional lenses of orange, iron stained sst. Grains all angular apart from pumice (sub-rounded), lots of black rock with vesicles (possibly scoria). Abundant volcanic glass. Very loose and friable, easy to dig by hand.

Face Log 2.2

Depth (m) From	Depth (m) To	Thickness	Description
0.00	1.02	1.02	CSS: Coarse sand, silt to pebble sized grains, light grey, brownish. Bands of silt and bands of black, scoria-like rock
1.02	1.30	0.28	ZST: Silt, light grey, brownish. Some orange staining
1.30	1.60	0.30	VCSS: Very coarse sandstone, coarse sand to granule. Light grey with bands of orange staining. Very distinctive band of orange granule sst at 1.46 to 1.51m

Face Log 3

Depth (m) From	Depth (m) To	Thickness	Description
0.00	0.20	0.20	Soil: Topsoil, brown
0.20	2.00	1.80	VCSS: Very coarse sandstone, medium sand to pebble size. Grey, with dark scoria-like rock. Many volcanic glass clasts. Angular grains
2.00	2.80	0.80	ZST: Silt, light grey, occasional iron staining. Soil horizon in the top 0.25m
2.80	4.00	1.20	VCSS: Very coarse sandstone, medium sand to granule. Light grey. Abundant volcanic glass, occasional pumice. Iron staining

Face Log 4

Depth (m) From	Depth (m) To	Thickness	Description
0.00	0.34	0.34	Soil: Topsoil, brown
0.34	1.12	0.78	VFS: Very fine sand, light grey. Some black laminations. Soft and friable.
1.12	1.38	0.26	VCSS: very coarse sandstone, medium sand to granule. Light grey. Very loose and friable. Angular grains
1.38	6.40	5.02	VCSS: Very coarse sandstone, fine sand to granule. Brown, orangeish. Grains angular apart from pumice which is generally rounded. Some black, scoria-like grains. Iron staining

Face Log 5

Depth (m) From	Depth (m) To	Thickness	Description
0.00	0.07	0.07	Soil: Topsoil, brown, organic material
0.07	0.40	0.33	VCSS: Very coarse sandstone, medium to granule grains. Light grey. Pumice and some volcanic glass present
0.40	0.50	0.10	Soil: Buried soil horizon, dark brown
0.50	0.60	0.10	VCSS: Very coarse sandstone, medium to granule grains. Grey, orangeish

Appendix H: Rolled thread results

Determination of plastic limit by rolling a thread

Sample	M1	M2	M3	M4	M5	Water content
1	13.468	15.812	14.999	0.813	1.531	53.10
2	13.423	16.059	15.246	0.813	1.823	44.60
3	13.49	15.467	14.888	0.579	1.398	41.42
4	13.746	17.236	16.033	1.203	2.287	52.60
6	13.582	17.824	16.594	1.23	3.012	40.84
7	13.49	17.054	16.077	0.977	2.587	37.77

M1	Mass of container
M2	Mass of container and wet soil
M3	Mass of container and dried soil
M4	Mass of water (M2-M3)
M5	Mass of dried soil (M3-M1)
Water content	(M4/M5)×100

Note: All weights in grams

Appendix I: Cone penetration results

Determination of Cone Penetration Limit and Water Content

Project:	Kawerau	Sample number:	**1**
Location:	Hole 3	Tested by:	HTM
Depth:	0.45-1.00m	Date:	30/11/2011
Sample history:	Disturbed, not dried		

Test number	1			2			3			4		
Initial dial	0	0	0	0	0	0	0	0	0	0	0	0
Final dial	14.9	13.94	15.2	18.1	19.26	18.9	21.6	21.8	21.45	22.85	23.15	24.1
Penetration	14.9	13.94	15.2	18.1	19.26	18.9	21.6	21.8	21.45	22.85	23.15	24.1
Av. Penetration	14.68			18.75			21.62			23.37		
Container no.	H1			H2			H3			H4		
M1	20.839			13.571			13.463			13.422		
M2	34.694			28.762			39.818			37.639		
M3	29.327			22.761			29.479			28.144		
M4	5.367			6.001			10.339			9.495		
M5	8.488			9.19			16.016			14.722		
Water content	63.23			65.30			64.55			64.50		

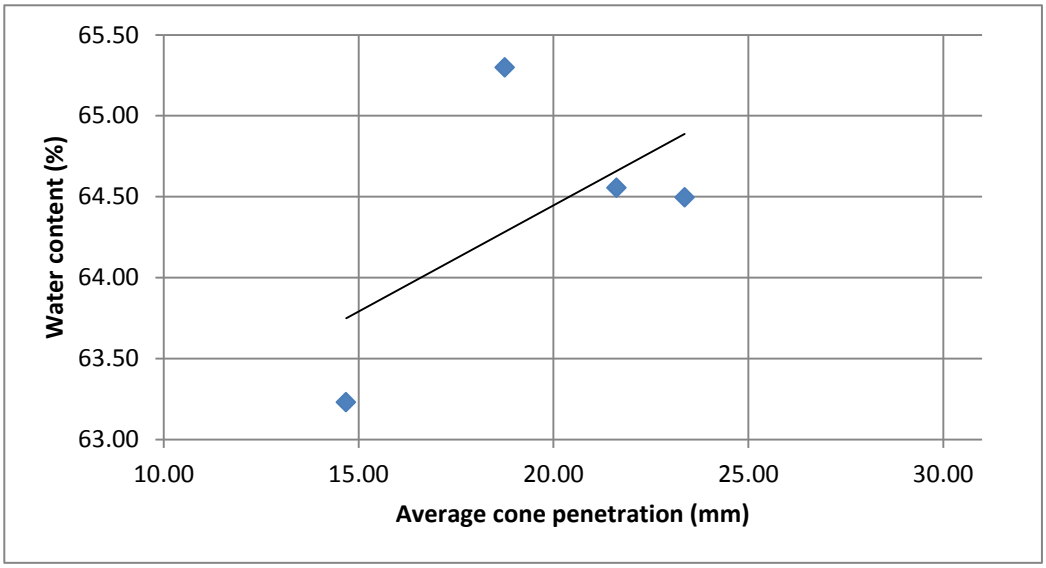

CPL: **64.5**

M1	Mass of container
M2	Mass of container and wet soil
M3	Mass of container and dried soil
M4	Mass of water (M2-M3)
M5	Mass of dried soil (M3-M1)
Water content	(M4/M5)×100

Note: All weights in grams

Determination of Cone Penetration Limit and Water Content

Project:	Kawerau	Sample number:	**2**
Location:	Hole 3	Tested by:	HTM
Depth:	0.03-0.25m	Date:	30/11/2011
Sample history:	Disturbed, not dried		

Test number	1			2			3			4		
Initial dial	0	0	0	0	0	0	0	0	0	0	0	0
Final dial	14.65	15.2	14.86	21	21.5	21.8	19.75	19.6	19.4	22.5	23.3	23.5
Penetration	14.65	15.2	14.86	21	21.5	21.8	19.75	19.6	19.4	22.5	23.3	23.5
Av. Penetration	14.90			21.43			19.58			23.10		
Container no.	H5			H6			H7			H8		
M1	13.21			13.337			13.39			13.488		
M2	33.708			41.28			46.943			44.63		
M3	26.765			31.557			35.337			33.823		
M4	6.943			9.723			11.606			10.807		
M5	13.555			18.22			21.947			20.335		
Water content	51.22			53.36			52.88			53.14		

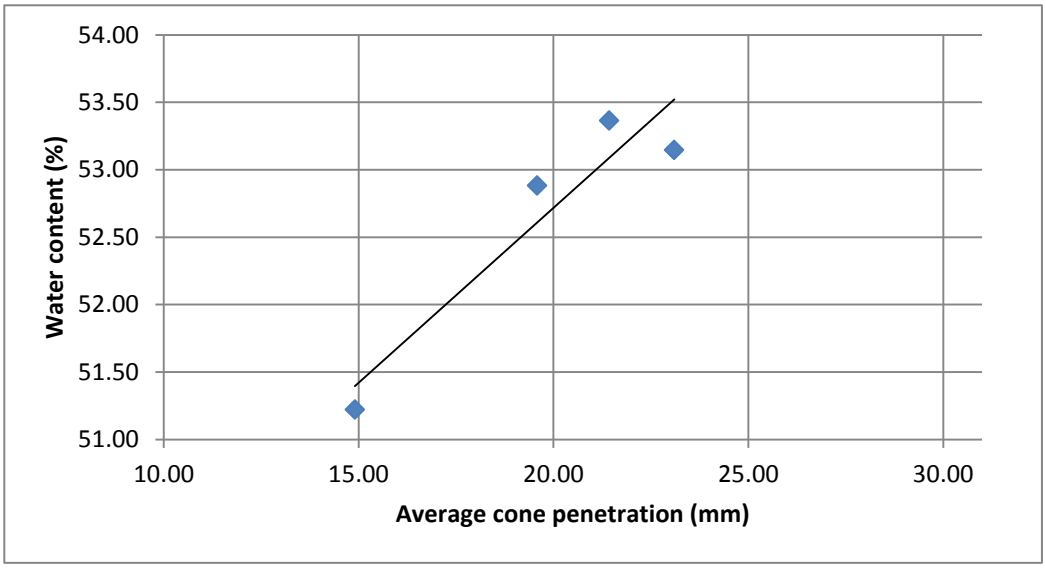

CPL: **52.75**

M1	Mass of container
M2	Mass of container and wet soil
M3	Mass of container and dried soil
M4	Mass of water (M2-M3)
M5	Mass of dried soil (M3-M1)
Water content	(M4/M5)×100

Note: All weights in grams

Determination of Cone Penetration Limit and Water Content

Project:	Kawerau	Sample number:	**3**
Location:	Hole 18	Tested by:	HTM
Depth:	0.9-1.4	Date:	30/11/2011
Sample history:	Disturbed, not dried		

Test number	1			2			3			4		
Initial dial	0	0	0	0	0	0	0	0	0	0	0	0
Final dial	21.9	21.8	0	22.1	22.2	0	20.2	20.45	19.6	12.6	12.1	12.7
Penetration	21.9	21.8	0	22.1	22.2	0	20.2	20.45	19.6	12.6	12.1	12.7
Av. Penetration	21.85			22.15			20.08			12.47		
Container no.	H1			H2			H3			H4		
M1	13.459			13.557			13.409			13.802		
M2	45.203			46.952			33.019			34.875		
M3	34.267			35.694			26.488			28.477		
M4	10.936			11.258			6.531			6.398		
M5	20.808			22.137			13.079			14.675		
Water content	52.56			50.86			49.94			43.60		

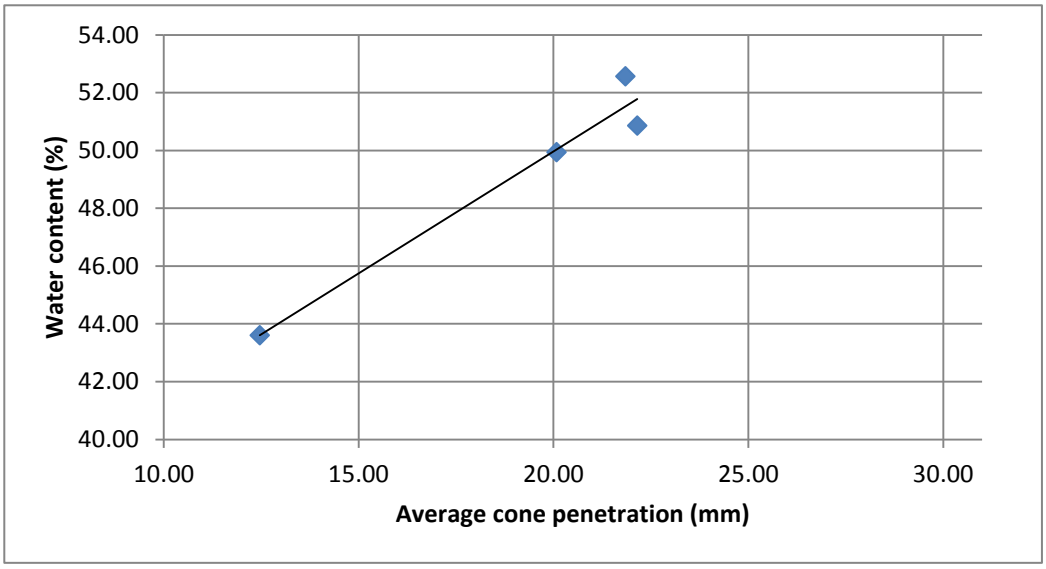

CPL: **50**

M1	Mass of container
M2	Mass of container and wet soil
M3	Mass of container and dried soil
M4	Mass of water (M2-M3)
M5	Mass of dried soil (M3-M1)
Water content	(M4/M5)×100

Note: All weights in grams

Determination of Cone Penetration Limit and Water Content

Project:	Kawerau	Sample number:	**4**
Location:	Hole 19	Tested by:	HTM
Depth:	0.4-1.0m	Date:	30/11/2011
Sample history:	Disturbed, not dried		

Test number	1			2			3			4		
Initial dial	0	0	0	0	0	0	0	0	0	0	0	0
Final dial	13.2	13.7	13.1	17.5	18.5	17.55	20.12	20.45	19.9	23.5	24.1	23.7
Penetration	13.2	13.7	13.1	17.5	18.5	17.55	20.12	20.45	19.9	23.5	24.1	23.7
Av. Penetration	13.33			17.85			20.16			23.77		
Container no.	H1			H2			H3			H4		
M1	13.572			13.563			13.584			13.414		
M2	37.997			39.194			42.734			43.76		
M3	29.684			30.396			32.698			33.143		
M4	8.313			8.798			10.036			10.617		
M5	16.112			16.833			19.114			19.729		
Water content	51.60			52.27			52.51			53.81		

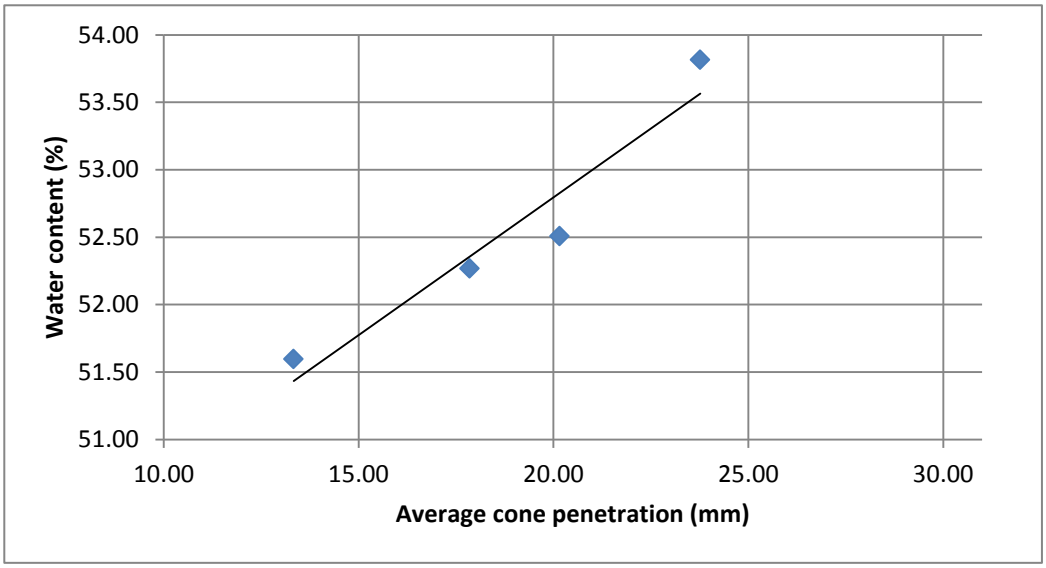

CPL: **52.75**

M1	Mass of container
M2	Mass of container and wet soil
M3	Mass of container and dried soil
M4	Mass of water (M2-M3)
M5	Mass of dried soil (M3-M1)
Water content	(M4/M5)×100

Note: All weights in grams

Determination of Cone Penetration Limit and Water Content

Project:	Kawerau	Sample number:	**6**
Location:	Hole 20	Tested by:	HTM
Depth:	2.8m	Date:	30/11/2011
Sample history:	Disturbed, not dried		

Test number	1			2			3			4		
Initial dial	0	0	0	0	0	0	0	0	0	0	0	0
Final dial	15.1	15	15.1	19.6	20.1	19.5	23.75	23.1	23.65	25.3	24.6	25.6
Penetration	15.1	15	15.1	19.6	20.1	19.5	23.75	23.1	23.65	25.3	24.6	25.6
Av. Penetration	15.07			19.73			23.50			25.17		
Container no.	H1			H2			H3			H4		
M1	13.499			13.544			13.468			13.469		
M2	41.969			47.397			40.006			36.977		
M3	32.825			36.29			31.276			29.266		
M4	9.144			11.107			8.73			7.711		
M5	19.326			22.746			17.808			15.797		
Water content	47.31			48.83			49.02			48.81		

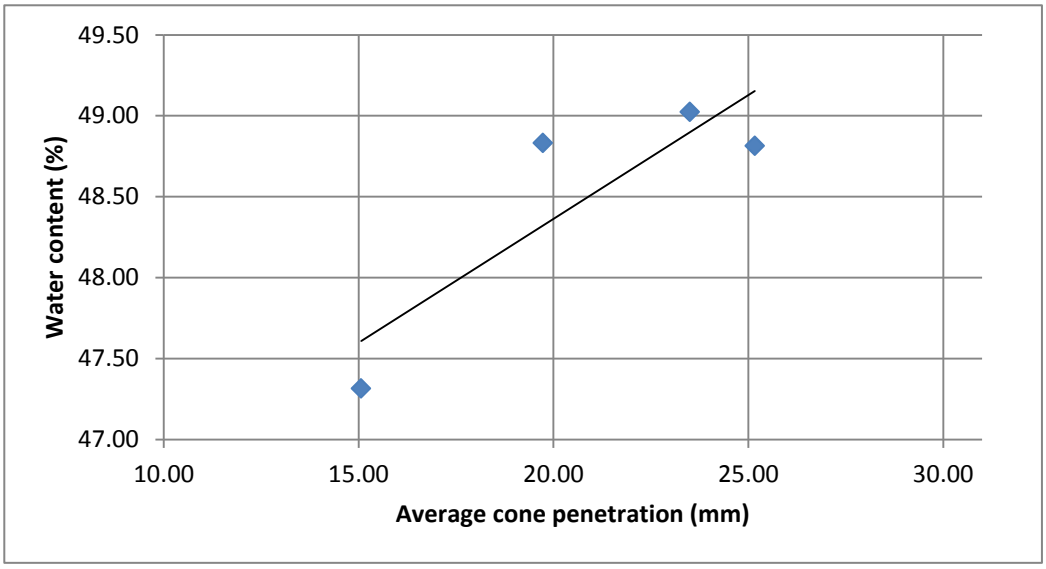

CPL: **48.35**

M1	Mass of container
M2	Mass of container and wet soil
M3	Mass of container and dried soil
M4	Mass of water (M2-M3)
M5	Mass of dried soil (M3-M1)
Water content	(M4/M5)×100

Note: All weights in grams

Determination of Cone Penetration Limit and Water Content

Project:	Kawerau	Sample number:	**7**
Location:	Hole 20	Tested by:	HTM
Depth:	1.8m	Date:	30/11/2011
Sample history:	Disturbed, not dried		

Test number	1			2			3			4		
Initial dial	0	0	0	0	0	0	0	0	0	0	0	0
Final dial	14	14	0	18.2	17.75	17.6	21.6	22.4	21.4	26.1	26	0
Penetration	14	14	0	18.2	17.75	17.6	21.6	22.4	21.4	26.1	26	0
Av. Penetration	14.00			17.85			21.80			26.05		
Container no.	H1			H2			H3			H4		
M1	13.537			13.31			13.564			13.47		
M2	32.682			36.71			34.272			36.98		
M3	26.71			29.454			27.893			29.36		
M4	5.972			7.256			6.379			7.62		
M5	13.173			16.144			14.329			15.89		
Water content	45.34			44.95			44.52			47.95		

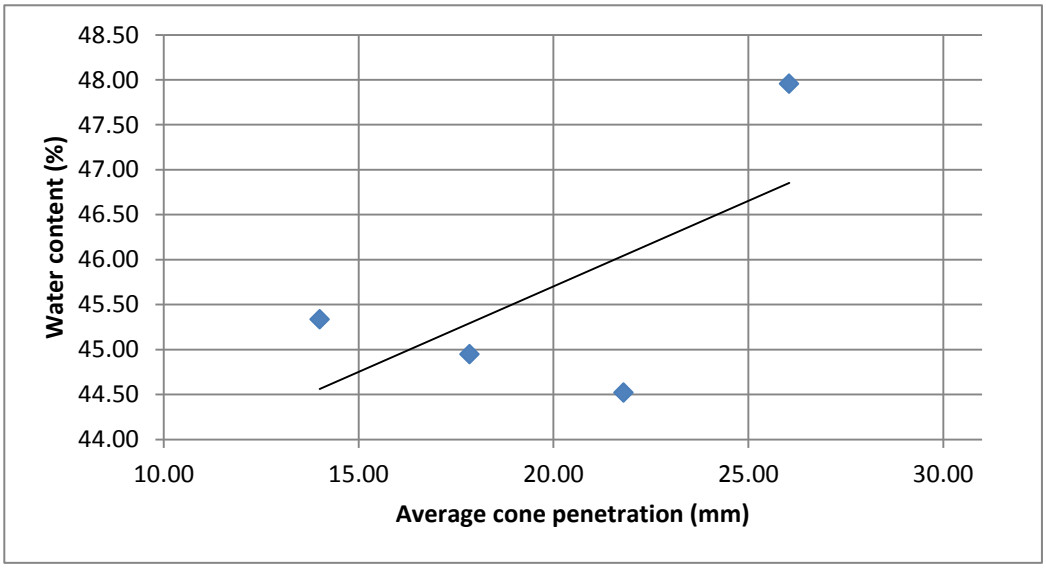

CPL: **45.75**

M1	Mass of container
M2	Mass of container and wet soil
M3	Mass of container and dried soil
M4	Mass of water (M2-M3)
M5	Mass of dried soil (M3-M1)
Water content	(M4/M5)×100

Note: All weights in grams

Appendix J: Emerson Aggregate Test methods

Department of Sustainable Natural Resources

SOIL SURVEY STANDARD TEST METHOD

EMERSON AGGREGATE TEST

ABBREVIATED NAME	EAT
TEST NUMBER	P9
TEST METHOD TYPE	B
VERSION NUMBER	2

SCOPE

This test classifies the behaviour of soil aggregates, when immersed, on their coherence in water. Testing is done only on soils with suitable aggregates. Sands and gravels are usually unsuitable for the test.

PRINCIPLE

This method describes the procedure for the determination of the Emerson class number of a soil. Soils are divided into seven classes on the basis of their coherence in water, with one further class being distinguished by the presence of calcium-rich minerals.

SPECIAL APPARATUS

- 250 mL beaker or similar container allowing a minimum depth of 30 mm of water.
- Spatula.
- Mixing bowl.
- Wash bottle containing deionised water.
- Test tubes.

PROCEDURE

1. Select 3 air-dry aggregates, 5–10 mm diameter.
2. Place 75 mL deionised water in the container. Place the 3 aggregates in the container of water, spaced equally around the side. Do not stir or otherwise disturb.
3. Record the time placed in the water. After 2 hours and 20 hours, assess aggregate behaviour according to the following:
    - Record whether slaking has occurred. (See Figure 1.) If there has been no slaking, record if there has been any swelling of the aggregate.
    - If the aggregate has dispersed, note the degree of dispersion. (See Figure 1.)
4. If the aggregate slakes but does not disperse, place about 20–40 g of soil (<2 mm) in the mixing bowl and add sufficient deionised water to bring the soil to a moisture content within the plastic range. Mix for 30 seconds.
5. Without using your fingers, form a 5 mm cube of the reworked soil using a spatula or mould. Place the cube of reworked soil into another container of deionised water. Do not stir or otherwise disturb. After 2 hours and 20 hours, rate the degree of dispersion. (See Figure 1.)
6. If the reworked aggregate disperses, note the degree of dispersion. (See Figure 1.)
7. If the reworked aggregate does not disperse, take 5 g of unworked soil and add a few drops of 1M HCl. Effervescence indicates carbonate is present.
8. If there is no carbonate present, prepare a 1:5 soil:water suspension. Shake for 10 minutes. Allow to stand for 5 minutes and note whether the suspension is dispersed or flocculated.
9. If the supernatant of the 1:5 soil:water suspension is clear, check for the presence of gypsum using 10% barium chloride solution.

DETERMINATION OF THE EMERSON AGGREGATE CLASS

Determine the Emerson Aggregate Class Number from Figure 1. Classes 2 and 3 are subdivided according to the degree of dispersion observed.

REFERENCES

Charman, PEV 1989, *Soils of New South Wales: Their Characterisation, Classification and Conservation*, Technical Handbook No 1. Soil Conservation Service of New South Wales.

Charman, PEV & Murphy, BW (eds) 1991, *Soils: Their Properties and Management: A Soil Conservation Handbook for New South Wales*, Sydney University Press in association with Oxford University Press, Sydney.

Emerson, WW 1967, A classification of soil aggregrates based on their coherence in water. *Australian Journal of Soil Research*, 5: 47-57.

Standards Australia. *AS 1289.C8.1-1980: Methods of testing soils for engineering purposes - Soil classification tests - Dispersion - Determination of Emerson class number of a soil.*

Figure 1. Determining the Emerson Class Number of Aggregates

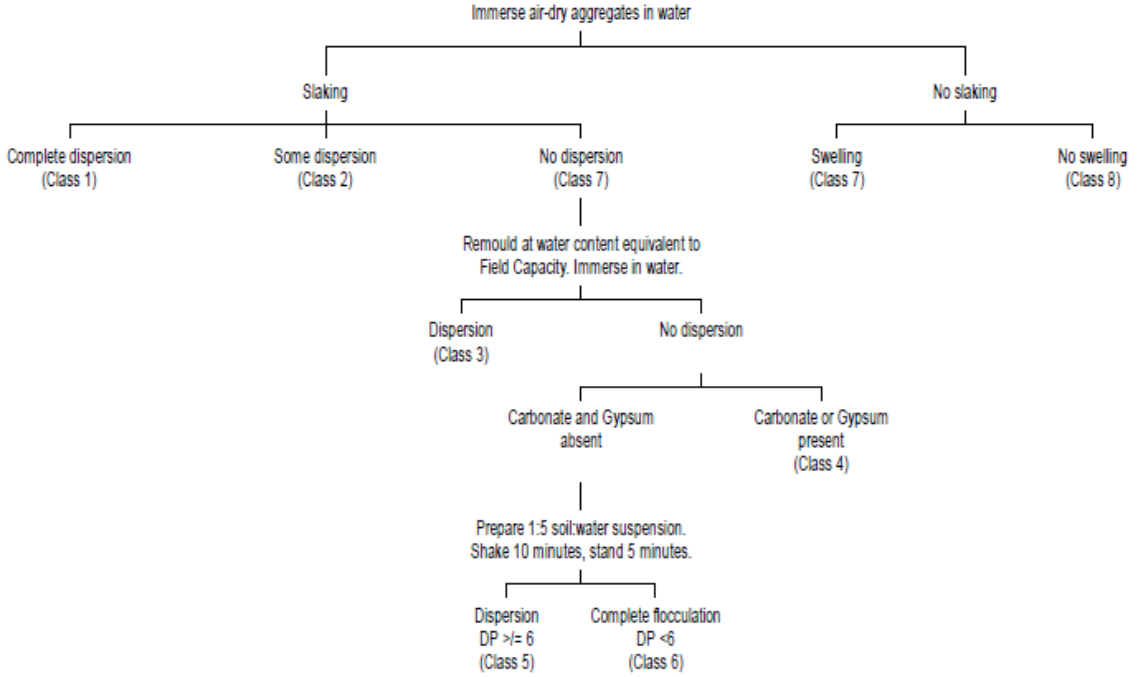

DISPERSION SUBCLASSES FOR TYPE 2 AND 3 AGGREGATES

1 Slight milkiness
2 Obvious milkiness, less than 50% of the aggregate affected
3 Obvious milkiness, greater than 50% of the aggregate affected
4 Total dispersion leaving only sand grains

Note: Class 2 (4) is equivalent to Class 1.

SLAKING

In situations where the degree of slaking is considered important, a slaking subclass is allowed:

0 No change
1 Aggregate breaks open but remains intact
2 Aggregate breaks down into smaller aggregates
3 Aggregate breaks down completely into sand grains

Appendix K: Emerson Aggregate Test results and photographs

Sample	*Hole*	*Depth (m)*	*T1*	*Comments*	*T2*	*Comments*	*T3*	*Comments*
1	3	0.45-1.00	20:03		22:03	No slaking		
2	3	0.03-0.25	20:05	Slaked immediately	22:05	Slaked	16:05	No change since T2
3	18	0.9-1.4	20:06		22:06	Slaked	16:06	No change since T2
4	19	0.4-1.0	20:07		22:07	Slaked	16:07	No change since T2
5	5	1.2-1.5	20:08		22:08	Slaked	16:08	No change since T2
6	20	2.8	20:09	Slaked immediately	22:09	Slaked	16:09	No change since T2
7	20	1.8	20:09	Slaked immediately	22:09	Slaked	16:09	No change since T2
8	20	3.5	20:10	Slaked immediately	22:10	Slaked	16:10	No change since T2

Sample	*Hole*	*Depth (m)*	*T4*	*Comments*	*T5*	*Comments*	*T6*	*Comments*	***CLASS***
1	3	0.45-1.00							**8**
2	3	0.03-0.25	13:29		15:29	Slaking and some dispersion	9:29	Slaking and some dispersion	**3**
3	18	0.9-1.4	13:31		15:31	Slaking and some dispersion	9:31	Slaking and some dispersion	**3**
4	19	0.4-1.0	13:33		13:33	Slaking and some dispersion	9:33	Slaking and some dispersion	**3**
5	5	1.2-1.5	13:35		13:35	Slaking and some dispersion	9:35	Slaked and no dispersion	**3**
6	20	2.8	13:37		13:37	Slaking and dispersion	9:37	Slaking and dispersion	**3**
7	20	1.8	13:39		13:39	Slaking and dispersion	9:39	Slaking and dispersion	**3**
8	20	3.5	13:41		13:41	Slaking and dispersion	9:41	Slaking and dispersion	**3**

T1: Time 0 hours, 1st test
T2: Time 2 hours, 1st test
T3: Time 20 hours, 1st test
T4: Time 0 hours, 2nd test
T5: Time 2 hours, 2nd test
T6: Time 20 hours, 2nd test

Note: Second test began 2 hours before the end of the 1st test as it was apparent samples were not dispersing

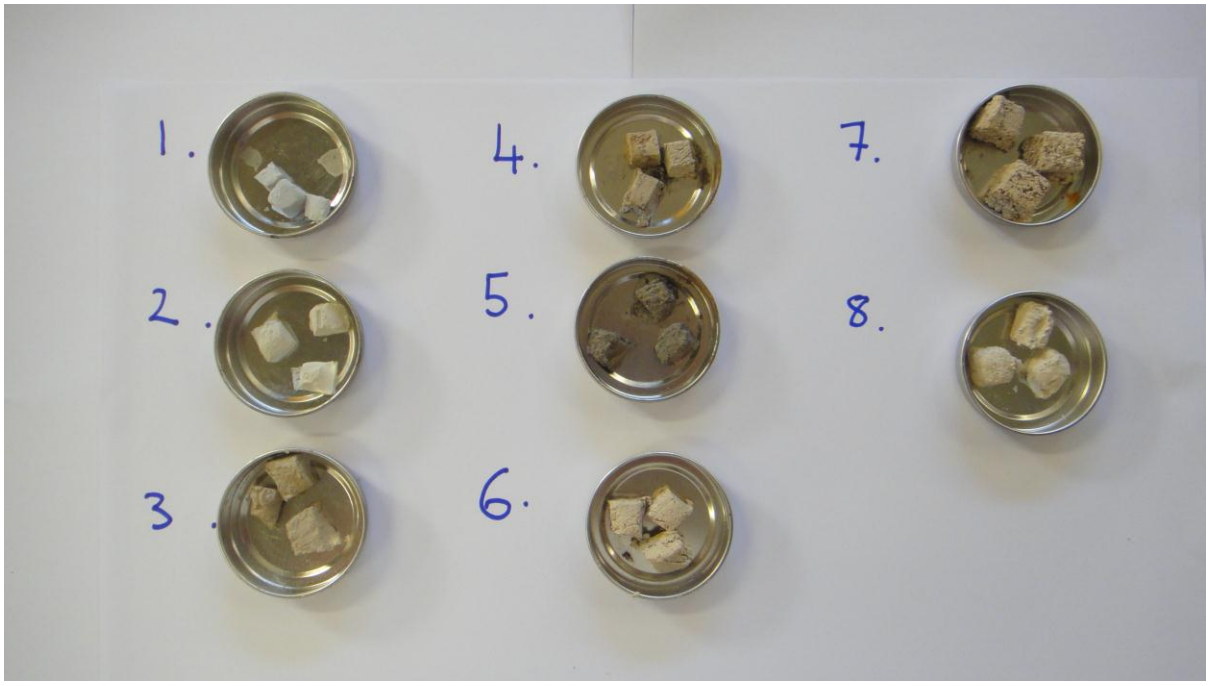
1.
4.
7.
2.
5.
8.
3.
6.


1.1

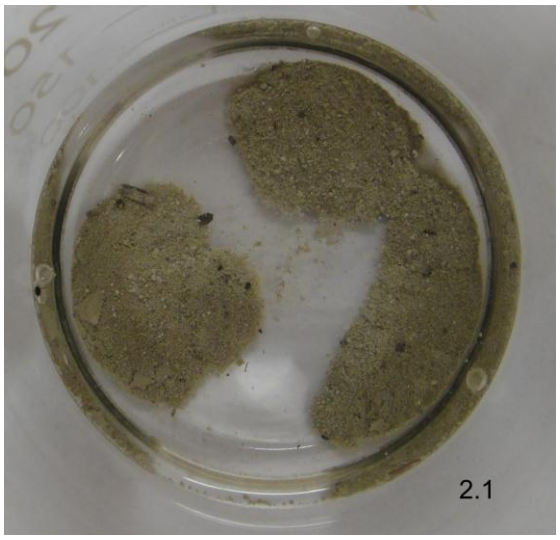
2.1

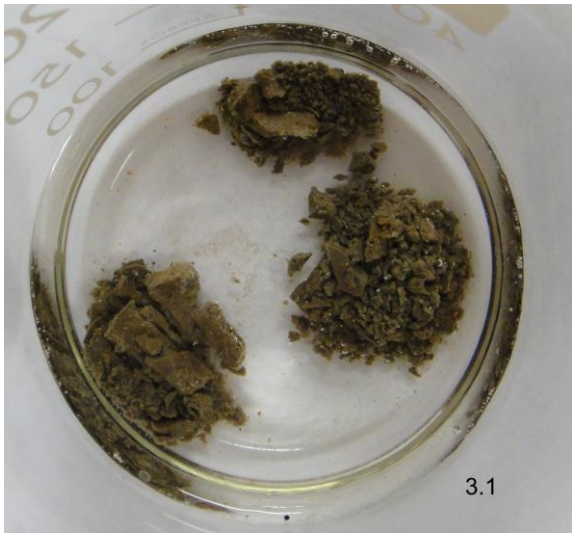
3.1

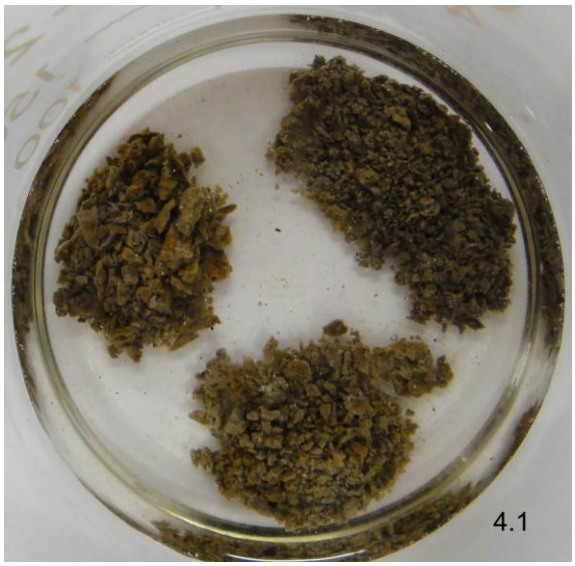
4.1

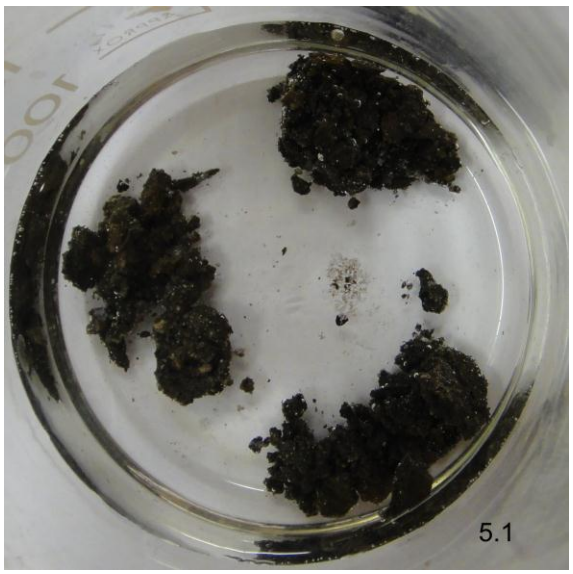
5.1

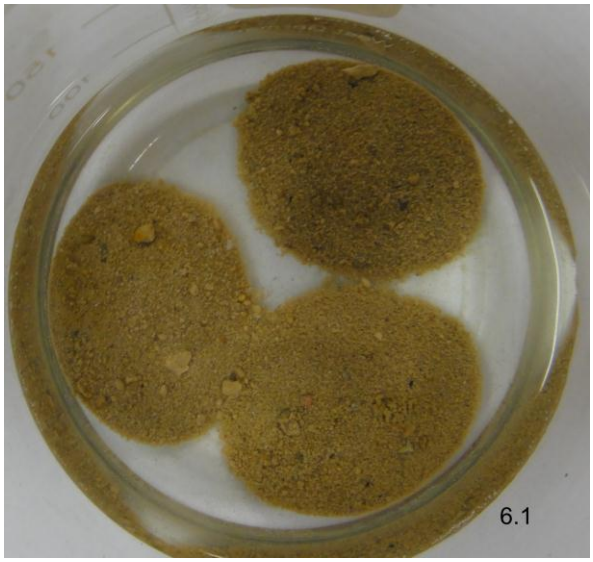
6.1

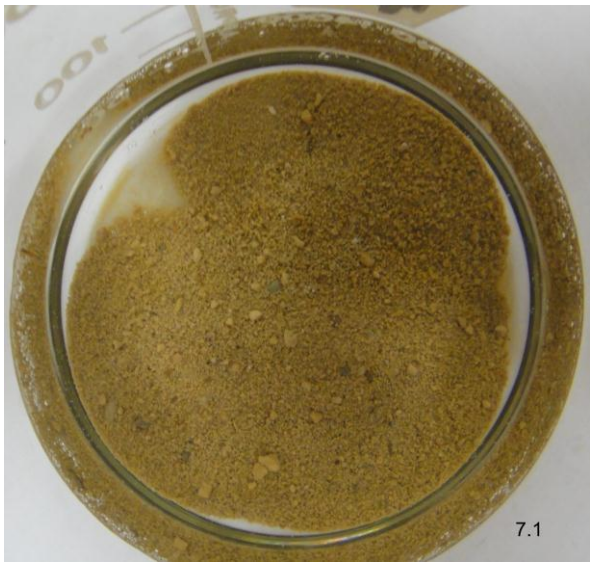
7.1

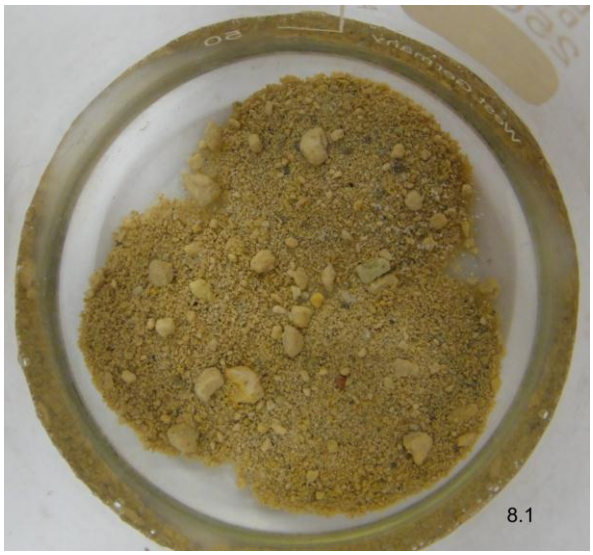
8.1

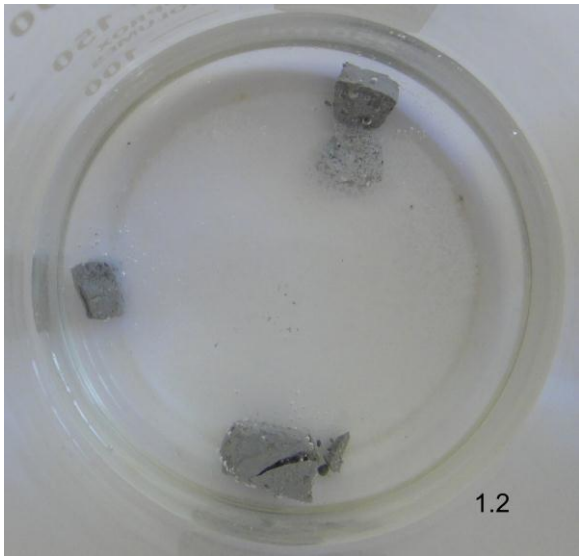
1.2

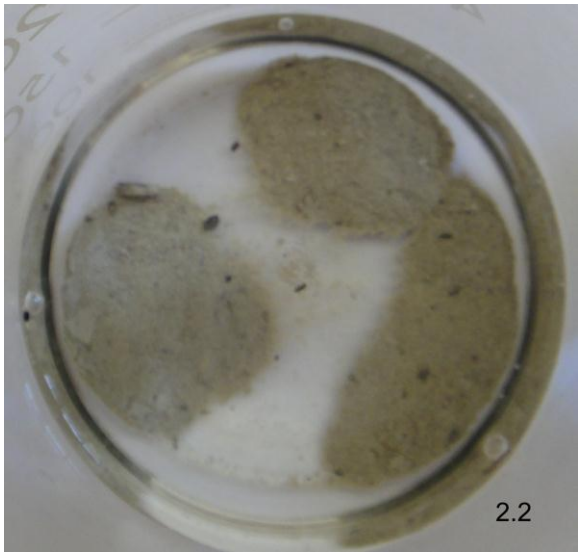
2.2

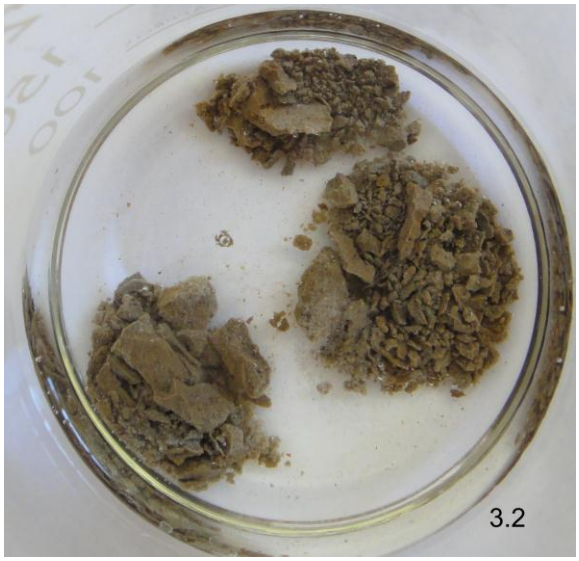
3.2

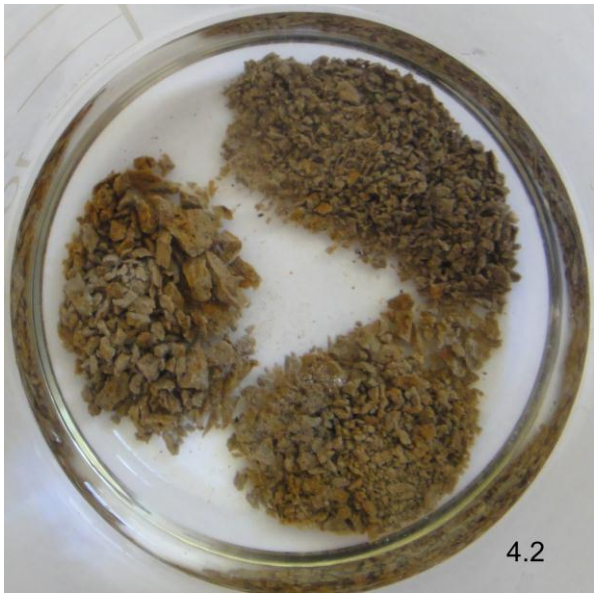
4.2


5.2

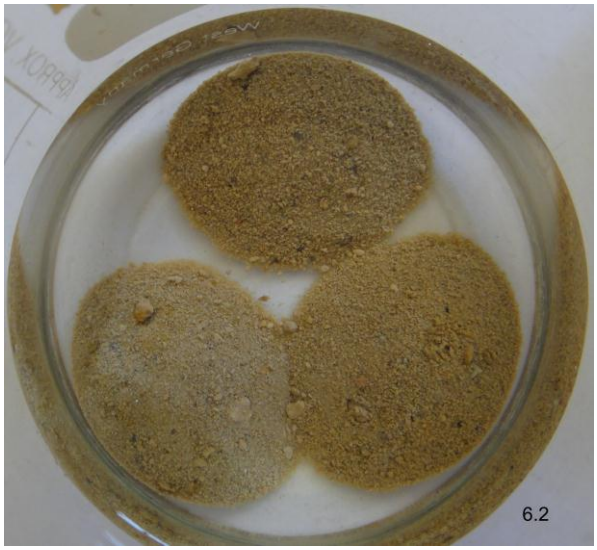
6.2

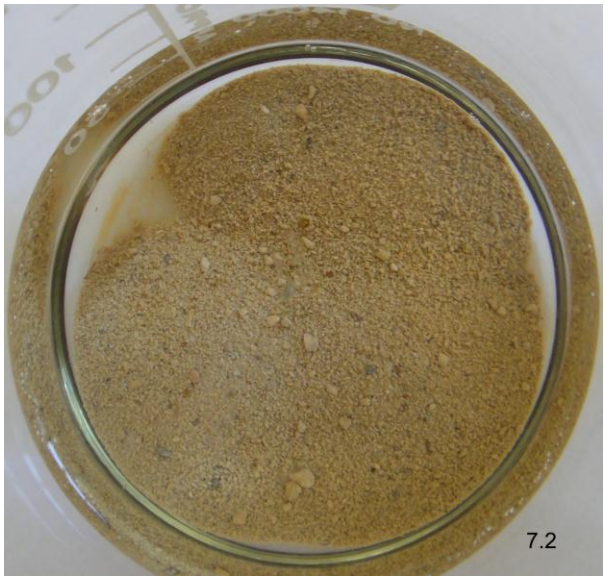
7.2


8.2

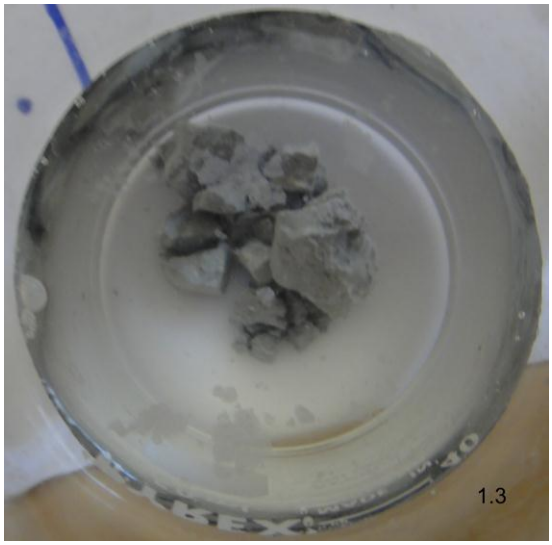
1.3


1.3


2.3

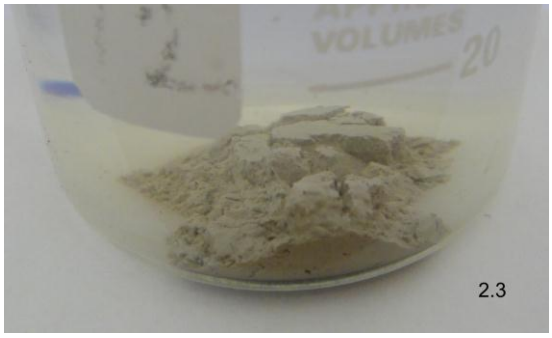
VOLUMES
20
2.3

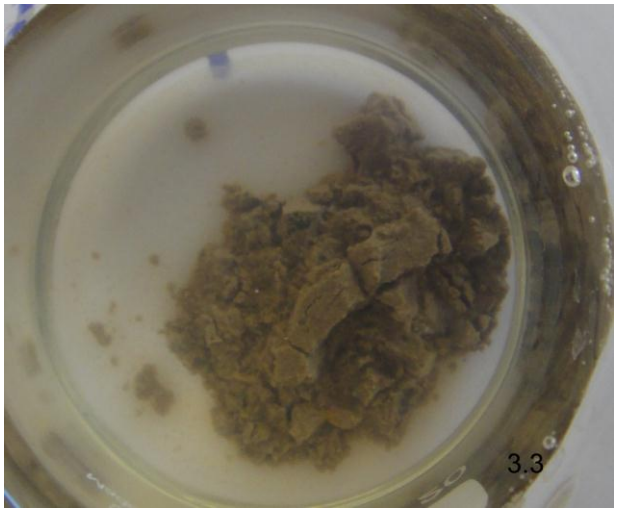
3.3


3.3

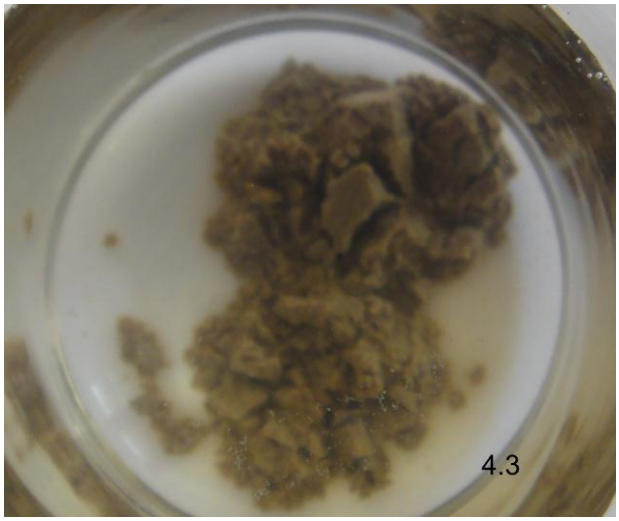
4.3


4.3

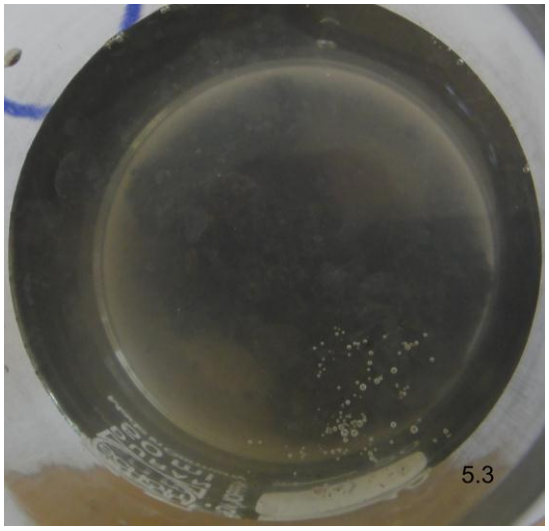
5.3

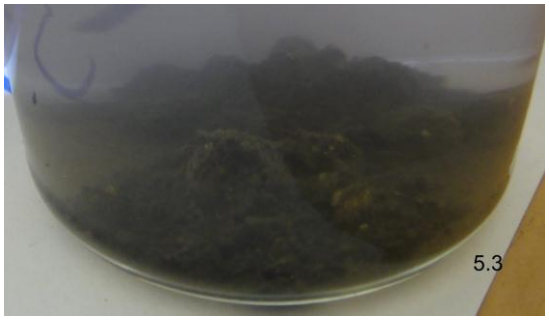
5.3

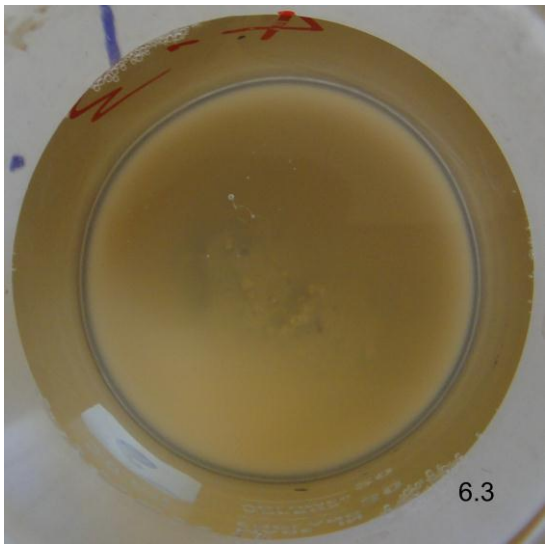
6.3


6.3

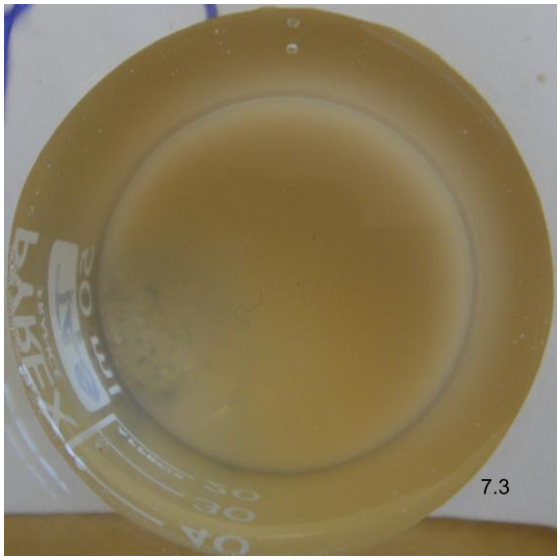
7.3


7.3

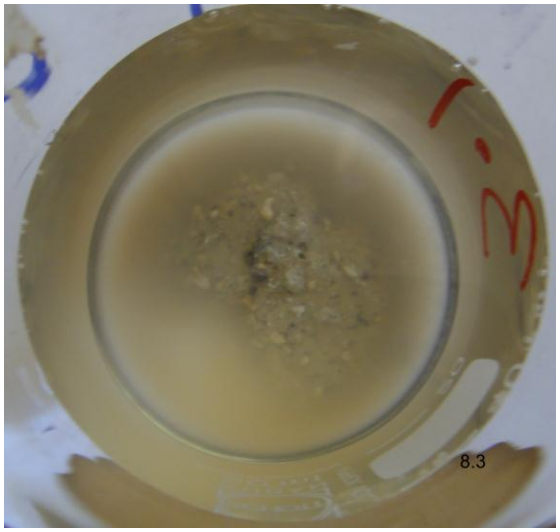
8.3

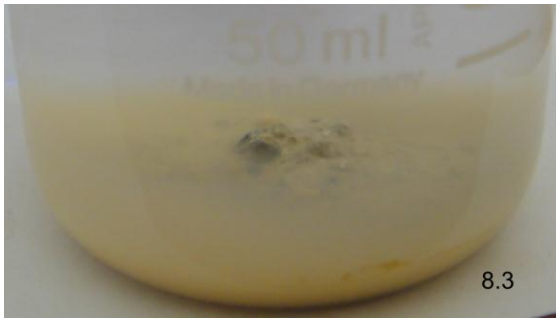
8.3

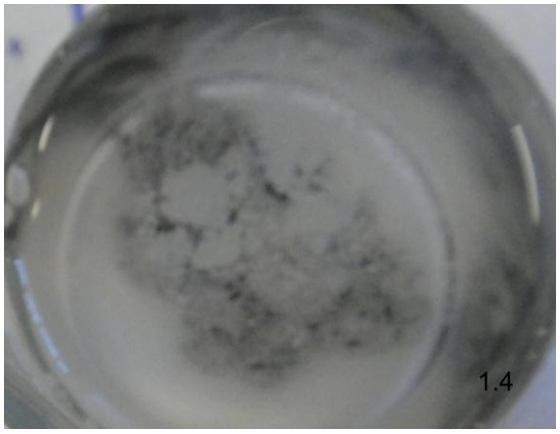
1.4


2.4

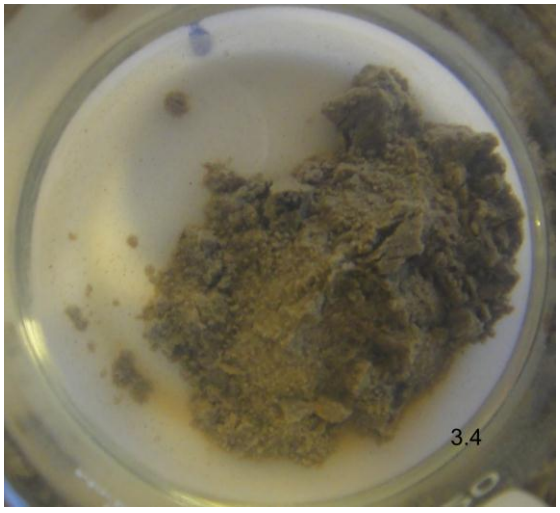
3.4


Germany
3.4


4.4

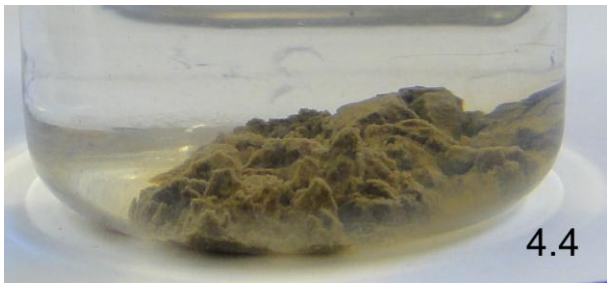
4.4

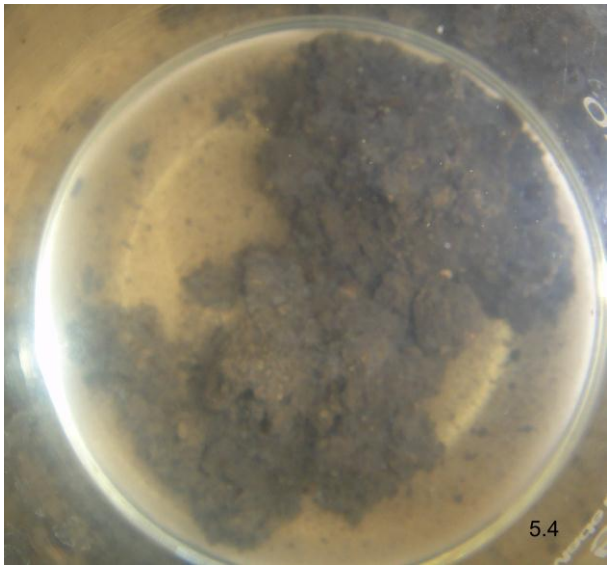
5.4


5.4

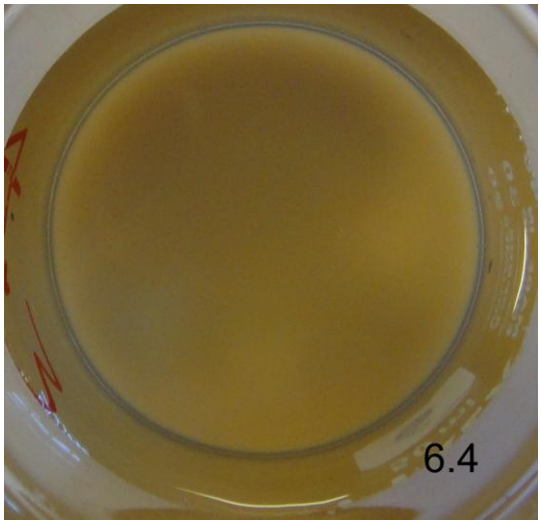
6.4

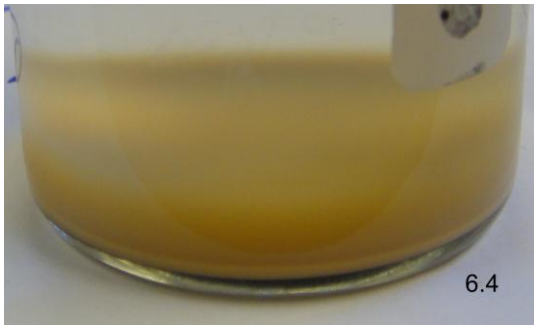
6.4

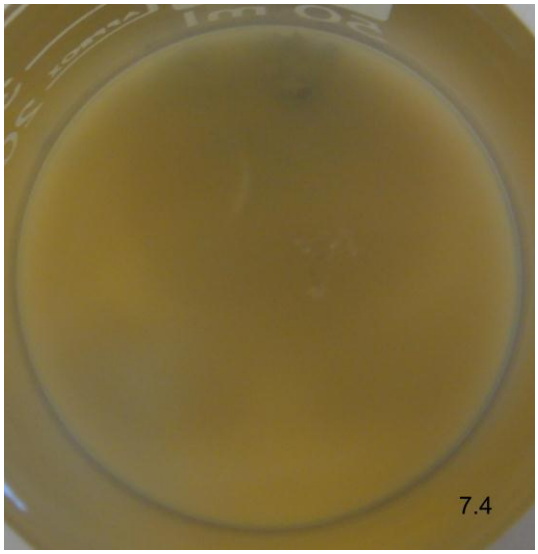
7.4


7.4

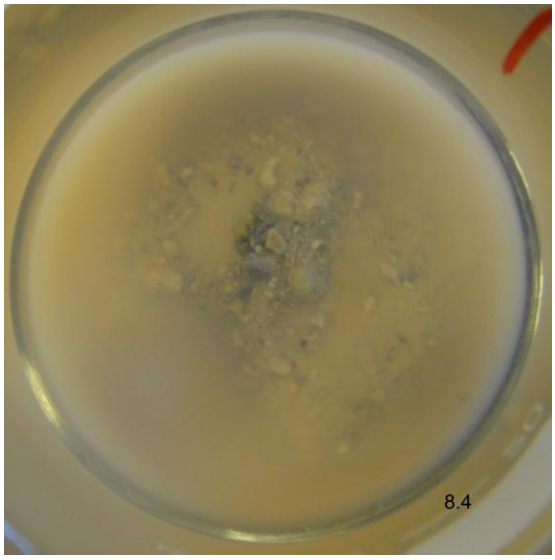
8.4


Made in Germany
8.4

Appendix L: Laser sizer results

micromeritics®

Micromeritics Instrument Corporation

Sample: LS1
Operator:
Submitter:
File: C:\...\HAYDEN\LS1.SMP

Test Number: 1
Analyzed: 5/12/2011 9:42:08p.m.
Reported: 5/12/2011 9:42:17p.m.
Background: 5/12/2011 9:34:27p.m.

Model: Fraunhofer, 1.331
Material: Fraunhofer / Water
Background: Water RI 1.331
Smoothing: Medium

Combined Report

Incremental Volume Percent vs. Particle Diameter Graph

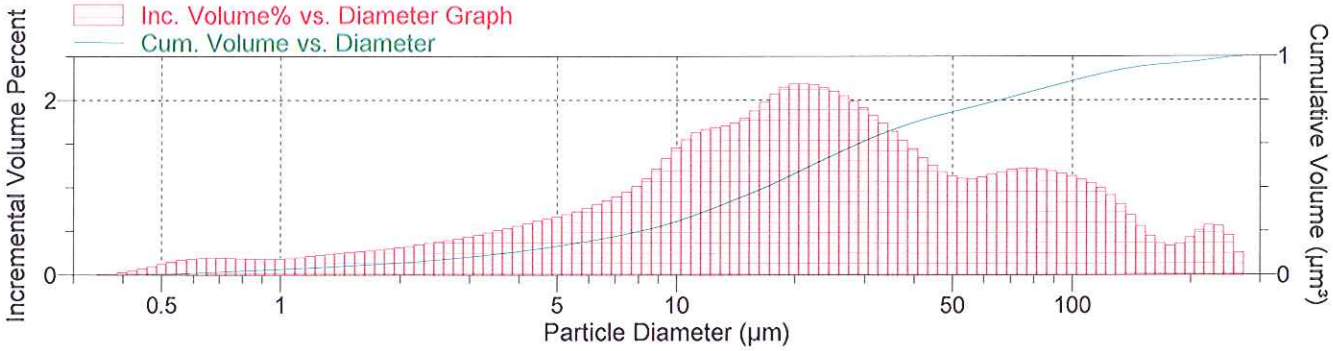

Summary Report

Sample

Sample Concentration: 0.00953 %
Obscuration: 16.7 %

Weighted Statistics (Volume Distribution)

		Std Dev of 1			Std Dev of 1
Mean	40.742	0.000	Mode	21.138	0.000
Median	21.867	0.000			

Peaks: Weighted Statistics (Volume Distribution)

Peak Number	Percent of Dist.*	Percent of Dist. Std Dev of 1	Mean	Mean Std Dev of 1	Median	Median Std Dev of 1	Mode
1	75.1	0.0	19.531	0.000	16.730	0.000	21.138
2	19.2	0.0	98.293	0.000	91.979	0.000	79.444

* Peaks must comprise at least 5.00 % of the distribution.

Sample: LS2
Operator:
Submitter:
File: C:\...\HAYDEN\LS2.SMP

Test Number: 1
Analyzed: 5/12/2011 9:57:17p.m.
Reported: 5/12/2011 9:57:24p.m.
Background: 5/12/2011 9:34:27p.m.

Model: Fraunhofer, 1.331
Material: Fraunhofer / Water
Background: Water RI 1.331
Smoothing: Medium

Combined Report

Incremental Volume Percent vs. Particle Diameter Graph

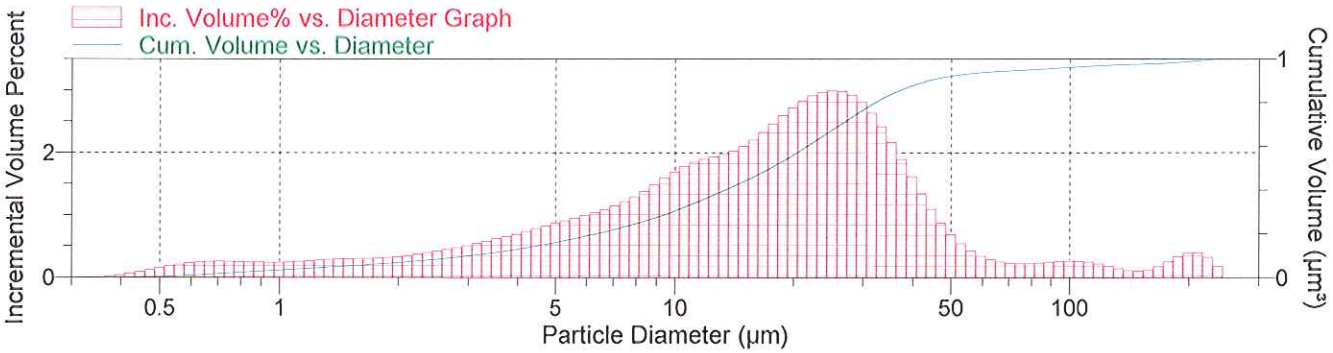

Summary Report

Sample

Sample Concentration: 0.00659 %
Obscuration: 14.4 %

Weighted Statistics (Volume Distribution)

		Std Dev of 1			Std Dev of 1
Mean	25.059	0.000	Mode	25.122	0.000
Median	17.426	0.000			

Peaks: Weighted Statistics (Volume Distribution)

Peak Number	Percent of Dist.*	Percent of Dist. Std Dev of 1	Mean	Mean Std Dev of 1	Median	Median Std Dev of 1	Mode
1	91.8	0.0	19.338	0.000	17.101	0.000	25.122

* Peaks must comprise at least 5.00 % of the distribution.

micromeritics®

Micromeritics Instrument Corporation

Sample: LS3
Operator:
Submitter:
File: C:\...\HAYDEN\LS3.SMP

Test Number: 1
Analyzed: 5/12/2011 10:07:04p.m.
Reported: 5/12/2011 10:07:08p.m.
Background: 5/12/2011 9:34:27p.m.

Model: Fraunhofer, 1.331
Material: Fraunhofer / Water
Background: Water RI 1.331
Smoothing: Medium

Combined Report

Incremental Volume Percent vs. Particle Diameter Graph

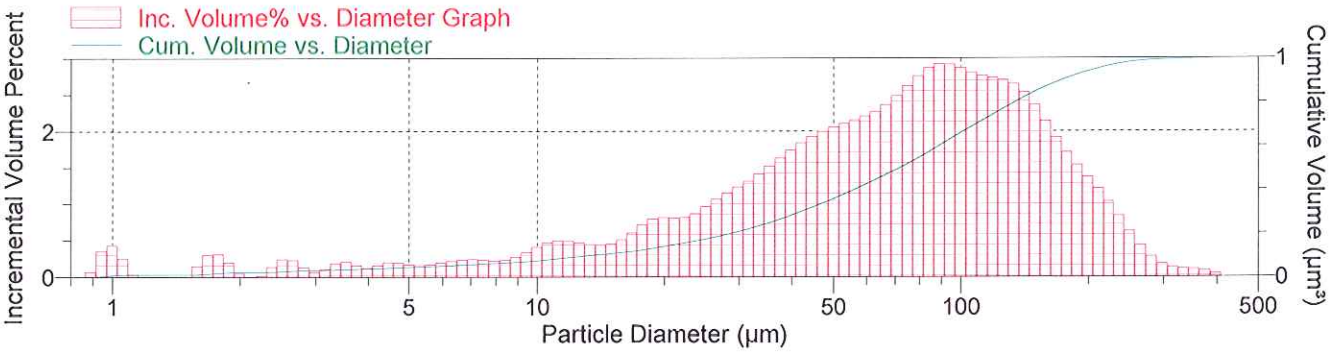

Summary Report

Sample

Sample Concentration: 0.02526 %
Obscuration: 16.2 %

Weighted Statistics (Volume Distribution)

		Std Dev of 1			Std Dev of 1
Mean	84.526	0.000	Mode	89.137	0.000
Median	72.020	0.000			

Peaks: Weighted Statistics (Volume Distribution)

Peak Number	Percent of Dist.*	Percent of Dist. Std Dev of 1	Mean	Mean Std Dev of 1	Median	Median Std Dev of 1	Mode
1	84.7	0.0	97.891	0.000	84.646	0.000	89.137

* Peaks must comprise at least 5.00 % of the distribution.

micromeritics®

Micromeritics Instrument Corporation

Sample: LS4
Operator:
Submitter:
File: C:\...\HAYDEN\LS4.SMP

Test Number: 1
Analyzed: 5/12/2011 10:18:28p.m.
Reported: 5/12/2011 10:18:32p.m.
Background: 5/12/2011 9:34:27p.m.

Model: Fraunhofer, 1.331
Material: Fraunhofer / Water
Background: Water RI 1.331
Smoothing: Medium

Combined Report

Incremental Volume Percent vs. Particle Diameter Graph

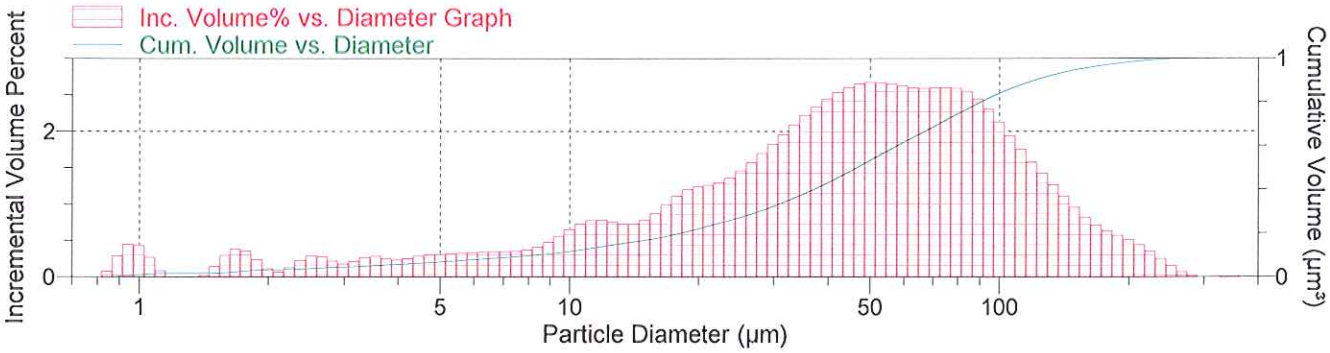

Summary Report

Sample

Sample Concentration: 0.02750 %
Obscuration: 24.0 %

Weighted Statistics (Volume Distribution)

		Std Dev of 1			Std Dev of 1
Mean	57.413	0.000	Mode	50.126	0.000
Median	46.460	0.000			

Peaks: Weighted Statistics (Volume Distribution)

Peak Number	Percent of Dist.*	Percent of Dist. Std Dev of 1	Mean	Mean Std Dev of 1	Median	Median Std Dev of 1	Mode
1	10.6	0.0	9.340	0.000	9.601	0.000	11.887
2	51.5	0.0	39.762	0.000	39.025	0.000	50.126
3	32.0	0.0	112.005	0.000	99.377	0.000	75.000

* Peaks must comprise at least 5.00 % of the distribution.

micromeritics®

Micromeritics Instrument Corporation

Sample: LS5
Operator:
Submitter:
File: C:\...\HAYDEN\LS5.SMP

Test Number: 1
Analyzed: 5/12/2011 10:30:36p.m.
Reported: 5/12/2011 10:30:40p.m.
Background: 5/12/2011 9:34:27p.m.

Model: Fraunhofer, 1.331
Material: Fraunhofer / Water
Background: Water RI 1.331
Smoothing: Medium

Combined Report

Incremental Volume Percent vs. Particle Diameter Graph

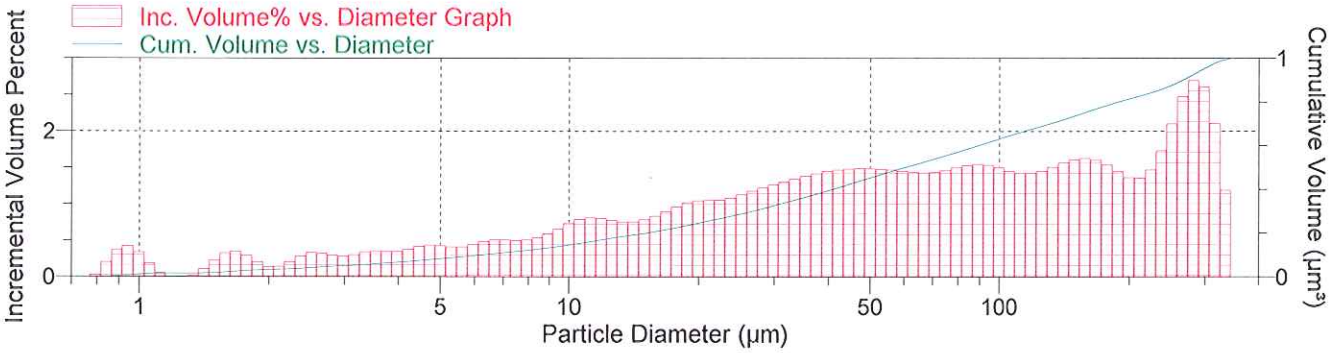

Summary Report

Sample

Sample Concentration: 0.01388 %
Obscuration: 13.6 %

Weighted Statistics (Volume Distribution)

		Std Dev of 1			Std Dev of 1
Mean	98.074	0.000	Mode	281.877	0.000
Median	59.745	0.000			

Peaks: Weighted Statistics (Volume Distribution)

Peak Number	Percent of Dist.*	Percent of Dist. Std Dev of 1	Mean	Mean Std Dev of 1	Median	Median Std Dev of 1	Mode
1	7.0	0.0	10.659	0.000	10.640	0.000	11.222
2	34.6	0.0	36.787	0.000	34.839	0.000	50.126
3	14.9	0.0	92.827	0.000	91.484	0.000	89.137
4	15.2	0.0	164.417	0.000	161.806	0.000	158.511
5	16.4	0.0	276.571	0.000	276.303	0.000	281.877

* Peaks must comprise at least 5.00 % of the distribution.

Sample: LS6
Operator:
Submitter:
File: C:\...\HAYDEN\LS6.SMP

Test Number: 1
Analyzed: 5/12/2011 10:38:52p.m.
Reported: 5/12/2011 10:38:57p.m.
Background: 5/12/2011 9:34:27p.m.

Model: Fraunhofer, 1.331
Material: Fraunhofer / Water
Background: Water RI 1.331
Smoothing: Medium

Combined Report

Incremental Volume Percent vs. Particle Diameter Graph

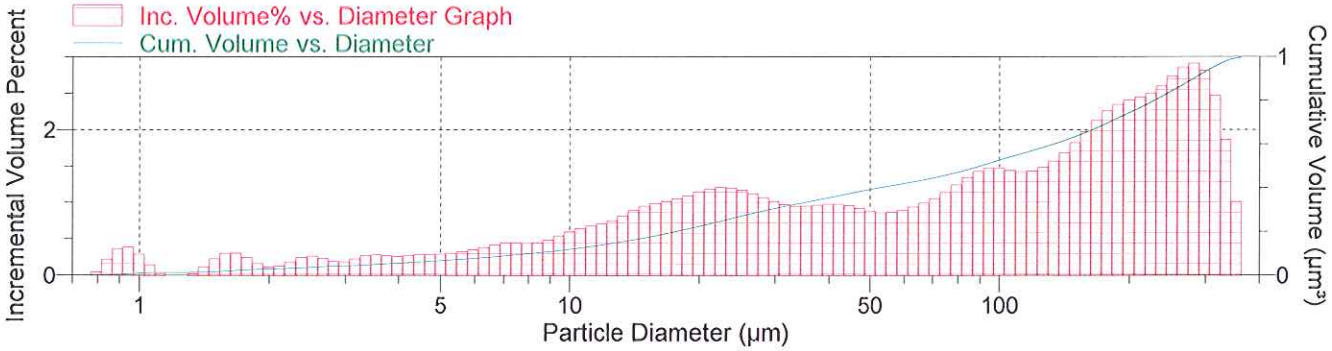

Summary Report

Sample

Sample Concentration: 0.01680 %
Obscuration: 14.6 %

Weighted Statistics (Volume Distribution)

		Std Dev of 1			Std Dev of 1
Mean	118.199	0.000	Mode	281.877	0.000
Median	89.201	0.000			

Peaks: Weighted Statistics (Volume Distribution)

Peak Number	Percent of Dist.*	Percent of Dist. Std Dev of 1	Mean	Mean Std Dev of 1	Median	Median Std Dev of 1	Mode
1	23.8	0.0	20.316	0.000	19.542	0.000	22.390
2	6.6	0.0	44.754	0.000	44.330	0.000	39.816
3	15.8	0.0	84.339	0.000	84.337	0.000	94.419
4	43.5	0.0	222.457	0.000	217.994	0.000	281.877

* Peaks must comprise at least 5.00 % of the distribution.

micromeritics®

Micromeritics Instrument Corporation

Sample: LS7
Operator:
Submitter:
File: C:\...\HAYDEN\LS7.SMP

Test Number: 1
Analyzed: 5/12/2011 10:52:49p.m.
Reported: 5/12/2011 10:52:54p.m.
Background: 5/12/2011 9:34:27p.m.

Model: Fraunhofer, 1.331
Material: Fraunhofer / Water
Background: Water RI 1.331
Smoothing: Medium

Combined Report

Incremental Volume Percent vs. Particle Diameter Graph

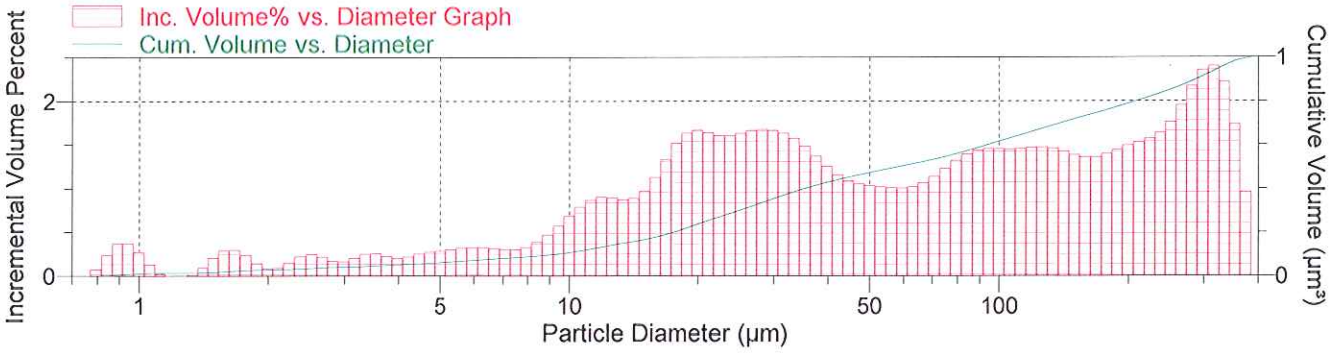

Summary Report

Sample

Sample Concentration: 0.02870 %
Obscuration: 23.6 %

Weighted Statistics (Volume Distribution)

		Std Dev of 1			Std Dev of 1
Mean	105.128	0.000	Mode	316.271	0.000
Median	58.270	0.000			

Peaks: Weighted Statistics (Volume Distribution)

Peak Number	Percent of Dist.*	Percent of Dist. Std Dev of 1	Mean	Mean Std Dev of 1	Median	Median Std Dev of 1	Mode
1	6.8	0.0	10.934	0.000	11.014	0.000	11.887
2	14.0	0.0	19.089	0.000	19.068	0.000	19.955
3	21.4	0.0	38.030	0.000	35.576	0.000	28.188
4	13.0	0.0	84.457	0.000	84.198	0.000	94.419
5	10.1	0.0	133.872	0.000	132.783	0.000	125.910
6	26.1	0.0	264.216	0.000	264.897	0.000	316.271

* Peaks must comprise at least 5.00 % of the distribution.

micromeritics®

Micromeritics Instrument Corporation

Sample: LS8
Operator:
Submitter:
File: C:\...\HAYDEN\LS8.SMP

Test Number: 1
Analyzed: 5/12/2011 11:06:06p.m.
Reported: 5/12/2011 11:06:10p.m.
Background: 5/12/2011 9:34:27p.m.

Model: Fraunhofer, 1.331
Material: Fraunhofer / Water
Background: Water RI 1.331
Smoothing: Medium

Combined Report

Incremental Volume Percent vs. Particle Diameter Graph

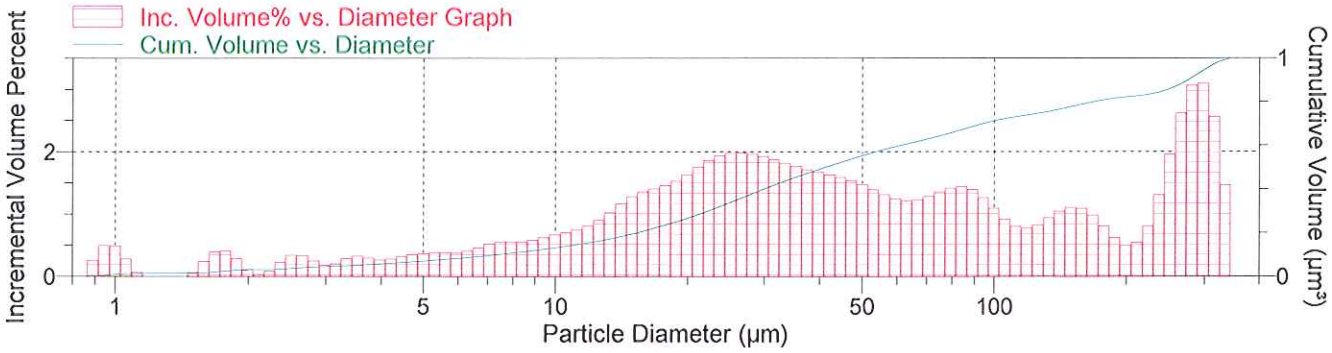

Summary Report

Sample

Sample Concentration: 0.01570 %
Obscuration: 15.0 %

Weighted Statistics (Volume Distribution)

		Std Dev of 1			Std Dev of 1
Mean	88.371	0.000	Mode	298.579	0.000
Median	41.009	0.000			

Peaks: Weighted Statistics (Volume Distribution)

Peak Number	Percent of Dist.*	Percent of Dist. Std Dev of 1	Mean	Mean Std Dev of 1	Median	Median Std Dev of 1	Mode
1	49.7	0.0	29.784	0.000	26.878	0.000	26.611
2	13.1	0.0	87.962	0.000	85.796	0.000	84.151
3	8.0	0.0	156.745	0.000	154.395	0.000	149.644
4	17.5	0.0	280.226	0.000	281.511	0.000	298.579

* Peaks must comprise at least 5.00 % of the distribution.

micromeritics®

Micromeritics Instrument Corporation

Sample: LS9
Operator:
Submitter:
File: C:\...\HAYDEN\LS9.SMP

Test Number: 1
Analyzed: 5/12/2011 11:28:36p.m.
Reported: 5/12/2011 11:28:40p.m.
Background: 5/12/2011 11:20:08p.m.

Model: Fraunhofer, 1.331
Material: Fraunhofer / Water
Background: Water RI 1.331
Smoothing: Medium

Combined Report

Incremental Volume Percent vs. Particle Diameter Graph

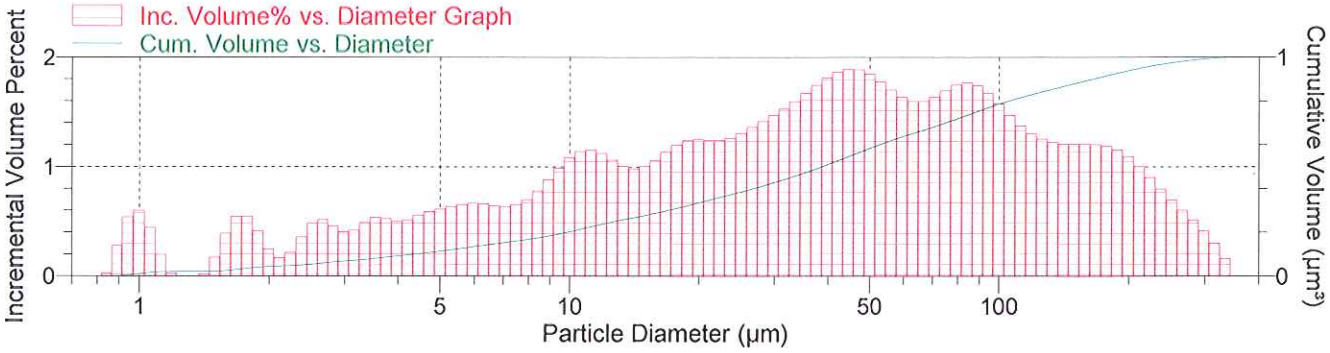

Summary Report

Sample

Sample Concentration: 0.01995 %
Obscuration: 23.8 %

Weighted Statistics (Volume Distribution)

		Std Dev of 1			Std Dev of 1
Mean	62.296	0.000	Mode	44.674	0.000
Median	38.496	0.000			

Peaks: Weighted Statistics (Volume Distribution)

Peak Number	Percent of Dist.*	Percent of Dist. Std Dev of 1	Mean	Mean Std Dev of 1	Median	Median Std Dev of 1	Mode
1	6.2	0.0	5.596	0.000	5.553	0.000	5.957
2	11.6	0.0	10.738	0.000	10.657	0.000	11.222
3	9.4	0.0	18.629	0.000	18.555	0.000	19.955
4	29.4	0.0	41.370	0.000	40.367	0.000	44.674
5	33.8	0.0	137.766	0.000	118.510	0.000	84.151

* Peaks must comprise at least 5.00 % of the distribution.

micromeritics®

Micromeritics Instrument Corporation

Sample: LS10
Operator:
Submitter:
File: C:\...\HAYDEN\LS10.SMP

Test Number: 1
Analyzed: 5/12/2011 11:39:11p.m.
Reported: 5/12/2011 11:39:15p.m.
Background: 5/12/2011 11:20:08p.m.

Model: Fraunhofer, 1.331
Material: Fraunhofer / Water
Background: Water RI 1.331
Smoothing: Medium

Combined Report

Incremental Volume Percent vs. Particle Diameter Graph

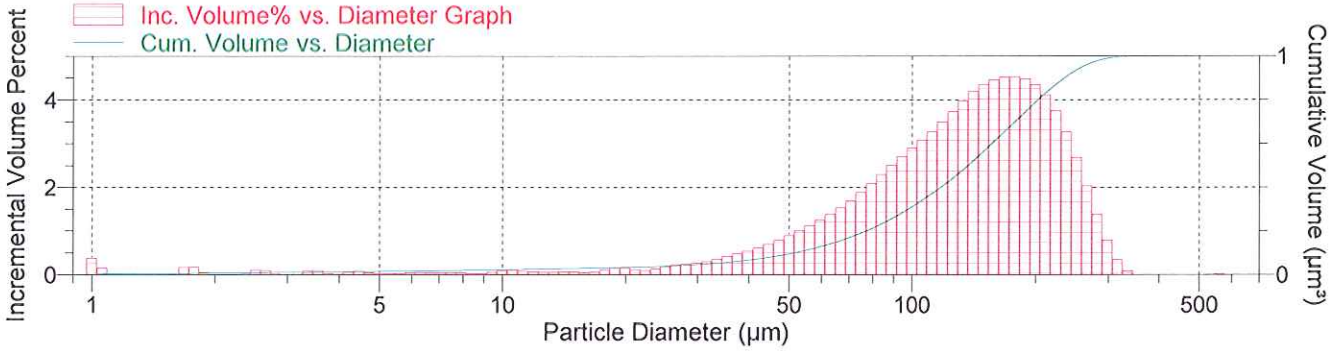

Summary Report

Sample

Sample Concentration: 0.04566 %
Obscuration: 13.5 %

Weighted Statistics (Volume Distribution)

		Std Dev of 1			Std Dev of 1
Mean	139.361	0.000	Mode	177.852	0.000
Median	136.427	0.000			

Peaks: Weighted Statistics (Volume Distribution)

Peak Number	Percent of Dist.*	Percent of Dist. Std Dev of 1	Mean	Mean Std Dev of 1	Median	Median Std Dev of 1	Mode
1	96.0	0.0	144.631	0.000	140.212	0.000	177.852

* Peaks must comprise at least 5.00 % of the distribution.

Sample: LS11
Operator:
Submitter:
File: C:\...\HAYDEN\LS11.SMP

Test Number: 1
Analyzed: 5/12/2011 11:51:22p.m.
Reported: 5/12/2011 11:51:26p.m.
Background: 5/12/2011 11:20:08p.m.

Model: Fraunhofer, 1.331
Material: Fraunhofer / Water
Background: Water RI 1.331
Smoothing: Medium

Combined Report

Incremental Volume Percent vs. Particle Diameter Graph

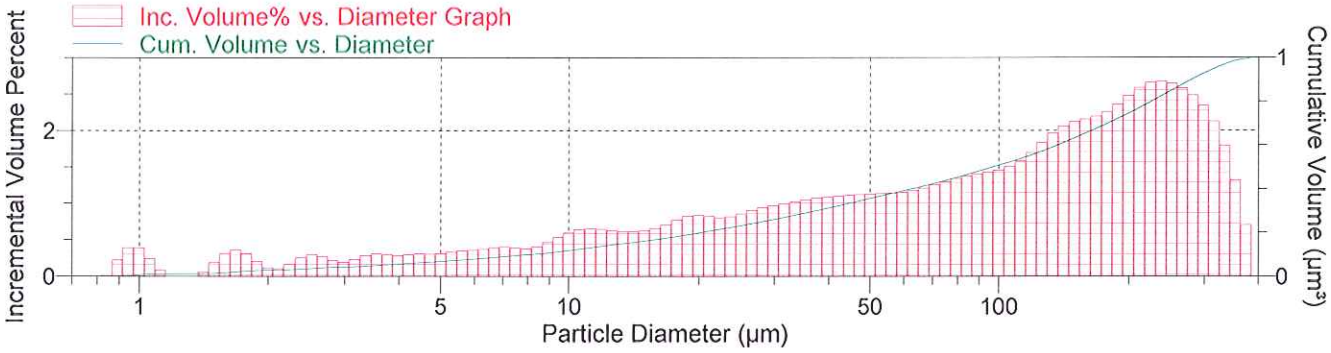

Summary Report

Sample

Sample Concentration: 0.01712 %
Obscuration: 13.9 %

Weighted Statistics (Volume Distribution)

		Std Dev of 1			Std Dev of 1
Mean	121.447	0.000	Mode	237.170	0.000
Median	95.908	0.000			

Peaks: Weighted Statistics (Volume Distribution)

Peak Number	Percent of Dist.*	Percent of Dist. Std Dev of 1	Mean	Mean Std Dev of 1	Median	Median Std Dev of 1	Mode
1	5.8	0.0	11.230	0.000	11.146	0.000	11.222
2	6.1	0.0	18.681	0.000	18.649	0.000	19.955
3	77.9	0.0	153.124	0.000	139.908	0.000	237.170

* Peaks must comprise at least 5.00 % of the distribution.

micromeritics®

Micromeritics Instrument Corporation

Sample: LS12
Operator:
Submitter:
File: C:\...\HAYDEN\LS12.SMP

Test Number: 1
Analyzed: 5/12/2011 11:59:53p.m.
Reported: 5/12/2011 11:59:57p.m.
Background: 5/12/2011 11:20:08p.m.

Model: Fraunhofer, 1.331
Material: Fraunhofer / Water
Background: Water RI 1.331
Smoothing: Medium

Combined Report

Incremental Volume Percent vs. Particle Diameter Graph

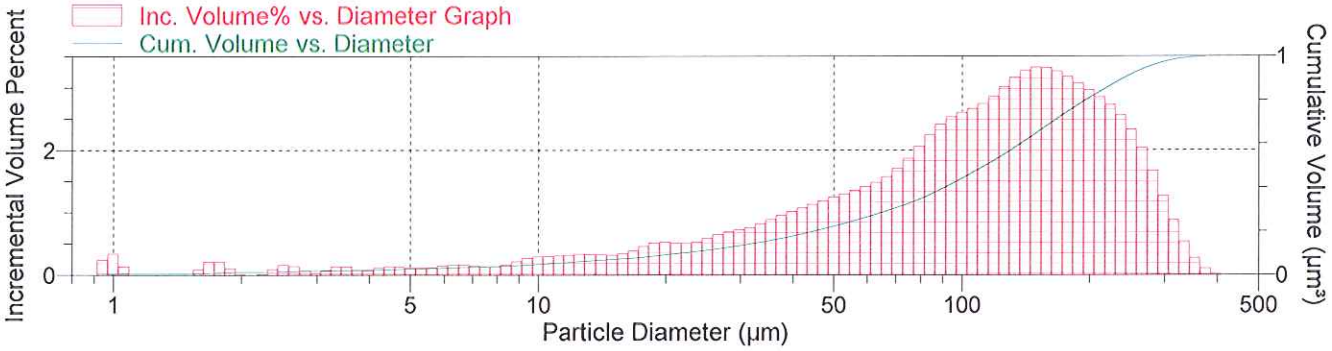

Summary Report

Sample

Sample Concentration: 0.03687 %
Obscuration: 16.4 %

Weighted Statistics (Volume Distribution)

		Std Dev of 1			Std Dev of 1
Mean	122.733	0.000	Mode	149.644	0.000
Median	112.679	0.000			

Peaks: Weighted Statistics (Volume Distribution)

Peak Number	Percent of Dist.*	Percent of Dist. Std Dev of 1	Mean	Mean Std Dev of 1	Median	Median Std Dev of 1	Mode
1	89.2	0.0	136.232	0.000	125.528	0.000	149.644

* Peaks must comprise at least 5.00 % of the distribution.

micromeritics®

Micromeritics Instrument Corporation

Sample: LS13
Operator:
Submitter:
File: C:\...\HAYDEN\LS13.SMP

Test Number: 1
Analyzed: 5/12/2011 12:10:16p.m.
Reported: 5/12/2011 12:10:21p.m.
Background: 5/12/2011 11:20:08p.m.

Model: Fraunhofer, 1.331
Material: Fraunhofer / Water
Background: Water RI 1.331
Smoothing: Medium

Combined Report

Incremental Volume Percent vs. Particle Diameter Graph

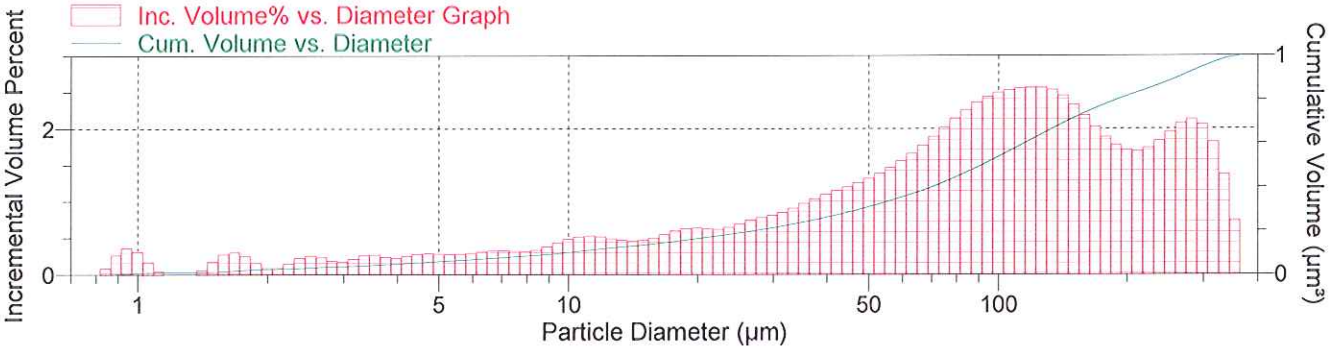

Summary Report

Sample

Sample Concentration: 0.01727 %
Obscuration: 12.9 %

Weighted Statistics (Volume Distribution)

		Std Dev of 1			Std Dev of 1
Mean	111.702	0.000	Mode	118.866	0.000
Median	90.897	0.000			

Peaks: Weighted Statistics (Volume Distribution)

Peak Number	Percent of Dist.*	Percent of Dist. Std Dev of 1	Mean	Mean Std Dev of 1	Median	Median Std Dev of 1	Mode
1	65.9	0.0	100.078	0.000	93.636	0.000	118.866
2	15.8	0.0	278.645	0.000	275.844	0.000	281.877

* Peaks must comprise at least 5.00 % of the distribution.

micromeritics®

Micromeritics Instrument Corporation

Sample: LS14
Operator:
Submitter:
File: C:\...\HAYDEN\LS14.SMP

Test Number: 1
Analyzed: 5/12/2011 12:33:54p.m.
Reported: 5/12/2011 12:34:00p.m.
Background: 5/12/2011 11:20:08p.m.

Model: Fraunhofer, 1.331
Material: Fraunhofer / Water
Background: Water RI 1.331
Smoothing: Medium

Combined Report

Incremental Volume Percent vs. Particle Diameter Graph

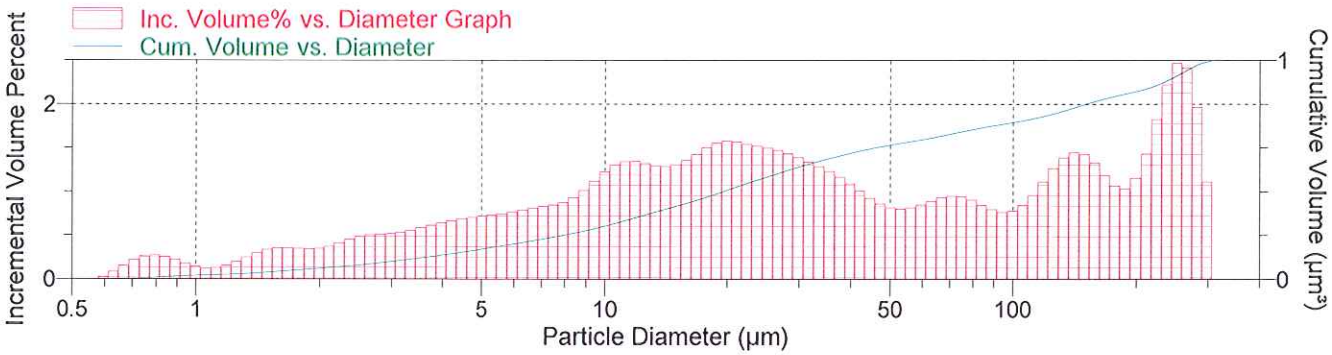

Summary Report

Sample

Sample Concentration: 0.00868 %
Obscuration: 13.2 %

Weighted Statistics (Volume Distribution)

		Std Dev of 1			Std Dev of 1
Mean	73.035	0.000	Mode	251.223	0.000
Median	28.147	0.000			

Peaks: Weighted Statistics (Volume Distribution)

Peak Number	Percent of Dist.*	Percent of Dist. Std Dev of 1	Mean	Mean Std Dev of 1	Median	Median Std Dev of 1	Mode
1	28.1	0.0	7.563	0.000	7.250	0.000	11.887
2	29.8	0.0	28.295	0.000	25.845	0.000	19.955
3	8.7	0.0	73.532	0.000	72.459	0.000	70.804
4	13.9	0.0	141.935	0.000	140.425	0.000	141.273
5	14.6	0.0	247.856	0.000	247.900	0.000	251.223

* Peaks must comprise at least 5.00 % of the distribution.

micromeritics®

Micromeritics Instrument Corporation

Sample: LS15
Operator:
Submitter:
File: C:\...\HAYDEN\LS15.SMP

Test Number: 1
Analyzed: 5/12/2011 12:46:11p.m.
Reported: 5/12/2011 12:46:15p.m.
Background: 5/12/2011 11:20:08p.m.

Model: Fraunhofer, 1.331
Material: Fraunhofer / Water
Background: Water RI 1.331
Smoothing: Medium

Combined Report

Incremental Volume Percent vs. Particle Diameter Graph

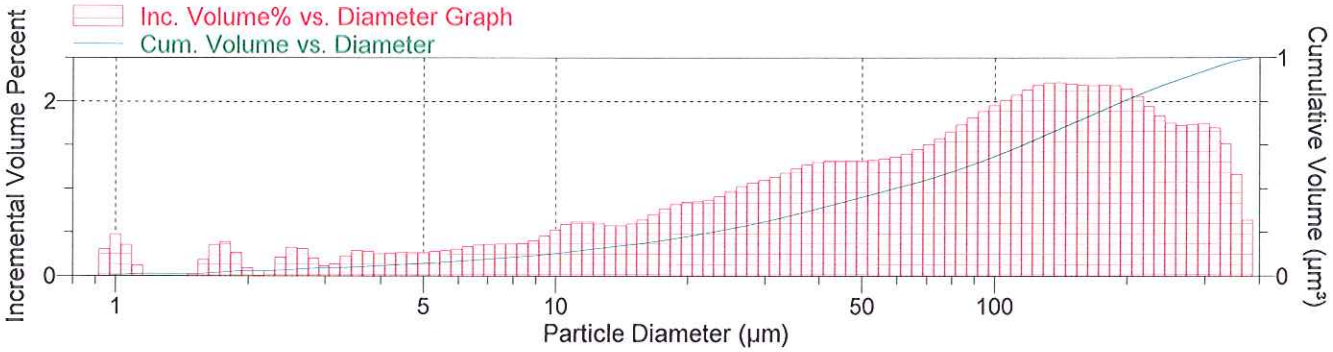

Summary Report

Sample

Sample Concentration: 0.01871 %
Obscuration: 13.9 %

Weighted Statistics (Volume Distribution)

		Std Dev of 1			Std Dev of 1
Mean	110.642	0.000	Mode	141.273	0.000
Median	85.318	0.000			

Peaks: Weighted Statistics (Volume Distribution)

Peak Number	Percent of Dist.*	Percent of Dist. Std Dev of 1	Mean	Mean Std Dev of 1	Median	Median Std Dev of 1	Mode
1	8.4	0.0	9.571	0.000	9.664	0.000	11.222
2	21.4	0.0	30.392	0.000	29.824	0.000	44.674
3	39.8	0.0	104.205	0.000	101.517	0.000	141.273
4	15.9	0.0	216.876	0.000	213.521	0.000	177.852
5	8.5	0.0	318.782	0.000	315.352	0.000	298.579

* Peaks must comprise at least 5.00 % of the distribution.

micromeritics®

Micromeritics Instrument Corporation

Sample: LS16
Operator:
Submitter:
File: C:\...\HAYDEN\LS16.SMP

Test Number: 1
Analyzed: 5/12/2011 13:04:37p.m.
Reported: 5/12/2011 13:04:42p.m.
Background: 5/12/2011 11:20:08p.m.

Model: Fraunhofer, 1.331
Material: Fraunhofer / Water
Background: Water RI 1.331
Smoothing: Medium

Combined Report

Incremental Volume Percent vs. Particle Diameter Graph

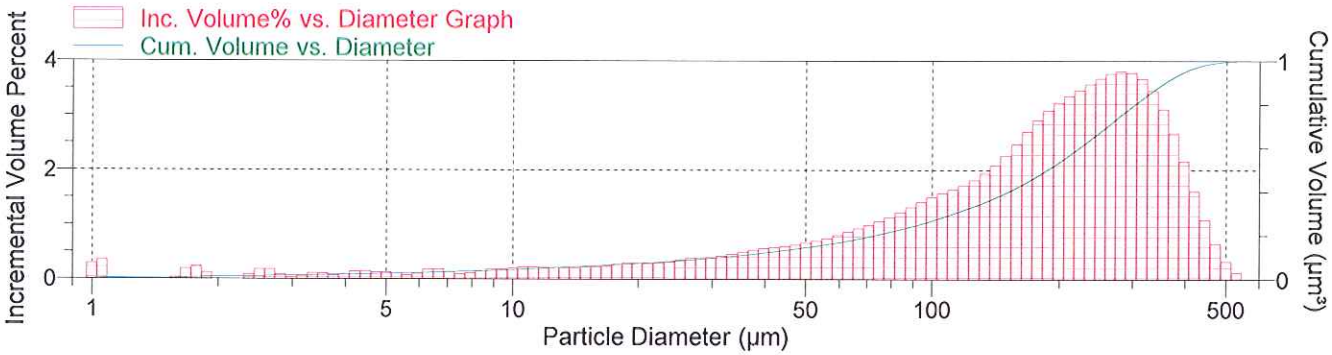

Summary Report

Sample

Sample Concentration: 0.03360 %
Obscuration: 12.5 %

Weighted Statistics (Volume Distribution)

		Std Dev of 1			Std Dev of 1
Mean	191.210	0.000	Mode	281.877	0.000
Median	185.831	0.000			

Peaks: Weighted Statistics (Volume Distribution)

Peak Number	Percent of Dist.*	Percent of Dist. Std Dev of 1	Mean	Mean Std Dev of 1	Median	Median Std Dev of 1	Mode
1	92.1	0.0	206.908	0.000	199.759	0.000	281.877

* Peaks must comprise at least 5.00 % of the distribution.

micromeritics®

Micromeritics Instrument Corporation

Sample: LS17
Operator:
Submitter:
File: C:\...\HAYDEN\LS17.SMP

Test Number: 1
Analyzed: 5/12/2011 13:17:07p.m.
Reported: 5/12/2011 13:17:11p.m.
Background: 5/12/2011 11:20:08p.m.

Model: Fraunhofer, 1.331
Material: Fraunhofer / Water
Background: Water RI 1.331
Smoothing: Medium

Combined Report

Incremental Volume Percent vs. Particle Diameter Graph

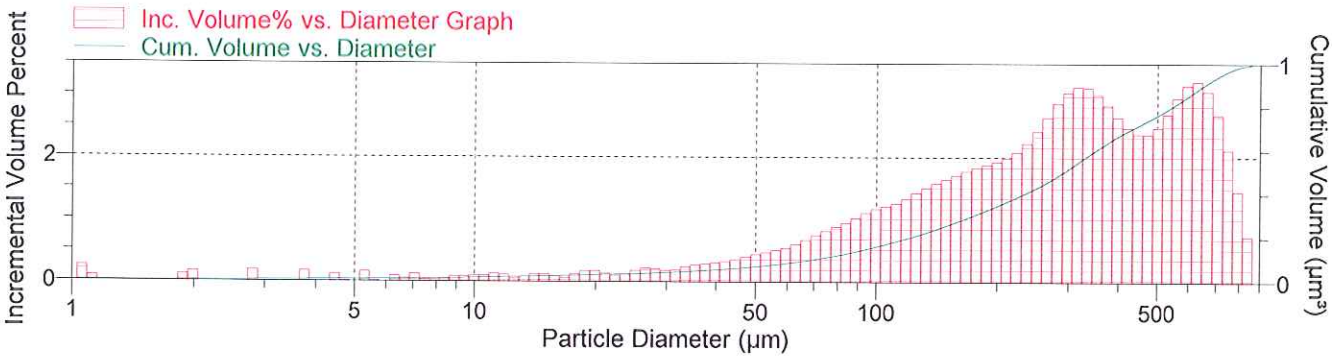

Summary Report

Sample

Sample Concentration: 0.06699 %
Obscuration: 12.8 %

Weighted Statistics (Volume Distribution)

		Std Dev of 1			Std Dev of 1
Mean	323.239	0.000	Mode	631.044	0.000
Median	287.844	0.000			

Peaks: Weighted Statistics (Volume Distribution)

Peak Number	Percent of Dist.*	Percent of Dist. Std Dev of 1	Mean	Mean Std Dev of 1	Median	Median Std Dev of 1	Mode
1	70.9	0.0	235.599	0.000	228.913	0.000	316.271
2	24.6	0.0	633.535	0.000	624.152	0.000	631.044

* Peaks must comprise at least 5.00 % of the distribution.